ISSI Scientific Report 11

Lennart Bengtsson · Roger-Maurice Bonnet
David Grinspoon · Symeon Koumoutsaris
Sebastien Lebonnois · Dmitri Titov *Editors*

Towards Understanding the Climate of Venus

Applications of Terrestrial Models to Our Sister Planet

INTERNATIONAL SPACE SCIENCE INSTITUTE

Springer

ISSI Scientific Report Series

For further volumes:
http://www.springer.com/series/10151

Lennart Bengtsson • Roger-Maurice Bonnet
David Grinspoon • Symeon Koumoutsaris
Sebastien Lebonnois • Dmitri Titov
Editors

Towards Understanding the Climate of Venus

Applications of Terrestrial Models to Our Sister Planet

Vol. No. 11

Springer

Editors
Lennart Bengtsson
International Space Science Institute
Bern, Switzerland

Roger-Maurice Bonnet
International Space Science Institute
Bern, Switzerland

David Grinspoon
Department of Space Science
Denver Museum of Nature and Science
Denver, CO, USA

Symeon Koumoutsaris
Peninsular House
Risk Management Solutions Ltd
London
United Kingdom

Sebastien Lebonnois
Laboratoire de Meterologie
Dynamique
Paris, France

Dmitri Titov
ESA-ESTEC
Noordwijk, The Netherlands

ISBN 978-1-4614-5063-4 ISBN 978-1-4614-5064-1 (eBook)
DOI 10.1007/978-1-4614-5064-1
Springer New York Heidelberg Dordrecht London

Library of Congress Control Number: 2012951841

Cover illustration:
– Galaxy, NASA/JPL-Caltech/C.Lonsdale (Caltech/IPAC) and the SWIRE Team
– Whole Earth, NASA
– Hemispheric view of Venus (Magellan), NASA/JPL-Caltech
– Ultraviolet image of Venus' clouds (Pioneer), NASA
– Artist's impression of Venus Express spacecraft, ESA-AOES Medialab

Printed on acid-free paper

Springer is part of Springer Science+Business Media (www.springer.com)

Foreword

Back in 2003, ISSI organized one of its regular internal reflexion meetings and invited a few scientists to share for two days their views on the future orientations of the scientific activities of the institute. Their scientific expertise covered a broad range of disciplines and interests, from astronomy to solar physics, planetology, and Earth sciences. One important recommendation of that meeting was to open ISSI activities to Earth sciences, in particular to atmospheric physics and dynamics, and also to the solid Earth, to volcanology and desertification, insisting that they be considered in the broader context of comparative planetology. A few years later these recommendations were implemented. A contract was established with the ESA Directorate of Earth Observations, and Lennart Bengtsson, the leading force behind the preparation of this book, was recruited as ISSI Director for Earth sciences. Lennart did not participate in the 2003 reflexion but he rapidly assimilated its conclusions, in particular as to what concerned Earth sciences and comparative planetology, as well as the unique opportunities offered by ISSI for hosting scientific visitors from all around the world and from many areas of space science. He rapidly proposed that ISSI dedicates one of its future Working Groups to the climate of Venus. The study of Venus climate would indeed offer a natural response to the 2003 meeting recommendations. Opening the ISSI program to the field of Earth sciences through comparative planetology was in continuity with the traditional space science orientations characterizing previous ISSI activities. When planetologists are asked to justify their activities and the costs of their space missions some very often respond that the study of planets should improve our understanding of the Earth.

Amazingly, the logics which led Lennart to establishing a Working Group on the climate of Venus is nearly the opposite, as the title of this book explicitly says: "Towards understanding the climate of Venus: Applications of terrestrial models to our sister planet"! The work reported here aims at showing how the modelling of the Earth atmosphere through General Circulation Models helps improving our understanding of Venus. In the Solar System, among all the other planets, the Earth is exhibiting the largest complexity. It is all at the same time: a solid planet, a magnetic planet, a liquid planet, an icy planet, and an atmospheric planet and last

but certainly not least a living planet (it hosts life). Venus is indeed often called our sister planet. It is rather our false twin. It was formed at the same time as the Earth 4.6 billion years ago from the same proto-solar nebula. With a diameter 95 % and a mass 80 % that of the Earth, Venus is a little smaller however. Both planets have nearly the same density and chemical composition. They both have an atmosphere and clouds. But they also have marked differences. Contrary to Venus, the Earth evidences plate tectonics, it has a magnetic field, and its surface is covered at 70 % by water. Venus had probably the same amount of water as the Earth but lost it very early in its history. Today, it is an arid desert and its surface temperature is 460 °C as a consequence of the enormous atmospheric pressure and the extreme greenhouse effect produced early in its life by the high concentration of CO_2, re-enforced by the presence of cloud particles and droplets of sulphuric acid. Besides the unbreathable atmosphere, at this temperature, life is impossible. The Russian probes which landed on Venus in 1970 and 1982 could transmit signals and pictures of the surface for no more than 2 h maximum (Venera-13), after which the heat destroyed the equipment. Furthermore, the absence of water that plays an essential lubrification role in Earth's tectonic activity has probably put to a standstill any such activity that might have existed on Venus, now a single-plate planet. Nevertheless, a comparative study of the poorly known atmosphere of Venus based on the models that have been developed for the extensive studies of the Earth atmosphere is an application that may help us understanding their enormous differences and forecasting their long-term evolution. For example, the Earth might follow the same trend as Venus when the increasing luminosity of the Sun at a rate of 1 % per 100 million years would have raised its temperature to the point where as was the case for the young Venus, water molecules would start being photo-dissociated, an irreversible process leading to the end of life in about one billion years. The problem is not that simple however, as the atmospheric circulation, very different on both planets, must play an important role in the process. Therefore, it is of importance to understand atmospheric circulation in the different physical conditions characterizing the two planets.

The work described in this book is unique and well in line with the inter-disciplinary approach that characterizes ISSI activities. While the Earth has been observed by several hundreds of artificial satellites, in addition to an enormous amount of in situ measurements, the number of satellites launched to Venus totals today just 40 (mostly Russian) of which only 20 were successful. The similarities and the large differences between the two planets would support a more continuous international effort in Venus exploration. This book offers an excellent basis on which to build the convincing arguments for sustaining such long-term exploration. Let me address my compliments to all the contributors to this book among whom I would like to explicitly mention Lennart Bengtsson who deserves special acknowledgements. Similarly, Simos Koumoutsaris should be acknowledged for his dedication and help in organizing the meetings and in the editing of the book.

Bern, Switzerland Roger-Maurice Bonnet

Contents

Chapter 1
Introduction

Lennart Bengtsson

The ultimate purpose of this book is to increase our understanding of the climate of planet Venus. We will endeavor to do so by bringing together recent observations from Venus with the general knowledge of the Earth's atmosphere that has been collected over a long period of time from modeling and data studies.

Superficially, there are many similarities between Earth and Venus when observed from a great distance but a close inspection reveals critical differences that make life on Venus inconceivable. In fact our sister planet is highly inhospitable. Its surface temperature is around 460 °C where lead and tin will start to melt, and it has a cloud cover where the droplets are not water but sulphuric acid. The cause of the high surface temperature is not that Venus is receiving more sunlight than the Earth. In fact it receives significantly less as can be seen in Table 1.1. Instead the high surface temperature of Venus results from the different composition of its atmosphere, consisting of 96 % carbon dioxide, as well as its huge atmospheric mass that is 92 times larger than that of the Earth's atmosphere. There are also marked differences due to the slow rotation of Venus, which means that the Coriolis force that is crucial in determining the dynamical structure of the Earth's atmosphere plays a secondary role on Venus.

The present understanding of Venus is the result of a large number of successful space missions to the planet that started in 1962 with Mariner 1. The latest in the series, to be discussed in more depth in this book, is the Venus Express mission of the European Space Agency. Venus Express, by now has been collecting information since April 2006.

However, our knowledge of planetary atmospheres does not come from empirical studies only but also from theoretical considerations by making use of our general knowledge of fluid mechanics and thermodynamics. This has been the alternative approach for the Earth's atmosphere through the use of physically based general

L. Bengtsson (✉)
International Space Science Institute, Bern, Switzerland
e-mail: Bengtsson@issibern.ch

L. Bengtsson et al. (eds.), *Towards Understanding the Climate of Venus*, ISSI Scientific Report Series 11, DOI 10.1007/978-1-4614-5064-1_1,

Table 1.1 Different physical values for Venus, Earth and Mars

Properties	Venus	Earth	Mars
Distance to sun	0.72 AU	1 AU	1.5 AU
Solar constant	2,622 W/m^2	1,364 W/m^2	589 W/m^2
Albedo	0.76	0.30	0.30
Eq. temperature	− 41 °C	−18 °C	−72 °C
Surf. temperature	+ 460 °C	+15 °C	−63 °C
Diurnal cycle	0 °C	20 °C	200 °C
Atmos. mass	92	1	0.006
Planetary emissivity (%)	0.01	0.59	0.84
CO_2 in %	96.5	0.039	95.3

Note the very high albedo of Venus compared to Earth and Mars. The outgoing radiation from Venus is consistent with a blackbody temperature of −41 °C. The planetary emissivity is calculated as the ratio between the blackbody radiation at the top of the atmosphere and at the surface

circulation models, GCMs. GCMs are based on the fundamental physical equations for energy, mass and momentum including sources and sinks. The first GCMs, developed in the late 1950s, were simple, but present models are highly sophisticated and are the main tools used to determine and predict the Earth's weather and climate. Present capabilities in understanding the climate of the Earth would be impossible without the use of GCMs. They have been the key factor that has transformed climatology from a pure empirical discipline in natural geography to a distinct discipline of classical physics. GCMs have in fact become the main numerical experimentation tool for theoretical analysis of different phenomena in planetary atmospheres. Furthermore, GCMs are also the main tools to study climate change resulting from changing the amount of greenhouse gases and the amount and nature of atmospheric aerosols.

Because of their general form the GCMs have also been applied to the atmospheres of other planets such as Venus, Mars and the Saturnian moon Titan. Venus in particular is a great challenge because of its very slow rotation and its mighty atmosphere consisting mainly of CO_2. Although modeling for different planets is based on the same physical laws as for the Earth, they also include the incorporation of many unresolved, small-scale processes that often are unique for any application and have to be parameterized in terms of available model parameters. Optimizing parameterization schemes requires numerical experiments and systematic testing over a period of time using observational data from the largest part of the planet as possible. That means in practice that certain aspects of a GCM will to some extent be tuned to the planetary atmosphere where it will be used. That is true for the Earth where parameterization of turbulence, moist convection and clouds could hardly be effectively done without detailed observing programs and systematic numerical experiments. As will be clarified in this book this is also the case for the atmosphere of Venus. In this respect observational explorations and numerical experiments should be considered as a combined approach.

The content of the book is organized as follows. We begin in Part I with a review of the present knowledge of Venus including a general background and

history of Venus observations. This will be followed by a comprehensive overview of the radiation balance, the composition of its atmosphere and the circulation and dynamics of its atmosphere.

An inspection of its radiation balance compared to the Earth shows large differences. Firstly, despite of its proximity to the sun Venus receives less net solar radiation than the Earth because of its high albedo. Furthermore, because of its high opacity, only a small amount of the solar radiation enters the depth of its atmosphere. At the surface of Venus only a mere $17\,\mathrm{Wm}^{-2}$ is received compared to almost 10 times as much at the Earth. On Venus most of the solar radiation is absorbed in the atmosphere. Most of the absorption occurs in the cloud layer 50–70 km above the surface with a minor part of some $30\,\mathrm{Wm}^{-2}$ in the atmosphere below the clouds. Secondly, there is no condensed surface water on Venus and consequently no latent heat flux from the surface and the sensible heat flux is maximised by the net surface energy. Thirdly, the black body radiation from the surface is some 40 times larger than for the Earth. Due to the high opacity of the Venus atmosphere there is no way for the planet to get rid of its heat by radiation and the upward flux of long wave radiation is more or less fully compensated by the downward long wave radiation flux. There is consequently only a limited amount of energy that is transported from the surface upwards as dry convective energy.

The main reason for the very high temperature of the surface of Venus is its atmospheric composition that consists of some 96 % carbon dioxide as well as other constituents such as clouds of sulphuric acid and water vapor. Another factor is the depth and size of its atmosphere, which insures that the temperature broadly follows a dry adiabatic lapse rate through a depth of some 70 km above the surface.

There are several indications that the composition of the Venus atmosphere has undergone large changes, such as an early runaway greenhouse climate, and it is likely that the planet has lost a large amount of water through dissociation of water in the upper atmosphere due to ultraviolet radiation and the subsequent escape of hydrogen. Later the free oxygen has reacted to create carbon dioxide and sulphur dioxide. The origin of the clouds on Venus and their lifetime is one of the many riddles of that mysterious planet. The source for both SO_2 and in fact also CO_2 can hardly be anything else than volcanic eruptions but no such eruptions have so far been directly observed. One reason could be that the volcanic eruptions could have a different character than on the Earth with either a steady flux from a low level activity or from major eruptions occurring at very rare intervals. There are indications from surface observations that the second alternative is the more likely.

A special aspect of this book is to try to bring some further understanding of the dynamics of the Venus atmosphere and the many puzzling features such as its super-rotation and its intriguing polar vortices. The main reason for the differences between the atmospheric general circulation of Venus and Earth can indeed be explained by the difference in solid body rotation. Numerical experiments as well as experiments with rotating annuli show that the general circulation is very sensitive to the rotation rate. For small rotation rates the Hadley circulation is extended to higher latitudes and the Ferrel circulation created by the activity of travelling extra-tropical cyclones weakens or disappears. Observations indicate that the Venus

general circulation is dominated by a huge Hadley cell transporting eddy momentum towards higher latitudes with a sharp transition to the polar vortex that is found on both hemispheres. The most likely explanation of the strong latitudinal jets is momentum transfer through the huge Hadley cell. The wind fields derived from temperature soundings using the cyclostrophic approximation show mid-latitude jets at 65–70 km and at 50–55 ° latitude in both hemispheres. The vortex eye resides inside the 70 °S latitude circle with striking similarity to a huge hurricane type circulation but in size more similar to a stratospheric winter polar vortex in the Earth's lower stratosphere.

Part II of the book is concerned with the modeling of the atmospheric circulation on Venus. The first section, outlined in Chap. 6 provides a detailed overview of the theoretical framework of the dynamics of the general circulation on Venus. The second section, Chap. 7 gives a background to the modeling efforts and some of the early results. The third part, Chap. 8, summarizes the latest achievements in the modeling of the Venus atmosphere by comparing results from recent numerical experiments. The fourth part, Chap. 9 provides a comparison with similar modeling efforts for the Earth using recent model results from the Earth's atmosphere from the troposphere through the stratosphere and the mesosphere.

In Part III of the book we endeavor to outline the prospects for future missions to Venus not the least based on what has been learned from the richness of information obtained from Venus Express.

Part I
What Do We Know About Venus?

Chapter 2
History of Venus Observations

Roger-Maurice Bonnet, David Grinspoon, and Angelo Pio Rossi

2.1 Knowledge of Venus Before the Space Age

Our image of Venus is that of a hellish, hot planet, permanently covered by fast-moving clouds, with its surface inaccessible to any Earth-based observer. But the perception and knowledge of our sister planet has been very different in the recent and more remote past.

Venus has been a prominent object in the sky since pre-historic times, being highly visible both at dawn and dusk. Also, contrary to many other planets, its apparent size did not change dramatically with time, due to a combined and inversely proportional effect of variable distance and phases (Goldstein 1972, and notes therein). In fact, the Latin name for Venus for its dawn appearance is lucifer (star carrying light) and for dusk, vesper (evening star), as derived from pre-existing Greek terms, respectively Phosphoros ($\Phi\omega\sigma\phi o\rho o\varsigma$) and Eosphoros ($E\omega\sigma\phi o\rho o\varsigma$).

Several ancient civilizations had knowledge of the existence of Venus, including, only to mention a few: Assyrians, who considered the planet under the rule of the Goddess Ishtar, Phoenicians (under the name of Astarte), Hindus (as Sukra), Greek, Roman and Mesoamerican peoples. A summary of the many different names attributed to Venus by various civilizations is provided by Grinspoon (1997).

Such clear visibility and awareness of Venus led to the creation of myths, stories and religious importance. As an example, the great importance attributed to Venus by Maya led them to precisely measure and predict its appearance in the sky.

R.-M. Bonnet (✉)
International Space Science Institute, Bern, Switzerland
e-mail: rmbonnet@issibern.ch

D. Grinspoon
Denver Museum of Nature & Science, Denver, USA

A.P. Rossi
Jacobs University Bremen, Bremen, Germany

L. Bengtsson et al. (eds.), *Towards Understanding the Climate of Venus*, ISSI Scientific Report Series 11, DOI 10.1007/978-1-4614-5064-1_2,

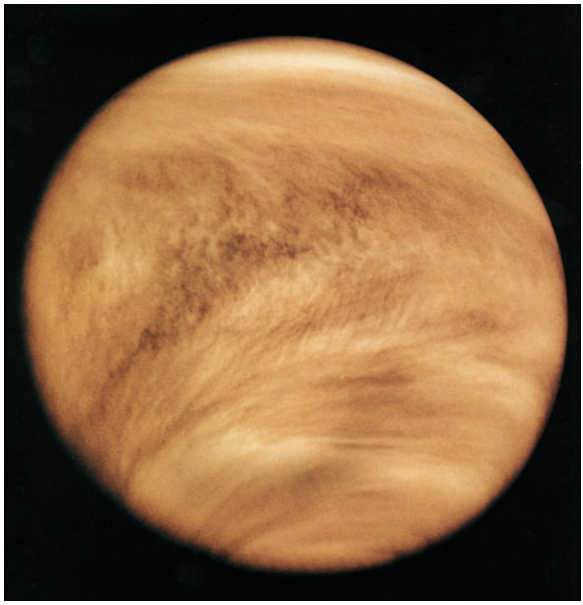

Fig. 2.1 Full disk image of Venus (from Pioneer-Venus, Credit: NASA/JPL)

Besides myths and stories, several accounts of astronomical observations and knowledge of Venus can be found among many different ancient peoples (e.g. Grinspoon 1997), including Babylonian, Greek and Mesoamerican such as the Aztecs, Mayans and Toltecs.

In the Middle Ages, Venus' position in the Ptolemaic system was considered below the Sun by Avicenna.

2.2 Telescopic Observations

Early telescopic observations of Venus, among other planets, were conducted by Galileo Galilei, who first measured Venus' phases in 1610 (e.g. Drake 1997; Palmieri 2001), determining its crescent disc shape and spherical geometry, confirming also its passage behind the Sun and thus validating Copernicus theory. Giandomenico Cassini observed Venus around 1666–1667 (Marov and Grinspoon 1998), detecting albedo variations, which, later in the eighteenth century were interpreted as possible continental and oceanic masses (Figs. 2.1–2.3).

Venus played a crucial role in measuring the distance between the Earth and the Sun, the so-called astronomical unit (AU): at its closest distance, the apparent disk of Venus, assuming to a first approximation the planet to have a size similar to that of the Earth, occupies an angle in the Sky of about 1 min of arc, from which it was possible to derive both the Venus-Earth and Earth-Sun distance, using Kepler's laws.

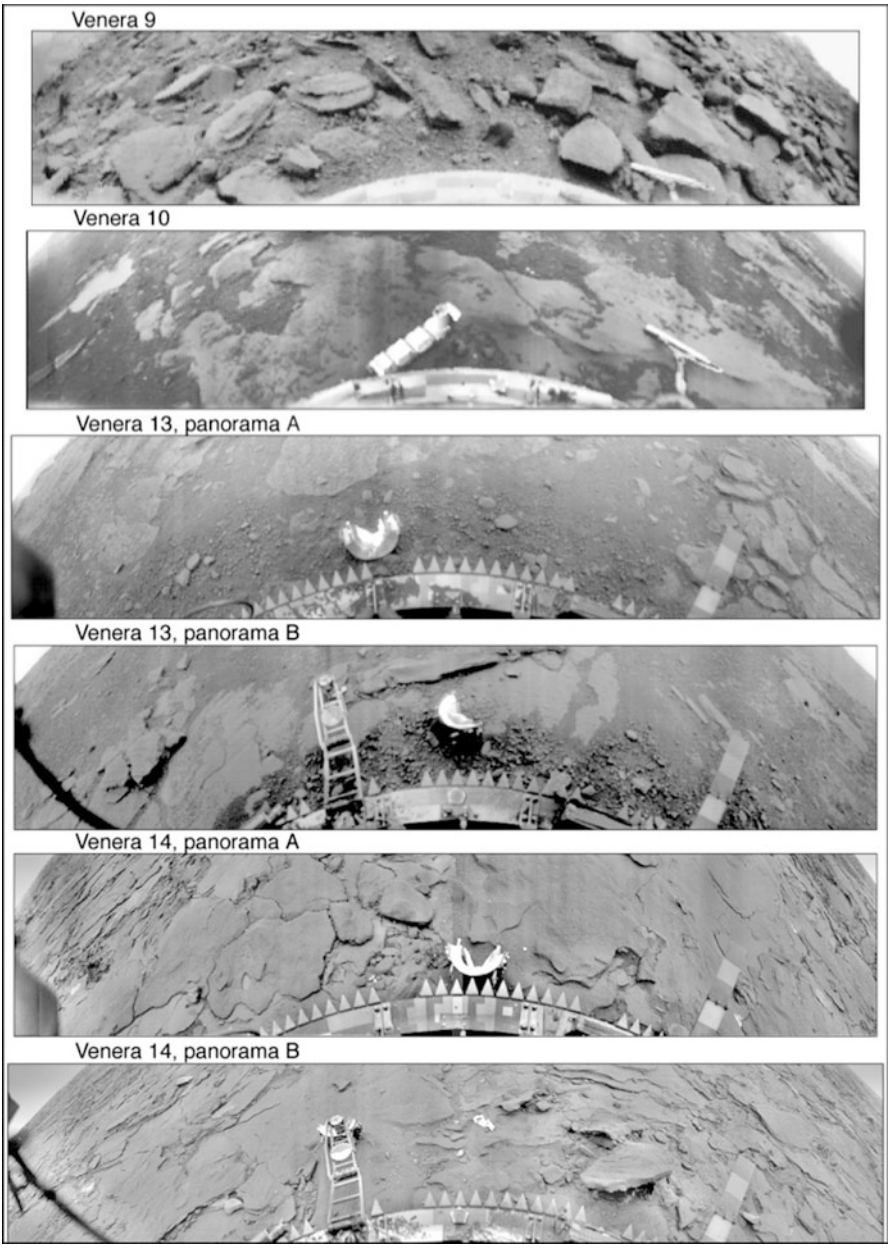

Fig. 2.2 Venera landings (Credit: Courtesy of Russian Academy of Science)

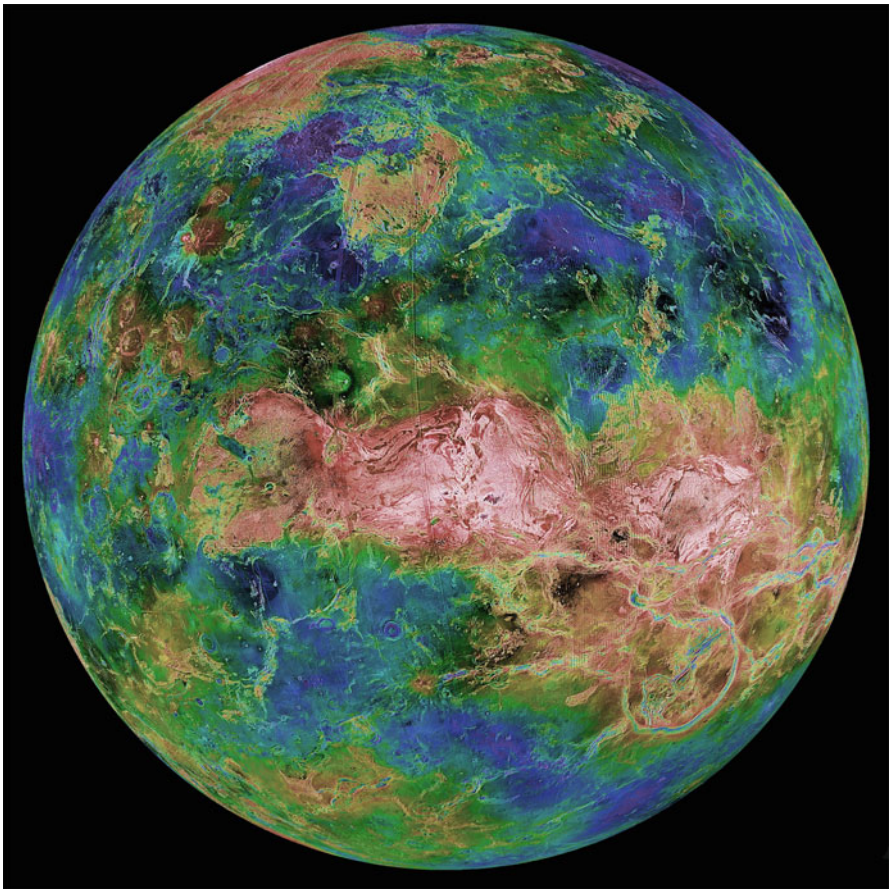

Fig. 2.3 Magellan view of Venus (Credit: NASA)

Transits of Venus in front of the Sun were particularly important for a variety of measurements (e.g. Chapman 1998; Teets 2003). In fact, transits were considered so important that even during exploration expeditions such as those of James Cook in the second half of the eighteenth century, they were studied systematically (e.g. Woolley 1969) and specific expeditions were organized for observing transits under favorable conditions. In fact, thanks to transits, the actual measurement of Venus' diameter was possible. Finally, the determination of the solar parallax, by means of measurements during the transits, was of paramount importance for determining the scale of the Solar System (e.g. Chapman 1998).

Therefore the determination of orbital and geometrical properties of Venus were of great importance for problems much wider than Venus itself, even before any hint about its surface conditions could be obtained.

The discovery that Venus actually has an atmosphere was made by M. Lomonosov in Russia during the observation of the Venus transit in 1761 (Lomonosov 1761; Marov and Grinspoon 1998). In fact, the existence of an atmosphere had already been proposed by William Herschel and Johann Schroter Grinspoon (1997).

Given the very similar sizes of the Earth and Venus, and the closer vicinity of the latter to the Sun, surface conditions were expected to be rather similar, Venus being possible slightly warmer than Earth. Based on the (false) assumption that the thick cloud cover of Venus was essentially due to water vapor, Nobel laureate Arrhenius in 1918 stated that "everything on Venus is dripping wet" which turned out, with subsequent astronomical and planetary exploration, to be far from the truth.

The determination of Venus' rotation rate, based on the search for surface periodic movements, was unsuccessful, due to its dynamical atmosphere. The first attempt was made by Cassini in 1667 (see Baum and Sheehan 1992). Optical (e.g. Slipher 1903; Richardson 1958) and radar (e.g. Dyce et al. 1967) measurements were performed in last few decades. Earth-based and space observations provided the currently known rotation rate of 243 days for an entire (retrograde) rotation. On a longer timescale, Venus' rotation itself, due to its chaotic evolution (Laskar and Robutel 1993), could have a resulting limited set of possible states due its dense, thick atmosphere (Correia and Laskar 2001). Compared with the solid planet rotation of 243 days, Venus' atmosphere rotates extremely fast (about 4 days at the equator). Such 'superrotation' was discovered in the 1960's (e.g. in Schubert 1983), mainly by Doppler experiments on the Soviet Venera 4 to 7 probes (reviewed by Dollfus (1975) and by Earth-based observations (e.g. Traub and Carleton 1975). CO_2 in Venus' atmosphere was first discovered and measured from the ground ((e.g. Adams and Dunham 1932), although its concentration was underestimated in these early observations. On the other hand, Earth-based measurements of H_2O have been much more challenging, given the strong absorption by the Earth's atmospheric water vapor: early measurements nevertheless already showed a very low concentration of H_2O (e.g. Spinrad 1962; Dollfus 1964). The discovery of hot millimeter waves radiation omitted by Venus made from Earth-based radioastronomy observations at the end of the 1950's was the first evidence that Venus is a hot planet Mayer et al. (1958).

2.3 History of Spacecraft Observations

In the space age, the robotic exploration of Venus was long and complicated, with variable, but in general positive results. In fact, the success rate for Venus space missions is higher than 50 % (higher than for Mars, overall): since 1961 space missions, including flybys, orbiters and landers performed successfully in 56 % of the cases, while failing in 44 %. Soviet missions constituted the bulk of these missions, counting for almost 3/4 of the total (43 so far). In addition to NASA (8 dedicated missions), ESA and Japan (JAXA) launched one mission each.

The first successful flyby of Venus was performed by the NASA Mariner 2 spacecraft whose radiometer confirmed the radioastronomy observations of an extremely high surface temperature of 460 °C, under a cloud-topped carbon dioxide atmosphere (Sonett 1963). The Soviet Venera programme revealed for the first time the atmospheric structure of the planet and its surface conditions through the use of different orbiters, atmospheric probes and landers. Venera 4 was the first mission to perform in situ atmospheric measurements, including temperature, pressure and density, from the surface to about 30 km (Vakhnin 1968). Venera 4 to 7 indeed confirmed earlier evidences of the super-rotation circulation (Dollfus 1975). The discovery of hot millimeter waves radiation omitted by Venus made from Earth-based radioastronomy observations at the end of the 1950's was the first evidence that Venus is a hot planet. Modern understanding of the Venus' atmosphere is derived largely from the heritage of Pioneer Venus (Colin and Hunten 1977) and from later Venera missions (e.g. Keldysh 1977; Avduevsky 1983). Their results included the measurement of atmospheric physical and chemical parameters and the determination of cloud microphysical properties, in addition to wind speeds. The Soviet VEGA mission in 1985 also carried French-built balloon experiments, which performed in situ measurements of pressure, temperature, wind velocity, ambient light, for more than 30 h (Blamont 1987, 2008).

Apart from several limited failures, most Venera landings were successful and provided data and imagery for slightly more than 2 h, a limitation imposed on the equipment by the very high surface temperature (e.g. Garvin et al. 1984). Among the many results of the Venera landings (e.g. Moroz 1983), elemental composition measurements were performed (e.g. Surkov et al. 1984), and widespread surface small-scale layer-like rock weathering was observed, most likely due to surface-atmospheric interactions (e.g. Barsukov et al. 1982; Wood 1997).

Late Venera missions (Venera 15 and 16) were equipped with imaging radars (e.g. Kotelnikov et al. 1985) allowing near-global coverage with low to moderate spatial resolution. That was later surpassed by the NASA Magellan mission launched in 1989 (Saunders et al. 1992). The combined results from Synthetic Aperture Radar imaging on board both Veneras and, in much higher resolution on board Magellan, provided the foundation for the reconstruction of Venus' geological history (e.g. Basilevsky and Head 1998).

A thorough review of Venus' spacecraft exploration and main scientific results until the late 1990's is provided by Marov and Grinspoon (1998). A further concise update until the mid 2000's, just before the launch of the European Space Agency (ESA) Venus Express (VEX) mission in 2005, the latest active mission to Venus, can be found in Titov et al. (2006). A more surface-oriented perspective on Venus landings is provided by Basilevsky et al. (2007). VEX is the first mission in two decades devoted to the study of Venus' atmosphere (Svedhem et al. 2007a,b). VEX has observed the dynamical features in the atmosphere with unprecedented spatial and temporal detail (Fig. 2.4). In particular it observed the detailed morphology of cloud patterns Markiewicz et al. (2007); Titov et al. (2011) and the complex atmospheric dynamics (e.g. Drossart et al. 2007). Several parameters of the cloud population have also been measured through imagery and tracking of their spatial

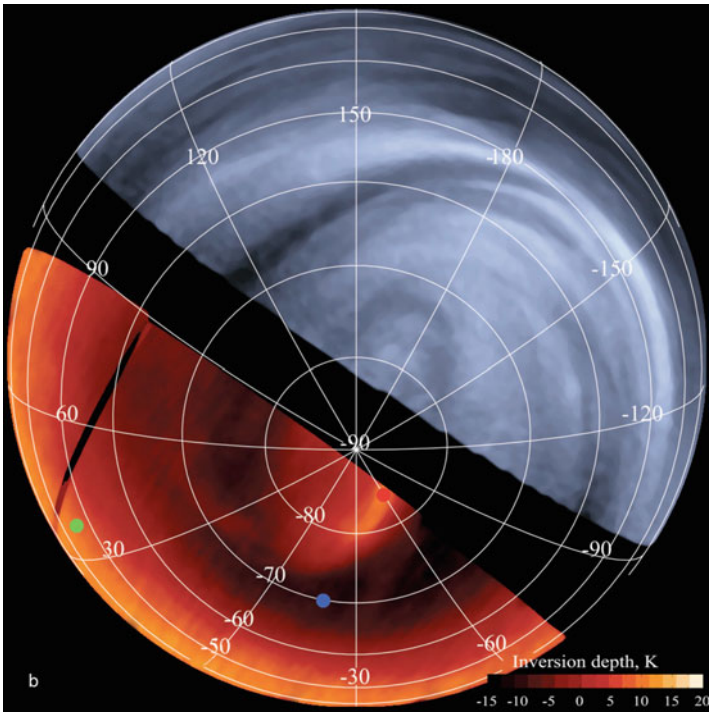

Fig. 2.4 Figure from VEX, the first ESA mission to Venus. Reprinted by permission from Macmillan Publishers Ltd: (from Titov et al. (2008))

and temporal variations, also allowing the derivation of wind velocities. Venus Express has also provided the first possible evidence of recent, possibly current, volcanic activity on Venus Smrekar et al. (2010), Svedhem et al. (2009), Titov et al. (2009).

The Japanese mission Akatsuki, launched 20 May 2010 also known as Venus Climate Orbiter or Planet-C (Nakamura et al. 2007) was designed for a wide range of meteorological studies and to scientifically and operationally benefit from synergic observations with VEX, in addition to the join data analysis and exploitation. In particular Akatsuki was meant to globally map clouds and minor atmospheric constituents thanks to a set of multispectral and hyperspectral imaging experiments, capable of sampling multiple depths within Venus' atmosphere. The failure of Akatsuki to achieve Venus orbit in December, 2010 was a set-back for Venus science. Plans are to relaunch Akatsuki in a strongly elongated orbit in 2015.

The future exploration of Venus will most likely have to rely on advanced mission architecture, involving multiple orbiters, landers, rovers and atmospheric probes (e.g. Bullock et al. 2009), such as balloons (e.g. Chassefiere et al. 2009). More advanced and complex mission scenarios will likely be put forward. Indeed ESA mission studies in the mid 1990's focused on the very challenging prospect of

collecting samples from the Venus surface and bringing them back to Earth (Scoon and Lebreton 1998), which would obviously constitute an extraordinary technical achievement, most likely lying outside the financial boundaries of any space agency in the present and near-future state of the necessary technologies.

Whatever will be the nature and elements of future Venus scientific exploration, an element of paramount scientific importance, and also technically challenging, will be a deeper understanding of the atmosphere properties and dynamics. In order to achieve this ambitious goal, more data should be gathered through instruments as those included onboard VEX and Akatsuki. But even more importantly, modeling efforts should be increased, coordinated and focused, as observational data should be assimilated into comprehensive models able to reproduce, reconstruct and predict the dynamical behavior of the atmosphere of the Morning Star.

Finally, a better understanding of the mechanisms at the base of Venus atmospheric circulation and processes would provide us with the best, although extreme, planetary analogue to Earth's own atmosphere. The following sections of this book provide an attempt for advancing our knowledge in this direction.

References

W. Adams, T. Dunham, Absorption bands in the infra-red spectrum of Venus. Publ. Astron. Soc. Pac. **44**, 243 (1932)

V. Avduevsky, Structure and parameters of the Venus atmosphere according to Venera probe data. Venus, Space Science Series, The University of Arizona press, pp. 280–298 (1983)

V.L. Barsukov, V.P. Volkov, I.L. Khodakovsky, The crust of Venus - theoretical-models of chemical and mineral-composition. J. Geophys. Res. **87**, A3–A9 (1982)

A.T. Basilevsky, J.W. Head, The geologic history of Venus: A stratigraphic view. J. Geophys. Res.-Planets **103**, 8531–8544 (1998)

A.T. Basilevsky, M.A. Ivanov, J.W. Head, M. Aittola, J. Raitala, Landing on Venus: Past and future. Planet Space Sci. **55**, 2097–2112 (2007)

R. Baum, W. Sheehan, Cassini and the rotation period of Venus-a common misconception. J. Hist. Astron. **23**, 299 (1992)

J. Blamont, The VEGA Venus balloon experiment. Adv. Space Res. **7**(12), 295–298 (1987)

J. Blamont, Planetary balloons. Exp. Astron. **22**, 1–39 (2008)

M.A. Bullock, D.A. Senske, T.S. Balint, A. Benz, B.A. Campbell, E. Chassefiere, A. Colaprete, J.A. Cutts, L. Glaze, S. Gorevan, D.H. Grisnspoon, J. Hall, G.L. Hashimoto, J.W. Head, G. Hunter, N. Johnson, V.V. Kerzhanovich, W.S. Kiefer, E.A. Kolawa, E. Kremic, J. Kwok, S.S. Limaye, S.J. Mackwell, M.Y. Marov, A. Ocampo, G. Schubert, E.R. Stofan, H. Svedhem, D.V. Titov, A.H. Treiman, A Venus flagship mission: Report of the Venus science and technology definition team, in *40th Lunar and Planetary Science Conference* (2009)

A. Chapman, The transits of Venus. Endeavour **22**(4), 148–151 (1998)

E. Chassefiere, O. Korablev, T. Imamura, K.H. Baines, C.F. Wilson, D.V. Titov, K.L. Aplin, T. Balint, J.E. Blamont, C.G. Cochrane, C. Ferencz, F. Ferri, M. Gerasimov, J.J. Leitner, J. Lopez-Moreno, B. Marty, M. Martynov, S.V. Pogrebenko, A. Rodin, J.A. Whiteway, L.V. Zasova, European Venus Explorer: An in-situ mission to Venus using a balloon platform. Adv. Space Res. **44**, 106–115 (2009)

L. Colin, D.M. Hunten, Pioneer Venus experiment descriptions. Space Sci. Rev. **20**, 451–525 (1977)

A.C.M. Correia, J. Laskar, The four final rotation states of Venus. Nature **411**, 767–770 (2001)

A. Dollfus, L'eau sur Venus et Mars, L'Astronomie, **78**, p. 41 (1964)
A. Dollfus, Venus – evolution of upper atmospheric clouds. J. Atmos. Sci. **32**, 1060–1070 (1975)
S. Drake, Galileo Kepler and phases of Venus. J. Hist. Astron. **15**, 198 (1984)
P. Drossart, G. Piccioni, J.C. Gerard, M.A. Lopez-Valverde, A. Sanchez-Lavega, L. Zasova, R. Hueso, F.W. Taylor, B. Bezard, A. Adriani, F. Angrilli, G. Arnold, K.H. Baines, G. Bellucci, J. Benkhoff, J.P. Bibring, A. Blanco, M.I. Blecka, R.W. Carlson, A. Coradini, A. Di Lellis, T. Encrenaz, S. Erard, S. Fonti, V. Formisano, T. Fouchet, R. Garcia, R. Haus, J. Helbert, N.I. Ignatiev, P. Irwin, Y. Langevin, S. Lebonnois, D. Luz, L. Marinangeli, V. Orofino, A.V. Rodin, M.C. Roos-Serote, B. Saggin, D.M. Stam, D. Titov, G. Visconti, M. Zambelli, C. Tsang, A dynamic upper atmosphere of Venus as revealed by VIRTIS on Venus Express. Nature **450**, 641–645 (2007)
R.B. Dyce, G.H. Pettengill, I.I. Shapiro, Radar determination of rotations of Venus and Mercury. Astron. J. **72**, 351–359 (1967)
J.B. Garvin, J.W. Head, M.T. Zuber, P. Helfenstein, Venus – the nature of the surface from Venera panoramas. J. Geophys. Res. **89**, 3381–3399 (1984)
B.R. Goldstein, Theory and observation in medieval astronomy. Isis **63**, 39–58 (1972)
D.H. Grinspoon, *Venus Revealed: A New Look Below the Clouds of Our Mysterious Twin Planet* (Helix Books, Perseus Piblishing, Cambridge, Massachusetts, 1997)
M.V. Keldysh, Venus Exploration With Venera 9 And Venera 10 Spacecraft. *Icarus* **30**, 605–625 (1977)
V.A. Kotelnikov, A.F. Bogomolov, O.N. Rzhiga, Radar study of Venus surface by the Venera-15 and -16 spacecraft. Adv. Space Res. **5**, COSPAR; IAU; Int. Assoc. Geomagetism & Aeronomy; et al. (1985)
J. Laskar, P. Robutel, The chaotic obliquity of the planets. Nature **361**, 608–612 (1993)
M.V. Lomonosov, in *The Appearance of Venus on Sun as it was Observed at the St Petersburg Emperor's Academy of Sciences on may 26, 1761*, Acad. of Sci. Office, St Petersburg., Memoirs in Physics, Astronomy and Instruments Building, USSR Acad. of Sci., Leningrad. (1761)
W.J. Markiewicz, D.V. Titov, S.S. Limaye, H.U. Keller, N. Ignatiev, R. Jaumann, N. Thomas, H. Michalik, R. Moissl, P. Russo, Morphology and dynamics of the upper cloud layer of Venus. Nature **450**, 633–636 (2007)
M.Y. Marov, D.H. Grinspoon, *The Planet Venus*, Yale University Press New Haven & London, Yale Planetary Exploration Series (1998)
C.H. Mayer, T. McCullough, R. Sloanker, Observations of venus at 3.15 cm wavelength. Ab. J. **127**, 1–10 (1958)
V. Moroz, Summary of preliminary results of the Venera 13 and Venera 14 missons, Venus, pp. 45–68 (1983)
M. Nakamura, T. Imamura, M. Ueno, N. Iwagami, T. Satoh, S. Watanabe, M. Taguchi, Y. Takahashi, M. Suzuki, T. Abe, G.L. Hashimoto, T. Sakanoi, S. Okano, Y. Kasaba, J. Yoshida, M. Yamada, N. Ishii, T. Yamada, K. Uemizu, T. Fukuhara, K.-I. Oyarna, Planet-C: Venus climate orbiter mission of Japan. Planet Space Sci. **55**, 1831–1842 (2007)
P. Palmieri, Galileo and the discovery of the phases of Venus. J. Hist. Astron. **32**(2), 109–129 (2001)
R.S. Richardson, Spectroscopic observations of Venus for rotation made at Mount Wilson in 1956. Publ. Astron. Soc. Pac. **70**, 251–260 (1958)
R.S. Saunders, A.J. Spear, P.C. Allin, R.S. Austin, A.L. Berman, R.C. Chandlee, J. Clark, A.V. Decharon, E.M. Dejong, D.G. Griffith, J.M. Gunn, S. Hensley, W.T.K. Johnson, C.E. Kirby, K.S. Leung, D.T. Lyons, G.A. Michaels, J. Miller, R.B. Morris, A.D. Morrison, R.G. Piereson, J.F. Scott, S.J. Shaffer, J.P. Slonski, E.R. Stofan, T.W. Thompson, S.D. Wall, Magellan mission summary. J. Geophys. Res.-Planets **97**, 13067–13090 (1992)
G. Scoon, J. Lebreton, Venus sample return assessment study report. Tech. Rep. pp. 16–19, ESA Report SCI (1998)
G. Schubert, General circulation and the dynamical state of the Venus atmosphere, in: Venus (A83-37401 17-91), Tucson, AZ, University of Arizona Press, p. 681–765, (1983)

V. Slipher, A spectographic investigation on the rotation velocity of Venus. Tech. Rep. 1, pp. 9–18, Lowell Observatory Bulletin (1903)

S.E. Smrekar, E.R. Stofan, N. Mueller, A. Treiman, L. Elkins-Tanton, J. Helbert, G. Piccioni, P. Drossart, Recent hotspot volcanism on Venus from VIRTIS emissivity data. Science **328**, 605–608 (2010)

C. Sonett, A summary review of the scientific findings of the Mariner Venus mission. Space Sci. Rev. **2**, 751–777 (1963)

H. Spinrad, A search for water vapor and trace constituents in the Venus atmospheres. *Icarus* **1**, 266–270 (1962)

Y. Surkov, V.L. Barsukov, L.P. Moskalyeva, V.P. Kharyukova, New data on the composition, structure, and properties of Venus rock obtained by Venera 13 and Venera 14, J. Geophys. Res. **89**, Lunar Planetary Inst.; NASA; AGU (1984)

H. Svedhem, D.V. Titov, D. McCoy, J.P. Lebreton, S. Barabash, J.L. Bertaux, P. Drossart, V. Formisano, B. Haeusler, O. Korablev, W.J. Markiewicz, D. Nevejans, M. Paetzold, G. Piccioni, T.L. Zhang, F.W. Taylor, E. Lellouch, D. Koschny, O. Witasse, H. Eggel, M. Warhaut, A. Accomazzo, J. Rodriguez-Canabal, J. Fabrega, T. Schirmann, A. Clochet, M. Coradini, Venus Express - the first european mission to Venus. Planet Space Sci. **55**, 1636–1652 (2007a)

H. Svedhem, D.V. Titov, F.W. Taylor, O. Witasse, Venus as a more Earth-like planet. Nature **450**, 629–632 (2007b)

H. Svedhem, D.V. Titov, F.W. Taylor, O. Witasse, The venus express mission. J. Geophys. Res. **114**, E00B33 (2009)

D.A. Teets, Transits of Venus and the astronomical unit. Math. Mag. **76(5)**, 335–348 (2003)

D. Titov, H. Svedhem, F. Taylor, in *The Atmosphere of Venus: Currenz Knowledge and Future Investigations*, ed. by P. Blondel, J.W. Mason. Solar System Update (Springer-Praxis, Berlin, 2006)

D. Titov, W. Markiewicz, N. Ignatiev, S. Li, S. Limaye, A. Sanchez-Lavega, J. Hesemann, M. Almeida, T. Roatsch, K.-D. Matz, F. Scholten, D. Crisp, L. Esposito, S. Hviid, R. Jaumann, H. Keller, R. Moissl, Morphology of the cloud tops as observed by the venus express monitoring camera. *Icarus*, **217**, 2, 682–701, doi:10.1016/j.icarus.2011.06.020 (2012)

D.V. Titov, H. Svedhem, F.W. Taylor, S. Barabash, J.L. Bertaux, P. Drossart, V. Formisano, B. Haeusler, O. Korablev, W.J. Markiewicz, D. Nevejans, M. Paetzold, G. Piccioni, J.A. Sauvaud, T.L. Zhang, O. Witasse, J.C. Gerard, A. Fedorov, A. Sanchez-Lavega, J. Helbert, R. Hoofs, Venus express: Highlights of the nominal mission. Solar Sys. Res. **43**, 185–209 (2009)

D.M. Titov, F.W. Taylor, H. Svedhem, N.I. Ignatiev, W.J. Markiewicz, G. Piccioni and P. Drossart, Atmospheric structure and dynamics as the cause of ultraviolet markings in the clouds of Venus, **456**, 620–623, doi:10.1038/nature07466, (2008)

W.A. Traub, N.P. Carleton, Spectroscopic observations of winds on Venus. J. Atmos. Sci. **32**, 1045–1059 (1975)

V.M. Vakhnin, A review of the Venera 4 flight and its scientific program. J. Atmos. Sci. **25**, 533–534 (1968)

J. Wood, Rock weathering on the surface of Venus. Tech. Rep. 637, Venus II (1997)

R. Woolley, Captain Cook and the transit of Venus of 1769. Notes Rec. Roy. Soc. **24**(1), 19–32 (1969)

Chapter 3
The Surface and Atmosphere of Venus: Evolution and Present State

David Grinspoon

3.1 Early Evolution of the Atmosphere

Most models of atmospheric evolution start with the reasonable but unverified assumption that the original atmospheric inventories of Venus and Earth were similar. Although the two planets have similar overall abundances of nitrogen and carbon, the present day water inventory of Venus is lower than that of Earth by a factor of 10^5. The original water abundance of Venus is highly unconstrained. The high D/H ratio observed, 2.5×10^{-2} or $\approx$150 times terrestrial (Donahue et al. 1997) has been cited as evidence of a large primordial water endowment (Donahue et al. 1982). Yet, given the likelihood of geologically recent water sources and the large uncertainty in the modern and past hydrogen and deuterium escape fluxes, the large D/H may not reflect the primordial water abundance but rather may result from the history of escape and resupply in the most recent $\approx 10^9$ years of planetary evolution (Grinspoon 1997, 1993; Donahue et al. 1997). Thus, at present the best arguments for a sizable early Venusian water endowment remain dependent on models of planet formation and early volatile delivery. Most models of water delivery to early Earth involve impact processes that would have also supplied Venus with abundant water (Morbidelli et al. 2000; Grinspoon 1987; Ip et al. 1998). Stochastic processes could have created large inequities in original volatile inventory among neighboring planets (Morbidelli et al. 2000). However, given the great similarity in bulk densities and their close proximity in the Solar System the best assumption at present is that Venus and Earth started with similar water abundances.

The loss of water has been modeled as occurring during a phase of hydrodynamic escape driven by the large early solar EUV flux in a runaway climate driven by water

D. Grinspoon
Denver Museum of Nature & Science, Denver, USA
e-mail: dgrinspoon@dmns.org

L. Bengtsson et al. (eds.), *Towards Understanding the Climate of Venus*, ISSI Scientific Report Series 11, DOI 10.1007/978-1-4614-5064-1_3,

vapor feedback (Kasting et al. 1984; Kasting 1988) followed by loss of hydrogen through various thermal and non thermal escape processes, including Jeans escape, charge exchange, collisional ejection (Kumar et al. 1983), and an electric field driven flow of ions in the night-side hydrogen bulge (Donahue et al. 1997).

Kasting (1988) derived a timescale of several hundred million years for the loss of water, but this timescale remains highly uncertain. One of the largest uncertainties in understanding the nature and timescale for water loss is understanding the effects of clouds on the early environment. Cloud feedback is not included in any of the currently published models of the moist greenhouse. Grinspoon and Bullock (2007) presented simple grey-model simulations that suggested the role of clouds in the thermal balance during water loss would be to stabilize surface temperatures and thus greatly prolong the period of stable surface water, perhaps extending to 2 or 3 billion years.

3.2 Geological and Climate Evolution

The Magellan mission mapped nearly the entire surface of Venus, revealing a surface dominated by volcanic features exhibiting wide variety of morphologies, ranging from vast basaltic plains which cover 80 % of the planet and blanket the low-land areas, to a wide range of individual edifices including annular volcanic/tectonic features called coronae, steep sided domes apparently formed from more viscous magmas, and shield volcanoes ranging in size from 5 to hundreds of kilometers across (Basilevsky and McGill 2007). The largest of these are clustered in areas that are believed to be "hot spots" or mantle plumes, on the basis of Magellan gravity data (Smrekar et al. 2007). This distribution, and the lack of large-scale linear tectonic features or chains of volcanic features have been used to infer that Venus lacks plate tectonics.

Approximately 8 % of the surface consists of highly faulted and folded tessera terrain, which lies topographically above the surrounding volcanic plains (Basilevsky and McGill 2007). The tesserae are the oldest areas of Venus and may represent remnants from an epoch of fundamentally different geological processes. Given the apparent strong coupling between surface and atmospheric evolution on Venus, this also suggests that the tesserae may have been witness to a great transition in the atmosphere and climate as well. The current lack of plate tectonics may reflect the interior dynamics of a desiccated Earth-like planet. Thus the loss of water over time may ultimately explain the very different geology of Venus and Earth as well as their climatic divergence (Grinspoon and Bullock 2007).

More than 960 impact craters have been identified in Magellan radar imagery (Schaber et al. 1992). Their size distribution is consistent with the filtering effects of the atmosphere, suggesting that the current thick atmosphere has existed for at least the age of the extensive global plains. This age has been estimated as 750 Myr, with an uncertainty of several hundred million years, on the basis of crater modeling and statistics. The observation that the spatial crater distribution is nearly

indistinguishable from a random distribution suggests that, to first order, the global plains were largely formed over a geologically short time. This, combined with the observation that the fraction of craters that have been volcanically and tectonically disturbed is quite small, suggests that the global resurfacing that created the plains was extensive enough to fully bury the pre-existing crater population, and ceased relatively suddenly, followed by more localized volcanic and tectonic activity which may continue to the present day. This interpretation has been disputed, and more data from future Venus missions, with high resolution surface imaging or direct surface sampling, will be required to resolve the resurfacing history of Venus. Recent near-infrared maps made with the VIRTIS instrument on Venus Express have revealed areas of anomalous surface emissivity around hot spot regions, which may indicate recent or ongoing volcanic activity (Smrekar et al. 2010). Such present-day activity may be consistent with either catastrophic or episodic models for the volcanic plains.

The more recent climate evolution of Venus, over the approximately age of the surface visible in Magellan global radar imagery, has likely been characterized by the balance between volcanic outgassing of radiatively active gases, especially SO_2 and H_2O, heterogeneous reactions with surface minerals, and exospheric outgassing of hydrogen. Without continued outgassing the clouds would largely dissipate on a timescale of ≈30 million years (Bullock and Grinspoon 2001), Thus, Venus may have experienced cloud-free epochs. The onset and cessation of episodes of global outgassing, of the style that some researchers have interpreted to be responsible for the globally extensive plains seen in Magellan mapping, may result in surface temperature changes of the order of several hundred degrees Kelvin (Bullock and Grinspoon 2001). Climate changes of this magnitude could result in surface thermal stresses that may help explain several puzzling geological features seen in Magellan imagery (Solomon et al. 1999).

3.3 The Lower and Middle Atmosphere

By 1971, after the Venera 7 and 8 landings, it was clear that Venus possessed a surface temperature of ≈735 K and a surface pressure of ≈90 bars (Marov et al. 1973). Approximately 10 % of the solar radiation absorbed by Venus diffuses to the surface through the thick clouds and atmosphere, amounting to 17 W/m^2 of surface insolation (Tomasko et al. 1980). Even with this rather low surface insolation, the opacity of the overlying atmosphere is sufficient to create massive greenhouse warming, raising the surface temperature to 735 K.

Table 3.1 summarizes some bulk qualities of the atmosphere of Venus. The lower atmosphere forms a deep, convective troposphere extending from the surface to the cloud base at 45 km. The temperature and pressure values measured by Venera and Pioneer Venus spacecraft, in comparison with adiabatic profiles, allowed estimates of the stability of the atmosphere. Early analyses suggested an essentially stable atmosphere (Avduevsky et al. 1968, 1970) with an overall vertical temperature

Table 3.1 Atmospheric properties of Venus

Surface pressure	92 Bar
Surface density	≈65 kg/m^3
Scale height	15.9 km
Total mass of atmosphere	≈4.8 x 10^{20} kg
Average surface temperature	735 K
Diurnal temperature change	≈0
Wind speeds at surface	0.3–1.0 m/s
Mean molecular weight	43.45 g/mol
Atmospheric composition (near surface, by volume)	
Major gases	CO_2 96.5 %
	N_2 3.5 %
Minor gases (ppm)	SO_2 130
	Ar 70
	H_2O 30
	CO 17
	He 12
	Ne 7

gradient of 7.7 K/km, substantially less than the adiabatic lapse rate of 8.9 K/km (Marov and Grinspoon 1998). Later analyses revealed evidence of zones of instability at altitudes of 20–30 km and 25–33 km (Seiff 1983). These regions of instability are believed to be associated with convective motions and zones of turbulence. A region of minor instability in the near-surface atmosphere below 10 km was inferred by Marov (1978) and Seiff et al. (1985).

The middle atmosphere above the clouds (60–100 km) exhibits even higher stability, with dT/dZ less than 3–4 K/km, suggesting a stratified middle atmosphere close to radiative equilibrium (Seiff 1983). Overall, the lower and middle atmosphere are close to the adiabatic lapse rate, a finding confirmed by the Vega 1–2 balloons in a large area of the middle cloud layer, where minor deviations from adiabatic suggested regions of slight stable stratification (Linkin et al. 1986). Knowledge of the structure and basic properties of the atmosphere up to 100 km, prior to the Venus Express mission, are summarized in the COSPAR reference model VIRA-85 (Seiff et al. 1985).

References

V.S. Avduevsky, N.F. Borodin, A.I. Kuznetsov, A.I. Lifshits, M.Y. Marov, V.V. Mikhnevich, M.K. Rozhdestvenskii, V.A. Sokolov, Temperature pressure and density of atmosphere of Venus from information supplied by Venus-4 Space Probe. Doklady Akademii Nauk SSSR **179**, pp. 310 (1968)

V.S. Avduevsky, M.Y. Marov, A.I. Noykina, V.I. Polezhaev, F.S. Zavelevich, Heat transfer in Venus atmosphere. J. Atmos. Sci. **27**, 569–579 (1970)

A. Basilevsky, G.E. McGill, in *Surface Evoluton of Venus, in Exploring Venus as a Terrestrial Planet*, ed. by L.W. Esposito, E.R. Stofan, T.E. Cravens (American Geophysical Union, Washington, DC, 2007)

M.A. Bullock, D.H. Grinspoon, The recent evolution of climate on Venus. *Icarus* **150**, 19–37 (2001)

T. Donahue, D.H. Grinspoon, R.E. Hartle, R.R. Hodges Jr, in *Ion/neutral Escape of Hydrogen and Deuterium: Evolution of Water* ed. by S.W. Bougher, D.M. Hunten, R.J. Phillips. Venus II Geology, Geophysics, Atmosphere and Solar Wind Environment (University of Arizona Press, Tucson, 1997)

T.M. Donahue, J.H. Hoffman, R.R. Hodges, A.J. Watson, Venus was wet – a measurement of the ratio of deuterium to hydrogen. *Science* **216**, 630–633 (1982)

D.H. Grinspoon, Was Venus wet – deuterium reconsidered. *Science* **238**, 1702–1704 (1987)

D.H. Grinspoon, Implications of the high D/H ratio for the sources of water in Venus atmosphere. Nature **363**, 428–431 (1993)

D.H. Grinspoon, *Venus Revealed: A New Look Below the Clouds of Our Mysterious Twin Planet* (Helix Books, Perseus Piblishing, Cambridge, Massachusetts, 1997)

D.H. Grinspoon, M.A. Bullock, in *Astrobiology and Venus Exploration*, ed. by L.W. Esposito, E.R. Stofan, T.E. Cravens. Exploring Venus as a Terrestrial Planet (American Geophysical Union, Washington DC, 2007)

W.H. Ip, D.J. Williams, R.W. McEntire, B.H. Mauk, Ion sputtering and surface erosion at Europa. Geophys. Res. Lett. **25**, 829–832 (1998)

J.F. Kasting, Runaway and moist greenhouse atmospheres and the evolution of Earth and Venus. *Icarus* **74**, 472–494 (1988)

J.F. Kasting, J.B. Pollack, T.P. Ackerman, Response of Earth's atmosphere to increases in solar flux and implications for loss of water from Venus. *Icarus* **57**, 335–355 (1984)

S. Kumar, D.M. Hunten, J.B. Pollack, Nonthermal escape of hydrogen and deuterium from Venus and implications for loss of water. *Icarus* **55**, 369–389 (1983)

V.M. Linkin, J. Blamont, A.N. Lipatov, A.A. Shurupov, C. Malique, S.P. Ignatova, G.A. Frank, L.I. Hlyustova, A.V. Terterashvili, A. Seiff, V.V. Kerzhanovich, B. Ragent, R. Young, E. Elson, R. Preston, A. Ingersoll, D. Crisp, Thermal structure of the Venus atmosphere in the middle cloud layer. Pis'ma v Astronomicheskie Zhurnal **12**, p. 36–40 (1986)

M.Y. Marov, Results of Venus missions. Ann. Rev. Astron. Astrophys. **16**, 141–169 (1978)

M.Y. Marov, D.H. Grinspoon, *The Planet Venus* (Yale University Press, New Haven, 1998)

M.Y. Marov, V.S. Avduevsk, N.F. Borodin, A.P. Ekonomov, V.V. Kerzhano, V.P. Lysov, B.Y. Moshkin, M.K. Rozhdest, O.L. Raybov, Preliminary results on Venus atmosphere from Venera-8 Descent Module. *Icarus* **20**, 407–421 (1973)

A. Morbidelli, J. Chambers, J.I. Lunine, J.M. Petit, F. Robert, G.B. Valsecchi, K.E. Cyr, Source regions and timescales for the delivery of water to the Earth. Meteorit. Planet. Sci. **35**, 1309–1320 (2000)

G.G. Schaber, R.G. Strom, H.J. Moore, L.A. Soderblom, R.L. Kirk, D.J. Chadwick, D.D., Dawson, L.R. Gaddis, J.M. Boyce, J. Russell, Geology and distribution of impact craters on Venus - what are they telling us. J. Geophys. Res.-Planets **97**, 13,257–13,301 (1992)

A. Seiff, Thermal structure of the atmosphere of Venus, in *Venus*, (A83-37401 17-31), ed. by D.M. Hunten, L. Colin, T.M. Donahue, V.I. Moroz, pp. 215–279 (Tucson, AZ, University of Arizona Press, 1983)

A. Seiff, J.T. Schofield, A.J. Kliore, F.W. Taylor, S.S Limaye, H.E. Revercomb, L.A. Sromovsky, V.V. Kerzahanovich, V.I. Moroz, M.Y. Marov, Models of the structure of the atmosphere of Venus from the surface to 100 kilometers altitude. Adv. Space Res. **5**(11), 3–58 (1985)

S. Smrekar, L. Elkins-Tanton, J. Leitner, A. Lenardic, L. Mackwell, L. Moresi, C. Sotin, E.R. Stofan, in *Tectonic and Thermal Evolution of Venus and the Role of Volatiles: Implications for Understanding the Terrestrial Planets*, ed. by L.W. Esposito, E.R. Stofan, T.E. Cravens. Exploring Venus as a Terrestrial Planet (American Geophysica Union, Washington DC, 2007)

S.E. Smrekar, E.R. Stofan, N. Mueller, A. Treiman, L. Elkins-Tanton, J. Helbert, G. Piccioni, P. Drossart, Recent hotspot volcanism on Venus from VIRTIS emissivity data. Science **328**, 605–608 (2010)

S.C. Solomon, M.A. Bullock, D.H. Grinspoon, Climate change as a regulator of tectonics on Venus. Science **286**, 87–90 (1999)

M.G. Tomasko, P.H. Smith, V.E. Suomi, L.A. Sromovsky, H.E. Revercomb, F.W. Taylor, D.J. Martonchik, A. Seiff, R. Boese, J.B. Pollack, A.P. Ingersoll, G. Schubert, C.C. Covey, The thermal balance of Venus in light of the Pioneer Venus mission. J. Geophys. Res.-Atmos., **85**, 8187–8199, doi:10.1029/JA085iA13p08187 (1980)

Chapter 4
Radiative Energy Balance in the Venus Atmosphere

Dmitrij V. Titov, Giuseppe Piccioni, Pierre Drossart, and Wojciech J. Markiewicz

This chapter reviews the observations of the radiative fluxes inside and outside the Venusian atmosphere, along with the available data about the planetary energy balance and the distribution of sources and sinks of radiative energy. We also briefly address the role of the radiation on the atmospheric temperature structure, global circulation, thermodynamics, climate and evolution of Venus and compare the main features of radiative balance on the terrestrial planets. We describe the physics of the greenhouse effect as it applies to the evolution of the Venusian climate, concluding with a summary of outstanding open issues. The article is to a great extent based on the paper by Titov et al. (2007) expanded by including recent results from the Venus Express observations relevant to the topic.

4.1 Introduction

Absorbed solar and thermal radiation internal to the atmosphere play a dominant role in many chemical and dynamical processes that define the climate of Venus. In some cases the radiative effects are pushed to their extremes in ways that make

D.V. Titov (✉)
ESA/ESTEC, The Netherlands
e-mail: dmitri.titov@esa.int

G. Piccioni
INAF-IASF, Rome, Italy
e-mail: giuseppe.piccioni@iasf-roma.inaf.it

P. Drossart
LESIA, Paris Observatory, Meudon, France
e-mail: pierre.drossart@obspm.fr

W.J. Markiewicz
MPS, Katlenburg-Lindau, Germany
e-mail: markiewicz@mps.mpg.de

L. Bengtsson et al. (eds.), *Towards Understanding the Climate of Venus*, ISSI Scientific Report Series 11, DOI 10.1007/978-1-4614-5064-1_4,

Venus unique among the terrestrial planets in the Solar System. The thick cloud layer that completely covers Venus and is one of the main climate forcing factors is a product of a photochemical "factory" that forms sulfuric acid aerosols from sulfur dioxide and water vapor in the middle atmosphere. The strongly scattering clouds reflect more than 75 % of incoming solar flux back to space, so that Venus absorbs less solar energy than the Earth does, even though it is 30 % closer to the Sun. Meanwhile, the cloud layer and atmospheric gases produce a powerful greenhouse effect that is responsible for maintaining globally-averaged surface temperature as high as 735 K, the highest among solar system planets. Venus is also remarkably different from the other terrestrial planets in terms of the distribution of energy sources and sinks in the atmosphere. Half of the solar flux received by the planet is absorbed at the cloud tops (≈65 km) by CO_2 and by the unknown UV absorber (Markiewicz et al. 2007; Titov et al. 2011). Only 2.6 % of the solar flux incident at the top of the atmosphere reaches the surface in the global average. This solar energy deposition pattern drives an unusual global circulation in the form of retrograde zonal super-rotation. This chapter reviews the current knowledge on radiative processes in the Venus atmosphere, including their interaction with the atmospheric dynamics, greenhouse effect, as well as their influence on climate stability and evolution. It is based on the earlier paper by Titov et al. (2007) updated with recent results from the Venus Express mission. Section 4.2 gives a synthesis of observations of the radiative fluxes inside and outside the atmosphere. Section 4.3 summarizes the available data about the planetary energy balance and distribution of sources and sinks of radiative energy. Implications of the radiative heat exchange to the forcing of the global circulation, greenhouse effect, current climate and its evolution are discussed in Sect. 4.4. The chapter concludes with a summary of outstanding open issues and future work.

4.2 Radiation Field: A Synthesis of Observations

Measurements of the radiation field within and outside of the Venus atmosphere during the past several decades have produced great progress in our understanding of conditions on Venus and of atmospheric processes on the planet. Remote sensing observations from Earth-based telescopes and orbiter instruments described the spectral dependence of the solar radiation reflected from the planet as well as the thermal radiation emitted to space. In situ measurements of scattered solar and thermal radiation from Venera and Pioneer-Venus descent probes provided constraints on the vertical distribution of radiation within the atmosphere. Recent multi-wavelength observations by Venus Express provided important new clues on variations of the radiative energy balance. This section gives a synthesis of the available observations.

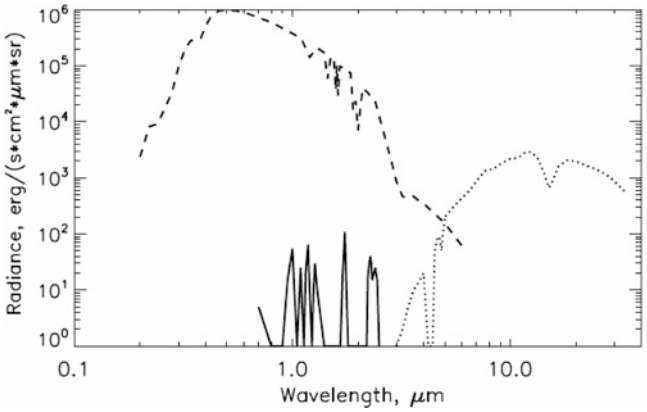

Fig. 4.1 General view of the Venus spectrum at a resolving power, $\lambda/\Delta\lambda$, of 200 as seen from space: the reflected solar light (*dashed line*), the thermal emission from the cloud tops and mesosphere (*dotted line*), and the night side emission escaping from the lower atmosphere (*solid line*). (From Titov et al. 2007)

4.2.1 A View From Space

The spectrum of Venus when observed from space can be roughly split in three components: reflected solar radiation, infrared thermal emission from the cloud tops, and emission from the hot deep atmosphere and the surface leaking to space through the narrow spectral transparency "windows". The first component dominates in the UV through the near-infrared range (0.2–4. μm) over the sunlit hemisphere, while the second one prevails at longer infrared wavelengths (4–50 μm). The third component is located in the spectral range 0.9–2.5 μm and is by several orders of magnitude weaker than the solar reflected light. Figure 4.1 shows typical spectra of all three components.

4.2.1.1 Reflected Solar Radiation and Albedo

Observations of the reflected solar spectrum of Venus are summarized in Moroz et al. (1983, 1985); Crisp and Titov (1997). A major fraction of the incoming solar flux is scattered back to space by thick clouds that are mainly composed of sulfuric acid and completely cover the planet. Estimates of the Bond albedo vary from 0.80±0.02 (Tomasko et al. 1980) to 0.76 ± 0.01 (Moroz et al. 1985). The clouds make Venus the most reflective planet in the Solar System. The spectral dependence of the Venus spherical albedo is presented in Fig. 4.2. The albedo curve shows a broad depression in the UV-blue range. At wavelengths below 0.32 μm this absorption is explained by the presence of SO_2 gas within and above the cloud tops. The absorption at longer wavelengths (0.32 μm-0.5 μm) is attributed to the

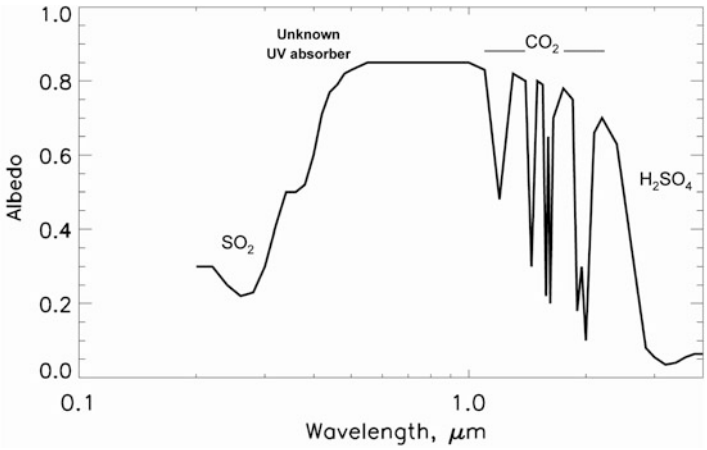

Fig. 4.2 Spectral dependence of the Venus spherical albedo. (From Titov et al. 2007)

presence of an unknown absorber in the upper cloud (58–65 km). Variability of the upper cloud structure and abundance of the absorbing species produces the well-known UV markings on the Venus disc with albedo variations of up to 30 % (Rossow et al. 1980; Markiewicz et al. 2007; Titov et al. 2011). In the near infrared (1–2 μm) sharp spectral features associated with absorption by CO_2 and H_2O within and above the cloud tops are clearly seen in the Venus spectrum. At wavelengths longer than 2.5 μm, the Venus albedo quickly drops to a few percent due to strong absorption by sulfuric acid aerosols (Fig. 4.2). Above 4 μm thermal radiation emitted by the cloud tops becomes comparable to the reflected solar light and its intensity rapidly increases with wavelength (Fig. 4.1).

4.2.1.2 Thermal Emission from the Cloud Tops

Even though Venus has a very high surface temperature, from space it appears as a rather cold object because the sulfuric acid clouds are opaque at $\lambda > 2.5\mu$m and the temperature of the cloud tops varies between 220 K and 260 K. Venus thermal radiation has been measured both from the ground and from space. The most comprehensive data sets were delivered by the Pioneer Venus Orbiter Infrared Radiometer (Taylor et al. 1980), the Venera 15 Fourier spectrometer (Oertel et al. 1985), the NIMS/Galileo infrared spectro-imager (Carlson et al. 1993), and the VIRTIS/Venus Express visible and infrared mapping spectrometer (Drossart et al. 2007; Piccioni et al. 2007). Figure 4.3 shows examples of the thermal infrared spectra of Venus. The spectrum of the planet at thermal wavelengths (5–50 μm) is close to that of a blackbody at the cloud top temperatures with spectral features mainly belonging to mesospheric CO_2, H_2O, SO_2, and other gases that absorb at levels within and above the clouds as well as broad signatures of sulfuric

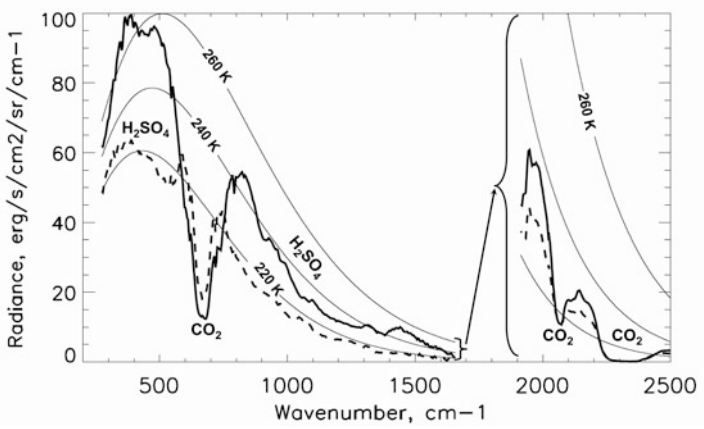

Fig. 4.3 Examples of the Venus thermal infrared spectra measured by the FTS/Venera 15 and NIMS/Galileo experiments in the equatorial (*solid*) and *middle (dashes)* latitudes. The NIMS spectra (1900–2500 cm^{-1}) are multiplied by a factor of 100. *Thin solid lines* show the blackbody spectra for the temperatures of 260 K, 240 K, and 220 K. (From Titov et al. 2007)

acid aerosols. The fundamental absorption bands of CO_2 at 4.3 μm, 4.8 μm, and 15 μm produce the strongest spectral features. These bands have been used to retrieve the temperature and aerosol altitude profiles in the mesosphere (Roos-Serote et al. 1995; Zasova et al. 2007; Grassi et al. 2010). The thermal structure of the Venus mesosphere varies strongly with latitude, with polar regions surprisingly being up to 20 K warmer than equatorial latitudes at most pressure levels between the cloud tops and 100 km. The thermal structure varies to a lesser extent with local time. Thermal infrared spectra also show a wealth of weaker absorption features belonging to hot and isotopic bands of CO_2 as well as SO_2, H_2O, and CO above the clouds and within the upper cloud.

The thermal emission spectra in Fig. 4.3 clearly show the atmospheric parameters and constituents that play the major role in radiative energy exchange with space. Thermal radiation leaves the planet mainly in the spectral range from 200 cm^{-1} to 1,000 cm^{-1} (50–10 μm). Strong infrared bands of CO_2 clearly seen in the thermal emission spectra in Fig. 4.3 are formed in the colder mesosphere and are responsible for cooling of the atmosphere above the clouds (up to $\approx$120 km).

4.2.1.3 Thermal Emission from the Lower Atmosphere

An efficient atmospheric greenhouse mechanism maintains Venus surface temperatures as high as 735 K. At this temperature, the surface emits substantial amounts of energy even in the near infrared range (1–5 μm). This emission was detected for the first time by the spectrophotometers onboard the Venera landers as an increase in the measured spectra at wavelengths above 0.8 μm. However, its importance

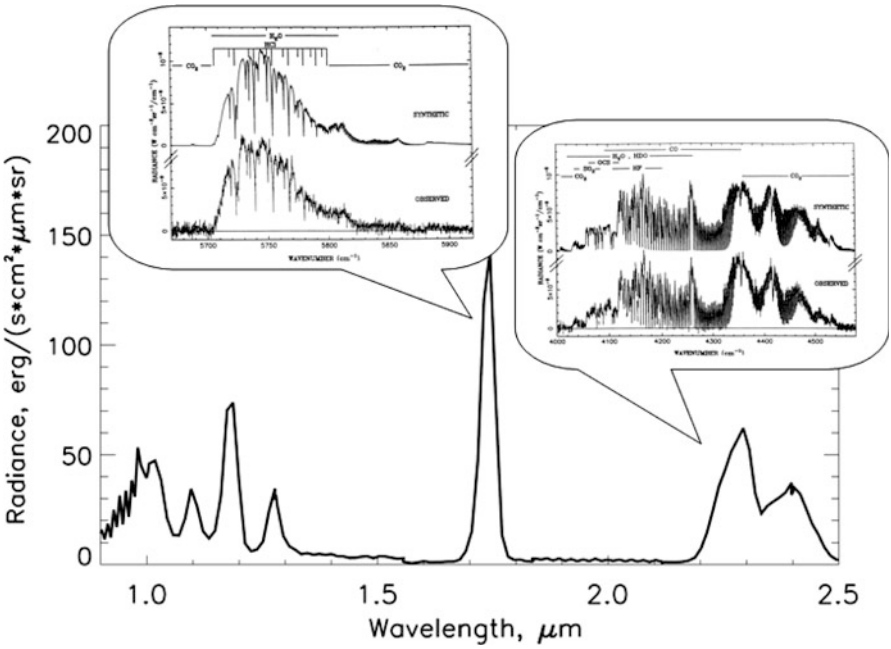

Fig. 4.4 NIMS/Galileo near infrared spectrum of the Venus night side. Ground based high resolution spectra of the emission at 1.7 μm and 2.3 μm (from Bezard et al. 1990 are shown in the inserts)

was fully recognized only after Allen and Crawford (1984) discovered that thermal radiation from the lower atmosphere leaks to space through partially transparent atmospheric "windows"—spectral gaps between strong CO_2 and H_2O absorption bands in the near infrared range. The discovery of the emissions on the Venus night side provided a powerful remote sensing tool to study composition of the lower atmosphere, to map the surface, and to monitor the cloud opacity and atmospheric dynamics in the cloud depth. This method is being successfully used by Venus Express (Titov et al. 2009). At wavelengths 0.8–2.4 μm the H_2SO_4 clouds are translucent. Aerosols are almost non-absorbing and their scattering properties have little variability with wavelength. The altitude of the origin of the night side emission is wavelength dependent and varies from the very surface at 1 μm to $\approx$35 km at 2.3 μm. These emissions are about 4 orders of magnitude weaker than the reflected solar component (Fig. 4.1) so they can be observed only on the night side.

Figure 4.4 shows examples of the Venus night side spectra measured by NIMS/Galileo and high resolution spectra of the same spectral "windows" from the Earth-based observations (Carlson and Taylor 1993; Crisp 1989; Crisp et al. 1991; Crisp et al. 1991; Bezard et al. 1990; Meadows and Crisp 1996; Taylor et al. 1997).

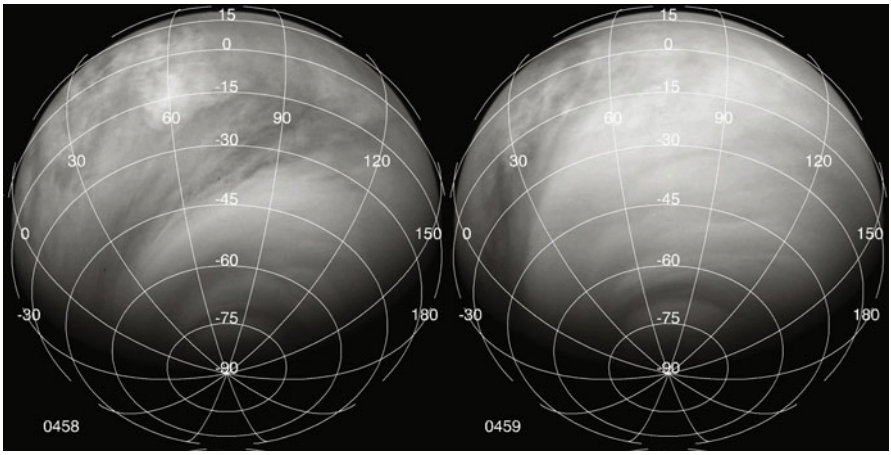

Fig. 4.5 UV images of Venus taken by VMC in orbits #458 and #459. Titov et al. (2011)

4.2.1.4 Variability of the Outgoing Radiation

Five years of continuous monitoring of the outgoing radiation field by Venus Express revealed strong changes of the atmospheric parameters (albedo, temperature, cloud top structure) that results in significant variations of the global radiative energy budget of the planet. Venus Monitoring Camera (VMC) images the planet in the narrow band filter centered at the characteristic band of the unknown UV absorber (365 nm) (Markiewicz et al. 2007; Titov et al. 2011) which is responsible for deposition of about half of solar energy that Venus receives from the Sun. Inhomogeneous distribution of the absorber at the cloud tops produces characteristic UV markings (Fig. 4.5) and strongly affects radiative energy deposition pattern. Figure 4.5 shows UV images captured by VMC in two successive orbits. The left one shows strong brightness contrast between dark low and bright high latitudes. The observed latitudinal variations of the UV albedo imply abrupt decrease in deposited solar energy by a factor of 3–4 from dark tropics to bright high latitudes on top of gradual decrease due to solar incidence angle. The energy is deposited at the cloud tops and is not buffered by the bulk of the atmosphere. This can trigger local dynamical response causing wind across the sharp albedo boundary—a mechanism similar to the mesoscale winds at the sea coasts on Earth or at the edge of the Martian polar cap. The right image in Fig. 4.5 shows rare global brightening event, when bright haze almost completely covered Venus in about a day (Markiewicz et al. 2007). Global changes of the planetary albedo during such events is likely to affect the radiative energy deposition pattern and thus will have an impact on the atmospheric dynamics.

Venus emits energy to space mainly due to thermal emission in the range 10–50 μm from the cloud tops (Fig. 4.1). The outgoing thermal flux depends on the temperature and aerosol distribution at the cloud top level. Venus Express observations revealed that both parameters change significantly with latitude resulting

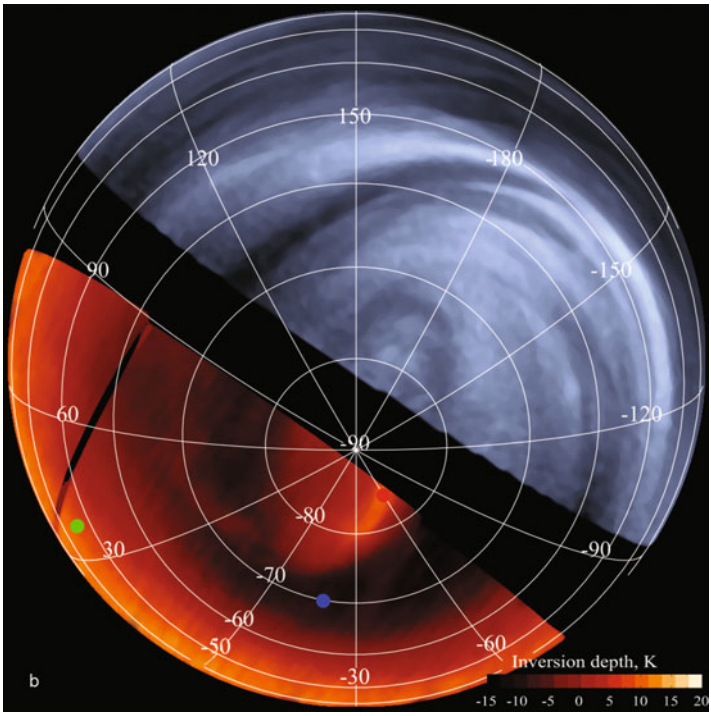

Fig. 4.6 Composite false color views of the Southern hemisphere: VIRTIS thermal-IR (5 μm) mosaic (*red*) and simultaneously captured VMC UV (0.365 μm) image (*grey*). Reprinted by permission from Macmillan Publishers Ltd: (from Titov et al. 2008). Brightness in the thermal IR images tracks the cloud top temperature. The bright oval feature close to the pole is the eye of the hemispheric vortex—a dynamical structure ≈3,000 km in size which is about 30 K warmer than its surroundings

in strong modulation of the thermal emission. Radio-occultation measurements showed that the temperature structure changes from monotonic profile in low latitudes to one with strong temperature inversions (Tellmann et al. 2009) that creates an annulus of cold air at 60–70 degrees latitude ("cold collar"). The cloud top structure changes in a correlated way with the temperature field. In low latitudes the cloud top is located at ≈72 km and the aerosol vertical scale height is of about 4 km. In the "cold collar" the cloud top descends to ≈64 km and has very sharp boundary coinciding with the altitude of temperature minimum (Ignatiev et al. 2009; Lee 2011). This combination of changes in the temperature and cloud structures results in the modulation of thermal flux observed from orbit. Figure 4.6 shows the VIRTIS thermal infrared (5 μm) mosaic captured by VIRTIS/Venus Express (Piccioni et al. 2007). The brightness temperature in low latitudes is few tens of degrees higher than the cold collar region at 60–70 °S. The polar eye of the planetary vortex is the brightest at thermal IR wavelengths. Comparison to the earlier observations indicate that this distribution of thermal flux is roughly similar to that in the Northern hemisphere (Taylor et al. 1980).

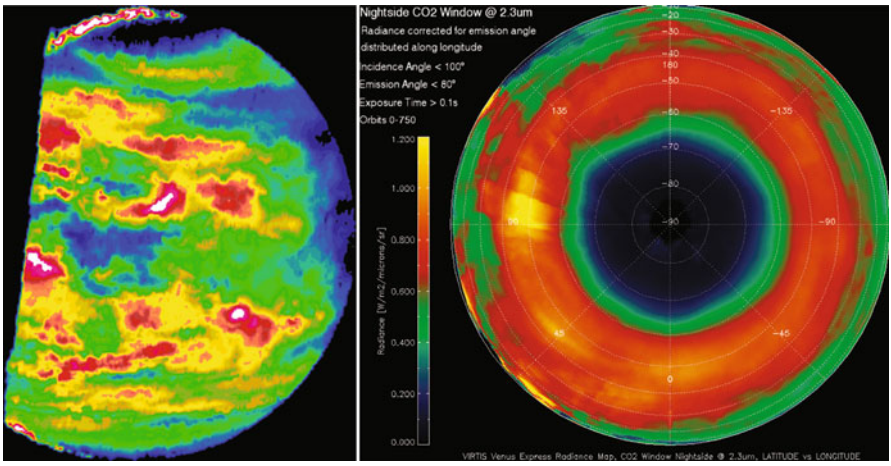

Fig. 4.7 Maps of the thermal emission escaping to space in the 2.3 μm "window" captured by VIRTIS/Venus Express (*left*) and NIMS/ Galileo (*right*) Carlson et al. (1993). *False colors* mark variations of brightness produced by spatial inhomogeneity of the total cloud opacity. *Red*—high flux and low cloud opacity, *blue*—low flux and high cloud opacity

The thermal radiation leaking to space from the hot lower atmosphere and the surface gives minor contribution to the global radiative energy balance due to weakness of the emission escaping through the thick cloud layer (Fig. 4.1). However the radiative effect of the lower atmosphere thermal emission on the lower cloud could be much stronger. Measurements of the flux in the near-IR transparency "windows" from orbit give an important clue on distribution of opacity over the globe. Figure 4.7 shows the maps of the emissions in the 2.3 μm "window". The VIRTIS/ Venus Express mean maps mosaics based on the southern hemisphere (left) indicates a factor of 5–7 decrease of the flux from low and middle latitudes to the polar regions that corresponds to about a factor of 2 increase in the cloud opacity. The NIMS/Galileo image (right) shows the view of Venus from equator indicating patchy morphology of the deep cloud.

4.2.2 Radiation Field Inside the Atmosphere

4.2.2.1 Scattered Solar Radiation

The solar radiation field inside the atmosphere was measured by spectrophotometers on several Venera descent probes (Ekonomov et al. 1983; Moroz et al. 1983). These observations provided a unique data set for characterizing the angular and spectral distribution of solar scattered light between 0.4 and 1.2 μm from $\approx$65 km down to

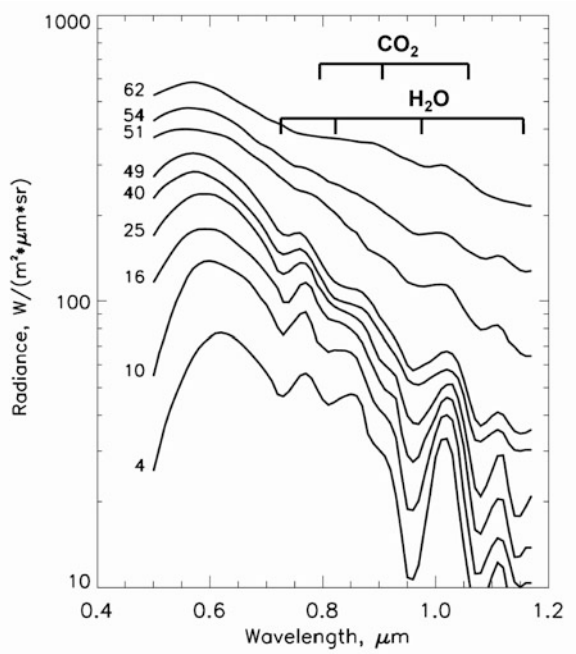

Fig. 4.8 Spectra of the downward scattered solar radiation measured by the Venera 13 descent probe. Lines are labelled with probed altitudes, in km. (From Ekonomov et al. 1983)

the surface. Figure 4.8 shows examples of the Venera-13 spectra. The intensity of solar radiation propagating downwards gradually decreases with altitude. Less than 10 % of the radiation that hits the top of the atmosphere reaches the surface and only about 2.5 % ($\approx$17 W/m^2) is absorbed at the ground (Crisp and Titov 1997). Increasing absorption in near-infrared by CO_2 and H_2O as well as absorption at the blue end of the spectrum is also evident as the probe descends. Analysis of these data supported the conclusion from ground-based near-infrared observations de Bergh et al. (1995) that the H_2O mixing ratio is nearly constant (30 $\pm$ 10 ppm) at altitudes between the cloud base and $\approx$16 km but shows a probable increase up to 50–70 ppm in the lower scale height (Ignatiev et al. 1997). Vertical profiles of the solar downward and upward fluxes and their divergence provide valuable information about the structure of the atmosphere and solar heating rates. The solar flux radiometer (LSFR) aboard the Pioneer Venus Large Probe measured solar fluxes during descent in a series of channels covering a broad range from 0.4 through 1.8 μm (Tomasko et al. 1980a). The Venera-13 and 14 descent probes also carried a photometric experiment to measure the distribution of UV radiation (Ekonomov et al. 1984). Figure 4.9 shows the vertical profiles of downward solar fluxes measured by the Venera and Pioneer-Venus descent probes. Their altitude derivative is proportional to the extinction coefficient of the scattering medium. These measurements show that UV and blue radiation are strongly absorbed in the upper cloud layer above 57 km. The abrupt change in the broadband radiance at $\approx$48 km clearly marks the location of the lower boundary of the cloud.

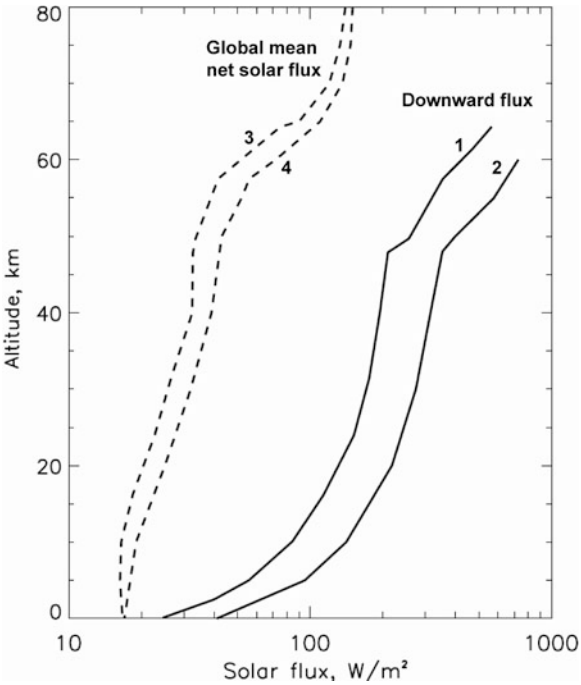

Fig. 4.9 Vertical profiles of the downward solar flux (*solid lines*) and global mean net solar flux (*dashed lines*) in the Venus atmosphere. The downward fluxes were measured by the Pioneer-Venus LSFR experiment (curve 1) Tomasko et al. (1980a)[Table 8] and spectrophotometers onboard the Venera 11, 13, 14 landers (curve 2) Moroz et al. (1985) [Tables 6 & 7]. The calculated global mean net solar fluxes are from Pioneer Venus (curve 3) and the Venus International Reference Atmosphere Moroz et al. (1985) (curve 4)

To find the global mean net solar flux, numerical models must be used to extend the spectral and spatial coverage provide by the experimental results. Figure 4.9 shows the results of two models (Tomasko et al. 1980a; Moroz et al. 1985). The deposition of solar energy occurs at altitudes of positive net flux divergence. The measurements and subsequent radiative transfer modeling reveal two regions where deposition of the solar energy is significant. The first one is located in the upper cloud layer above ≈57 km and is possibly caused by the unknown UV absorber and by absorption beyond 3 μm by the H_2SO_4 cloud particles. The second region is located in the lower atmosphere (40–20 km) where solar energy is absorbed by CO_2 and H_2O in the near-infrared and possibly elemental sulfur in the UV-blue range. Surprisingly, almost no absorption of sunlight occurs between 57 and 48 km where the bulk of the cloud layer is located.

4.2.2.2 Thermal Fluxes in the Atmosphere

The vertical distribution of thermal fluxes depends on the profiles of temperature and opacity sources in the atmosphere. The vertical net thermal flux divergence defines the thermal cooling rate which, in combination with net solar heating, determines the radiative energy balance in the atmosphere. Experimental characterization of the thermal fluxes was the goal of three net flux radiometers (SNFR) on the Pioneer

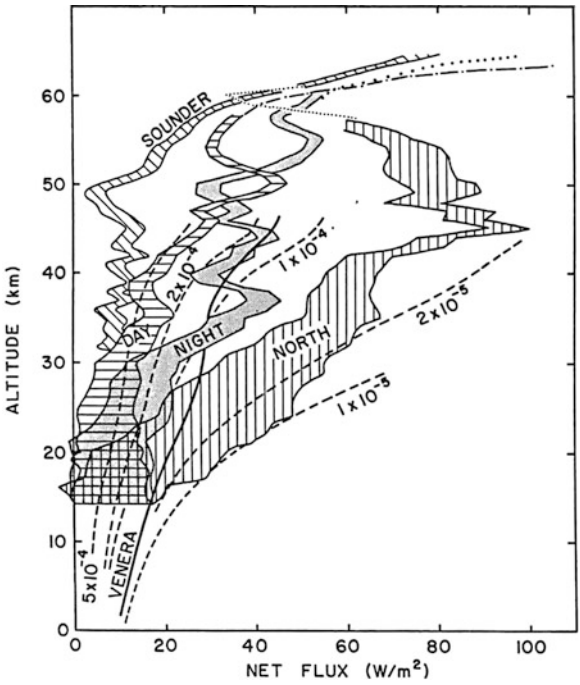

Fig. 4.10 Net thermal fluxes in the Venus atmosphere derived from the SNFR and LIR measurements on the Pioneer Venus descent probes (from Revercomb et al. 1985). *Dashed lines* show the modeled profiles of the net thermal fluxes for different water vapor mixing ratio (numbers at the curves)

Venus Small Probes (Suomi et al. 1980) and an infrared radiometer (LIR) on the PV Large Probe (Boese et al. 1979). The original data were affected by a significant error whose source was discovered in laboratory testing after the mission was completed. Revercomb et al. (1985) corrected the measurements and analyzed their implications for the cloud structure, water vapor distribution in the lower atmosphere, and radiative cooling. Figure 4.10 shows the corrected net fluxes at four descent sites and compares them to model calculations for different water abundances below the clouds.

The measured thermal fluxes indicate the presence of an additional either gaseous or particulate source of opacity above 60 km. Below the clouds, the measurements suggest a strong increase of the net flux and its divergence from equator to pole. Because the temperature structure below the clouds varies little with latitude, this trend implies a strong latitude variability of infrared opacity sources. Since sulfur dioxide has fairly low absorption, Revercomb et al. (1985) concluded that the net flux measurements imply a significant latitude trend in the water mixing ratio below the clouds. This conclusion, however, contradicts the results of a recent re-analysis of spectrophotometry on the Venera descent probes (Ignatiev et al. 1997) and observations in the near IR windows (Crisp et al. 1991; Drossart et al. 1993; de Bergh et al. 2006; Bezard et al. 2009) which imply an H_2O mixing ratio of $\approx$30 ppm without significant latitude variability below the clouds. However, the near IR observations show that there is significant spatial variability of the cloud

opacity, with persistently low optical depths at latitudes between 40 and 60 degrees (Crisp et al. 1991). The low cloud optical depths at latitudes where the Pioneer Venus North Probe entered the atmosphere may explain the large thermal net flux divergences near the cloud base inferred from the net flux radiometer results (Crisp and Titov 1997). The vertical divergence of the measured net thermal fluxes that defines the cooling rate also shows a significant latitude gradient. Comparisons of the thermal flux divergence in Fig. 4.10 with the divergence of solar flux (heating rate) in Fig. 4.9 suggest strong net radiative cooling of the lower atmosphere at high latitudes. To maintain the observed thermal structure in the presence of this high latitude cooling, the net atmospheric transport must be descending there.

4.3 Radiative Energy Balance

The measurements described in Sect. 4.2 were used to develop models of the distribution of opacity sources and temperatures in the atmosphere. These models were then used to calculate broadband radiative fluxes in and outside the atmosphere, and to assess the distribution of radiative energy sources and sinks. This section summarizes the results of this radiative balance modeling.

4.3.1 Global Budget

Observations by the Pioneer Venus and Venera orbiters and descent probes provided a substantial amount of information about scattering and absorbing properties of the Venus atmosphere. Several comprehensive radiative transfer models consistent with the data were developed at that time (Tomasko et al. 1980a, 1985). The authors calculated the global balance of radiative energy and solar heating rates in the atmosphere. The total solar flux at the Venus orbit is $2622 \pm 6\,\mathrm{W/m^2}$ (Moroz et al. 1985). Due to its high albedo the planet absorbs only $157 \pm 6\,\mathrm{W/m^2}$ on average, less than that deposited on Earth ($\approx 240\,\mathrm{W/m^2}$), despite the fact that Venus is 30 % closer to the Sun. Both models and observations show that less than 10 % of the total solar energy incident on Venus reaches the surface, and only 2.5 % is absorbed there. The largest portion of solar energy is absorbed above 57 km by the unknown UV absorber at the cloud tops. This is in contrast with the Earth, where 74 % of the non-reflected solar energy is absorbed directly at the ground (Arking 1996).

The outgoing thermal radiation has been characterized by the Pioneer Venus Orbiter Infrared Radiometer (Taylor et al. 1980), the Venera 15 Fourier transform spectrometer (Oertel et al. 1985), and VIRTIS/ Venus Express (Drossart et al. 2007). These observations were analyzed to retrieve the temperature and aerosol structure of the Venus mesosphere and to calculate the outgoing thermal flux (Schofield and Taylor 1982; Zasova et al. 2007; Grassi et al. 2010; Tellmann et al. 2009).

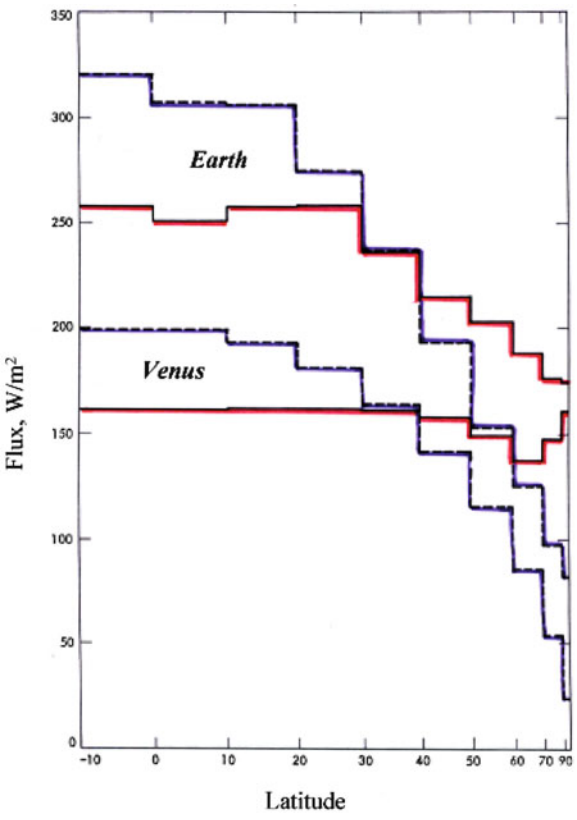

Fig. 4.11 Latitude dependence of the zonally averaged net incident solar (*blue*) and outgoing thermal (*red*) fluxes (from Schofield and Taylor 1982). Similar curves for the Earth are also shown for comparison

The globally averaged effective temperature as measured by Pioneer Venus is $\approx$230 K which corresponds to an outgoing thermal flux of $\approx$160 W/m^2. This value is slightly different from the mean solar flux deposited on the planet but given the uncertainties in both values this discrepancy cannot be interpreted as an indication of global energy imbalance. Venus Express delivered significant amount of data on the outgoing thermal emission especially in the Southern polar regions that showed highly variable structure of the polar eye of the global vortex (Fig. 4.6) (Piccioni et al. 2007). Available observations and models quantify the planetary radiation budget (Tomasko et al. 1980; Schofield and Taylor 1982). Figure 4.11 compares the mean latitude distributions of solar radiation received by the planet and thermal radiation emitted to space for Venus and Earth. Both planets receive solar energy mainly at low latitudes with the incident flux strongly decreasing toward the poles. Earth has similar trend in latitude distribution of the outgoing thermal radiation. On Venus, however, the outgoing thermal flux is almost constant with latitude indicating that atmospheric dynamics are more efficient in transporting energy from equator to pole.

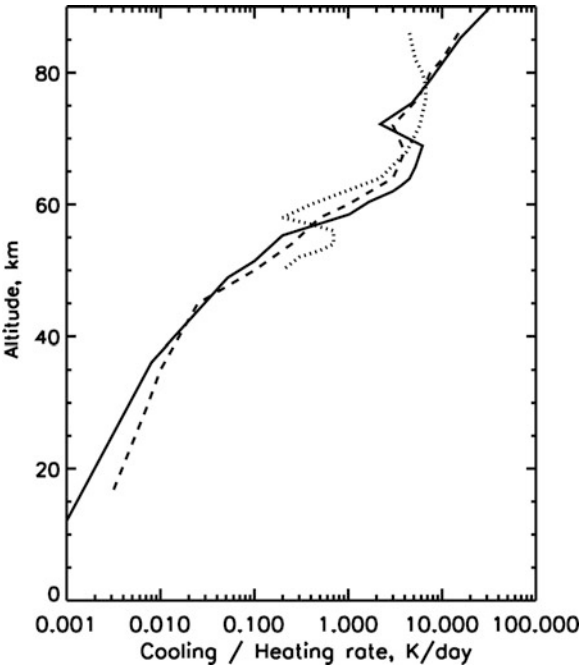

Fig. 4.12 Vertical profiles of globally averaged solar heating (*solid line*—Tomasko et al. (1985); *dashed line*—Crisp and Titov (1997) and thermal cooling rates (*dotted line*—Crisp and Titov (1997)

4.3.2 Distribution of Sources and Sinks

The vertical divergence of the net solar and thermal fluxes gives the radiative heating and cooling rates in the atmosphere. These sources and sinks of radiative energy force the atmospheric dynamics. Radiative transfer models of the Venus atmosphere have progressed together with the accumulation of observational data (Pollack et al. 1980; Tomasko 1983). Tomasko et al. (1985) used an atmospheric radiative transfer model derived from the Pioneer-Venus and Venera measurements to calculate solar fluxes and heating rates (Fig. 4.12).

Observations by the Pioneer Venus, Venera 15 and Venus Express orbiters significantly improved our knowledge of the temperature and aerosol structure of the mesosphere (Schofield and Taylor 1982; Zasova et al. 2007; Grassi et al. 2010; Ignatiev et al. 2009; Lee et al. 2011; Tellmann et al. 2009). This inspired extensive numerical modeling of the radiative balance in the Venus mesosphere (Crisp 1986, 1989; Haus and Goering 1990; Titov 1995; Crisp and Titov 1997; Lee 2011). These studies confirmed that the radiative forcing is very sensitive to atmospheric parameters such as temperature structure, aerosol composition and distribution, and abundance of trace gases. Figure 4.12 shows the vertical profiles of globally averaged cooling and heating rates in the Venus atmosphere. Above the clouds the radiative energy exchange occurs mainly in the CO_2 bands. Both cooling and heating rates gradually decrease from $\approx$50 K/day near the top of the mesosphere

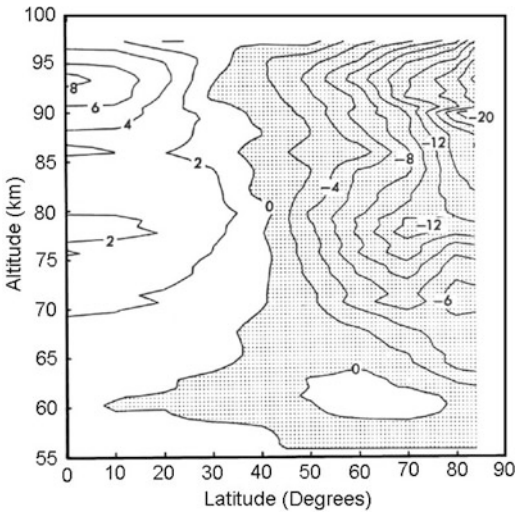

Fig. 4.13 The altitude-latitude field of the net radiative heating (K/day) in the Venus mesosphere calculated for the Pioneer Venus OIR thermal structure. (From Crisp 1989)

(90 km) to few K/day at the cloud tops (70 km). Absorption by the unknown UV absorber and the H_2SO_4 cloud particles above 57 km in the upper cloud creates a heating rate peak of up to 8K/day in the global average. About 10 % of the solar energy incident on the top of the atmosphere or half of the solar energy absorbed by the planet is deposited in this altitude range. Radiative cooling cannot compensate for this heating at low latitudes, creating a region of net heating in the upper cloud. Below the clouds (<48 km), both cooling and heating rates gradually decrease from 0.1–1 K/day at the cloud base to ≈0.001 K/day at the surface. Figure 4.13 shows the altitude-latitude field of net radiative heating calculated for the mesospheric temperature structure retrieved from the Pioneer Venus OIR remote sensing data (Crisp 1989).

The observed thermal structure can be maintained in the presence of the net solar heating at low latitudes and net thermal cooling near the poles if the mesospheric circulation is characterized by rising motion at low latitudes, poleward flow near the mesopause (≈100 km) and subsidence over at high latitudes (Crisp 1986). Measurements of scattered solar radiation below the clouds (Moroz et al. 1983; Ekonomov et al. 1984) indicate that the atmosphere at these levels is only slightly heated by absorption of sunlight in weak near-IR CO_2 and H_2O bands and by additional UV absorption. Thermal infrared fluxes and cooling rates in the lower atmosphere are very poorly constrained by the observations and the models. Although Revercomb et al. (1985) managed to correct the Pioneer Venus thermal flux measurements, the error bars are still quite large such that these results should still be used with caution in thermal balance studies. Spatial variability of the cloud opacity, which can be as large as a factor of 2 (20–40) (Fig. 4.7), can also cause significant variations of thermal radiative forcing at levels within and below the clouds affecting the local temperatures and heat fluxes (Crisp and Titov 1997).

For example, the temperatures measured by the Vega-1 balloon were systematically 6.5 K higher than those observed by Vega-2 at similar levels within the middle cloud region at equatorial latitudes (Linkin et al. 1986; Crisp et al. 1990). The amplitude of this zonal temperature contrast was surprising because it is almost as large as the pole to equator gradient at these levels. This phenomenon can be explained if Vega-1 balloon flew in a denser cloud that was heated more strongly as it absorbed upwelling thermal flux from the deep atmosphere (Crisp and Titov 1997).

4.4 Role of Radiation on The Climate and Evolution of Venus

Radiation plays an important role on the physical and chemical processes on Venus due to the high density of its atmosphere, great amount of radiatively active species, and peculiarities of the energy deposition pattern. This section summarizes the role of radiation on the Venus climate and compares it to the other terrestrial planets.

4.4.1 Radiative Forcing of the Atmospheric Circulation

Remote sensing by the Pioneer Venus, Venera-15, and Venus Express spacecraft revealed significant latitudinal variations in the mesospheric temperature and cloud structure (Taylor et al. 1980; Lellouch et al. 1997; Zasova et al. 2007; Grassi et al. 2010; Tellmann et al. 2009). In particular, both the cloud top altitude and aerosol scale height at the cloud tops decreased from equator to the pole (Ignatiev et al. 2009; Lee et al. 2011), with simultaneous development of a strong temperature inversion in the "cold collar" at 60–70 degrees in both hemispheres (Fig. 4.14). Early estimates of the net radiative forcing have been combined with measurements of the anomalous thermal structure to infer several interesting features of the mesospheric dynamics (Crisp 1986, 1989; Haus and Goering 1990; Titov 1995; Crisp and Titov 1997). First, radiative transfer models confirmed that the mesospheric temperature contrasts between equator and pole indicate that these regions are in strong radiative disequilibrium. Radiative energy transport would have quickly destroyed this feature (Fig. 4.14). Its persistence therefore implies significant meridional heat transport by the global circulation. The meridional circulation could produce adiabatic cooling in its rising branch at low latitudes and compression heating in the descending polar branch. Crisp (1989) found that mean subsidence velocities of $\approx$1cm/s were enough to produce adiabatic heating compensating for radiative cooling.

Measurements of the mesospheric temperature structure have been used to infer the zonal circulation at theses levels (Lellouch et al. 1997; Zasova et al. 2007; Piccialli et al. 2008, 2012) and to correlate it with the net radiative heating pattern. If the zonal winds in the mesosphere remain in cyclostrophic balance (e.g. the latitudinal pressure gradient is balanced by centrifugal force in the zonal

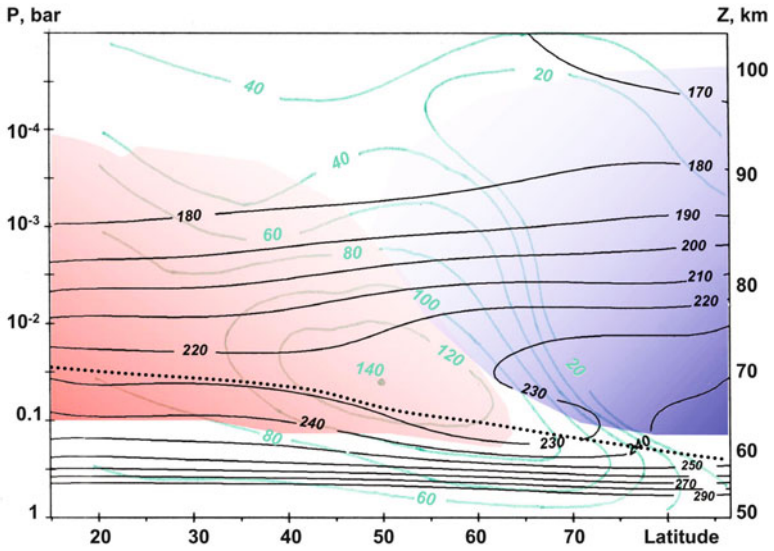

Fig. 4.14 Latitude-altitude fields of physical parameters in the mesosphere of Venus. Black and green curves, respectively, are the isolines of atmospheric temperature (in K) and thermal wind field (in m/s) derived from the Venera-15 remote sounding experiment (Lellouch et al. 1997). Dotted line shows the cloud top altitude (Zasova et al. 2007). Pink and blue areas mark the regions with net radiative heating and cooling whose maximum/minimum values reach ±10 K/day (Titov et al. 2007)

circulation), the observed temperature structure indicates that the super-rotating cloud top winds should decay with altitude. It also suggests the presence of a strong jet stream with wind velocities of 120–140 m/s near the cloud tops at mid-latitudes (50–60 degrees) (Fig. 4.15).

Pioneer Venus OIR and Venera-15 observations indicated the existence of a solar-locked component in the mesospheric temperature field, the diurnal and semi-diurnal thermal tides (Taylor et al. 1983; Zasova et al. 2007). The peak velocity of the mid-latitude, cloud-top thermal wind jet was found to vary by 10–20 % in correlation with local solar time thus indicating the importance of radiative forcing. Theoretical and numerical studies showed that thermal tides play an important role in the maintenance of strong zonal winds in the mesosphere (Forbes 2004). The third peculiarity of the Venus radiative balance that has implications for atmospheric dynamics is the vertical distribution of radiative heating. As noted above, on Venus, most of the solar energy is deposited in the upper cloud (>57 km) rather than at the surface. This makes Venus a special case among terrestrial planets because its atmosphere is heated from the top while the atmospheres of Mars and Earth receive most of their solar energy at the surface. This peculiarity should have consequences for the global dynamics, but details of these circulations still remain to be studied.

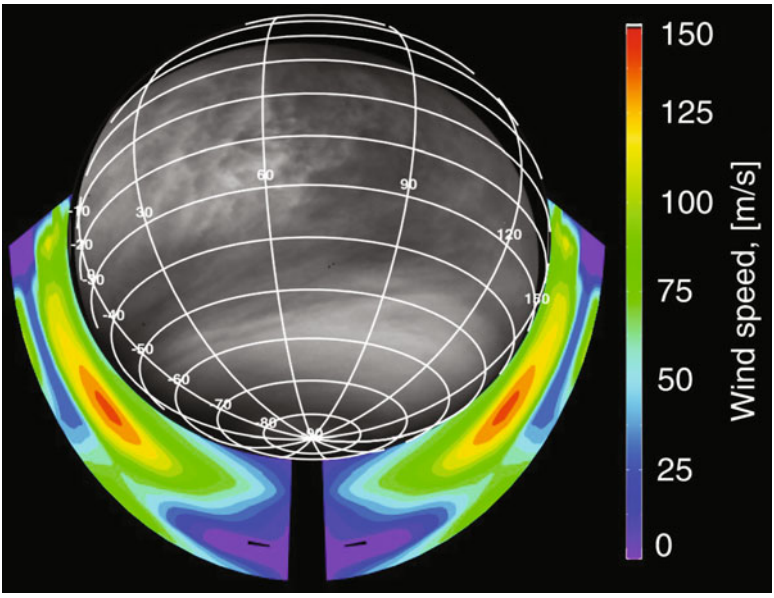

Fig. 4.15 Sketch of the zonal cyclostrophic wind derived from VeRa temperature soundings (color latitude-altitude cross section) plotted together with a VMC image. Reprinted from Icarus, 217, (from Piccialli et al. 2012 with permission from Elsevier)

4.4.2 Global Balance of Radiative Entropy

Radiation carries not only energy but also entropy. Its flux is proportional to that of the radiative flux divided by the temperature at which energy is deposited or emitted. Since heating by solar radiation and cooling by thermal emission occur at different altitudes and temperatures, planets have non-zero (usually negative) balance of radiative entropy. This flux is balanced by the entropy production in the irreversible (dissipative) processes such as viscous and turbulent dissipation, phase transitions, and precipitation. The radiative entropy flux can be estimated from the radiative energy balance and is a measure of cumulative effect of all dissipative processes on a planet. The radiative energy balance in the Venusian atmosphere was described in Sect. 4.3. Figure 4.16 shows a sketch of the global mean budgets of energy and entropy on the planet. At the cloud level Venus receives $\approx 400\,\mathrm{mW/m^2/K}$ of entropy from solar radiation and looses $\approx 600\,\mathrm{mW/m^2/K}$ from thermal emission. A relatively small amount of energy and entropy is delivered to the lower atmosphere and the surface by the solar flux (Fig. 4.16). The net global mean budget of radiative entropy on Venus is about $-100\,\mathrm{mW/m^2/K}$.

Comparison of the entropy budget on Venus with that on Earth can shed light on the differences in irreversible processes on both planets (Table 4.1). Goody (2000) assessed their effect on Earth. The total mean flux of radiative entropy

Table 4.1 Comparison of sources and sinks of the planetary entropy for Venus and Earth

	Earth, mW/m^2/K (Goody 2000)	Venus, mW/m^2/K Titov et al. (2007)
Net radiative sink	−70	−100
Moist convection	+55	0
Mechanical dissipation	+12	≈1
Net balance	−3	−100

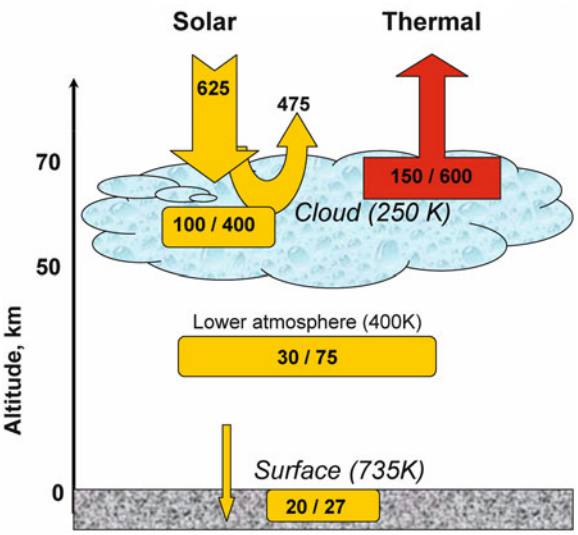

Fig. 4.16 Globally mean budgets of energy E and entropy (S=E/T) on Venus. The figures separated by slashes are energy in W/m^2 and entropy in mW/m^2/K. Credit: Titov et al. (2007)

on Earth is about –60 mW/m^2/K. Viscous and turbulent dissipation, water phase transitions and precipitation were found to be the main sources of entropy on Earth (Goody 2000; Renno 2001). The Venus dry climate suggests negligible role of the dissipative mechanisms associated with transport, phase transitions of water and precipitation. Observations suggest rather weak turbulence within the cloud layer with eddy diffusion coefficient of 10^4–10^3 cm^2/s (Kerzhanovich and Marov 1983) and corresponding entropy production not exceeding 1 mW/m^2/K. Thus, the entropy sources and sinks on Earth are quite different from those on Venus. However, the role of large scale dynamics, chemical reactions, and cloud processes on the Venusian entropy budget still needs to be studied.

Another difference between the entropy balances on Earth and Venus is the vertical distribution of the radiative sinks and sources of entropy. Earth receives solar energy and entropy mainly at the surface and emits them to space mostly from the atmosphere (Renno and Ingersoll 1996; Renno 1997; Goody 2000). On Venus the sources of radiative entropy at the surface and in the lower atmosphere represent only 20 % of the total balance (Fig. 4.16). The largest sinks and sources of radiative entropy on Venus are both located in the upper cloud deck.

General principles of dynamical system when applied to the Venus climate can lead to interesting, although so far only qualitative, conclusions. Nonlinear

dynamics shows that the emergence of higher levels of order in dissipative systems that exchange energy and entropy with environment is typical of both hydrodynamics (e.g., Rayleigh-Benard convection) and chemistry (e.g Zhabotinsky reaction) (Prigogine 1980). Strong external forcing can push such systems to a stationary state that is far from thermodynamic equilibrium and which is characterized by the maximum entropy production (MEP). The MEP principle was applied to planetary atmospheres and successfully predicted such general parameters of the Earth climate as surface temperature, cloud coverage, meridional energy transport (Paltridge 1975; Grassl 1981) and equator-to-pole temperature contrasts (Lorenz et al. 2001). Venus gives another example of such systems. The general circulation is in a steady but strongly non-equilibrium state. The super-rotating Venusian atmosphere (Gierasch et al. 1997) has rather high level of organization and, thus, low entropy maintained by energy and entropy exchange with the Sun and space. However, a detailed analysis of the Venus climate based on these principles is still awaited.

4.4.3 Greenhouse Effect and Climate Evolution

The planets receive solar energy in the ultraviolet, visible, and near-infrared spectral ranges, in which their atmospheres are relatively transparent. The surface and the lower atmosphere eliminate the absorbed energy by emitting radiation at infrared wavelengths. Strong absorption bands of gases and aerosols trap the heat in the lower atmosphere that results in raising the surface temperature. This process is referred to as the atmospheric greenhouse effect. The larger the infrared opacity, the higher surface temperature is required to balance the incoming solar flux. The difference between the actual surface temperature and the effective temperature of the planet without an atmosphere is a measure of the greenhouse effect. Its value reaches $\approx$735 K on Venus, which is by far the largest on the terrestrial planets. Bullock and Grinspoon (2001) used a one-dimensional, two-stream radiative-convective equilibrium (RCE) model to calculate the globally averaged temperature structure of the Venus atmosphere, study its sensitivity to various model parameters, and possible evolution with time. Gaseous opacities were obtained from the correlated-k coefficients (Goody et al. 1989) for CO_2 and the eight radiatively active trace gases (Fig. 4.17) with line parameters taken from the HITRAN (Rothman et al. 1998) and HITEMP (Wattson and Rothman 1992) spectral databases. CO_2 (Moskalenko et al. 1979) and H_2O continuum opacities (Liou 1992) were included, as were Rayleigh scattering by CO_2 and N_2 (Van de Hulst 1981). Absorption and scattering in the clouds was calculated assuming spherical particles in the globally-averaged cloud model based on the Pioneer Venus measurements (Knollenberg and Hunten 1980).

The lower atmosphere is opaque at infrared wavelengths, CO_2 being the principal source of absorption at wavelengths near 2.0, 2.7, 4.3, 4.8, 5.2, and 15 microns. Water vapor, SO_2, CO, and the H_2SO_4 clouds provide the primary sources of opacity between these bands thus strongly affecting the energy balance of the atmosphere (Fig. 4.18). The most significant windows between CO_2 bands are between

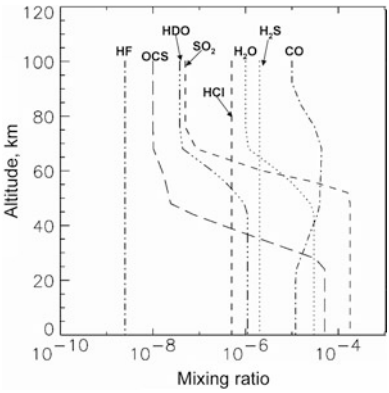

Fig. 4.17 A model of globally averaged chemical abundances of the radiatively active gases in the Venus atmosphere based on the Pioneer Venus and the ground-based observations. N_2 is also present, as the second most abundant gas in the Venus atmosphere, with constant mixing ratio of 0.0365 (Oyama et al. 1980)

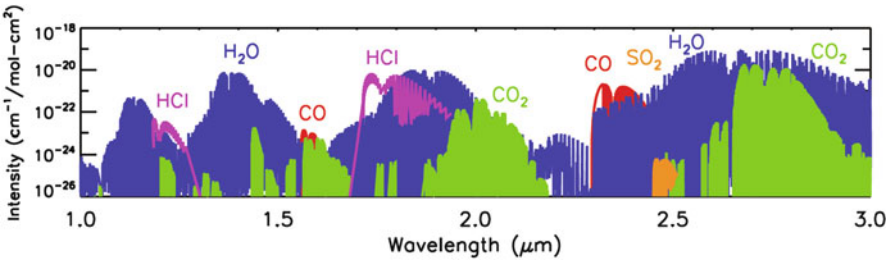

Fig. 4.18 Spectral line intensities as a function of wavelength in microns, for CO_2 (*green*), H_2O (*blue*), CO (*red*), SO_2 (*orange*) and HCl (*purple*). Line intensities are from the HITRAN 2004 data base (Rothman et al. 2005) and do not reflect their weighting due to mixing ratios in the Venus atmosphere

1–1.2 μm, where only H_2O absorbs, at 1.7 μm where HCl and CO are also detectable, and between 2.2 and 2.5 μm, where absorption by CO and SO_2 may be seen. Because absorption by these species occurs between bands of the major absorber, CO_2, changes in their abundance have a large, disproportionate influence on the Venus greenhouse effect. For instance, the water vapor mixing ratio on average is only 30 ppm, but it contributes about 70 K to the greenhouse effect due to absorption bands at 1.4, 1.9, and 2.5 μm. Therefore natural variations of the atmospheric water abundance have a significant effect on the surface temperature. To a lesser extent than water vapor, perturbations to atmospheric SO_2 abundance can be expected to alter the efficiency of the Venus greenhouse effect.

By subtracting out one atmospheric absorber at a time and re-calculating the thermal fluxes and the equilibrium state of the atmosphere we obtain the contribution of each constituent to the greenhouse effect (Table 4.2).

Contributions of the atmospheric components are not additive because of strong overlap between the absorption bands. Thus, the cumulative contribution of all opacity sources in Table 4.2 exceeds the observed greenhouse effect. These numerical experiments take into account only changes in the atmospheric opacity

Table 4.2 The effect of the removal of infrared opacity sources on the surface temperature. (From Titov et al. 2007)

Source	Change in surface temperature, K
CO_2	−420
Clouds	−140
H_2O	−70
OCS	−12
CO	−3
SO_2	−3
HCl	−2

due to removal of each trace gas, but neglect their effect on cloud formation. For instance, removal of sulfur dioxide as an optical agent from the model only marginally affects the greenhouse effect (Table 4.2), while actual removal of this gas from the atmosphere would cause the disappearance of the clouds. This would in turn reduce the greenhouse effect due to infrared scattering within the clouds, along with a decrease in the planetary albedo. The implications of this kind of change for the surface temperature, with competing albedo and greenhouse forcing, is not obvious without detailed calculations. The surface temperature sensitivity of a fully coupled radiative/convective and cloud microphysical model to the variations of water vapor and sulfur dioxide abundance is discussed in detail by Bullock et al. (2007).

The greenhouse effect also acts on Mars and Earth, although it results in less dramatic changes in surface temperature. On both planets it is mainly due to the presence of H_2O and CO_2 in the atmosphere and reaches few degrees on Mars and 30–40 K on Earth. Although the greenhouse effect on our planet is rather moderate it is obviously responsible for maintaining surface temperature above the freezing point and climate conditions comfortable for life. Without the greenhouse effect the mean temperature would fall to $\approx -20\,^{\circ}\mathrm{C}$, ocean would freeze, and life would become impossible. Since the conditions on the terrestrial planets and especially the amount of CO_2 and H_2O in the atmosphere could have varied over the geological history the greenhouse effect could have played more important role in the past.

The greenhouse effect seems to have played an important role in the evolution of the atmospheres on all terrestrial planets and, in particular, on Venus (Ingersoll 1969; Pollack 1971; Rasool and de Bergh 1970). Theories about the planets formation suggest that the neighboring planets Earth, Mars and Venus received similar amounts of water during their formation (Ip and Fernandez 1988). However, the atmosphere of Venus currently has about 100,000 times less water than the oceans and atmosphere of the Earth and is strongly enriched in deuterium. The measurements on Venus give D/H = 150±30 of the terrestrial value (Donahue et al. 1997; de Bergh et al. 2006). This suggests that Venus lost most of its water at some time in the past. The efficiency of escape depends strongly on the amount of hydrogen and deuterium in the upper atmosphere. The important result of the radiative-convective models of the early Venus atmosphere is that the greenhouse mechanism efficiently forces water into the stratosphere, where solar UV photons

readily dissociate H_2O molecules thus creating favorable conditions for hydrogen escape. The hydrodynamic escape is rapid enough to eliminate a large ocean in less than 600 million years (Kasting et al. 1984; Kasting 1988). Current Venus climate is a system with complex feedback between radiative effects, cloud formations processes, and surface-atmosphere interactions with water vapor and sulfur dioxide playing the key role in this balance. Bullock and Grinspoon (2001) used their RCE model to study sensitivity of the Venus climate to perturbations in these species due to global resurfacing event that assumed to have happened several hundreds millions years ago (McKinnon et al. 1997). The Venus climate appears to be stable within broad range of H_2O mixing ratios. However, at about 50 times the current abundance the enhanced water greenhouse begins to warm the atmosphere, evaporating and thinning the clouds from below. This reduces the albedo, further warming the atmosphere, and further evaporating the clouds. This positive feedback destroys the massive H_2SO_4/H_2O clouds and replaces them with thin, high water-rich clouds increasing the surface temperature to about 920 K. Further raising of the atmospheric H_2O content does not increase surface temperatures substantially, mostly because it does not enhance the greenhouse effect as much as before, and also because the high water clouds become thicker and more reflective, offsetting the greenhouse effect. Thus, the Venusian climate reaches equilibrium with surface temperatures limited to about 920 K, over a wide range of atmospheric water abundance. If either H_2O or SO_2 abundance fall below 0.5 ppm the clouds also disappear but the surface temperature stabilizes at $\approx$700 K (Bullock et al. 2007).

4.5 Open Issues and Perspectives

Observations, numerical modeling and theoretical studies have all revealed the extremely important role that radiation plays in various processes on Venus, both now and early in its history. The large opacity of the atmosphere and the presence of great amounts of radiatively active gases and aerosols give Venus its unique place among the terrestrial planets. The greenhouse mechanism has clearly been very effective in forming the current and early climate on Venus, while the peculiar distribution of the radiative energy sinks and sources drives the remarkable super-rotation of the entire atmosphere. Chemical interactions between different gaseous and aerosol species and the importance of non-linear feedbacks make the Venus climate a very complex system.

Previous investigations of radiation in the Venus atmosphere provided a general understanding of the distribution of fluxes, sources and sinks of radiative energy, and of the radiative forcing of the atmospheric dynamics and climate. At the same time they left a great number of unsolved problems. One of the most important open issues in this field is the variability of atmospheric properties such as the abundance of radiatively active gases, cloud microphysical and optical properties and total opacity, and the influence of these on the energy balance. The second problem concerns the radiative forcing of the atmospheric global circulation. How does the

distribution of the sources and sinks of radiative energy drives the atmospheric dynamics? The thermodynamics of the Venus atmosphere is the third issue needing to be clarified and quantified. New studies of the fluxes and balance of energy and entropy, the role of dissipative processes and efficiency of the Venus heat engine would help us to understand the Venus climate-forming mechanisms. The forth open question concerns the role of radiation in the evolution of the Venus atmosphere, the early greenhouse effect and the loss of water from the planet, as well as recent climate perturbations during global resurfacing. Resolving these open issues in Venus physics would result in significant progress in comparative planetology and climatology of the terrestrial planets in general and in the study of the Earth's climate evolution in particular.

Future work would require a combination of new observations, laboratory studies, numerical modeling, and theoretical investigations. Remote sensing of the Venus mesosphere will provide the global temperature and aerosol structure, distribution and variations of the radiatively active gases, and characterize the aerosol properties and total cloud opacity with complete latitude and local time coverage. Observations of the night side in the near-IR transparency "windows" from orbit will provide access to the composition and cloud properties in the middle and lower atmosphere—the regions that had been so far reachable by descent probes only. Measurements of the reflected solar and outgoing thermal fluxes from orbit are required to quantify the details of energy and entropy budgets.

The details of the atmospheric properties and especially their vertical distribution require in-situ measurements. The first priority here is the characterization of the aerosol population including number density, particle size distribution and optical properties as well as their composition. Special attention should be paid to the identification of the unknown UV absorber and understanding of its distribution due to its important role in the radiative balance. Accurate measurements of the vertical profiles of the radiatively active gases and their spatial variations are important for development of the models of the Venus greenhouse. Vertical profiles of the radiative heat fluxes are poorly known and new in-situ observations are required. And finally, precise measurements of the vertical profiles of atmospheric temperatures in the deep atmosphere would constrain models of the Venus greenhouse and to determine the regions of convective stability.

The Venus lower atmosphere is an example of an extreme environment. The spectral properties of the atmospheric gases at such conditions must be measured in laboratories to support the analysis of remote and in-situ measurements and state-of-the-art radiative transfer models to study the radiative energy balance and forcing of the global circulation and climate and their sensitivity to the variation of the atmospheric optical properties.

Venus Express remote sensing observations have recently provided a great amount of new data on the above mentioned topics. The spacecraft that began orbital operations on April 11, 2006 (Svedhem et al. 2007) carries a powerful suite of spectral and imaging instruments that aims at a global study of the structure, composition and dynamics of the Venus atmosphere and plasma environment. A versatile program of orbital observations includes global monitoring and close-up

imaging of the atmosphere, solar, stellar and Earth radio occultation to study its structure and composition, and in-situ measurements of neutral atoms, plasma, and the magnetic field (Titov et al. 2006). The mission extension is approved till the end of 2014.

The next logical step in the Venus exploration would be in-situ studies by descent probes and balloons that would investigate the composition and microphysical and optical properties of the clouds, as well as measure the fluxes of solar and thermal radiation within the atmosphere. Although no such investigation is so far approved by the world's space agencies, the science goals, payloads and possible space platforms are well identified and are well within current technological capabilities (Crisp et al. 2002; Chassefiere et al. 2002; Baines et al. 2007).

References

D.A. Allen, J.W. Crawford, Cloud structure on the dark side of Venus. Nature **307**, 222–224 (1984)

A. Arking, Absorption of solar energy in the atmosphere: Discrepancy between model and observations. Science **273**, 779–782 (1996)

K.H. Baines, R.W. Atreya, D. Carlson, D. Crisp, D. Grinspoon, C.T. Russel, G. Schubert, K. Zahnle, in *Experiencing Venus: Clues to the Origin, Evolution, and Chemistry of Terrestrial Planets via in-situ Exploration of our Sister World*, ed. by L.W. Esposito, E.R. Stofan, T.E. Cravens. Exploring Venus as a Terrestrial Planet (American Geophysical Union, Washington, DC, 2007)

B. Bezard, C. DeBergh, D. Crisp, J.P. Maillard, The deep atmosphere of Venus revealed by high-resolution nightside spectra. Nature **345**, 508–511 (1990)

B. Bezard, C.C.C. Tsang, R.W. Carlson, G. Piccioni, E. Marcq, P. Drossart, Water vapor abundance near the surface of Venus from Venus Express/VIRTIS observations. J. Geophys. Res.-Planets **114**, E00B39 (2009)

R.W. Boese, J.B. Pollack, P.M. Silvaggio, 1st results from the large probe infrared radiometer experiment. Science **203**, 797–800 (1979)

M.A. Bullock, D.H. Grinspoon, The recent evolution of climate on Venus. Icarus **150**, 19–37 (2001)

M.A. Bullock, D.H. Grinspoon, S.C. Solomon, J.W. Head, R.J. Phillips, in *Climate change and tectonics on Venus*, ed. by L.W. Esposito, E.R. Stofan, T.E. Cravens. Exploring Venus as a Terrestrial Planet (American Geophysical Union, Washington, DC, 2007)

R.W. Carlson, F.W. Taylor, The Galileo Encounter With Venus – results from the near-infrared mapping spectrometer. Planet Space Sci. **41**, 475–476 (1993)

R.W. Carlson, L.W. Kamp, K.H. Baines, J.B. Pollack, D.H. Grinspoon, T. Encrenaz, P. Drossart, F.W. Taylor, Variations in Venus cloud particle properties – a new view of Venus' cloud morphology as observed by the Galileo Near-Infrared Mapping Spectrometer. Planet Space Sci. **41**, 477–485 (1993)

E. Chassefiere, J.J. Berthelier, J.L. Bertaux, E. Quemerais, J.P. Pommereau, P. Rannou, F. Raulin, P. Coll, D. Coscia, A. Jambon, P. Sarda, J.C. Sabroux, G. Vitter, A. Le Pichon, B. Landeau, P. Lognonne, Y. Cohen, S. Vergniole, G. Hulot, M. Mandea, J.F. Pineau, B. Bezard, H.U. Keller, D. Titov, D. Breuer, K. Szego, C. Ferencz, M. Roos-Serote, O. Korablev, V. Linkin, R. Rodrigo, F.W. Taylor, A.M. Harri, The Lavoisier mission: A system of descent probe and balloon flotilla for geochemical investigation of the deep atmosphere and surface of Venus. Planet. Atmos. **29** (2002)

D. Crisp, Radiative forcing of the Venus mesosphere. 1. solar fluxes and heating rates. Icarus **67**, 484–514 (1986)

D. Crisp, Radiative forcing of the Venus mesosphere. 2. thermal fluxes, cooling rates, and radiative equilibrium temperatures. Icarus **77**, 391–413 (1989)
D. Crisp, D.V. Titov, in *The Thermal Balance of the Venus Atmosphere*, ed. by S.W. Bougher, D.M. Hunten, R.J. Phillips. Venus-II (The University of Arizona Press, Tucson, Arizona, 1997)
D. Crisp, A.P. Ingersoll, C.E. Hildebrand, R.A. Preston, Vega balloon meteorological measurements. Venus Atmosp. **10**, 109–124 (1990)
D. Crisp, D.A. Allen, D.H. Grinspoon, J.B. Pollack, The dark side of Venus – near-infrared images and spectra from the Anglo-Australian-Observatory. Science **253**, 1263–1266 (1991)
D. Crisp, S. McMuldroch, S.K. Stephens, W.M. Sinton, B. Ragent, K.-W. Hodapp, R.G. Probst, L.R. Doyle, D.A. Allen, J. Elias, Ground-based near-infrared imaging observations of Venus during the Galileo encounter. Science **253**, 1538–1541 (1991)
D. Crisp, M.A. Allen, V.G. Anicich, R.E. Arvidson, S.K. Atreya, K.H. Baines, W.B. Banerdt, G.L. Bjoraker, S.W. Bougher, B.A. Campbell, R.W. Carlson, G. Chin, A. Chutjian, R.T. Clancy, B.C. Clark, T. Cravens, Divergent evolution among Earth-like planets: The case for venus exploration, the future of solar system exploration, 2003–2013. In Community contributions to the NRC solar system exploration survey, ASP Conference Series, vol. 272, ed. M. Sykes, ISBN: 1-58381-113-3, San Francisco, pp. 5–34 (2002)
C. de Bergh, B. Bezard, D. Crisp, J.P. Maillard, T. Owen, J. Pollack, D. Grinspoon, Water in the deep atmosphere of Venus from high-resolution spectra of the night side. Explorat. Venus Mars Atmosp. **15** (1995)
C. de Bergh, V.I. Moroz, F.W. Taylor, D. Crisp, B. Bezard, L.V. Zasova, The composition of the atmosphere of Venus below 100 km altitude: An overview. Planet Space Sci. **54**, 1389–1397 (2006)
T. Donahue, D.H. Grinspoon, R.E. Hartle, R.R. Hodges Jr, in *Ion/Neutral Escape of Hydrogen and Deuterium: Evolution of Water*, ed. by S.W. Bougher, D.M. Hunten, R.J. Phillips. Venus II Geology, Geophysics, Atmosphere and Solar Wind Environment (University of Arizona Press, Tucson, 1997)
P. Drossart, B. Bezard, T. Encrenaz, E. Lellouch, M. Roos, F.W. Taylor, A.D. Collard, S.B. Calcutt, J. Pollack, D.H. Grinspoon, R.W. Carlson, K.H. Baines, L.W. Kamp, Search for spatial variations of the H2O abundance in the lower atmosphere of Venus From Nims-Galileo. Planet Space Sci. **41**, 495–504 (1993)
P. Drossart, G. Piccioni, J.C. Gerard, M.A. Lopez-Valverde, A. Sanchez-Lavega, L. Zasova, R. Hueso, F.W. Taylor, B. Bezard, A. Adriani, F. Angrilli, G. Arnold, K.H. Baines, G. Bellucci, J. Benkhoff, J.P. Bibring, A. Blanco, M.I. Blecka, R.W. Carlson, A. Coradini, A. Di Lellis, T. Encrenaz, S. Erard, S. Fonti, V. Formisano, T. Fouchet, R. Garcia, R. Haus, J. Helbert, N.I. Ignatiev, P. Irwin, Y. Langevin, S. Lebonnois, D. Luz, L. Marinangeli, V. Orofino, A.V., Rodin, M.C. Roos-Serote, B. Saggin, D.M. Stam, D. Titov, G. Visconti, M. Zambelli, C. Tsang, A dynamic upper atmosphere of Venus as revealed by VIRTIS on Venus Express. Nature **450**, 641–645 (2007)
A.P. Ekonomov, Y. Golovin, V.I. Moroz, B. Moshkin, Solar scattered radiation measurements by venus probes. Venus (A83-37401 17-91) Tucson, AZ, University of Arizona Press 632–649 (1983)
A.P. Ekonomov, V.I. Moroz, B.E. Moshkin, V.I. Gnedykh, Y.M. Golovin, A.V. Crigoryev, Scattered UV solar-radiation within the clouds of Venus. Nature **307**, 345–347 (1984)
J.M. Forbes, Tides in the middle and upper atmospheres of Mars and Venus. Planetary Atmospheres, Ionospheres And Plasma Interactions. Comm. Space Res. **33** (2004)
P.J. Gierasch, R.M. Goody, R.E. Young, D. Crisp, C. Edwards, R. Kahn, D. Rider, A. Del Genio, R. Greeley, A. Hou, C.B. Leovy, D. McCleese, M. in Newman, *The General Circulation of the Venus Atmosphere: An Assessment*, ed. by S.W. Bougher, D.M. Hunten, R.J. Philips. Venus II: Geology, Geophysics, Atmosphere, and Solar Wind Environment, Tucson, AZ, University of Arizona Press p. 459 (1997)
R. Goody, Sources and sinks of climate entropy. Quart. J. R. Meteor. Soc. **126**, 1953–1970 (2000)
R. Goody, West, R., L. Chen, D. Crisp, The correlated-k method for radiation calculations in nonhomogeneous atmospheres. J. Quant. Spectrosc. Radiat. Transfer **42**, 539–550 (1989)

D. Grassi, A. Migliorini, L. Montabone, S. Lebonnois, A. Cardesin-Moinelo, G. Piccioni, P. Drossart, L.V. Zasova, Thermal structure of Venusian nighttime mesosphere as observed by VIRTIS-Venus Express. J. Geophys. Res.-Planets **115**, E09007 (2010)

H. Grassl, The climate at maximum-entropy production by meridional atmospheric and oceanic heat fluxes. Quart. J. R. Meteor. Soc. **107**, 153–166 (1981)

R. Haus, H. Goering, Radiative energy-balance of the Venus mesosphere. Icarus **84**, 62–82 (1990)

N.I. Ignatiev, V.I. Moroz, B.E. Moshkin, A.P. Ekonomov, V.I. Gnedykh, A.V. Grigoriev, I.V. Khatuntsev, Water vapour in the lower atmosphere of Venus: A new analysis of optical spectra measured by entry probes. Planet Space Sci. **45**, 427–438 (1997)

N.I. Ignatiev, D.V. Titov, G. Piccioni, P. Drossart, W.J. Markiewicz, V. Cottini, T. Roatsch, M. Almeida, N. Manoel, Altimetry of the Venus cloud tops from the Venus Express observations. J. Geophys. Res.-Planets **114**, E00B43 (2009)

A.P. Ingersoll, Runaway greenhouse – a history of water on Venus. J. Atmos. Sci. **26**, 1191–1198 (1969)

W.H. Ip, J.A. Fernandez, Exchange of condensed matter among the outer and terrestrial protoplanets and the effect on surface impact and atmospheric accretion. Icarus **74**, 47–61 (1988)

J.F. Kasting, Runaway and moist greenhouse atmospheres and the evolution of Earth and Venus. Icarus **74**, 472–494 (1988)

J.F. Kasting, J.B. Pollack, T.P. Ackerman, Response of Earth's atmosphere to increases in solar flux and implications for loss of water from Venus. Icarus **57**, 335–355 (1984)

V.V. Kerzhanovich, M. Marov, The atmospheric dynamics of venus according to doppler measurements by the venera entry probes. Venus, Ed. D.M. Hunten, L. Colin, T.M. Donahue, V.I. Moroz, Tucson, AZ, University of Arizona Press (1983)

R.G. Knollenberg, D.M. Hunten, The microphysics of the clouds of venus: Results of the pioneer venus particle size spectrometer experiment. J. Geophys. Res. **85**, 8039–8058 (1980)

Y.J. Lee, Venus cloud structure and radiative energy balance of the mesosphere, Ph.D. thesis, TU Braunschweig (2011)

Y.J. Lee, D. Titov, S. Tellmann, A. Piccialli, N. Ignatiev, M. Pätzold, B. Häusler, G. Piccioni, P. Drossart, Vertical structure of the Venus cloud top from the VeRa and VIRTIS observations onboard Venus Express, Icarus, in press, doi:10.1016/j.icarus.2011.07.001 Icarus **217**(2), 599–609 (2012)

E. Lellouch, T. Clancy, D. Crisp, A. Kliore, D. Titov, S.W. Bougher, *Monitoring of Mesospheric Structure and Dynamics, Venus II* University of Arizona Press (1997)

V.M. Linkin, J. Blamont, A.N. Lipatov, A.A. Shurupov, C. Malique, S.P. Ignatova, G.A. Frank, L.I. Hlyustova, A.V. Terterashvili, A. Seiff, V.V. Kerzhanovich, B. Ragent, R. Young, E. Elson, R. Preston, A. Ingersoll, D. Crisp, Thermal structure of the Venus atmosphere in the middle cloud layer. Pis'ma v Astronomicheskie Zhurnal, **12** (1986)

K.N. Liou, *Radiation and Cloud Processes in the Atmosphere*. (Oxford University Press, New York, 1992)

R.D. Lorenz, J.I. Lunine, P.G. Withers, C.P. McKay, Titan, Mars and Earth: Entropy production by latitudinal heat transport. Geophys. Res. Lett. **28**, 415–418 (2001)

W.J. Markiewicz, D.V. Titov, S.S. Limaye, H.U. Keller, N. Ignatiev, R. Jaumann, N. Thomas, H. Michalik, R. Moissl, P. Russo, Morphology and dynamics of the upper cloud layer of Venus. Nature **450**, 633–636 (2007)

W.B. McKinnon, K.J. Zahnle, H.J. Melosh, in *Cratering on Venus: Models and Observations*, ed. by S.W. Bougher, D.M. Hunten, R.J. Phillips. Venus-II (The University of Arizona Press, Tucson, Arizona, 1997)

V.S. Meadows, D. Crisp, Ground-based near-infrared observations of the Venus nightside: The thermal structure and water abundance near the surface. J. Geophys. Res.-Planets **101**, 4595–4622 (1996)

V.I. Moroz, A. Ekonomov, B. Moshkin, H. Revercomb, L. Sromovsky, J. Schofield, D. Spaenkuch, F. Taylor, M. Tomasko, Solar and thermal radiation in the Venus atmosphere. Adv. Space Res. **5**, 197–232 (1985)

V.I. Moroz, A.P. Ekonomov, Y.M. Golovin, B.E. Moshkin, N.F. Sanko, Solar-radiation scattered in the Venus Atmosphere – The Venera 11,12 Data. Icarus **53**, 509–537 (1983)

N.I. Moskalenko, Y.A. Ilin, C.N. Parzhin, L.V. Rodionov, Pressure-induced IR radiation absorption in atmospheres. Izvestiya Akademii Nauk Sssr Fizika Atmosfery I Okeana **15**, 912–919 (1979)

D. Oertel, D. Spankuch, H. Jahn, H. Becker-Ross, W. Stadthaus, J. Nopirakowski, W. Dohler, K. Schafer, J. Guldner, R. Dubois, V.I. Moroz, V.M. Linkin, V.V. Kerzhanovich, I.A. Matsgorin, A.N. Lipatov, A.A. Shurupov, L.V. Zasova, E.A. Ustinov, Infrared spectrometry of venus from 'venera-15' and 'venera-16', COSPAR; IAU; Int. Assoc. Geomagnetism & Aeronomy. Adv. Space Res. **5**, 25–36 (1985)

V.I. Oyama, G.C. Carle, F. Woeller, S. Rocklin, J. Vogrin, W. Potter, G. Rosiak, C. Reichwein, Pioneer Venus sounder probe gas-chromatograph. IEEE T. Geosci. Remote. **18**, 85–93 (1980)

G.W. Paltridge, Global dynamics and climate – system of minimum entropy exchange. Quart. J. R. Meteor. Soc. **101**, 475–484 (1975)

A. Piccialli, D.V. Titov, D. Grassi, I. Khatuntsev, P. Drossart, G. Piccioni, A. Migliorini, Cyclostrophic winds from the visible and infrared thermal imaging spectrometer temperature sounding: A preliminary analysis. J. Geophys. Res.-Planets **113**, E00B11 (2008)

A. Piccialli, S. Tellmann, D. Titov, S.S. Limaye, I.V. Khatuntsev, M. Patzold, B. Haussler, Dynamical properties of the Venus mesosphere from the radio-occultation experiment Vera onboard Venus Express. Icarus **217**, 669–681 (2012)

G. Piccioni, P. Drossart, A. Sanchez-Lavega, R. Hueso, F.W. Taylor, C.F. Wilson, D. Grassi, L. Zasova, M. Moriconi, A. Adriani, S. Lebonnois, A. Coradini, B. Bezard, F. Angrilli, G. Arnold, K.H. Baines, G. Bellucci, J. Benkhoff, J.P. Bibring, A. Blanco, M.I. Blecka, R.W. Carlson, A. Di Lellis, T. Encrenaz, S. Erard, S. Fonti, V. Formisano, T. Fouchet, R. Garcia, R. Haus, J. Helbert, N.I. Ignatiev, P.G.J. Irwin, Y. Langevin, M.A. Lopez-Valverde, D. Luz, L. Marinangeli, V. Orofino, A.V. Rodin, M.C. Roos-Serote, B. Saggin, D.M. Stam, D. Titov, G. Visconti, M. Zambelli, South-polar features on venus similar to those near the North Pole. Nature **450**, 637–640 (2007)

J.B. Pollack, Nongrey calculation of runaway greenhouse - implications for Venus past and present, Icarus **14**, 295–306 (1971)

J.B. Pollack, O.B. Toon, R. Boese, Greenhouse models of Venus' high surface temperature, as constrained by Pioneer Venus measurements. J. Geophys. Res. **85**, 8223–8231 (1980)

I. Prigogine, *From Being to Becoming: Time and Complexity in the Physical Sciences* ISBN 0-7167-1107-9, W.H. Freeman & Co. Ltd, San Francisco (1980)

S.I. Rasool, C. de Bergh, Runaway greenhouse and accumulation of CO2 in Venus atmosphere. Nature **226**, 1037–1039 (1970)

N.O. Renno, Multiple equilibria in radiative-convective atmospheres. Tellus Ser. A-Dyn. Meteorol. Oceanograp. **49**, 423–438 (1997)

N.O. Renno, Comments on "frictional dissipation in a precipitating atmosphere". J. Atmos. Sci. **58**, 1173–1177 (2001)

N.O. Renno, A.P. Ingersoll, Natural convection as a heat engine: A theory for CAPE. J. Atmos. Sci. **53**, 572–585 (1996)

H.E. Revercomb, L.A. Sromovsky, V.E. Suomi, R.W. Boese, Net thermal-radiation in the atmosphere of Venus. Icarus **61**, 521–538 (1985)

M. Roos-Serote, P. Drossart, T. Encrenaz, E. Lellouch, R.W. Carlson, K.H. Baines, F.W. Taylor, S.B. Calcutt, The thermal structure and dynamics of the atmosphere of Venus between 70 and 90 Km from the Galileo-Nims Spectra. Icarus **114**, 300–309 (1995)

W.B. Rossow, A.D. Del Genio, S.S. Limaye, L.D. Travis, P. Stone, Cloud morphology and motions from Pioneer Venus images. J. Geophys. Res. **85**, 8107–8128 (1980)

L.S. Rothman, C.P. Rinsland, A. Goldman, S.T. Massie, D.P. Edwards, J.M. Flaud, A. Perrin, C. Camy-Peyret, V. Dana, J.Y. Mandin, J. Schroeder, A. McCann, R.R. Gamache, R.B. Wattson, K. Yoshino, K.V. Chance, K.W. Jucks, L.R. Brown, V. Nemtchinov, P. Varanasi, The HITRAN molecular spectroscopic database and HAWKS (HITRAN Atmospheric Workstation): 1996 edition. J. Quant. Spectrosc. Radiat. Transfer **60**, 665–710 (1998)

L.S. Rothman, D. Jacquemart, A. Barbe, D.C. Benner, M. Birk, L.R. Brown, M.R. Carleer, C. Chackerian, K. Chance, L.H. Coudert, V. Dana, V.M. Devi, J.M. Flaud, R.R. Gamache, A. Goldman, J.M. Hartmann, K.W. Jucks, A.G. Maki, J.Y. Mandin, S.T. Massie, J. Orphal, A. Perrin, C.P. Rinsland, M.A.H. Smith, J. Tennyson, R.N. Tolchenov, R.A. Toth, J. Vander Auwera, P. Varanasi, G. Wagner, The HITRAN 2004 molecular spectroscopic database. J. Quant. Spectrosc. Radiat. Transfer **96**, 139–204 (2005)

J.T. Schofield, F.W. Taylor, Net global thermal emission from the Venusian atmosphere. Icarus **52**, 245–262 (1982)

V.E. Suomi, L.A. Sromovsky, H.E. Revercomb, Net radiation in the atmosphere of Venus: measurements and interpretation. J. Geophys. Res. **85**, 8200–8218 (1980)

H. Svedhem, D.V. Titov, D. McCoy, J.P. Lebreton, S. Barabash, J.L. Bertaux, P. Drossart, V. Formisano, B. Haeusler, O. Korablev, W.J. Markiewicz, D. Nevejans, M. Paetzold, G. Piccioni, T.L. Zhang, F.W. Taylor, E. Lellouch, D. Koschny, O. Witasse, H. Eggel, M. Warhaut, A. Accomazzo, J. Rodriguez-Canabal, J. Fabrega, T. Schirmann, A. Clochet, M. Coradini, Venus Express – the first european mission to Venus. Planet Space Sci. **55**, 1636–1652 (2007)

F. Taylor, R. Beer, M. Chahine, D. Diner, L. Elson, R. Haskins, D. McCleese, J. Martonchik, P. Reichley, S. Bradley, J. Delderfield, J. Schofield, C. Farmer, L. Froidevaux, J. Leung, M. Coffey, J.C. Gille, Structure and meteorology of the middle atmosphere of Venus: infrared remote sensing from the Pioneer obiter. J. Geophys. Res. **85**, 7963–8006 (1980)

F. Taylor, D. Crisp, B. Bezard, in *Near-infrared sounding of the lower atmosphere of Venus*, ed. by S.W. Bougher, D.M. Hunten, R.J. Phillips. Venus-II (The University of Arizona Press, Tucson, Arizona, 1997)

F.W. Taylor, D.M. Hunten, L.V. Ksanfomaliti, The thermal balance of the middle and upper atmosphere of venus, Venus (A83-37401 17-91), Tucson, AZ, University of Arizona Press, p. 650–680, (1983)

S. Tellmann, M. Paetzold, B. Haeusler, M.K. Bird, G.L. Tyler, Structure of the Venus neutral atmosphere as observed by the Radio Science experiment VeRa on Venus Express. J. Geophys. Res.-Planets **114**, E00B36 (2009)

D.V. Titov, M. Bullock, D. Crisp, N. Renno, F. Taylor, L. Zasova, in *Radiation in the Atmosphere of Venus*, ed. by L.W. Esposito, E.R. Stofan, T.E. Cravens. Exploring Venus as terrestrial planet. Geophysical Monograph, vol 176 (American Geophysical Union, Washington, DC, 2007)

D.V. Titov, W. Markiewicz, N. Ignatiev, S. Li, S. Limaye, A. Sanchez-Lavega, J. Hesemann, M. Almeida, T. Roatsch, K.-D. Matz, F. Scholten, D. Crisp, L. Esposito, S. Hviid, R. Jaumann, H. Keller, R. Moissl, Morphology of the cloud tops as observed by the venus express monitoring camera. Icarus, **21**(2) p. 682–701, doi:10.1016/j.icarus.2011.06.020, (2012)

D.V. Titov, Radiative balance in the mesosphere of venus from the venera-15 infrared spectrometer results. Explor. Venus Mars Atmos. **15** p. 73–77 (1995)

D.V. Titov, H. Svedhem, F.W. Taylor, in *The Atmosphere of Venus: Current Knowledge and Future Investigations*, ed. by Ph. Blondel, J.W. Mason. Solar System Update (Springer-Praxis, Berlin, 2006)

D.V. Titov, F.W. Taylor, H. Svedhem, N.I. Ignatiev, W.J. Markiewicz, G. Piccioni, P. Drossart, Atmospheric structure and dynamics as the cause of ultraviolet markings in the clouds of Venus. Nature **456**, 620–623 (2008)

D.V. Titov, H. Svedhem, F.W. Taylor, S. Barabash, J.L. Bertaux, P. Drossart, V. Formisano, B. Haeusler, O. Korablev, W.J. Markiewicz, D. Nevejans, M. Paetzold, G. Piccioni, J.A. Sauvaud, T.L. Zhang, O. Witasse, J.C. Gerard, A. Fedorov, A. Sanchez-Lavega, J. Helbert, R. Hoofs, Venus express: Highlights of the nominal mission. Solar Sys. Res. **43**, 185–209 (2009)

M.G. Tomasko, L. Doose, P. Smith, A. Odell, Measurements of the flux of sunlight in the atmosphere of Venus. J. Geophys. Res. **85**, 8167–8186 (1980a)

M.G. Tomasko, The thermal balance of the lower atmosphere of Venus. *Venus*, Ed. D.M. Hunten, L. Colin, T.M. Donahue, V.I. Moroz, Tucson, AZ, University of Arizona Press (1983)

M.G. Tomasko, P.H. Smith, V.E. Suomi, L.A. Sromovsky, H.E. Revercomb, F.W. Taylor, D.J. Martonchik, A. Seiff, R. Boese, J.B. Pollack, A.P. Ingersoll, G. Schubert, C.C. Covey, The

thermal balance of Venus in light of the Pioneer Venus mission. J. Geophys. Res.-Atmos, doi: 10.1029/JA085iA13p08187 85, A13, 8187–8199(1980)
M.G. Tomasko, L.R. Doose, P.H. Smith, The absorption of solar energy and the heating rate in the atmosphere of Venus. Adv. Space Res. **5**, 71–79 (1985)
H.C. Van de Hulst, *Light Scattering by Small Particles* (Dover, New York, 1981)
R.B. Wattson, L.S. Rothman, Direct numerical diagonalization – wave of the future. J. Quant. Spectrosc. Radiat. Transfer **48**, 763–780 (1992)
L.V. Zasova, N. Ignatiev, I. Khatuntsev, V. Linkin, Structure of the Venus atmosphere. Planet Space Sci. **55**, 1712–1728 (2007)

Chapter 5
Atmospheric Circulation and Dynamics

Sanjay S. Limaye and Miriam Rengel

5.1 Introduction

The deep atmosphere of Venus (~180 km including the thermosphere) presents both observational and modeling challenges. Its thick, nearly uniform global cloud cover makes it difficult to fathom the vertical structure of the global circulation through available techniques that are applied to Earth's atmosphere. Further, the slow rotation of the planet and the consequential prevailing cyclostrophic balance restricts easy inferences about the meridional flow and circulation (Schubert et al. 2007; Gierasch et al. 1997; Read 1986).

Different observational methods have been used to measure the atmospheric circulation from near surface to the thermosphere. A summary of the observations at different altitudes can be found in many review articles (Schubert 1983; Gierasch et al. 1997; Bougher et al. 2006; Lellouch et al. 1997; Brecht 2011) while some limitations and need for future observations have been presented (Limaye 2007; Limaye et al. 2010). For the sake of completeness, a brief overview of the atmospheric circulation observations and the deficiencies are summarized in this chapter. The different methods have different spatial and temporal coverage and some limitations which cannot be ignored. These techniques include Doppler Spectroscopic (restricted to Line-of-Sight measurements only), tracking of atmospheric entry probes and balloons anemometers, and tracking of cloud features. The Doppler spectroscopic technique has been used so far only from Earth based telescopes (e.g. Widemann et al. 2007, 2008) and hence the spatial coverage and

S.S. Limaye (✉)
Space Science and Engineering Center, University of Wisconsin, Wisconsin, USA
e-mail: SanjayL@ssec.wisc.edu

M. Rengel
Max-Planck-Institut fur Sonnensystemforschung, Lindau, Germany

L. Bengtsson et al. (eds.), *Towards Understanding the Climate of Venus*, ISSI Scientific Report Series 11, DOI 10.1007/978-1-4614-5064-1_5,

resolution are severely limited to infer detailed horizontal structure and temporal coverage as typically such observations are feasible only when the Earth-Venus geometry is favorable when Venus is near quadrature. The wind field can also be approximative determined by making use of the cyclostrophic balance. In this way profiles of pressure with altitude have been derived from Venus Express (Piccialli et al. 2012; Zasova et al. 2007) and Pioneer Venus (Limaye 1985) from radio occultation technique, and from Pioneer entry probe profiles (Seiff 1983; Sromovsky et al. 1985). The results obtained in this way are in general agreement with the averaged cloud tracking results both for the gross latitudinal dependence as well as providing confirmation of their general altitude level. Further, it has been shown that the magnitude of the zonal flow is dependent on the vertical resolution of the temperature profiles as evidenced by the large discrepancy in the flow derived under the assumption of a lower boundary profile of zonal flow and the thermal wind equation for cyclostrophic flow using infrared retrievals from VIRTIS observations (Piccialli et al. 2012). Using derived thermal profiles obtained by radio occultation yields results similar in magnitude to those obtained from the direct application of the balance equation and the meridional gradient of pressure.

Since the discovery that the cloud top level (∼70 km) "4-day" super-rotation of the atmosphere of Venus was first inferred from the movement of large scale cloud features in images taken through ultraviolet or blue filter from Earth based telescopes (Boyer and Guerin 1969), much has been learned about the global atmospheric circulation. Although the knowledge that the bulk of the atmosphere of Venus rotates faster than the underlying solid planet and in the same direction for nearly four decades, its origins and the mechanisms that maintain it are unknown. Leovy (1973) pointed out that the super-rotation is likely in a state of cyclostrophic balance given the very small Coriolis force due to the slow rotation of the planet. While observations of the thermal structure have shown this to be the case, the unbalanced part of the circulation must be a main component of the Venus atmosphere and likely a key aspect of the atmospheric processes that maintain the super-rotation.

At least at the ultraviolet cloud level (as measured repeatedly from the ultraviolet images obtained from Mariner 10, Pioneer Venus, Galileo Orbiter and Venus Express), the rapid flow is weakly directed toward the respective rotation pole in each hemisphere. The presence of the weak poleward component leads to a state of non rigid body rotation in the low and mid latitudes and the build up of mid latitude jets which have cores located at ∼62 km altitude at ∼45 degrees latitude as inferred from thermal structure data and the existence of cyclostrophic balance. The mean meridional flow transports absolute angular momentum which must be dissipated in polar latitudes due to viscous forces that leads to a tendency towards rigid body rotation in polar latitudes, consistent with the Rankine vortex structure that Venus exhibits. The resupply of the angular momentum in equatorial regions to maintain the super-rotation has been suggested to occur through one or both of two key atmospheric processes—solar thermal tides and eddy circulations associated with atmospheric waves ranging from small scale gravity waves to a single Kelvin wave. Yet, dynamical observations (Limaye 2007) available to date have been

unable to verify this equator-ward transport of angular momentum. Lorenz (1967) laid out the framework to diagnose or to explore the general circulation of the Earth's atmosphere in terms of mean and eddy circulations that also can be used for diagnosing the maintenance of the super-rotation of the Venus atmosphere by determining the global mean and eddy circulations and the accompanying meridional transports of angular momentum and energy. This is limited obviously by the available observations of the global circulation of Venus, and measurements of cloud motions provide the only data to achieve this at present (Limaye and Suomi 1981; Limaye et al. 1988; Rossow et al. 1990; Moissl et al. 2009). However, this is possible only at the ultraviolet cloud level and only on the day-side. Although near infrared observations from Venus Express have yielded some cloud motions (Hueso et al. 2012), no estimates of the eddy transports from night side measurements are yet available due to insufficient measurements and accuracies.

There are few observations of winds between the cloud top level (73 km, equatorial and ~65 km polar latitudes) and the lowest accessible level for Doppler spectroscopic measurements (~90 km). The atmospheric entry probes generally provide measurements below ~64 km at best and the radio occultation technique generally provides information below ~85 km as it requires a "guess" value at the upper boundary and the derived profile becomes insensitive to the assumed value at the upper boundary at ~85 km. Thus only the balanced zonal flow can be estimated between the cloud top level and 85 km. There is thus a critical unfilled gap in the observations between ~85 and 90 km levels about the nature and magnitude of the winds.

Venus General Circulation Models (GCM) currently in varying state of maturity (see Chaps. 7 and 8) show that both super-rotation and polar vortex circulation are present, but as yet there is not unanimity in their relative significance or prominence. The maturity of the circulation models themselves as well as realism of the models regarding the physical processes in the Venus atmosphere appear to be the main issues and it is likely that future developments will narrow the gap between the simulation results.

Eventually, once the Venus GCMs are mature enough, they should be capable of providing some guidance on long term evolution of the climate on Venus and the rotation state of the solid planet by examining the exchange of angular momentum with the atmosphere. This would help understand how Venus came to rotate about itself in an anomalous way.

5.2 Meso-Thermosphere (Day-Night Circulation)

There is a lack of a consistent picture of the circulation of the upper atmosphere of Venus. However, Earth-based observations indicated that the atmospheric circulation above 100 km exhibits the sub-solar point to anti-solar point (SSAS) flow (Bougher et al. 1997; Lellouch et al. 1997) originally anticipated for Venus before

the discovery of the super-rotation of the cloud level atmosphere. Because the zonal rotation of the lower atmosphere and the diurnal circulation (day-to-night flow) of the thermosphere, the region above the cloud top (from ∼80 km to 110 km), is characterized by extremely complex dynamics. Then the global circulation in this region is difficult to characterize in detail and even more, the temporal variability is poorly understood. Wind measurements are important to help constrain global circulation models which help to provide a better overall understanding of Venus' upper atmosphere. Most of the available measurements of the combined circulation associated with zonal and SSAS winds are from Earth-based telescopes at different wavelengths using Doppler line shift measurements of selected spectral lines. Mapping of oxygen airglow at 1.27 μ and of NO in UV from Earth-based telescopes and from the VIRTIS instrument on Venus Express is now enabling some indirect inferences of vertical motions in the lower mesosphere. Whether or not the airglow feature motions represent the atmospheric flow remains to be confirmed, but kinematic models suggest that they are likely to indicate the bulk atmospheric flow. A summary of the Earth-based wind measurements can be found in Lellouch et al. (1997), and more recently, in Brecht (2011) and is also presented in Table 5.1 on page 59.

There is strong evidence of Venus' highly varying winds and complex dynamics between ∼70 km and 110 km. At the cloud tops, observations of Doppler shifts in solar Fraunhofer lines at visible wavelengths provide direct retrograde wind velocity measurements of around 100 m s^{-1} (Widemann et al. 2007; Gabsi et al. 2008; Gaulme et al. 2008; Widemann et al. 2008). This provides a general validation of the cloud tracking method from ultraviolet images, corresponding to the unity optical depth, somewhat lower than the Doppler observations. Heterodyne spectroscopy at milli-submillimeter wavelengths achieves the detection of the Doppler shift of selected molecular lines, which provides the capacity of direct measurements of the mesospheric winds, from ∼90 to 110 km. The mesospheric circulation has been observed primarily from Earth-based telescopes at milli-submillimeter wavelengths (e.g. Gurwell et al. 1995; Clancy et al. 2008; Lellouch et al. 2008; Rengel et al. 2008a,b), including interferometer facilities (Sagawa et al. 2010). Although direct comparison of the results from different instruments must be considered cautiously (requires us to assume that all instrument-related offsets have been accounted for), in general, the data show that this region is the place of strong and temporally variable winds (both retrograde super-rotating zonal "RSZ" and subsolar-to-antisolar "SSAS" winds), increasing with altitude. Near 0.1 mbar (∼93 km), winds generally strongly increase from typically 30–50 m s^{-1} with altitude to 90–120 m s^{-1} near 0.01 mbar (∼102 km) (Lellouch et al. 2008; Shah et al. 1991) with a combination of the zonal super-rotating flow and SSAS flow with fair amount of variability. At 100–110 km near-supersonic retrograde wind speeds characterizes the circulation over afternoon to evening local times (Clancy et al. 2008). On scales of ∼2,000 km the nightside wind field is variable with evidence of meridional winds. Dayside winds at low mesospheric altitudes are poorly sampled by observations. They have been measured as a predominantly zonal, 85 m s^{-1} flow at 100 km (Shah et al. 1991). Between 85 and 110 km, short-term day-to-

Table 5.1 Summary of results of measurements of thermospheric zonal flow

Altitude (km)	Observation date	Wind velocity (m s^{-1})				Method	References
		Zonal	SS-AS	Night-side	Day-side		
66	Jan. 2003	66±5–91±6				Visible/solar rad.	Gabsi et al. (2008)
67	July 2007	151±16				Visible/solar rad.	Gaulme et al. (2008)
68	Jun., Aug. 2007	90–150, 104±10				Visible/solar rad.	Widemann et al. (2008)
74	2001, 2002	83±27				Visible/CO_2	Widemann et al. (2007)
74	2001, 2002	67±21				Visible/solar rad.	Widemann et al. (2007)
∼70–80	Apr.-May 1977	94±6	-35±6			10μm heterodyna	Goldstein et al. (1991)
∼100	Feb., Apr. 1977, 1978		Detected			CO mm/submm	Gulkis et al. (1977); Schloerb et al. (1980)
∼90–105	1978–1982	Detected (weak)	Detected			CO mm/submm	Clancy and Muhleman (1985)
∼90–105	Mar. 1985, May 1988, Feb. 1990	Detected (weak)	Detected			CO mm/submm	Clancy and Muhleman (1991)
∼90–105	Dec. 1986, Apr.-May 1988	Detected (strong)	Detected			CO mm/submm	Gurwell et al. (1995)
∼90–105	Aug. 1991	Detected				CO mm/submm	Lellouch et al. (1994)
∼90–105	May-Jun. 1993		Detected (strong)			CO mm/submm	Rosenqvist et al. (1995)
∼90–105	Jun. 2009	25±8		60–110	85	CO mm/submm	Moullet et al. (2010)
95	Aug. 1991	35±15	45±15			CO mm/submm	Lellouch et al. (1994)
95±6	Nov. 1994	45±30	50±35			CO mm/submm	Rosenqvist et al. (1995)

(continued)

Table 5.1 (continued)

Altitude (km)	Observation date	Wind velocity ($m\ s^{-1}$)				Method	References
		Zonal	SS-AS	Night-side	Day-side		
~95–110	Jul.-Oct. 1991, Mar.-May 1993	Detected (var.)				O_2 IR nightglow	Crisp et al. (1996)
99±6	Apr.-May 1988	132±10	<40			CO mm/submm	Shah et al. (1991)
102	Jun. 2007	131±13	290±44	147±3		CO mm/submm	Lellouch et al. (2008)
102	Jun. 2007	46±19	114±41		63±10	CO mm/submm	Lellouch et al. (2008)
102	Aug. 2007	-30±53	55±53	120±36		CO mm/submm	Lellouch et al. (2008)
102	Aug. 2006	40±30	40±45	120±90	120±90	CO mm/submm	Lellouch et al. (2008)
103	Jun. 2007	195±70		235±70	235±70	CO mm/submm	Clancy et al. (2008)
105	Aug. 1991	95±10	95±10			CO mm/submm	Lellouch et al. (1994)
~105	Jan. 2009	Detected		~200	~0	CO mm/submm	Sagawa et al. (2010)
105±9	Nov. 1994	75±20	110±20			CO mm/submm	Rosenqvist et al. (1995)
109±1	Dec. 1985, OCt. 1986, Mar. 1987	25±15	120±30			10μ CO_2 heterodyne	Goldstein et al. (1991)
110	1990	40±3	119±2			10μ CO_2 heterodyne	Schmuelling et al. (2000)
110	1991	66±5–91±6				10μ CO_2 heterodyne	Schmuelling et al. (2000)
~110	Jun. 2007	~20–200		205–355	68–280	CO mm/submm	Rengel et al. (2008a)
110	May-Jun. 2007	3±7, 18±4	52±18			10μ CO_2 heterodyne	Sornig et al. (2008)
~100–110	Sep. 1994	140±45				CO 5 μm	Maillard et al. (1995)
~125–145	Sep. 1994	200±50				CO 5 μm	Maillard et al. (1995)

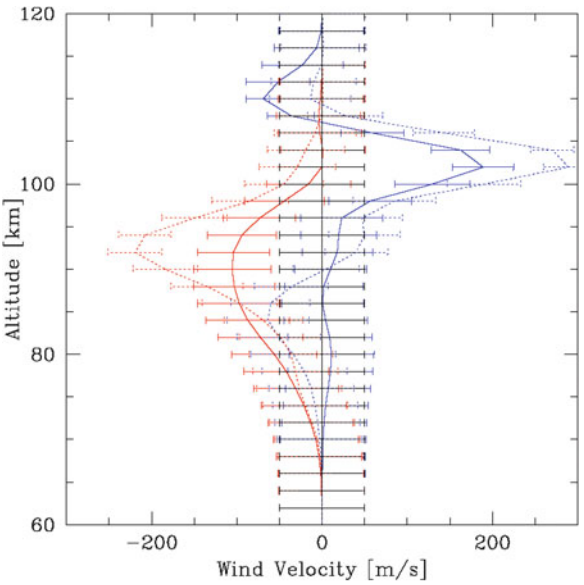

Fig. 5.1 Beam-integrated wind velocities retrieved from ^{12}CO J=2-1 spectral line observations (Rengel et al. (2008a) at two consecutive observing days, 14 and 15 June 2007 (*solid and dashed lines*) at night and day-sides (*blue and red lines*, respectively). Error bars represent the total error in the retrieval

day and also day-to-night winds have been measured from CO line observations (Rengel et al. 2008a Fig. 5.1). Day side winds are generally slower than on the night side. Measurements acquired at longer observing periods would define a pattern of variation (if any). The observational differences found between day and night is in close agreement with Zhang et al. (1996) model result. The strong cross-terminator horizontal temperature gradient is a dominant physical driver of the diurnal behavior of zonal wind in the lower mesosphere. The SSAS and zonal winds discussed above refer to the net flow-field over the observed hemisphere, whether dayside or nightside. At smaller horizontal scales, spatial and temporal variations are observed and often stronger than hemispheric temporal variations also.

The circulation at ∼95 km level is also being inferred from oxygen airglow observations from Venus Express (Gerard et al. 2009). Earth-based observations of the night side oxygen air glow show very large spatial and temporal variations suggesting that the controlling atmospheric circulation is likely to be caused by the highly variable atmospheric circulation of the nightside thermosphere (Crisp et al. 1996; Ohtsuki et al. 2008; Bailey et al. 2008).

Around 110 km, there is evidence that the RSZ winds are present but are usually weak, while the SSAS winds are ∼120 m s^{-1}. At these altitudes, the narrow non-LTE emission lines of CO_2 at 10 μm and CO at 5 μm induced by solar input enable a Doppler spectroscopic determination of winds using a similar technique as in the milli-submillimeter observations (Goldstein et al. 1991; Maillard et al. 1995; Schmuelling et al. 2000; Sornig et al. 2008). A SSAS circulation of 90–150 ms^{-1} (cross-terminator) horizontal velocities has been found (Goldstein et al. 1991). Sornig et al. (2008) report a smaller footprint than the other methods and infer a

non-existent zonal wind. However, such observations have not yet been made at polar latitudes to determine the meridional signature of the SSAS circulation in the meridional direction. Sornig et al. (2008) observed dayside winds and are also generally slower than on the night side (less than 50 m s^{-1}). They find daytime zonal wind speeds are never faster than 50 m s^{-1} at 110 km, consistent with all previous daytime zonal winds determined with this observing method, much slower than the (Clancy et al. 2007, 2008) night time zonal wind.

5.3 Transition Region

The available thermal structure observations suggest that the cyclostrophic balance breaks down at altitudes near 85 km at low latitudes (Newman et al. 1984; Limaye 1985; Piccialli et al. 2012). This is suggestive of a reversal of the meridional pressure gradient, indicating that the cyclostrophic balance does not hold. Not surprisingly, this is also the region of chaotic winds as only turbulent friction and the minuscule Coriolis force are available to balance the pressure gradient force.

The cloud top level, where the discovery of the super-rotation of Venus was made has since been measured on the day side with varying detail and temporal coverage, mostly from spacecraft data. Below the clouds the discovery of the infrared "windows" into the lower atmosphere (Allen and Crawford 1984) have yielded information about movements of the lower atmosphere attributed to between 47–53 km (Carlson et al. 1991; Crisp et al. 1991; Sanchez-Lavega et al. 2008).

5.4 Horizontal Structure/Organization

The global cloud morphology and cloud level winds are consistent with the atmospheric circulation being organized into a vortex in each hemisphere. This was first shown from Mariner 10 images acquired in 1974 and later from Pioneer Venus. In 2006, Venus Express observations showed that the vortex organization was present Limaye (2007), and in fact was identified on the day and night side simultaneously from the VIRTIS reflected solar ultraviolet and emitted near infrared observations. Although the northern hemisphere is not observed sufficiently by Venus Express due to the nature of its orbit, it is believed that the northern hemisphere also likely exhibited a similar vortex centered over the pole.

The vortex is characterized at the ultraviolet cloud level (~67 km at the equator, ~70 km at about 45 to 50 degrees latitude and ~65 km over the pole) by a gradual increase in the rotational velocity from equator to about 45 degrees latitude and weakening towards the pole at a rate comparable to but not exactly, solid-body rotation. The accompanying meridional flow at the cloud level on the dayside starts from near zero magnitude near the equator and peaks near the latitude where the

angular velocity peaks. It then weakens toward the pole. This is characteristic of the Rankine vortex, which has been extensively studied in fluid dynamics. The flow and the morphology of the ultraviolet clouds are visually very similar to a mature tropical cyclone, except for the size. Another example is having similar dimensions are the winter polar stratospheric vortices on Earth.

The vortex structure on Venus is intriguing in that it has been observed for over three decades and may be a very long term feature of the Venus atmosphere, just like the super-rotation. While the basic characteristics of the Venus vortex have been observed, many others remain unknown. Examples of such questions are given below. It is believed that suitably designed numerical simulations might at least partially answer them.

The global circulation at the level of the ultraviolet cloud tops was first deduced from Mariner 10 images (Suomi 1974; Limaye and Suomi 1981) following the discovery of the "4-day" rotation of the atmosphere from ground based telescopic images by Boyer and Guerin (1969), and from the Pioneer Venus Orbiter (Limaye et al. 1982, 1988; Rossow et al. 1990) and Galileo Fly-by observations (Belton et al. 1991; Toigo et al. 1994; Smith and Gierasch 1996; Peralta et al. 2007) and most recently from Venus Express (Moissl et al. 2009; Markiewicz et al. 2010). An assessment of these results in terms of the inferences from the cloud motions was presented by Limaye (2007).

The global cloud level morphology is also seen to evolve over time on different scales, sometimes changing in brightness and contrast very quickly (two or three orbits) and dissipating just as soon while longer term variations are also seen. The connection between cloud morphology and the measured cloud winds is difficult to ascertain with confidence as we lack means to measure the cloud top level independently.

Figure 5.2 shows composite views of the southern hemisphere in polar stereographic projection, three days apart. The features at high latitudes are influenced by the presence of dynamical instabilities which arise in the presence of latitudinal shear in the zonal flow (Limaye et al. 2009) also seen in tropical cyclones. Luz et al. (2011) provide evidence of asymmetry in the inner core region of this hemispheric vortex.

5.5 Cloud Level Zonal Average Flow

For the purpose of comparisons with the GCM results, the cloud tracking results provide the best coverage over latitude-longitude, temporal coverage and time of day variations. We now have estimates for the cloud level flow over a span of 35 years between Mariner 10 results obtained in 1974 and those being obtained from Venus Express at present (UV cloud top level and a lower level from NIR images from VIRTIS). The results obtained so far (e.g. Figs. 5.3 and 5.4) from Venus Express VMC (Moissl et al. 2009) have been from somewhat lower resolution

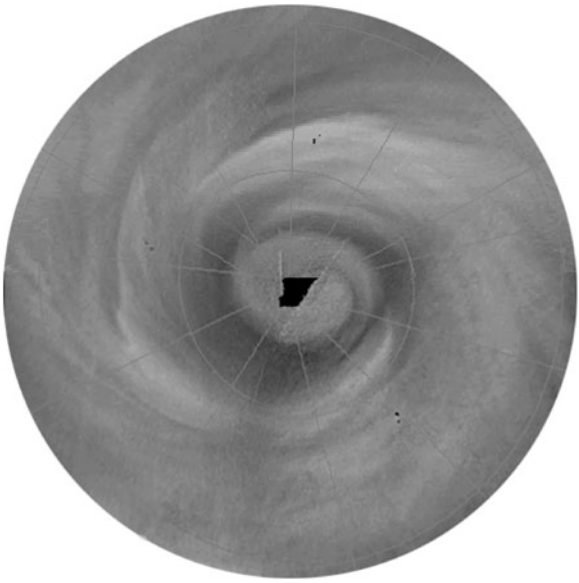

Fig. 5.2 Space-time composite views of the southern hemisphere of Venus created from ultraviolet images from the Venus Monitoring Camera on Venus Express (three consecutive orbits). The outer periphery is the equator and the South Pole is at the center. The nearly continuous coverage from Venus Express shows a constantly evolving vortex structure (Credit: ESA)

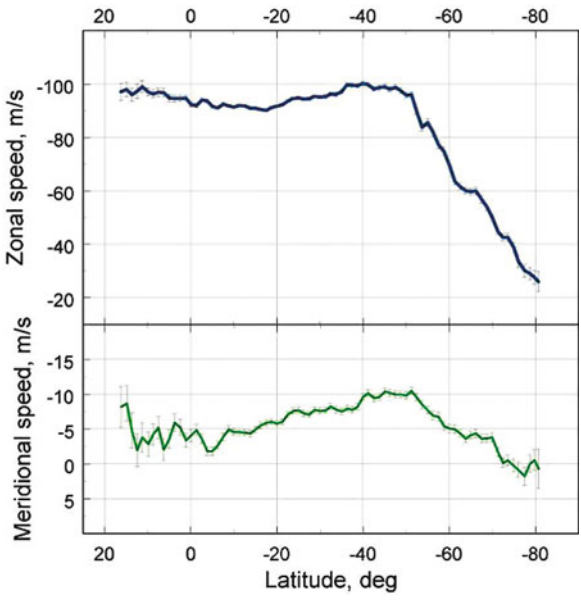

Fig. 5.3 Visual cloud tracking results from VMC UV (from (Markiewicz et al. 2010). The E-W component and N-S components are shown as a function of the average latitudes of the tracked clouds. The *smooth curve* represents a polynomial fit to the data

(∼40 km per pixel) and may be indicative of very large scale flow, somewhat slower than the ambient winds. This is indicated by the disagreement with the balanced zonal flow estimated from thermal structure and the inferred cloud top level altitude (Ignatiev et al. 2009; Piccialli et al. 2012).

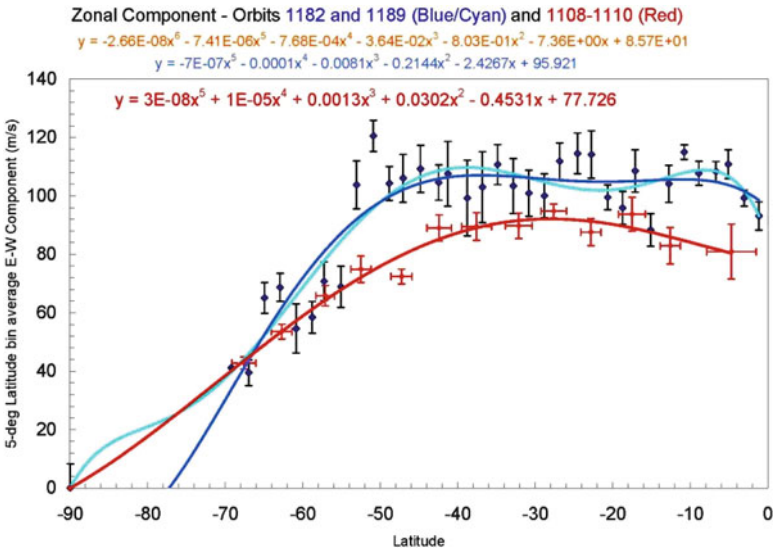

Fig. 5.4 Digital cloud tracking results obtained at University of Wisconsin from VMC images acquired on orbits 1108–1109 and during 1182–1189, showing a somewhat different latitudinal dependence. The E-W component is shown as a function of the average latitudes of the tracked clouds. The smooth curve represents a polynomial fit to the data. Similar results have been obtained from visual and digital tracking at IKI from VMC data and VIRTIS-M data (Hueso et al. 2012)

5.6 Circulation: Varying Winds or Varying Cloud Height?

Analysis of the VIRTIS data has indicated that the UV cloud top altitude varies gradually from near the equator to the South Pole (Ignatiev et al. 2009). It is quite possible and likely that the cloud top altitude also varies over time and with longitude. It is thus quite likely that the observed cloud motions refer to different altitudes. The observed thermal structure from radio occultation and VIRTIS inferred temperature profiles from infrared spectral observations show that the thermal wind (vertical shear of the zonal flow) with assumed cyclostrophic balance between 60–70 km is $\sim$10 m s^{-1}/km as estimated from the Venus Express radio occultation profiles (Piccialli et al. 2012).

Figure 5.4 shows a comparison of the day-side longitude average of the zonal component over two short periods separated by about 11 weeks to illustrate the differences over time. Similar differences are seen on shorter time scales which have been interpreted in the past as indicative of planetary scale waves (Del Genio and Rossow 1990). What has not been confirmed however, is whether this change is due to real changes in the mass field or spurious due to change in the effective level of cloud motions. This is supported by the significant level of vertical shear of the zonal flow indicated by the thermal data and the balanced flow assumption (4.15, from Piccialli et al. 2012). Another concern is that the short term variations are

accompanied by some changes in the cloud morphology, which impacts the number of suitable discrete cloud features available for tracking. Thus, the changes in the measured cloud motions could be simply a sampling effect which provides far fewer discrete cloud features that can be tracked unambiguously. Following (Limaye et al. 2010), we summarize aspects of the circulation as requiring additional observations are as follows:

- Global longitudinal and latitudinal structure of the zonal and meridional flow at a known level over at least one Venus day
- Vertical structure of the horizontal flow, which is also critical to understanding the Hadley cell structure at multiple levels
- Amplitudes and phases of solar thermal tidal winds at any level
- Reliable estimates of zonal and time-averaged latitudinal profiles of the meridional transports of absolute angular momentum, heat and trace species at any level
- Exchange of angular momentum between the atmosphere and the solid planet over time
- Middle atmosphere circulation (70–140 km) at high spatial and temporal resolution
- Structure of planetary and small scale waves and their role in the atmospheric circulation
- Some information about the near surface winds to elucidate the momentum exchange between the surface and the solid planet. Measurements of the wind speed and direction at low, mid and high latitudes are essential, but very difficult to obtain.

Future missions, which are capable of returning such measurements are discussed in Chap. 10.

5.7 Transport of Momentum

One goal of cloud tracking measurements is to estimate the transport of angular momentum across latitudes. The VMC cloud tracking measurements have a limiting resolution of > 5 m s^{-1} in the zonal and meridional components and for this reason such estimates have not yet been attempted.

The published results from recent GCMs achieve super-rotation and one or both mechanisms that have been invoked to maintain the super-rotation of the Venus atmosphere—the so called Gierasch mechanism in which angular momentum is transported to the equatorial region by the eddies at the cloud top level, and the solar thermal tides which have been invoked primarily to transport angular momentum in the vertical direction towards the surface. However, we are not yet at a point where we can make detailed comparisons of observations with model results.

A lot more work is needed to improve the models but also to obtain detailed wind field estimates at multiple levels of the Venus atmosphere for both day and night

sides. Tracking clouds is essential for obtaining estimates of the eddy circulation, but other emerging tools such as Doppler LIDAR from orbiting spacecraft may also provide better measurements in the future. The question of obtaining a reliable longitudinal average of zonal and meridional components at the same level on day and night side at any level is presently possible only from deployment of long-lived balloons in the Venus atmosphere.

References

D.A. Allen, J.W. Crawford, Cloud structure on the dark side of Venus. Nature **307**, 222–224 (1984)

J. Bailey, S. Chamberlain, D. Crisp, V.S. Meadows, Near infrared imaging spectroscopy of Venus with the Anglo-Australian telescope. Planet Space Sci. **56**, 1385–1390 (2008)

M.J.S. Belton, P.J. Gierasch, M.D. Smith, P. Helfenstein, P.J. Schinder, J.B. Pollack, K.A. Rages, A.P. Ingersoll, K.P. Klaasen, J. Veverka, C.D. Anger, M.H. Carr, C.R. Chapman, M.E. Davies, F.P. Fanale, R. Greeley, R. Greenberg, J.W. Head, D. Morrison, G. Neukum, C.B. Pilcher, Images from Galileo of the Venus cloud deck. Science **253**, 1531–1536 (1991)

S.W. Bougher, M.J. Alexander, H.G. Mayr, Upper atmosphere dynamics: global circulation and gravity waves, in *Venus II: Geology, Geophysics, Atmosphere, and Solar Wind Environment*, ed. by S.W. Bougher, D.M. Hunten, R.J. Philips Tucson, AZ, University of Arizon Press (1997), pp. 259–291

S.W. Bougher, S. Rafkin, P. Drossart, Dynamics of the Venus upper atmosphere: Outstanding problems and new constraints expected from Venus Express. Planet Space Sci. **54**, 1371–1380 (2006)

C. Boyer, P. Guerin, Study of retrograde rotation, in 4 days, of exterior cloud layer of Venus. Icarus **11**, 338–351 (1969)

A.S. Brecht, *Tracing the Dynamics in Venus' Upper Atmosphere*, Ph.D. Thesis, University of Michigan (2011)

R.W. Carlson, K.H. Baines, L.W. Kamp, P.R. Weissman, W.D. Smythe, A.C. Ocampo, T.V. Johnson, D.L. Matson, J.B. Pollack, D. Grinspoon, Galileo infrared imaging spectroscopy measurements at Venus. Science **253**, 1541–1548 (1991)

R. Clancy, B.J. Sandor, G.H. Moriarty-Schieven, Dynamics of the Venus upper atmosphere: Global-temporal distribution of winds, temperature, and CO at the Venus mesopause. Bull. Amer. Astron. Soc. **39**, 539 (2007)

R.T. Clancy, D.O. Muhleman, Diurnal CO variations in the Venus mesosphere from CO Microwave-Spectra. Icarus **64**, 157–182 (1985)

R.T. Clancy, D.O. Muhleman, Long-term (1979–1990) changes in the thermal, dynamical, and compositional structure of the Venus mesosphere as inferred from microwave spectral line observations of C-12O, C-13O, and CO-18. Icarus **89**, 129–146 (1991)

R.T. Clancy, B.J. Sandor, G.H. Moriarty-Schieven, Venus upper atmospheric CO, temperature, and winds across the afternoon/evening terminator from june 2007 JCMT sub-millimeter line observations. Planet Space Sci. **56**, 1344–1354 (2008)

D. Crisp, S. McMuldroch, S.K. Stephens, W.M. Sinton, B. Ragent, K.-W. Hodapp, R.G. Probst, L.R. Doyle, D.A. Allen, J. Elias, Ground-based near-infrared imaging observations of Venus during the Galileo encounter. Science **253**, 1538–1541 (1991)

D. Crisp, V.S. Meadows, B. Bezard, C. deBergh, J.P. Maillard, F.P. Mills, Ground-based near-infrared observations of the Venus nightside: 1.27-μ m o-2(a(1)delta(g)) airglow from the upper atmosphere. J. Geophys. Res.-Planets **101**, 4577–4593 (1996)

A.D. Del Genio, W.B. Rossow, Planetary-scale waves and the cyclic nature of cloud top dynamics on Venus. J. Atmos. Sci. **47**, 293–318 (1990)

Y. Gabsi, J.-L. Bertaux, A. Hauchecorne, J. Schmitt, S. Guibert, Measuring Venus' winds using the absolute astronomical accelerometer: solid superrotation model of Venus' clouds. Plan. Space Sci. **56**, 1454–1466 (2008). doi:10.1016/j.pss.2008.07.016

P. Gaulme, F. Schmider, C. Grec, A. Lopez-Ariste, T. Widemann, B. Gelly, Venus wind map at cloud top level with the MTR/THEMIS visible spectrometer, I: instrumental performance and first results. Planet. Space Sci. **56**, 1335–1343 (2008). doi:10.1016/j.pss.2008.06.014

J.C. Gerard, C. Cox, L. Soret, A. Saglam, G. Piccioni, J.L. Bertaux, P. Drossart, Concurrent observations of the ultraviolet nitric oxide and infrared O(2) nightglow emissions with Venus Express. J. Geophys. Res.-Planets **114**, E00B44 (2009)

P.J. Gierasch, R.M. Goody, R.E. Young, D. Crisp, C. Edwards, R. Kahn, D. Rider, A. Del Genio, R. Greeley, A. Hou, C.B. Leovy, D. McCleese, M. Newman, The general circulation of the Venus atmosphere: an assessment, in *Venus II: Geology, Geophysics, Atmosphere, and Solar Wind Environment*, ed. by S.W. Bougher, D.M. Hunten, R.J. Philips, Tucson, AZ, University of Arizon Press, p. 459 (1997)

J.J. Goldstein, M.J. Mumma, T. Kostiuk, D. Deming, F. Espenak, D. Zipoy, Absolute wind velocities in the lower thermosphere of Venus using infrared heterodyne spectroscopy. Icarus **94**, 45–63 (1991)

S. Gulkis, R.K. Kakar, M.J. Klein, E.T. Olsen, W.J. Wilson, Venus – detection of variations in stratospheric carbon monoxide, in *Proceedings of the 19th Symposium on Planetary Atmospheres (A79-13101 03-91)*, Ottawa, 16–19 August 1977 (Royal Society of Canada, Ottawa, 1977), pp. 61–65

M.A. Gurwell, D.O. Muhleman, K.P. Shah, G.L. Berge, D.J. Rudy, A.W. Grossman, Observations of the co bulge on Venus and implications for mesospheric winds. Icarus **115**, 141–158 (1995)

R. Hueso, J. Peralta, A. Sanchez-Lavega, Assessing the long-term variability of Venus winds at cloud level from VIRTIS-Venus Express. Icarus **217**, 585–598 (2012)

N.I. Ignatiev, D.V. Titov, G. Piccioni, P. Drossart, W.J. Markiewicz, V. Cottini, T. Roatsch, M. Almeida, N. Manoel, Altimetry of the Venus cloud tops from the Venus Express observations. J. Geophys. Res.-Planets **114**, E00B43 (2009)

E. Lellouch, J.J. Goldstein, J. Rosenqvist, S.W. Bougher, G. Paubert, Global circulation, thermal structure, and carbon-monoxide distribution in Venus mesosphere in 1991. Icarus **110**, 315–339 (1994)

E. Lellouch, T. Clancy, D. Crisp, A. Kliore, D. Titov, and S.W. Bougher, *Monitoring of Mesospheric Structure and Dynamics, Venus II* (Tucson, AZ, University of Arizona Press, 1997)

E. Lellouch, G. Paubert, R. Moreno, A. Moullet, Monitoring Venus' mesospheric winds in support of Venus Express: IRAM 30-m and APEX observations. Planet Space Sci. **56**, 1355–1367 (2008)

C.B. Leovy, Rotation of the upper atmosphere of Venus. J. Atmos. Sci. **30**, 1218–1220 (1973). doi:10.1175/1520-0469(1973)030

S. Limaye, M. Allen, S. Atreya, K. Baines, J.-L. Bertaux, G. Bjoraker, M. Bullock, E. Chassefiere, G. Chin, C. Covey, D. Grinspoon, S. Gulkis, V. Kerzhanovich, S. Lewis, K. McGouldrick, W. Markiewicz, R. Pertzborn, C. Rozoff, G. Piccioni, G. Schubert, L. Sromovsky, C. Wilson, Y. Yung, Venus atmosphere: Major questions and required observations. input to the national academies planetary science decadal survey, Tech. Rep., Lunar and Planetary Institute, URL www.lpi.usra.edu/vexag (2010)

S.S. Limaye, Venus atmospheric circulation: Observations and implications of the thermal structure. Adv. Space Res. **5**, 51–62 (1985)

S.S. Limaye, Venus atmospheric circulation: Known and unknown. J. Geophys. Res. **112**, E04S09 (2007). doi:10.1029/2006JE002814

S.S. Limaye, V.E. Suomi, Cloud motions on Venus – global structure and organization. J. Atmos. Sci. **38**, 1220–1235 (1981)

S.S. Limaye, C.J. Grund, S.P. Burre, Zonal mean circulation at the cloud level on Venus – spring and fall 1979 ocpp observations. Icarus **51**, 416–439 (1982)

S.S. Limaye, C. Grassotti, M.J. Kuetemeyer, Venus – cloud level circulation during 1982 as determined from pioneer cloud photopolarimeter images. 1. time and zonally averaged circulation. Icarus **73**, 193–211 (1988)

S.S. Limaye, J.P. Kossin, C. Rozoff, G. Piccioni, D.V. Titov, W.J. Markiewicz, Vortex circulation on Venus: Dynamical similarities with terrestrial hurricanes. Geophys. Res. Lett. **36**, L04204 (2009). doi:10.1029/2008GL036093

E.N. Lorenz, *The Nature and Theory of the General Circulation of the Atmosphere* (World Meteorological Organization Monograph, Geneva, 1967)

D. Luz, D.L. Berry, G. Piccioni, P. Drossart, R. Politi, C.F. Wilson, S. Erard, F. Nuccilli, Venus's southern polar vortex reveals precessing circulation. Science **332**, 577–580 (2011)

E. Maillard, J.-P. abd Lellouch, J. Crovisier, C. de Bergh, B. Bezard, Carbon monoxide 4.7 μm emission: A new dynamical probe of Venus' thermosphere. Bull. Amer. Astron. Soc. **27**, 1080 (1995)

W.J. Markiewicz, D. Titov, E. Petrova, N. Ignatiev, I. Khatuntsev, R. Moissl, S.S. Limaye, O. Shalygina, M. Almeida, 1500 Earth days around Venus imaging with Venus, monitoring camera on Venus Express. Presented at the VEXAG International Conference. URL http://venus.wisc.edu/workshop/VEXAG_2010_Workshop_Abstracts_%Portfolio.pdf (2010)

R. Moissl, I. Khatuntsev, S.S. Limaye, D.V. Titov, W.J. Markiewicz, N.I. Ignatiev, T. Roatsch, K.-D. Matz, R. Jaumann, M. Almeida, G. Portyankina, T. Behnke, S.F. Hviid, Venus cloud top winds from tracking UV features in Venus monitoring camera images. J. Geophys. Res. **114**, E00B31 (2009). doi:10.1029/2008JE003117

A. Moullet, R. Moreno, E. Lellouch, H. Sagawa, M. Gurwell, Wind measurements in Venus' upper mesosphere with the IRAM-Plateau De Bure interferometer. Bull. Am. Astron. Soc. **42**, 974 (2010)

M. Newman, G. Schubert, A.J. Kliore, I.R. Patel, Zonal winds in the middle atmosphere of Venus from Pioneer Venus radio occultation data. J. Atmos. Sci. **41**, 1901–1913 (1984)

S. Ohtsuki, N. Iwagami, H. Sagawa, M. Ueno, Y. Kasaba, T. Imamura, K. Yanagisawa, E. Nishihara, Distributions of the Venus 1.27-μm O-2 airglow and rotational temperature. Planet Space Sci. **56**, 1391–1398 (2008)

J. Peralta, R. Hueso, A. Sanchez-Lavega, A reanalysis of venus winds at two cloud levels from Galileo SSI images. Icarus **190**, 469–477 (2007)

A. Piccialli, S. Tellmann, D. Titov, S.S. Limaye, I.V. Khatuntsev, M. Patzold, B. Haussler, Dynamical properties of the Venus mesosphere from the radio-occultation experiment Vera onboard Venus Express. Icarus **217**, 669–681 (2012)

P. Read, Super-rotation and diffusion of axial angular momentum: II. A review of quasi-axisymmetric models of planetary atmospheres. Quater. J. R. Met. Soc. **112**, 253–272 (1986)

M. Rengel, P. Hartogh, C. Jarchow, HHSMT observations of the Venusian mesospheric temperature, winds, and CO abundance around the MESSENGER flyby. Planet Space Sci. **56**(13), doi:10.1016/j.pss.2008.07.014 Asia Oceania Geosci. Soc. (2008a)

M. Rengel, P. Hartogh, C. Jarchow, Mesospheric vertical thermal structure and winds on Venus from HHSMT CO spectral-line observations. Planet Space Sci. **56**, 1368–1384 (2008b)

J. Rosenqvist, E. Lelloucj, T. Encrenaz, G. Paubert, Global circulation in Venus' mesosphere from IRAM CO observations (1991–1994): A tribute to Jan Rosenqvist. Bull. Am. Astron. Soc. **27**, 1080 (1995)

W.B. Rossow, A.D. DelGenio, T. Eichler, Cloud-tracked winds from Pioneer-Venus Ocpp images. J. Atmos. Sci. **47**, 2053–2084 (1990)

H. Sagawa, P. Hartogh, M. Rengel, Interferometric measurements of Venus mesospheric wind using millimeter/submillimeter interferometers, in *International Venus Conference*, Aussois, 20–26 June 2010

A. Sanchez-Lavega, R. Hueso, G. Piccioni, P. Drossart, J. Peralta, S. Perez-Hoyos, C.F. Wilson, F.W. Taylor, K.H. Baines, D. Luz, S. Erard, S. Lebonnois, Variable winds on Venus mapped in three dimensions. Geophys. Res. Lett. **35**, L13204 (2008)

F.P. Schloerb, S.E. Robinson, W.M. Irvine, Observations of CO in the stratosphere of Venus via its J = O-1 rotational transition. Icarus **43**, 121–127 (1980)

F. Schmuelling, J. Goldstein, T. Kostiuk, T. Hewagama, D. Zipoy, High precision wind measurements in the upper Venus atmosphere. Bull. Am. Astron. Soc. **32**, 1121 (2000)
G. Schubert, General circulation and the dynamical state of the Venus atmosphere. Venus (1983)
G. Schubert, S.W. Bougher, C.C. Covey, A.D. Del Genio, A.S. Grossman, J.L. Hollingsworth, S.S. Limaye, R.E. Young, Venus atmosphere dynamics: A continuing enigma, in *Exploring Venus as a Terrestrial Planet*, ed. by L.W. Esposito, E.R. Stofan, T.E. Cravens (American Geophysical Union, Washington, DC, 2007), pp. 101–120
A. Seiff, Thermal structure of the atmosphere of Venus, in *Venus*, ed. by D.M. Hunten, L. Colin, T.M. Donahue, V.I. Moroz (Tucson, AZ, University of Arizona Press, 1983), pp. 215–279
K.P. Shah, D.O. Muhleman, G.L. Berge, Measurement of winds in Venus upper mesosphere based on doppler shifts of the 2.6-Mm (Co)-C-12 line. Icarus **93**, 96–121 (1991)
M.D. Smith, P.J. Gierasch, Global-scale winds at the venus cloud-top inferred from cloud streak orientations. Icarus **123**, 313–323 (1996)
M. Sornig, T. Livengood, G. Sonnabend, P. Kroetz, D. Stupar, T. Kostiuk, R. Schieder, Venus upper atmosphere winds from ground-based heterodyne spectroscopy of CO2 at 10 mu m wavelength. Planet Space Sci. **56**, 1399–1406 (2008)
L.A. Sromovsky, H.E. Revercomb, V.E. Suomi, Temperature structure in the lower atmosphere of Venus: New results derived from Pioneer Venus entry probe measurements. Icarus **62**, 458–493 (1985)
V.E. Suomi, (1974) Observations of cloud motions. Presented at the conference of the atmosphere of venus, Tech. Rep., Goddard Institute of Space Studies, NASA Report SP-382
A. Toigo, P.J. Gierasch, M.D. Smith, High-resolution cloud feature tracking on Venus by Galileo. Icarus **109**, 318–336 (1994)
T. Widemann, E. Lellouch, A. Campargue, New wind measurements in Venus' lower mesosphere from visible spectroscopy. Planet. Space Sci. **55**, 1741–1756 (2007). doi:10.1016/j.pss.2007.01.005
T. Widemann, E. Lellouch, J.-F. Donati, Venus doppler winds at cloud tops observed with ESPaDOnS at CFHT. Planet. Space Sci. **56**, 1320–1334 (2008). doi:10.1016/j.pss.2008.07.005
L.V. Zasova, N. Ignatiev, I. Khatuntsev, V. Linkin, Structure of the Venus atmosphere. Planet Space Sci. **55**, 1712–1728 (2007)
S. Zhang, S.W. Bougher, M.J. Alexander, The impact of gravity waves on the Venus thermosphere and O-2 IR nightglow. J. Geophys. Res.-Planets **101**, 23195–23205 (1996)

Part II
Modeling the Atmospheric Circulation of Venus

Chapter 6
The Dynamics and Circulation of Venus Atmosphere

Peter L. Read

In this chapter we introduce a number of basic dynamical ideas and concepts that are useful in understanding the large-scale circulation of Venus's atmosphere. Some of these are of interest from an historical viewpoint, having influenced thinking on this subject at an earlier time. But most are still very relevant for interpreting modern observations, measurements and for formulating and interpreting models. We begin by considering basic conservation principles that provide key constraints on the circulation and go on to investigate the main dynamical balances prevalent in the atmosphere. The chapter goes on to discuss the main eddy processes that are likely to play a significant role in maintaining Venus's atmospheric super-rotation, including planetary waves, gravity waves and thermal tides, their likely origins and how they interact with the zonal flow. The chapter concludes with a brief discussion of how the atmosphere interacts with the underlying surface.

6.1 Introduction

As a result of the slow rotation of the planet, its near circular orbit and small obliquity, the underlying circulation of Venus' atmosphere is relatively simple in form. The Sun is always close to being directly overhead above the equator at local noon, to within a couple of degrees, so the air warmed at low latitudes rises and moves towards the poles, where it cools and descends before returning equatorwards at lower altitudes. On top of this simple picture are superimposed various complications. One that has been observed for many decades, but remains difficult to explain, is the global 'super-rotation', which manifests itself in cloud structures

P.L. Read (✉)
Atmospheric, Oceanic & Planetary Physics, University of Oxford, UK
e-mail: p.read1@physics.ox.ac.uk

L. Bengtsson et al. (eds.), *Towards Understanding the Climate of Venus*, ISSI Scientific Report Series 11, DOI 10.1007/978-1-4614-5064-1_6,

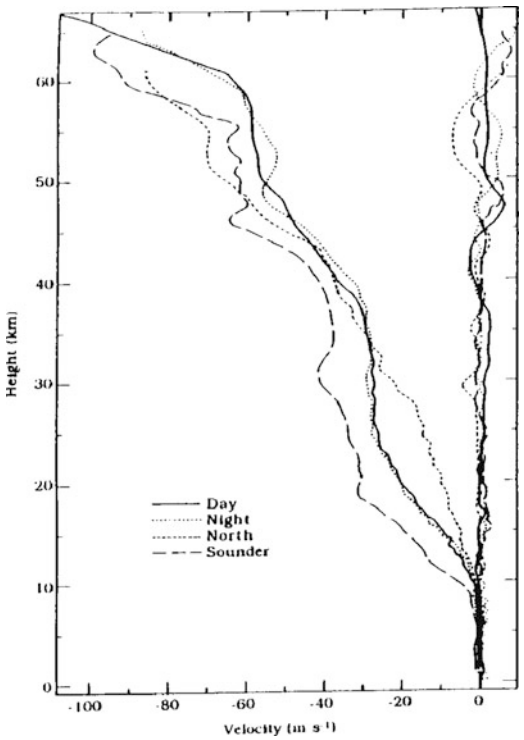

Fig. 6.1 Profiles of the zonal (east-to-west) and meridional (equator-to-pole) wind on Venus as measured by tracking the Pioneer Venus entry probes, after Counselman et al. (1980). Note the suggestion of global layering, which has been interpreted as suggesting stacked "Hadley" circulation cells of considerable latitudinal extent

which move rapidly around the planet in a direction almost parallel to the equator. The cloud markings, which appear with high contrast through an ultraviolet filter, have their origin at heights 60 or 70 km above the surface (where the pressure is of the order of 10 hPa) and travel around the equator in 4–5 days, corresponding to speeds near 100 m s^{-1}. This is more than 50 times faster than the rotation rate of the surface below. Measurements of the winds below the clouds (Fig. 6.1; Counselman et al. (1980)), and calculations (from temperature data) of the winds above the cloud tops, show that the zonal wind speed declines at higher and lower levels, reaching values near zero at about 100 km and near the surface respectively. Direct measurements of the winds 1 m or so above the surface by the Russian landers Venera 9 and 10, found velocities of $\leq$1 m s^{-1}. Tracking of the Pioneer and Venera landers during their descent showed that there is a steady decrease with height from the 100 m s^{-1} or so observed in the ultraviolet markings near the cloud tops. Earth-based observers had earlier shown, by the measurement of Doppler shifted emission lines from atmospheric gases, that the cloud-tracked winds do, in fact, apply to mass motions, rather than the phase speed of waves as had also been suggested.

6.2 Basic Equations and Cyclostrophic Balance

In common with other planetary atmospheres, the dynamics of the Venus atmosphere are governed by a combination of the Navier-Stokes equation, together with equations of continuity and thermodynamic energy conservation and a suitable equation of state. For most purposes, the Navier-Stokes equations are usually approximated by the so-called meteorological primitive equations for a shallow atmosphere on the sphere, expressed in component form as

$$Du/Dt - uv\,\tan\phi/a - 2\Omega v\,\sin\phi + 1/(\rho a\,\cos\phi)\partial p/\partial\lambda = F_\lambda \tag{6.1}$$

$$\underset{(1)}{Dv/Dt} + \underset{(2)}{u^2\tan\phi/a} + \underset{(3)}{2\Omega u\,\sin\phi} + \underset{(4)}{1/(\rho a)\partial p/\partial\phi} = \underset{(5)}{F_\phi} \tag{6.2}$$

$$g + \frac{1}{\rho}\frac{\partial p}{\partial z} = 0. \tag{6.3}$$

The continuity equation can be written most simply using pressure as the vertical coordinate as

$$\frac{1}{a\,\cos\phi}\frac{\partial u}{\partial\lambda} + \frac{1}{a\,\cos\phi}\frac{\partial}{\partial\phi}(v\,\cos\phi) + \frac{\partial\omega}{\partial p} = 0, \tag{6.4}$$

where $\omega = Dp/Dt$ represents the vertical velocity expressed in terms of pressure. The thermodynamic energy equation for a dry atmosphere is most simply represented in terms of potential temperature as

$$\frac{D\theta}{Dt} = \frac{Q}{c_p}\left(\frac{p}{p_0}\right)^{-\kappa}, \tag{6.5}$$

where $\theta = T(p_0/p)^\kappa$, $\kappa = R/c_p$ with specific gas constant R, heat capacity at constant pressure, c_p and reference pressure, p_0. For the equation of state, this is usually taken as the perfect gas law

$$p = \rho RT. \tag{6.6}$$

Equation (6.3) represents hydrostatic balance, which is a considerable simplification of the full vertical equation of motion but is a very good approximation for large-scale motion. For rapidly rotating planets, Ω is relatively large so that the dominant balance in (6.2) is between terms (3) and (4), and is known as *geostrophic*. For slowly rotating planets, such as Venus, however, term (3) in (6.2) is too small to balance the pressure gradient (term (4)) so that the centrifugal term (2) takes over. The resulting balance between terms (2) and (4) is known as *cyclostrophic*, as first identified by Leovy (1973). For intermediate rotation rates, terms (2), (3) *and* (4) are of comparable magnitude and the resulting balance of these three terms is known as *gradient wind* balance.

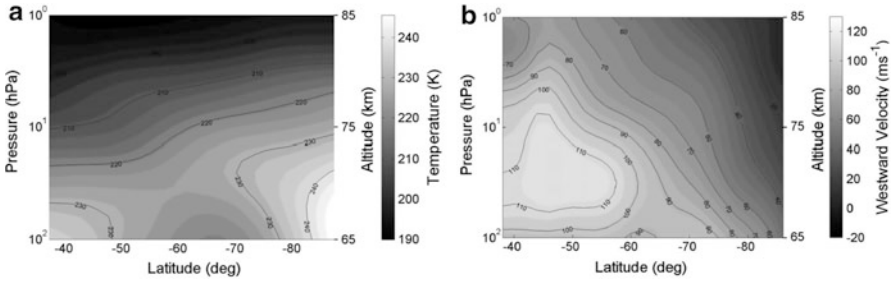

Fig. 6.2 (**a**) Temperature field in the meridional plane on Venus for 24.00 local time from the VIRTIS instrument on the Venus Express spacecraft Grassi et al. 2010, (**b**) zonal velocity field retrieved by vertical integration of the cyclostrophic thermal wind equation by Mendonca et al. (2012). Reprinted with the permission from Elsevier

By combining Eqs. (6.2), (6.3) and (6.6), a further equation can be derived for the vertical derivative of u. In pressure coordinates, this becomes

$$\frac{\partial u^2}{\partial \zeta} = -\frac{R}{\tan\phi}\left(\frac{\partial T}{\partial \phi}\right)_p, \tag{6.7}$$

where $\zeta = \ln(p/p_0)$, and is referred to as the *cyclostrophic thermal wind equation*.

In so far as cyclostrophic balance is approximately satisfied by the flow, given a latitudinal profile of $\overline{u}(\phi)$ at a particular pressure level, (6.7) can be integrated upwards to recover the complete field of $\overline{u}$ in ζ and ϕ. An example of this is shown in Fig. 6.2, using temperature measurements obtained by the VIRTIS instrument on the Venus Express spacecraft (Grassi et al. 2010)This 'super-rotation' of the Venus atmosphere is perhaps the most remarkable feature of its dynamical behavior, and so we go on now to consider how to understand and investigate this phenomenon from a quantitative point of view. But first of all, how should we define super-rotation in a quantitative manner, and why is it so remarkable?

6.3 Angular Momentum and Hide's Theorems

In any atmospheric circulation system the flow must everywhere satisfy certain key conservation principles in relation to energy, momentum and angular momentum. The latter two quantities are strictly vectors, but in the case of angular momentum, it is straightforward to show that the axial component may be conserved under certain circumstances that we will now explore.

In practice, it is most convenient to consider the absolute axial component of specific angular momentum, m, which we can define in conventional meteorological spherical polar coordinates as

$$m = a\ \cos\phi(\Omega a\ \cos\phi + u), \tag{6.8}$$

where a is the planetary radius, Ω the planetary rotation speed, u is the zonal velocity as measured in the frame rotating with the planet and ϕ is latitude.

6.3.1 Hide's Theorem I

First consider the situation where the flow is frictionless and axisymmetric about the pole of the planet, with no other body force acting. Under these circumstances, the zonal equation of motion becomes

$$\frac{\partial u}{\partial t} + \frac{v}{a}\frac{\partial u}{\partial \phi} + w\frac{\partial u}{\partial z} - \frac{uv\,\tan\phi}{a} - 2\Omega v\,\sin\phi = 0. \tag{6.9}$$

From a comparison of $a\,\cos\phi\times$ (6.8) with (6.9), one can substitute m for u to obtain

$$\frac{\partial m}{\partial t} + \frac{v}{a}\frac{\partial m}{\partial \phi} + w\frac{\partial m}{\partial z} = \frac{Dm}{Dt} = 0. \tag{6.10}$$

This implies that the axial component of absolute axial angular momentum, m, is conserved following the motion in the meridional (ϕ, z) plane, meaning that axial angular momentum per unit mass in rings of fluid aligned along latitude circles behaves like a conserved tracer. Once a ring of fluid has been initialized with a certain value of m, there is no means of changing it in the absence of friction or body forces. In other words, there can be no torque on such a ring of fluid unless we relax one of the conditions relating to axisymmetry, friction or some other external force acting in the zonal direction.

In the case of a planet like Venus, therefore, the fact that u is observed to be large on the equator and in the same sense as the planetary rotation implies that m must exceed Ωa^2, which is the maximum value of m for any point on the planet that co-rotates with the planet itself. In a sense, this serves as a 'conceptual speed limit' for atmospheric flow, since if we observe $m > \Omega a^2$ anywhere in the atmosphere, it cannot have acquired this without a special initial condition in the absence of friction or non-axisymmetric motion (and consequent zonal pressure torques). It also suggests a way to define a non-dimensional measure of 'local super-rotation' in the form

$$s = \frac{m}{\Omega a^2} - 1, \tag{6.11}$$

so that $s \leq 0$ for any flow starting with initial conditions in solid body rotation with the underlying surface.

The globally integrated axial angular momentum in such a system is similarly constrained to a constant value set by the initial conditions, suggesting a further measure of 'global super-rotation', S, defined by

$$S = \int\int\int m\,dV/M_0 - 1 \tag{6.12}$$

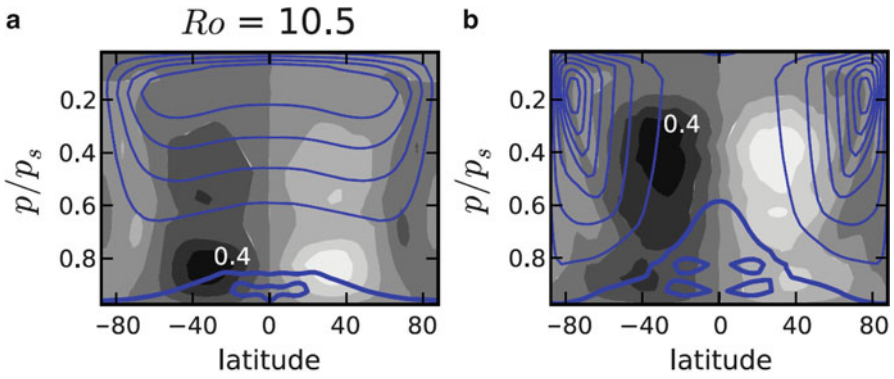

Fig. 6.3 Contour maps of zonal mean zonal flow and meridional stream function for the equilibrated flow in a slowly-rotating atmospheric simulation (**a**) in a fully three-dimensional simulation and (**b**) in a two-dimensional, axisymmetric simulation under the same thermal forcing and boundary conditions. Adapted from the results of simulations by Mitchell and Vallis (2010). Solid contours represent the zonal velocity and shaded contours the meridional mass streamfunction

where dV is an element of volume and M_0 represents the integrated absolute angler momentum of the fluid in solid-body rotation at rotation rate Ω.

For a purely inviscid, axisymmetric system, therefore, both s and S can never exceed zero without invoking rather special initial conditions. This was a result first discussed in this context by Hide (1969) and is sometimes referred to as "Hide's first theorem" (e.g. Read 1986), and was used, for example, by Hide (1970) to refute the suggestion by Gierasch and Stone (1968) that inviscid, symmetric baroclinic instability could account for the super-rotating equatorial jet stream on Jupiter. Hide's arguments were subsequently borne out by later work that included the effects of viscous friction (Walton 1975). It can also be clearly illustrated in numerical simulations where care is taken to minimise the effects of internal numerical diffusion. Figure 6.3 shows two examples that illustrate and contrast the resulting flows when eddy-zonal flow interactions are suppressed (Fig. 6.3b) from those with fully three-dimensional eddies present. The 2D flow spins up high latitude prograde jets but with essentially no zonal flow over the equator. With resolved eddies, however, the equator can be brought into near-solid body rotation with higher latitudes (Fig. 6.3a) because of eddy fluxes of angular momentum.

6.3.2 Hide's Theorem II

When non-axisymmetric eddies (or viscous friction) are present, these arguments can be further generalized (Schneider 1977; Held and Hou 1980), based on the suppose properties of angular momentum transfer by an 'eddy viscosity'. In these arguments, it is suggested that steady, prograde equatorial flow cannot occur, even in

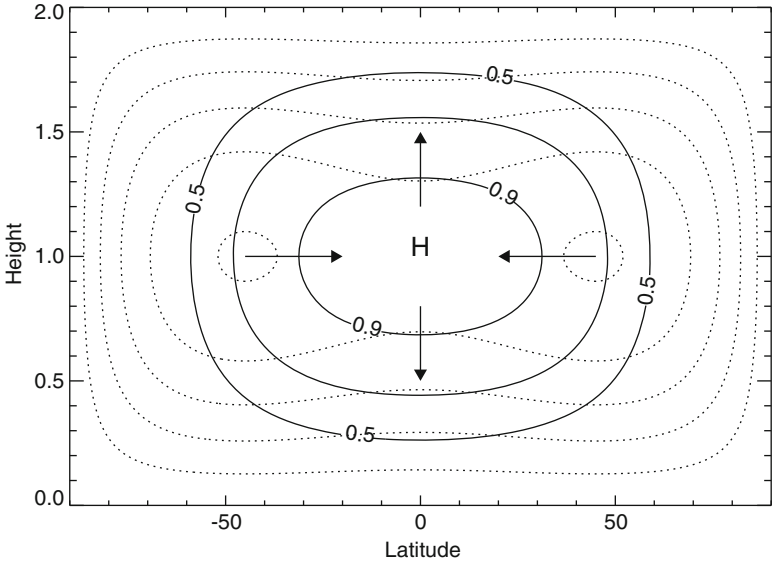

Fig. 6.4 Schematic contour map in the meridional (latitude, height) plane of absolute axial angular momentum per unit mass, $\overline{m}$, in a hypothetical zonally averaged flow on a sphere. Arrows indicate the directions of $\overline{\mathbf{F}}$ consistent with (6.17). Dotted contours schematically represent a plausible variation of prograde zonal velocity, consistent with the contoured field of $\overline{m}$

a viscous fluid, unless the effective eddy viscous diffusion coefficient, ν, is negative (thereby implying an effect obtainable *only* by non-axisymmetric processes, e.g. see Starr 1968). In the presence of eddies (and/or molecular viscosity), the zonally averaged form of (6.9) is

$$\frac{\partial \overline{u}}{\partial t} + \overline{\mathbf{u}} \cdot \nabla m = \overline{\mathcal{F}} \tag{6.13}$$

where $\overline{\mathcal{F}}$ represents the net zonal acceleration due to real or 'eddy' viscosity. If we now identify a prograde equatorial flow as one for which there is a local maximum of absolute, axial angular momentum per unit mass ($m = m_0$, say) at upper levels near the equator (see Fig. 6.4, although similar arguments will apply to any local extremum of m), we may draw a closed contour in the meridional plane $m = m_0 - \delta$, where δ can be arbitrarily small and positive.

Integrating the steady form of (6.13) over the entire toroidal volume enclosed by the $m_0 - \delta$ contour, it is straightforward to show via the Divergence Theorem that

$$\int\int\int \nabla.(\overline{m}\overline{\mathbf{u}})\, dV = (m_0 - \delta) \int\int \overline{\mathbf{u}}.d\mathbf{n}, \tag{6.14}$$

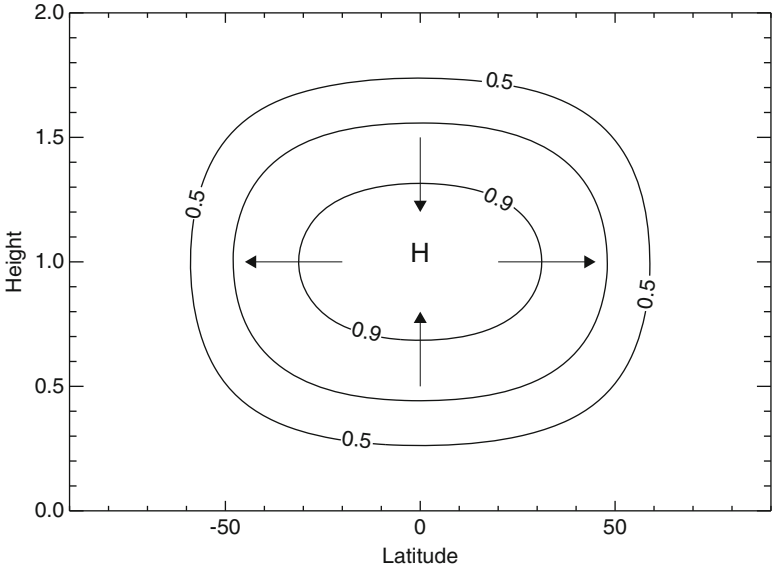

Fig. 6.5 Similar schematic contour map to Fig. 6.4 but in which the directions of **F** have been reversed, also consistent with (6.17)

where $d\mathbf{n}$ is the outward normal vector element of surface area. By conservation of mass, however,

$$\int\int \overline{\mathbf{u}} \cdot d\mathbf{n} = 0 \tag{6.15}$$

for a steady flow, implying also, therefore, that

$$\int\int\int \overline{\mathcal{F}}\, dV = 0. \tag{6.16}$$

If $\overline{\mathcal{F}}$ can be written as $-\nabla \cdot \overline{\mathbf{F}}$, however, where $\overline{\mathbf{F}}$ represents either the viscous flux or the notional zonally-averaged eddy angular momentum flux in the meridional plane, then (6.16) can be written as

$$\int\int \overline{\mathbf{F}} \cdot d\mathbf{n} = 0. \tag{6.17}$$

Excluding the trivial case, this implies either that $\overline{\mathbf{F}}$ must be everywhere parallel to the $m_0 - \delta$ contour *or* have components somewhere that act against the gradient of $\overline{m}$. Schematic examples are illustrated in Figs. 6.4 and 6.5 and are implicit in the three-dimensional simulation shown in Fig. 6.3a.

This is sometimes quoted by itself as an argument that eddies are necessary for super-rotation, although the situation in reality is somewhat more subtle.

While it is certainly the case that eddies can spontaneously act to transfer angular momentum up-gradient, either in the horizontal or vertical directions, such transfers can also occur due to simple, isotropic molecular viscosity. This is because Newtonian viscosity acts to mix momentum (both linear and angular) towards a state of uniform *angular* velocity. There is nothing in principle to prevent the gradient of angular velocity being in the opposite sense to that of angular momentum, *but only in the horizontal direction* (Plumb 1977; Read 1986). Figure 6.4 illustrates a simple conceptual example in which the zonal flow (dotted contours) exhibits weak jets at mid-latitudes consistent with a poleward gradient of angular velocity whilst still having a maximum of m on the equator. With this *caveat*, *at least in principle*, a super-rotating flow with a local maximum of m on the equator can be maintained in a purely axisymmetric flow by viscosity alone.

In practice, however, molecular viscosity coefficients of gases are far too small to sustain an equator-ward diffusive flux of angular momentum large enough to balance the direct advection of m by thermally-direct meridional circulations without impossibly large horizontal shears. Eddies are much more efficient at effecting this transfer than molecular viscosity, and so eddies are much more able to maintain a steady super-rotation with much more moderate shear in the zonal flow. Moreover, it is common in many atmospheric models to parameterize internal diffusion (necessary e.g. for stability of the numerical integration method) as a purely vertical Laplacian viscosity. Such an anisotropic viscosity is fundamentally unable to transport m up-gradient (Read 1986), and so eddies are then essential in the maintenance of super-rotation. A clearer statement of Hide's (second) theorem might then be that *an axisymmetric atmosphere cannot super-rotate at the equator if small-scale mixing of angular momentum is everywhere down-gradient*.

Finally, there is nothing in principle to prevent eddies transporting angular momentum up-gradient in the vertical direction as well as in the horizontal. Thus, eddies allow a wider range of possible configurations of $\overline{\mathbf{F}}$, e.g. including the alternative configuration illustrated in Fig. 6.5, in which up-gradient fluxes act in the vertical directions with down-gradient fluxes in the horizontal.

6.4 Hadley Circulations

Despite the important role of eddies in sustaining a Venus-like super-rotation, a great deal of useful insight can be gained from studying simple Hadley-type flows without explicit inclusion of eddies. The effects of adding eddies can then be easily identified. A particularly useful and simple approach to this problem was first presented by Schneider (1977) and Held and Hou (1980) with the Earth's tropical Hadley circulation in mind, but later elaborated by Hou (1984) to slowly rotating planets such as Venus.

While the full treatment entails the numerical solution of some complex equations, the essence of these models can be expressed relatively simply. Consider a two layer, axisymmetric atmosphere in which the lower layer is strongly coupled

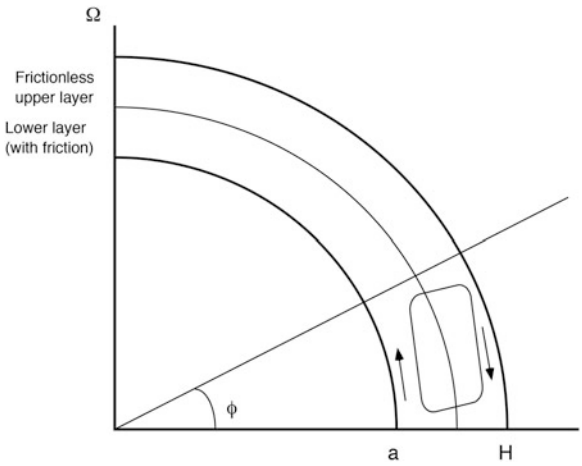

Fig. 6.6 Schematic diagram of the formulation of the simple model of weakly viscous Hadley circulations on the sphere by Held and Hou (1980)

to the surface via friction while the upper layer is almost inviscid. An overturning Hadley circulation moves air polewards in the upper layer and equator-wards in the lower layer (see Fig. 6.6).

In the upper layer, specific angular momentum m is conserved and the flow will approximate to one in which m is constant with latitude, while in the lower layer the zonal flow is relatively weak because of the action of friction. We may also invoke a balance requirement on the zonal flow, which may be purely geostrophic or the more complicated gradient wind balance for slowly rotating planets. In addition, thermal diffusion effects are also assumed to be negligible.

Held and Hou (1980) simplify the forcing by assuming that the atmospheric temperature relaxes towards a specified 'radiative equilibrium' potential temperature distribution with the simple, analytical form

$$\theta_E = \theta_0 \left[1 - \frac{2}{3}\Delta_h \, P_2(\sin\phi) + \Delta_v \left(\frac{z}{H} - \frac{1}{2} \right) \right], \tag{6.18}$$

where θ_0 is a reference potential temperature, Δ_h and Δ_v are dimensionless measures of the equator-pole and vertical temperature gradients (by θ_0), H is the vertical depth of the atmosphere and P_2 is the second Legendre polynomial $P_2(x) = (3x^2 - 1)/2$. This takes the form of an inverted parabolic profile of temperature with latitude, as illustrated in the solid line in Fig. 6.7.

If the steady state zonal flow in the upper layer is assumed to conserve m, it will adopt a profile $u_m(\phi)$ in which m is invariant in latitude. From the definition of m in (6.8), therefore,

$$m = \Omega a^2 = a \, \cos\phi (u_m + \Omega a \, \cos\phi) \tag{6.19}$$

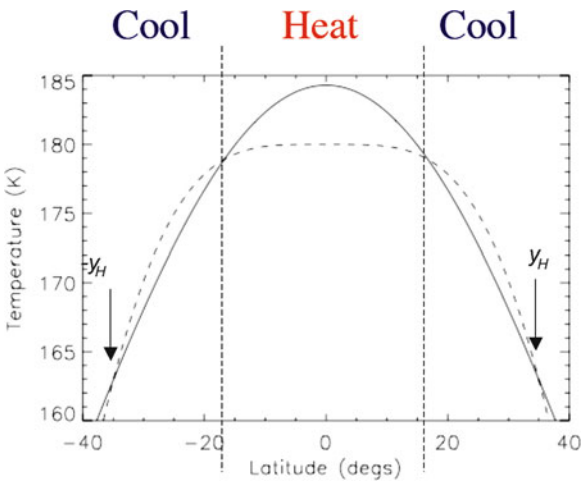

Fig. 6.7 Schematic profiles of zonal velocity in the simple model of weakly viscous Hadley circulations on the sphere by Held and Hou (1980)

so u becomes

$$u_m = \frac{\Omega a \ \sin^2 \phi}{\cos \phi}. \tag{6.20}$$

Such a profile of u_m is illustrated in Fig. 6.7, showing the quadratic increase of u away from the equator (where u is taken here to be zero). Figure 6.7 also shows the dynamically consistent profile of zonal velocity in the lower layer. This cannot really be zero, as approximated above, since otherwise friction would not be able to add or remove angular momentum to the flow. Note, however, that u in the lower layer has to include both positive and negative flows at different latitudes (in this case retrograde near the equator and prograde at higher latitudes) in order to result in zero *net* torque on the atmosphere.

For the case of the Earth, the problem can be significantly simplified (a) by applying geostrophic balance and (b) by invoking the small angle approximation, so that $u_m \simeq \Omega y^2/a$, where $\sin \phi \simeq y/a$. If u in the lower layer is assumed to be small, we can obtain a simple expression for the potential temperature profile at mid-level, θ_m, consistent with u_m in geostrophic balance,so that

$$\frac{\partial u_m}{\partial z} \simeq \frac{u_m}{H} \simeq \frac{\Omega y^2}{aH} \simeq -\frac{ga}{2\Omega\theta_0 y}\frac{\partial \theta_m}{\partial y}. \tag{6.21}$$

This can be solved analytically in this case for the small-angle form of balanced potential temperature to obtain

$$\theta_m = \theta_{m0} - \frac{\Omega^2 a^2 \theta_0}{2gH} y^4, \tag{6.22}$$

where θ_{m0} is a constant of integration. The resulting profile $\theta_m(y)$ is shown as the dashed curve in Fig. 6.8.

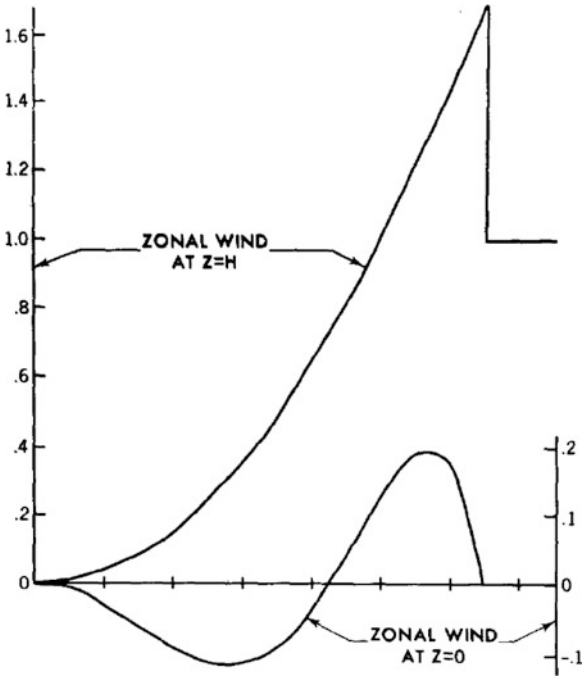

Fig. 6.8 The meridional distribution of idealized radiative equilibrium temperature, θ_R (*dashed line*), assumed in the simple Hadley circulation model of Held and Hou (1980), together with the assumed temperature distribution, θ_M (*solid line*), consistent with angular momentum conservation (see text)

The final step in the process is then to constrain the constants θ_{m0} and θ_{E0} by assuming the Hadley circulation to be driven by a simple linear relaxation heating/cooling of the form

$$Q = \frac{\theta_E - \theta}{\tau_R}, \tag{6.23}$$

where τ_R is a radiative time constant. If the Hadley circulation is assumed to be a closed system in which the net heating integrates to zero, we can write

$$\int_0^{y_H} \theta_m - \theta_E \, dy = 0 \tag{6.24}$$

assuming symmetry about the equator. Given the forms of θ_E and θ_m in Eqs. (6.18) and (6.22), this reduces to the solution of a pair of algebraic equations for the parameters y_H and $\theta_{m0} - \theta_{E0}$. Thus we can obtain expressions for the width of the Hadley circulation and the maximum departure of θ_m from radiative equilibrium at the equator from the other parameters of the problem.

$$y_H = \left(\frac{2gH\Delta_h}{3\Omega^2}\right)^{1/2} = a\left(\frac{2\Theta}{3}\right)^{1/2} \tag{6.25}$$

$$\theta_{m0} - \theta_{E0} = \frac{5gH\theta_0\Delta_h^2}{18a^2\Omega^2} = \Delta\theta_h \frac{5\Theta}{18}, \tag{6.26}$$

where Θ is a dimensionless parameter,

$$\Theta = \frac{g\Delta_h H}{\Omega^2 a^2}, \tag{6.27}$$

known as the *Thermal Rossby number*, and $\Delta\theta_h = \theta_0\Delta_h$ is the equator-pole thermal contrast. Thus, we see that both the width of the Hadley circulation and the thermal offset depend directly on the Thermal Rossby number Θ, which turns out to be a fundamental parameter for a number of aspects of the circulation. If we put in suitable numbers for the Earth, Θ comes out to be around 0.1, leading to a Hadley cell width of around 1,500 km or $\sim$15° in latitude, and a thermal offset $\sim$ 0.8 K. Putting in the corresponding numbers for Venus, however, leads to value for y_H that is much larger than the radius of the planet. This is a clear indication that the small angle approximation is no longer valid, nor is the geostrophic balance condition satisfied. For this case, the parameters y_H and $\theta_{m0} - \theta_{E0}$ need to be obtained from a solution to the full problem without these approximations.

If we relax the small angle approximation, (6.21) must be replaced by

$$u_m = \frac{\Omega a}{(1-y^2)^{1/2}} y^2 \tag{6.28}$$

and with a gradient wind balance condition instead of pure geostrophic balance, (6.22) becomes

$$\theta_m = \theta_{m0} - \frac{\Omega^2 a^2 \theta_0}{gH} \frac{y^4}{1-y^2}. \tag{6.29}$$

The determination of y_H and $\theta_{m0} - \theta_{E0}$ then reduces to the solution of the transcendental equation (Held and Hou 1980; Hou 1984)

$$\frac{(4\Theta - 1)y_H^3}{3} - \frac{y_H^5}{1-y_H^2} - y_H + \frac{1}{2}\ln\left[\frac{1+y_H}{1-y_H}\right] = 0. \tag{6.30}$$

This can be solved numerically to obtain the solid curve for y_H shown in Fig. 6.9. This can be shown to reduce to the asymptotic form (6.25) for $\Theta \ll 1$ and $y_H \to 1 - 3/8\Theta$ for $\Theta \gg 1$. The appropriate value of Θ for Venus probably lies around 300–400, indicating that y_H closely approaches the full width of the hemisphere and the corresponding Hadley circulation extends almost all the way from equator to pole (much as apparently observed).

Hou (1984) also developed a number of other Hadley circulation solutions which include heat and momentum sources intended to represent the effects of eddy processes, which was further developed by Hou and Goody (1985) to obtain diagnostic estimates of the actual eddy processes active on Venus from Pioneer Venus observations. These estimates were not, however, able to discern precisely which eddy processes were dominant in maintaining the observed zonal mean circulation.

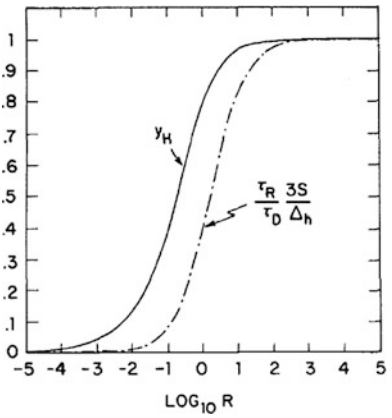

Fig. 6.9 The meridional width of the Hadley circulation, y_H, non-dimensionalised in terms of cos(latitude), as a function of the external thermal Rossby number, R_T (*solid line*), obtained by Hou (1984). The dashed line plots the ratio, τ_R/τ_D, of the radiative and dissipative timescales, scale by $\Delta_h/3S$

6.5 "Classical" and "Non-classical" Gierasch-Rossow-Williams Mechanisms

Somewhat before the analysis of Held and Hou (1980), the notion that the Hadley circulation on Venus played a major role in generating its super-rotation had been suggested, most notably by Gierasch (1975) who devised a reasonably complete scenario for the production and maintenance of super-rotation. This approach included a simple diffusive parameterization of the role of eddies in transporting angular momentum so as not to violate Hide's theorems. However, it was necessary to make certain assumptions about the way eddies mix momentum, vorticity and heat in order not that they should not remove thermal gradients or mix angular momentum in the vertical too effectively. Gierasch (1975) placed emphasis on the effects of eddies primarily as *horizontal* mixing agents of *vorticity*, which enables eddy diffusion to transport angular momentum up-gradient in a similar manner to horizontal molecular viscosity (Plumb 1977; Read 1986). This emphasis on the role of eddies as horizontal vorticity mixers was taken up subsequently by Rossow and Williams (1979), who investigated the possible role of large-scale barotropically unstable eddies under Venus-like conditions and also demonstrated numerical solutions of super-rotating flows in a shallow-water model. These combined insights have led to an important paradigm in our understanding of the super-rotation model, now known as the "Gierasch-Rossow-Williams" mechanism and which we now explore.

6.5.1 "Classical" GRW Mechanism

The "classical" form of this scenario can be understood with reference to the schematic diagram in Fig. 6.10, which illustrates the main transports and

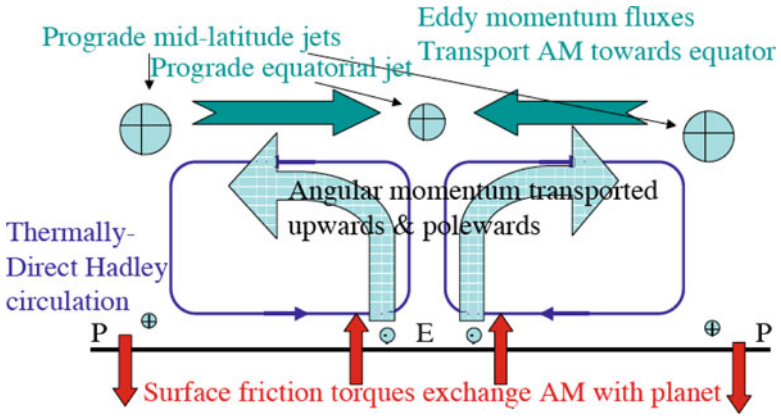

Fig. 6.10 Schematic diagram illustrating the main features of the "classical" Gierasch-Rossow-Williams mechanism for atmospheric super-rotation

circulation processes. The mechanism can be considered in two phases: (i) a 'spin-up' phase in which the atmosphere first gains angular momentum from the solid planet, and (ii) the equilibration of the final super-rotation.

In the 'spin-up' phase, we envisage the atmosphere initially at rest with respect to the underlying (slowly rotating) planet when differential heating/cooling between the tropics and polar latitudes is activated. Heating over the equator and cooling in polar regions respectively leads to rising and sinking motion as the initial Hadley circulation is initiated. Continuity of mass requires air near the surface to move towards the equator, initially conserving its angular momentum as it moves along the surface and further away from the rotation axis of the planet. Hence, westward zonal flow is induced at low latitudes which is then acted on by surface friction. Frictional drag weakens the westward near-surface flow, thereby increasing its absolute specific angular momentum and injecting positive m into the flow (see red upward arrows in Fig. 6.10). Once it reaches the tropics, however, the air begins to rise and become decoupled from the ground. From now on, angular momentum is approximately conserved following the motion (cf. Sect. 6.3). Hence, the newly injected m at the surface is effectively transported upwards and polewards by the continuity preserving poleward flow at upper levels (light green arrows in Fig. 6.10).

The movement of upper level air from the tropics back towards high latitudes will now lead to the spin-up of eastward flow at these levels, increasing in strength as the flow approaches the poles. This cannot continue all the way to the poles, otherwise a singularity is produced, so in reality this may be expected to lead to an eastward jet surrounding a vortex over the pole itself, with strong shear towards the equator, where the zonal flow remains close to zero up to this stage since there are no eddies to exert a torque on the flow and increase the angular momentum beyond $\Omega^2 a$.

At this point, Gierasch (1975); Rossow and Williams (1979) suppose that the strong equator-pole shear in the upper level flow will lead to the generation of

eddies, most likely from the action of an instability. These eddies are assumed to act to mix the flow towards a state of uniform relative or absolute vorticity, which is likely if they arise from an instability associated with an inflection point in the flow. Here, there is a clear analogy with the effects of Newtonian viscosity, which acts to mix towards a state of solid body rotation and uniform angular velocity, since a flow with uniform angular velocity will also have a uniform vorticity with latitude. Thus, the development of such eddies will lead to a flux of angular momentum towards the equator, thereby setting the seed for the formation of a local maximum in m over the equator itself (dark green arrows in Fig. 6.10; cf. also Fig. 6.4). In the more mature stages of the spin-up, eastward flow from the mid-latitude jets extends towards the ground, due to the downward transport in the descending branch of the Hadley circulation. This is necessary for the final equilibration of the process, since eastward flow near the equator allows friction to remove angular momentum from the atmosphere, thereby providing a region of negative torque to balance the positive torque acting near the equator on the equatorward low-level flow. In the final stages, this region of negative torque grows in strength until it balances the positive torques and a steady state is reached. By this point, the upper level flow has evolved towards a state of almost uniform absolute vorticity (and angular velocity) with an angular velocity that approaches that of the mid-latitude jets. Such a flow will now have a strong positive maximum of m over the equator and a super-rotating state has been attained. The strength of the super-rotation so attained is evidently dependent on a number of factors, but essentially requires the upper levels to become strongly isolated from the lower atmosphere so the accumulation of angular momentum at upper midlatitudes does not leak away too rapidly. This places constraints on the vertical structure of static stability and requires the eddies to transport angular momentum preferentially in the horizontal direction. Gierasch (1975) estimates the strength of super-rotation to depend on the dimensionless parameter $S_G = (D\tau_v/H\tau_d)$, where D/H is the depth of the atmospheric circulation normalized by the pressure scale height, H, τ_v is the timescale associated with vertical diffusion of momentum and τ_d the dynamical overturning timescale of the principal Hadley circulation. When S_G is large, strong super-rotation will be observed, but if it is small e.g. because the circulation is shallow or the vertical eddy mixing is very efficient, then super-rotation will be comparatively weak. The nature of the main eddies in this scenario were not discussed in detail by Gierasch, but one possibility was considered by Rossow and Williams (1979), namely, large-scale waves and eddies formed from barotropic instability. This was shown by Rossow and Williams (1979) to be a viable possibility, at least in principle, with eddy fluxes of zonal momentum in the poleward direction, but this is by no means the only possible configuration. Indeed, one of the key issues in understanding of Venus's atmospheric circulation is the nature and role of various eddy processes in transporting angular momentum and contributing to sustaining super-rotation. Such a situation has been further complicated by a lack of a clear observational confirmation of the poleward nature of eddy momentum transports. But results have instead tended to be somewhat ambiguous and inconclusive (Limaye 2007).

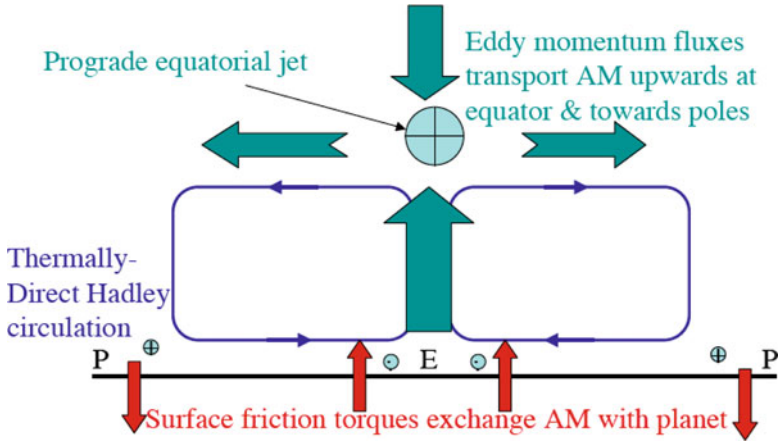

Fig. 6.11 Schematic diagram illustrating the main features of the alternative to the "classical" Gierasch-Rossow-Williams mechanism for atmospheric super-rotation, in which up-gradient fluxes of angular momentum occur in the vertical (see text)

6.5.2 A "Non-classical" GRW Scenario

An alternative, though somewhat related, scenario is illustrated in Fig. 6.11. In this case, a thermally-direct Hadley circulation acts as before to extract angular momentum from the solid planet in the tropics during spin-up, and to transport m upwards and polewards to form mid-latitude jets. Unlike in the "classical" GRW scenario, however, in this alternative approach the eddies are assumed to transport m predominantly up-gradient in the *vertical* direction instead of in the horizontal. Such a configuration can be equally valid in the context of Hide's theorems (cf. Sect. 6.3), supporting a local maximum in m over the equator, provided any horizontal momentum fluxes are predominantly *poleward* instead of equator-ward (cf. Figs. 6.4 and 6.5).

Eddies acting in this way are likely to have a quite different origin from the vorticity mixing, predominantly barotropic eddies invoked in the "classical GRW" mechanism, but there are a number of plausible candidates. These and the likely waves and eddies contributing to the GRW mechanism will now be reviewed in the next section.

6.6 Waves and Eddies

In common with the Earth and other planetary atmospheres, Venus's atmosphere is capable of supporting a wide range of different wave modes and eddies, energised by a variety of sources, that could contribute to the transport of momentum, vorticity

and other tracers and thereby play a significant role in developing and maintaining the strong atmospheric super-rotation. In the following, we treat these in three main categories, namely,

1. Quasi-horizontal waves and eddies, mostly on a large, near-planetary scale;
2. Diurnally-forced eddies, thermal tides and day-night circulations; and
3. Small-scale gravity waves and turbulence.

These are mostly processes that occur in the free atmosphere, well away from the ground, although it is possible in principle for interactions with the planetary surface to lead to topographically forced waves. These and other surface processes will be considered in the following Sect. 6.7.

6.6.1 Quasi-Horizontal Free Waves and Eddies

Since the early work of Rossow and Williams (1979), it has been common practice to consider the behavior of many quasi-horizontal dynamical processes on Venus in the context of a single, homogeneous fluid layer, either in the form of a barotropic flow on the sphere or in the context of the shallow water equations (e.g. see Iga and Matsuda 2005). The latter in particular are quite general and apply equally well to both rapidly rotating planets such as the Earth as well as to slow rotators such as Venus. The shallow water equations on the sphere are equivalent to the nonlinear form of the Laplace tidal equations (e.g. Vallis 2006)

$$\begin{aligned}\frac{Du}{Dt} - fv &= \frac{\partial u}{\partial t} + \frac{u}{a\,\cos\phi}\frac{\partial u}{\partial \lambda} + \frac{v}{a}\frac{\partial u}{\partial \phi} - \frac{uv\,\tan\phi}{a} - fv \\ &= -\frac{g}{a\,\cos\phi}\frac{\partial h}{\partial \lambda} \end{aligned} \tag{6.31}$$

$$\begin{aligned}\frac{Dv}{Dt} + fu &= \frac{\partial v}{\partial t} + \frac{u}{a\,cos\phi}\frac{\partial v}{\partial \lambda} + \frac{v}{a}\frac{\partial v}{\partial \phi} + \frac{u^2\tan\phi}{a} + fu \\ &= -\frac{g}{a}\frac{\partial h}{\partial \phi} \end{aligned} \tag{6.32}$$

$$\begin{aligned}\frac{\partial h}{\partial t} &= -\nabla\cdot(\mathbf{u}h) \\ &= -\frac{1}{a\,\cos\phi}\left[\frac{\partial}{\partial\lambda}(hu) + \frac{\partial}{\partial\phi}(hv\,\cos\phi)\right] \end{aligned} \tag{6.33}$$

where $f = 2\Omega\,\sin\phi$ and h is the depth of the fluid layer. Waves supported in such a system are frequently interpreted in terms of the principal eigenmodes of the linearized form of these equations, which represent the spectrum of different

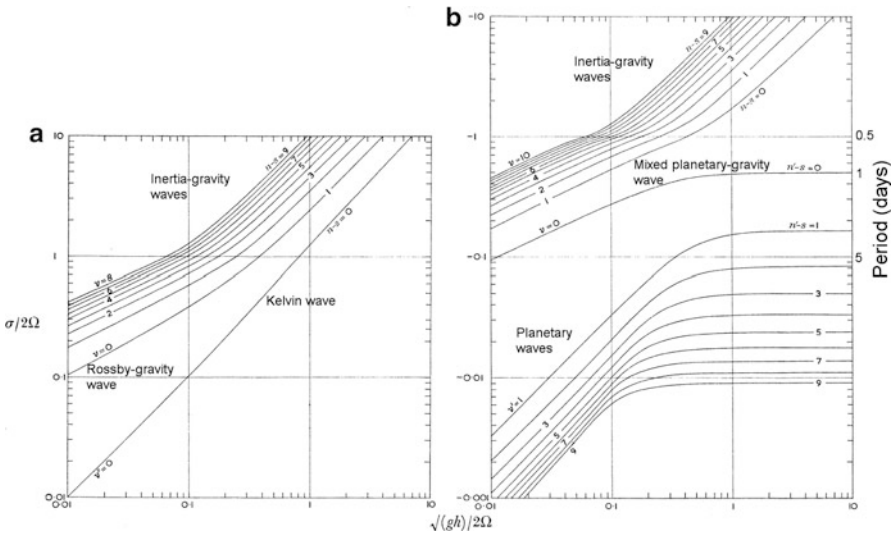

Fig. 6.12 Plots of $(g|h|)^{1/2}/(2\Omega a)$ versus frequency σ for zonal wavenumber $s = 1$ in the linearized Laplace tidal equations for positive equivalent depth h: (**a**) eastward phase speeds ($\sigma > 0$) and (**b**) westward phase speeds ($\sigma < 0$). Figure adapted from Longuet-Higgins (1968). Reprinted with the permission from the Royal Society

possible wave modes that combine the effects of rotation and buoyancy (representing the effect of gravity on the top free surface). Some examples of the main eigenfrequencies are illustrated in Fig. 6.12, which shows the variation of frequency σ with the so-called Lamb parameter $\gamma_L = \sqrt{g|h|}/(2\Omega a)$, assuming a perturbation of the form

$$\{u', v', \Phi\} \propto \exp i(s\lambda - 2\Omega\sigma t), \tag{6.34}$$

with zonal wavenumber s for a range of values of integer indices n, n' or ν (e.g. see Longuet-Higgins 1968 and Andrews et al. 1987) that principally determine the meridional structure of each mode and positive equivalent depth h.

These show the eigenmodes to fall into several families. Westward modes (Fig. 6.12a) include high frequency, inertia-gravity waves ($\nu \geq 0$) and the equatorially-trapped Kelvin wave ($\nu' = 0$). Eastward modes (Fig. 6.12b include high frequency inertia-gravity waves ($\nu \geq 1$) similar to their westward counterparts, low frequency planetary Rossby waves ($\nu' \geq 1$) and the intermediate mixed planetary-gravity mode ($\nu = 0$).

The low frequency westward planetary Rossby waves are directly related to the well known Rossby-Haurwitz waves in terrestrial meteorology (Rossby 1939; Haurwitz 1940). In the low rotation limit ($\gamma_L \to \infty$) these waves are of planetary scale and are dispersive and non-divergent. The upper branches of both eastward and westward inertia-gravity waves are also of planetary scale for $\gamma_L \to \infty$ but then become divergent but irrotational. The eastward (a) $n - s = \nu'' = 0$ and

(b) $n - s = 1; \nu = 0$ branches of the eastward modes have a particular identity as equatorial Kelvin and Rossby-gravity modes. For small γ_L the waves become trapped either towards the equator ($h > 0$) or towards the poles ($h < 0$) and may be approximated by mathematically simpler solutions on a tangent β-plane (see Andrews et al. 1987 and Longuet-Higgins 1968 for further details).

Rossow and Williams (1979) noted that various extensions to the Rossby-Haurwitz planetary wave solutions can be made with the addition of zonally-symmetric flow components, including a simple solid-body flow with angular velocity Ω' and other, more complex zonal flows with meridional vorticity gradients. Following the original suggestions of Craig (1945). Neamtan (1946) and Thompson (1948), wave-like solutions of *permanent form* to the full barotropic vorticity equation (i.e. which propagate at uniform speed without change of amplitude or form) can be obtained with the dispersion relation

$$c = U_0 - \frac{\beta - \partial^2 U_0/\partial y^2}{k^2 + m^2}, \tag{6.35}$$

where U_0 is the background zonal velocity component (in general in a frame rotating at $\Omega + \Omega'$), $\beta = \partial f/\partial y$ and k and m are the zonal and meridional wavenumbers (assuming a simple, Cartesian β-plane geometry here for simplicity). For some situations where the planetary rotation is negligible, therefore, the flow can still support large-scale 'advective Rossby wave flows' Rossow and Williams (1979) whose character is defined by uniform propagation without change of form or shape with respect to the frame in solid body rotation with the dominant zonal flow.

The transformation to a frame moving with the solid-body component of the zonal wind can also be applied to the other modes of the shallow water equations, allowing us, for example, to use the equatorial β-plane approximation to consider modes such as the Kelvin and mixed Rossby-gravity waves. For such an equatorial β-plane, the linearized shallow-water equations become

$$\frac{\partial u}{\partial t} - \beta' y v = -g\frac{\partial h}{\partial x} \tag{6.36}$$

$$\frac{\partial v}{\partial t} + \beta' y u = -g\frac{\partial h}{\partial y} \tag{6.37}$$

$$\frac{\partial h}{\partial t} = -h_0 \nabla \cdot (\mathbf{u}), \tag{6.38}$$

where h_0 is a constant mean (equivalent) depth and $\beta' = 2\Omega'/a$ is the 'planetary vorticity gradient' at the equator relative to the solid-body component of the zonal wind. If we seek a wave-like solution for which $v = 0$, taking the form $u = U(y)p(x - ct)$; $h = \alpha U(y)p(x - ct)$, this leads to

$$u = U_1 \exp -\left[\frac{\beta' y^2}{2c}\right] \exp i[kx - \omega t)], \tag{6.39}$$

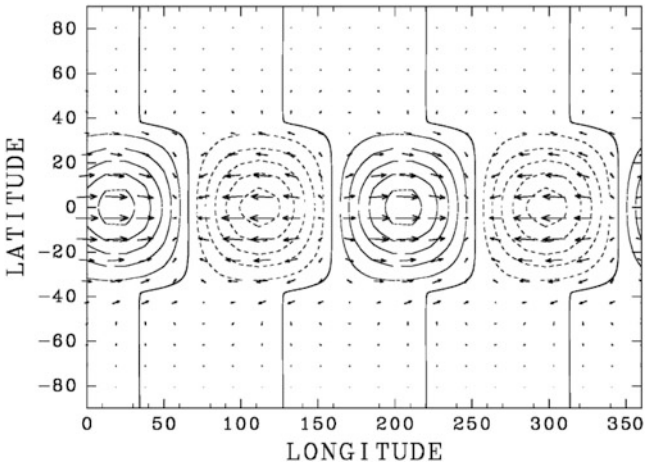

Fig. 6.13 Contours of height perturbation with velocity vectors for an unstable equatorial Kelvin-like mode in a shallow water model. Figure adapted from Iga and Matsuda (2005)

where U_1 is a constant and $c = +\sqrt{gh_0}$ for meridionally bounded solutions. This represents the simplest form of the equatorial Kelvin wave in the context of the equatorial β-plane. Note that this solution has a gaussian variation with y that is symmetric about the equator ($y = 0$) and has a characteristic width $L = (2c/\beta')^{1/2}$. For the Venus cloud-level mean atmospheric rotation rate, $\beta' \simeq 6 \times 10^{-12}$ m^{-1}s^{-1}, so $c \simeq 16$ m s^{-1} and $L \simeq 2300$ km or around $a/3$. A solution of similar form can be seen in Fig. 6.13, which illustrates a growing Kelvin-like solution in a shallow water numerical model (Iga and Matsuda 2005). The strongly anisotropic horizontal velocity field is clearly seen, with weak v except near critical latitudes (where $c \sim \overline{u}$).

For modes for which $v \neq 0$ in a solid-body flow at Ω', the dispersion relation becomes

$$\left(\frac{\omega}{c}\right)^2 - k^2 - \frac{\beta' k}{\omega} = \frac{2(n+1)\beta'}{c}; \quad n = -1, 0, 1 \ldots \tag{6.40}$$

for which the case $n = -1$ can be identified as the Kelvin mode. Other examples of the height and velocity fields associated with $n = 0$ (mixed Rossby-Gravity) and $n = 1$ (Rossby) modes are illustrated in Fig. 6.14, showing more complex structures than for the Kelvin mode. Note that the $n = 0$ mode is antisymmetric about the equator and $n = 1$ symmetric.

6.6.2 Vertically-Propagating Free Waves and Eddies

For the waves and eddies discussed in the previous section, their vertical structure was not considered in detail in order to focus on their horizontal structure and

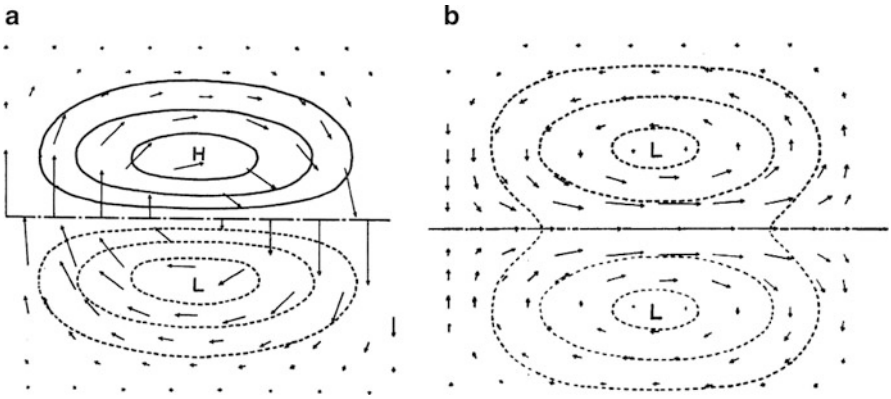

Fig. 6.14 Contours of height perturbation with velocity vectors for linear equatorial wave modes (**a**) $n = 0$ westward mixed Rossby-gravity wave, and (**b**) $n = 1$ westward equatorial Rossby wave. After Matsuno (1966). Reprinted with the permission from the Meteorological Society of Japan

propagation. In a stratified atmosphere, however, there are a number of other types of wave mode with more complex vertical structure that propagate both vertically and horizontally, carrying momentum, vorticity and energy across the planet. The simplest of these are the internal gravity waves, which are supported by the buoyancy restoring force associated with statically stable stratification. These waves mostly occur on relatively short space and timescales compared with the planetary rotation period, so can be modelled theoretically without needing to take explicit account of background rotation. Linearizing the primitive equations about a state of rest in a compressible atmosphere, the basic equations of motion, continuity and buoyancy become (Andrews et al. 1987)

$$\frac{\partial u'}{\partial t} = -\frac{\partial \Phi'}{\partial x} \tag{6.41}$$

$$\frac{\partial v'}{\partial t} = -\frac{\partial \Phi'}{\partial y} \tag{6.42}$$

$$\frac{\partial u'}{\partial x} + \frac{\partial v'}{\partial y} + \frac{1}{\rho_0}\frac{\partial(\rho_0 w')}{\partial z} = 0 \tag{6.43}$$

$$\frac{\partial^2 \Phi'}{\partial t \partial z} + w' N^2 = 0, \tag{6.44}$$

where $\rho_0(z)$ is the background density profile, $N^2 = -g/\theta_0 \partial\theta/\partial z$ is the squared buoyancy or Brunt-Väisälä frequency and primed quantities represent departures from the time-independent basic state. These equations support wave-like solutions of the form

$$(u', v', w', \Phi') = \exp\left(\frac{z}{2H}\right)(\hat{u}, \hat{v}, \hat{w}, \hat{\Phi}) \exp[i(kx + ly + mz - \omega t)], \tag{6.45}$$

where $\hat{()}$ quantities are constants representing the amplitude of each variable, H is the pressure scale height, ω is the frequency and k, l, m are the wavenumbers in the x, y and z directions respectively. These solutions imply a dispersion relation relating ω and the horizontal and vertical wavenumbers

$$\omega^2 = \frac{N^2(k^2 + l^2)}{m^2 + 1/(4H^2)}. \tag{6.46}$$

Note that this can be written in terms of the equivalent depth, h_0, used above as

$$\omega^2 = gh_0(k^2 + l^2) \tag{6.47}$$

if $m^2 = (N^2/gh_0) - 1/(4H^2)$. For waves with a relatively short vertical wavelength compared with H such that $m^2 \gg 1/(4H^2)$, the term in H can be neglected and we recover the Boussinesq form of the dispersion relation.

The dispersion relation (6.46) implies various properties of internal gravity waves (e.g. see Gill 1982). This includes the property that $|\omega| \leq N$ and, in the hydrostatic limit $|\omega| \ll N$ (Gill 1982), implying that the wave period is much greater than $2\pi/N$ and that the vertical wavelength $2\pi/m \ll$ the horizontal wavelength $2\pi/(k^2 + l^2)^{1/2}$. In this limit also it can be shown (e.g. see Andrews et al. 1987) that the velocity vector (u', v', w') is approximately perpendicular to the wave vector $\mathbf{k} = (k, l, m)$, so that the velocity vector lies along lines of constant phase and the orbits of individual air parcels are along straight lines perpendicular to $\mathbf{k}$.

The group velocity determines the propagation of energy or 'information' and is given by

$$\mathbf{c_g} = \left(\frac{\partial\omega}{\partial k}, \frac{\partial\omega}{\partial l}, \frac{\partial\omega}{\partial m}\right). \tag{6.48}$$

For a simple plane wave aligned in the x, z-plane, for which $\mathbf{k} = (k, 0, m)$, the group velocity becomes

$$\mathbf{c_g} = \frac{N}{m^2}(-m, 0, k), \tag{6.49}$$

so that for a wave with phase propagation upwards and towards positive x, $m < 0$. Equation (6.49) implies that $\mathbf{c_g}$ will be perpendicular to $\mathbf{k}$ and the vertical component of group velocity, c_g^z, is positive (upwards). This is illustrated in Fig. 6.15, which shows the relative alignment of phase lines, parcel velocities and group velocity.

Note that much of the above theory is for small amplitude waves propagating in a resting atmosphere with uniform N^2. It may be generalized, however, for cases where N^2 and the background flow vary with space and time, and for waves of finite amplitude (e.g. see Andrews et al. 1987 and references therein). In the presence of a simple, uniform zonal flow, $\overline{u}$, the analysis above can be straightforwardly modified to replace the frequency ω with the Doppler shifted *intrinsic frequency*, $\tilde{\omega} = \omega - \overline{u}k$. Where the background flow varies with position, however, there is the possibility of encountering a situation where $c = \omega/k = \overline{u}$, known as a *critical*

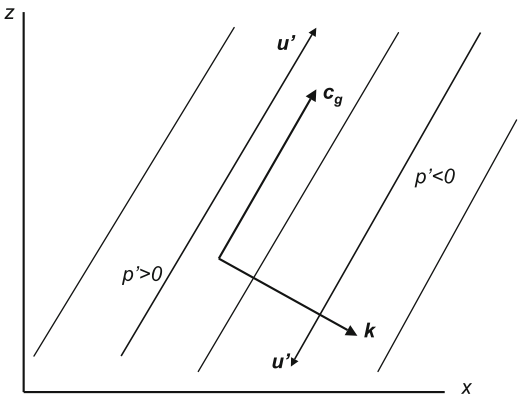

Fig. 6.15 Schematic cross-section through a plane internal gravity wave for which $k > 0$, $\omega > 0$ and $m < 0$ so that $c_g^{(z)} > 0$. Thin sloping lines indicate lines of constant phase and thin arrows indicate the perturbation velocities. The phase lines propagate in the direction of the wave vector **k** as indicated

line or *critical level*. In the vicinity of such a critical level, the intrinsic frequency tends to zero and wave propagation may be inhibited, leading to a build-up of wave activity and ultimately to wave breaking and dissipation. This is an important region where waves can deposit momentum as they dissipate and lead to acceleration of the background flow. This situation will be discussed more generally in Sect. 6.6.5.

Evidence for the occurrence of gravity waves on Venus comes from several sources, including in situ entry probes, the Soviet VEGA balloons, as well as from remote sensing from radio occultation profiles (Hinson and Jenkins 1995) and in ultraviolet and infrared images of Venus's clouds (e.g. Peralta et al. 2008). Two examples are illustrated in Fig. 6.16. Figure 6.16a shows a typical profile of a mid-latitude gravity wave profile with a wave of vertical wavelength ∼2.5 km, apparently stationary with respect to the planet, that grows in amplitude with height above the clouds before saturating. Figure 6.16b shows a 1.75 μm image from VEX-VIRTIS of the lower cloud deck on Venus, within which a train of ∼zonally propagating waves are visualized in variable cloud opacity.

If we add planetary rotation and spherical geometry back into the problem, as may be necessary for long wavelength disturbances with frequencies comparable with the rotation period either of the planet itself or the background zonal flow, we recover the full meteorological primitive equations. In the horizontal direction, however, the equations still resemble the shallow water equations discussed above. In this case, we recover a similar set of rotationally-modified modes to those presented in Sect. 6.6.1, including Kelvin, Rossby and inertia-gravity waves, but for which

$$h_0 = \frac{N^2}{g}\left[\frac{1}{m^2 + 1/(4H^2)}\right]. \tag{6.50}$$

For $m \neq 0$, these modes will now have a wave-like component that propagates in the vertical direction, also with a non-zero vertical component in group velocity. It is

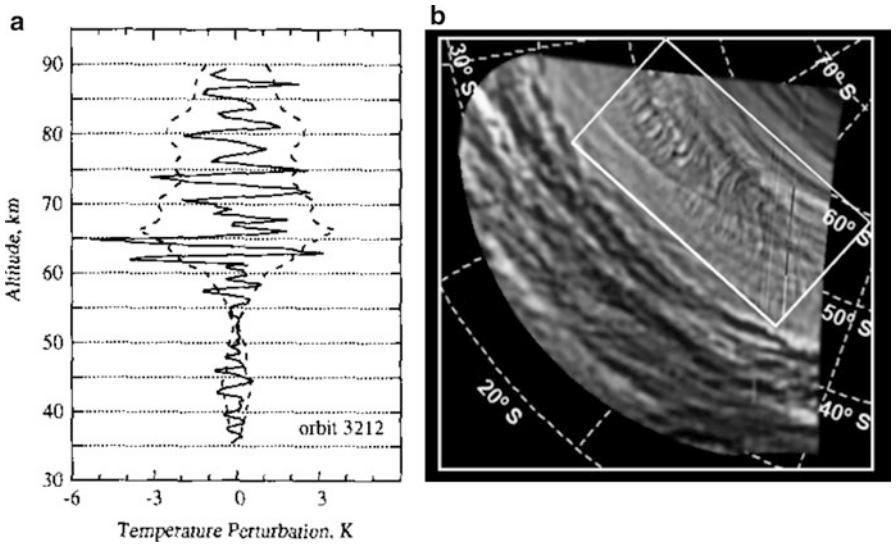

Fig. 6.16 Two examples of observational evidence for internal gravity wave activity on Venus (**a**) from Magellan radio-occultation measurements of temperature profiles at 67 °N Hinson and Jenkins (1995), reprinted with the permission from Elsevier and (**b**) in near infrared images of Venus's southern hemisphere from the VIRTIS instrument on Venus Express Peralta et al. (2008)

still possible, however, to have $m = 0$, with no phase variation with height. Such modes are known as *external modes*, and may be associated e.g. with the presence of sharp interfaces in stratification.

6.6.3 *Instabilities and the Generation of Free Waves and Eddies*

At least three types of instability process may lead to the generation of the types of wave and eddy discussed so far. On the largest scale, barotropic instabilities may directly energize zonally-propagating Rossby and equatorial planetary waves. Close to the equator, many of the conditions necessary for inertial instability are also satisfied, although the direct observational evidence for this instability is somewhat elusive. At certain locations, however, the local static stability may become relatively weak, especially near the surface and within the main cloud decks around 40–55 km altitude, leading to the possibility of vertical shear instabilities and even unstably-stratified direct convection.

6.6.3.1 Large-Scale Barotropic/Baroclinic Instability

Well away from the equator, classical barotropic instability is likely to be a dominant process on Venus. Barotropic instability is a horizontal shear instability of the Rayleigh (inflection-point) variety, for which a necessary (but not sufficient) condition for its occurrence, e.g. see Holton (2004). Andrews et al. (1987); Vallis (2006) is for the meridional gradient of absolute or potential vorticity

$$\frac{\partial \overline{q}}{\partial y} = \beta - \frac{\partial^2 \overline{u}}{\partial y^2} \tag{6.51}$$

(or its equivalent in spherical geometry) to change sign somewhere within the horizontal domain of interest. This is often known as the *Rayleigh-Kuo stability criterion* (e.g. Vallis 2006) for barotropic instability. For zonal flows that fulfill this necessary condition and are actually unstable, the typical result is a growing, wave-like disturbance that propagates zonally, effectively energizing a barotropic Rossby wave in mid-latitudes. The essential mechanism can be viewed as resulting from the mutual interaction between two zonally-propagating Rossby waves, supported by two adjacent regions of $\partial \overline{q}/\partial y$ of opposite sign (e.g. see Lindzen 1988, Vallis 2006), leading to a meridional flux of zonal momentum ($\overline{u'v'}$) in the same sense as $\partial \overline{u}/\partial y$. This requires the resulting waves to 'lean into' the shear of the background zonal flow so as to increase the kinetic energy of the waves at the direct expense of the zonal flow.

The length scale favored by this instability depends to some extent on the precise configuration of zonal flow under consideration, but for simple, rectilinear, inviscid flows or jets with a meridional length scale of L, the wavelength of maximum growth rate, λ_{max}, is often found to be comparable to

$$\lambda_{max} \simeq \pi L \sqrt{2} \tag{6.52}$$

(Howard and Drazin 1964). This scale is roughly borne out in laboratory experiments on barotropic instability (Sommeria et al. 1991; Niino and Misawa 1984; Fruh and Read 1999; Aguiar et al. 2010) but the precise scale is affected by other factors such as the curvature of a zonal jet or viscous effects.

In the context of Venus, the most likely location for barotropic instability is in the vicinity of the main cloud decks, where the zonal flow is strongest, close to the edge of the polar vortex in each hemisphere. Figure 6.17a shows a meridional profile of relative vorticity in the north polar vortex of Venus, obtained by Limaye et al. (2009), which shows a peak in vorticity close to the boundary of the inner vortex. From this, it is clear that the poleward gradient of vorticity must change sign either side of this peak, satisfying the Rayleigh-Kuo criterion for barotropic instability. Figure 6.17b shows the result of a barotropic model simulation that uses as a background state a smooth version of the vorticity profile in Fig. 6.17a (which tends

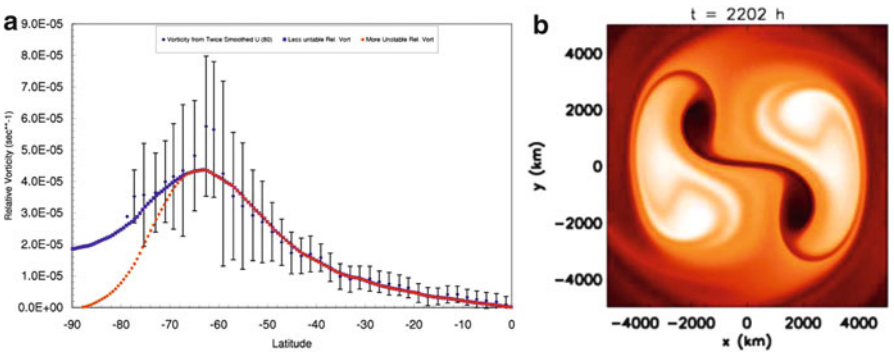

Fig. 6.17 (**a**) Latitudinal profiles of relative vorticity close to the north polar vortex of Venus, obtained from Pioneer Venus (points with error bars) and idealized in smooth profiles by Limaye et al. (2009); (**b**) finite amplitude, $s = 2$ equilibrated barotropic instability, obtained in the numerical model of Limaye et al. (2009) after ∼2000 days using one of the initial vorticity profiles shown in (**a**)

to zero at the pole). The initially unstable jet develops a wavenumber $s = 2$ zonally travelling wave that grows in amplitude and eventually equilibrates to a strong double-vortex structure that continues to rotate around the pole. The influence of the $s = 2$ pattern, however, penetrates across a wide range of latitudes, effectively transporting zonal momentum towards the equator on the equator-ward side of the jet. This broadly confirms a range of earlier studies of barotropic instability on Venus by Elson (1982), Michelangeli et al. (1987) and others, who were seeking a possible origin for the Venus 'polar dipole' features found by Pioneer Venus.

The possible occurrence of baroclinic instability has also been discussed on Venus (Young et al. 1984). The very low rotation rate of Venus itself would seem to make this mechanism unlikely to occur in weak zonal flow, because the first baroclinic Rossby deformation radius NH/f is much larger than the radius of the planet. But close to the visible clouds, the local rotation rate is much faster (period around 4 Earth days) and more conducive to baroclinic instability.

A necessary condition for baroclinic instability, analogous to the Rayleigh-Kuo condition for barotropic instability, is that the horizontal gradient of potential vorticity, $\partial\overline{q}/\partial y$, must change sign *in the vertical direction* (Holton 2004; Vallis 2006). This was satisfied close to the main cloud decks in the idealized basic states investigated by Young et al. (1984), and led to the identification of growing instabilities of zonal wavenumber $s = 2$ close to the pole. The potential vorticity structure in more realistic flows may be more complicated than was assumed by Young et al. (1984), and so the precise role of such forms of baroclinic instability remains somewhat uncertain. More likely in practice, perhaps, is the occurrence of instabilities with a mixed barotropic-baroclinic character, although the relative dominance of either type on Venus remains to be established conclusively.

6.6.3.2 Inertial Instability

Another form of instability is found if the product $f\overline{q} < 0$ anywhere within the domain, where $\overline{q}$ may be either absolute vorticity or (Ertel) potential vorticity (e.g. see Andrews et al. 1987). Such a condition, where the absolute or potential vorticity takes the 'wrong' sign in a given hemisphere, is most likely to occur close to the equator, for which cross-equatorial transport of vorticity can lead to positive $\overline{q}$ crossing into the southern hemisphere and *vice versa*.

The manifestation of this instability is 'classically' of a zonally symmetric form, with vertically stacked rolls in the meridional plane of relatively short vertical wavelength and small lateral scale. This is often to be seen in numerical model simulations, for example, where grid-length perturbations occur close to the equator in zonal mean fields of temperature and velocity. But other forms may be possible, especially if the instability occurs at the same time as other types of instability so their effects reinforce each other. To date, however, there are few if any clear examples of phenomena on Venus that can be unambiguously attributed to inertial instability.

6.6.3.3 Convective and Shear Instability

The other main form of instability that can lead to the generation of propagating waves on Venus is associated with statically unstable or very weakly stable conditions. In this case, the main criterion for instability is provided by the Richardson number (e.g. Drazin and Reid 1981),

$$Ri = \frac{N^2}{(\partial \overline{u}/\partial z)^2}. \tag{6.53}$$

Where the flow is statically stable ($N^2 > 0$), the horizontal roll-like Kelvin-Helmholtz shear instability typically appears for $Ri \leq 0.25$, leading to the development of turbulent flow, although the precise value for the onset of this turbulence is somewhat controversial (e.g. see Galperin et al. 2007). Where $N^2 < 0$ the stratification becomes statically unstable and, provided viscous diffusion is weak enough, the flow becomes convectively unstable and will tend to overturn.

Either of these situations will lead to turbulence production, either from mechanical sources ($Ri > 0$) or thermal convection ($Ri < 0$), and may often lead to the generation of gravity wave activity, especially in stably-stratified regions that may be adjacent to those where the instability breaks out.

Figure 6.18a shows an example of a measured profile of static stability, obtained from radio-occultation measurements of temperature from the Magellan mission by Hinson and Jenkins (1995). This clearly shows a region around 50–55 km altitude where $N^2 \simeq 0$, which is indicative of a well mixed convective layer. This lies within one of the main cloud decks on Venus, where cloud opacity is large and convection

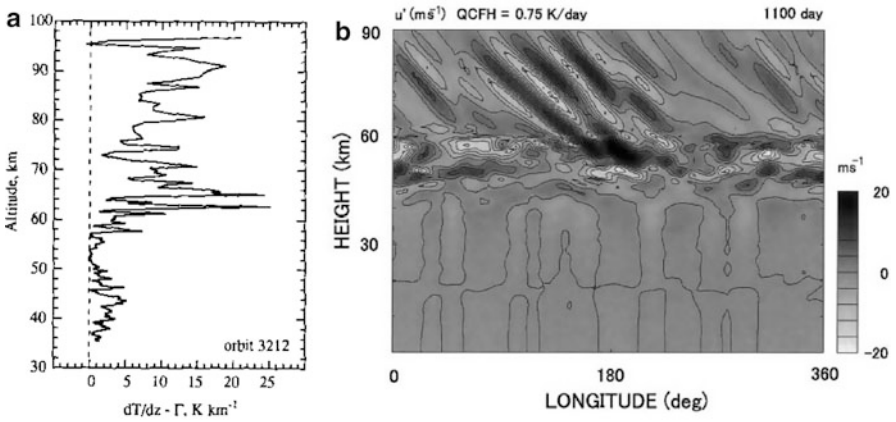

Fig. 6.18 (**a**) Vertical profile of static stability on Venus, obtained via radio-occultation during the Magellan mission by Hinson and Jenkins (1995) and showing evidence for a convective region around 50–55 km altitude, reprinted with the permission from Elsevier; (**b**) generation of vertically-propagating gravity waves in the stable layer overlying a convective layer on Venus, obtained in the numerical model of Yamamoto (2003) after ∼1100 days using a static stability profile similar to a smoothed version of the one shown in (**a**). Figure 6.18b has been reprinted with the permission from the Meteorological Society of Japan

is almost certainly driven by strong absorption of sunlight in the layer immediately below the convection. This layer of convection is bounded on either side by statically stable regions, within which oscillatory activity is visible, likely due to the presence of gravity waves. This is confirmed in model studies, such as those of Yamamoto (2003), illustrated in Fig. 6.18b, which clearly shows vertically-propagating gravity waves in the layer above 60 km altitude emerging from the convective layer between 50 and 60 km. This mechanism has also been extensively studied in similar models by Schubert and Walterscheid (1984), Hou and Farrell (1987), Gierasch (1987), Schnider et al. (1990), Leroy and Ingersoll (1995), Baker et al. (2000a,b) and others.

6.6.4 Forced Waves and Thermal Tides

Another major means of exciting eddies and waves in Venus's atmosphere is through direct forcing of wave activity, of which the most significant is due to the zonal variation in solar heating. The response of the atmosphere to the day-night contrast in solar heating depends strongly on the ratio of the radiative time constant of the atmosphere, τ_R, to the length of the solar day. In general, τ_R is given by

$$\tau_R = \frac{c_p \rho H}{8\sigma_{SB} T^3}, \tag{6.54}$$

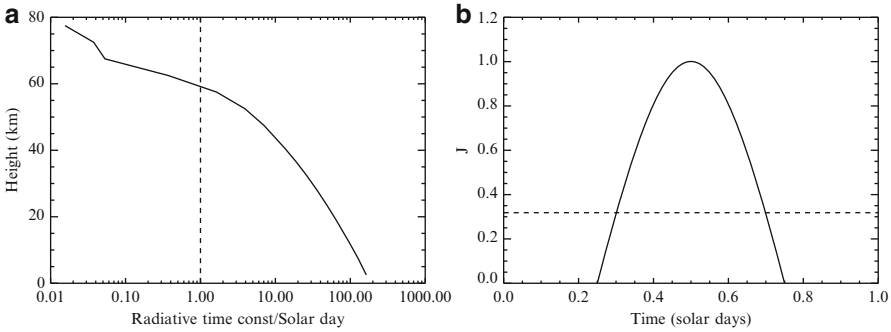

Fig. 6.19 (**a**) Variation with altitude of the ratio of the radiative time constant in the Venus atmosphere to the length of the solar day (116.25 Earth days), as computed by Pollack and Young (1975), and (**b**) idealized variation of solar heating rate J with time of solar day

where c_p is the specific heat capacity of the atmosphere at constant pressure, ρ its density, H the scale height as before and σ_{SB} the Stephan-Boltzmann constant. This is a strong function of height on Venus, not least because ρ is proportional to pressure, $H = H(T)$ and $c_p = c_p(T)$. This variation is illustrated from early computations by Pollack and Young (1975) in Fig. 6.19, which clearly shows that the radiative time constant is much longer than the solar day below the main cloud decks, but becomes comparable to, or significantly smaller than, the solar day above an altitude of around 60 km (where the pressure is around 200 hPa). For altitudes above 50–60 km, therefore, the atmosphere is able to respond rapidly to changes in solar heating on timescales comparable with the solar day.

The variation in direct solar heating is illustrated schematically in Fig. 6.19b, which shows a roughly sinusoidal variation during the daylit period but with zero heating during the night. The response to such a variation of heating rate is typically to force an ensemble of waves, whose period and direction of propagation are likely to be closely related to that of the solar day. On the largest scales, these take the form of westward propagating planetary waves, for which the gravest (zonal wavenumber $s = 1$) corresponds to the diurnal period thermal tide and the first harmonic ($s = 2$) corresponds to the semi-diurnal tide. In general, however, a whole series of other waves may be excited, ranging from planetary scale waves to localized, small-scale gravity waves (e.g. Fels and Lindzen 1974).

A key property of the main thermal tides, however, is their wavelike quality in the vertical as well as the horizontal. In particular, the vertical wavelength of each tidal mode determines to a large extent the strength of its response to diurnal heating. This is because the solar heating is distributed in the vertical over a distance at least comparable with the pressure scale height. The horizontal and vertical structure of tidal modes is well described by classical tidal theory (Chapman and Lindzen 1970) for a stratified atmosphere at rest. For an atmosphere in motion, however, the theory is more complicated and generally requires solution using numerical techniques. For Venus, the diurnal tide typically has a relatively short vertical wavelength (~20 km;

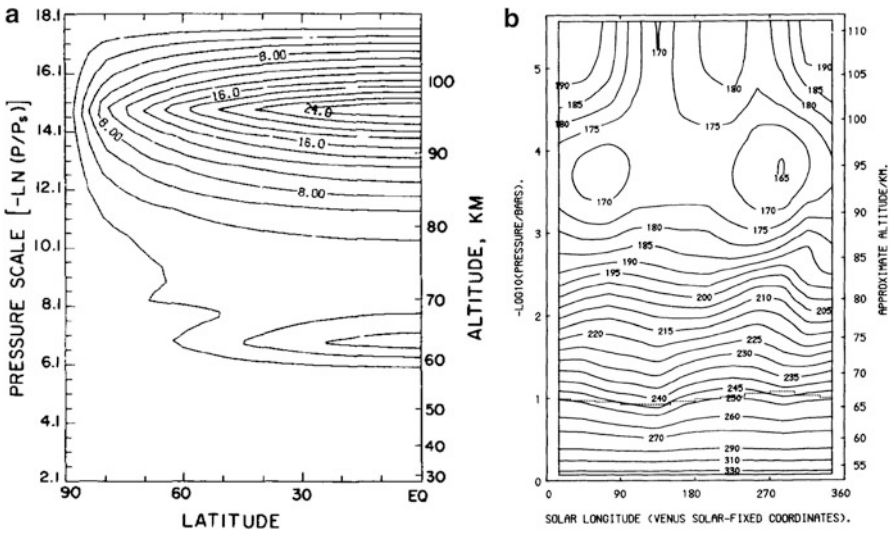

Fig. 6.20 (**a**) Variation of the effective heating rate of the semi-diurnal tide on Venus as a function of height and latitude, derived by Baker and Leovy (1987) reprinted with the permission from Elsevier; (**b**) observed thermal structure of Venus along the equator as a function of longitude and height, obtained from Pioneer Venus infrared sounding by Schofield and Taylor (1983)

Baker and Leovy 1987) compared with the vertical scale of the heating, so the net response to solar heating may be relatively weak. The semi-diurnal tide, however, has a typical wavelength much longer than this and so couples more strongly to the solar heating distribution. The strongest tidal response is therefore expected to be in the $s = 2$ semi-diurnal mode.

Figure 6.20a illustrates a typical distribution of heating rate in height and latitude for the semi-diurnal tide on Venus (Baker and Leovy 1987), that clearly shows a strong peak just above the clouds and a larger secondary peak at higher altitudes around 100 km. The resulting semi-diurnal response can be seen in the observed temperature field from Schofield and Taylor (1983) in Fig. 6.20b, which clearly shows a strong $s = 2$ response at most altitudes above the clouds, peaking in amplitude around 100 km. There is a clear tilt of the phase fronts with altitude characteristic of vertical propagation. This semi-diurnal tide is a major feature in the near-equatorial atmospheric circulation on Venus, that may be expected to play a significant role in its energy and momentum budget.

On smaller scales, convectively generated gravity waves may also be generated within regions that follow the motion of the sub-solar point. This was apparent, for example, in the gravity waves discussed in Sect. 6.6.2 found in Magellan radio-occultation profiles. Such waves were found to have a horizontal phase speed close to zero (Hinson and Jenkins 1995), indicating a connection with the slowly-moving sub-solar point and associated region of strong localized heating.

At high altitudes (>100 km), the radiative time constant becomes so short that the thermal tide circulation may become dominant. In this case, the planetary scale circulation may transition from being dominated by zonally-symmetric equator-pole Hadley circulations towards a three-dimensional flow with rising motion over the sub-solar point and sinking above the anti-solar points. Such a sub-anti-solar circulation is typical of flow in the thermosphere (e.g. Bougher et al. 1997).

6.6.5 *Eddy-Mean Flow Interactions*

The discussion above has so far concentrated on identifying the key classes of waves and eddies in the Venus atmosphere and mechanisms for their generation. But a major role that propagating waves and eddies can play in a stratified atmosphere is to transport heat and momentum across the planet and to deposit these quantities in particular regions.

The detailed quantitative theory of how waves and eddies of finite amplitude interact nonlinearly with background mean zonal flows was developed extensively in the 1980s in the context of a generalized Eliassen-Palm theorem and Lagrangian mean (e.g. see Andrews and McIntyre 1978, Andrews et al. 1987). This generalized Eliassen-Palm theorem can be interpreted as a conservation law for *wave activity density*, A, for which

$$\frac{\partial A}{\partial t} + \nabla \cdot \mathbf{F} = D[+O(\alpha^3)], \tag{6.55}$$

where α represents the amplitude of the wave and $\mathbf{F}$ is the so-called *Eliassen-Palm flux*, given by

$$\mathbf{F} = (0, F_\phi, F_z) \tag{6.56}$$

$$F_\phi = \rho_0 a \cos\phi \left(\frac{\partial \overline{u}}{\partial z} \frac{\overline{u'\theta'}}{\partial \overline{\theta}/\partial z} - \overline{u'v'} \right) \tag{6.57}$$

$$F_z = \rho_0 a \cos\phi \left(\left[f - \frac{1}{a \cos\phi} \frac{\partial (\overline{u} \cos\phi)}{\partial \phi} \right] \frac{\overline{v'\theta'}}{\partial \overline{\theta}/\partial z} - \overline{w'\theta'} \right). \tag{6.58}$$

For many purposes, however, an intuitive understanding of the processes involved can be guided by a few relatively straightforward principles.

(i) In the absence of transient growth or decay of wave amplitude (e.g. due to instability), dissipation or active forcing, waves and eddies will propagate without interaction with the background zonal flow;

(ii) Where irreversible dissipation of wave activity takes place, a nonlinear interaction between the wave and the background zonal mean flow can occur, leading to an acceleration of the mean zonal flow. This will typically act in the same sense as the phase speed of the propagating waves or eddies.

(iii) This interaction may be especially strong in *critical layers*, where the phase speed $c \simeq \overline{u}$ and the Doppler-shifted wave frequency in a frame moving with $\overline{u} \rightarrow 0$.
(iv) Where wave-forcing takes place, momentum of the same sign as c is removed from the mean zonal flow, leading to a net wave-induced acceleration in the opposite sense to c.

Thus, we can see that where the retrograde-propagating semi-diurnal tide is being actively forced, this will tend to lead to a prograde zonal acceleration. As the tide propagates away from its source region and begins to dissipate elsewhere, that region will experience a wave-induced retrograde acceleration unless a critical layer develops. In this way, tides can produce zonal accelerations in either sense, depending upon the details of where they are actively forced or dissipated. Similar considerations will also apply to small-scale gravity waves, driven e.g. by sub-solar convection. Conversely, waves driven via interactions with the surface will tend to have a zonal phase speed close to zero relative to the underlying planet. Where such waves are dissipated, the zonal flow will tend to experience a wave-induced 'drag' towards zero.

The role of eddies emerging as the result of large-scale instabilities is somewhat less straightforward to explain. According to the GRW scenario discussed in Sect. 6.5, eddies may be generated spontaneously on the equator-ward side of the zonal flow at mid-latitudes on Venus, which can transport angular momentum equator-wards to counteract the poleward transport of angular momentum due to the thermally-direct Hadley circulation. This picture is consistent with ideas based on vorticity mixing in planetary atmospheres (e.g. see Read 1986). However, the waves resulting from barotropic instability of the mid-latitude zonal 'jets' on Venus are essentially 'westward-propagating' Rossby waves, so will tend to produce retrograde accelerations if they propagate equator-wards and dissipate in the tropics. This is broadly what appears to happen in the Earth's atmosphere, leading to tropical easterlies in the mid-upper troposphere. Recent work by Williams (2003) and Mitchell and Vallis (2010), however, suggest that other kinds of instability at tropical and sub-tropical latitudes may be necessary during the spin-up phase to produce an equilibrated super-rotating state at the equator itself.

Mitchell and Vallis (2010) note that the dominant instability during spin-up of a model atmosphere from rest with slow planetary rotation is of a mixed barotropic-baroclinic character and of global scale. So the simple paradigm outlined above for spatially separated wave generation and dissipation in a critical layer does not apply. In practice, the dominant instability during spin-up takes a form similar to an equatorial Kelvin mode in the tropics of wavenumber $s = 1$, leading to prograde acceleration over the equator. As the spin-up progresses, the horizontal reversal of potential vorticity gradient on either side of the equator is reduced to ∼zero, expelling the strong gradients towards the fringes of the polar vortex and across the equator, much as now observed on Venus. Evidence for the dominant planetary-scale waves that might be responsible for the acceleration of the atmosphere close to the equator is fairly elusive in observations, although some indication of global waves with plausible frequencies and phase speeds were found from analyses of

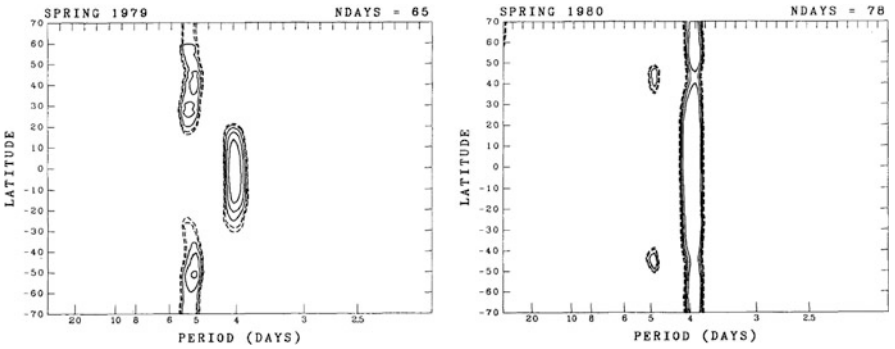

Fig. 6.21 Frequency spectra of ultraviolet cloud brightness as a function of latitude, obtained by Del Genio and Rossow (1990) from Pioneer Venus images at two different times

ultraviolet images of Venus taken by Pioneer Venus (see Del Genio and Rossow 1990). Figure 6.21 shows two examples of cloud brightness frequency spectra of the $s = 1$ zonal wavenumber features, derived from time series of Pioneer Venus ultraviolet images by Del Genio and Rossow (1990). These indicate some significant variability, but the occurrence of coherent features with relatively short period ($\sim$4 Earth days) close to the equator appears to be common and sometimes seen to extend across the whole planet, much as seen in the models of Mitchell and Vallis (2010). At other times, however, the equatorial and mid-latitude features decouple into separate components, with the mid-latitudes exhibiting a lower frequency feature with a period closer to 5 Earth days. Such features appear to have aspects in common with the discrete Kelvin, Rossby and Rossby-gravity modes discussed above.

Another aspect of eddy-mean flow interaction is the effect of eddies on the transport of quasi-conserved tracers such as vorticity and chemical constituents. In regions where eddies propagate but are not irreversibly breaking or dissipating, material transport across strong gradients of (potential) vorticity tends to be inhibited, leading to the concept of an *eddy transport barrier* (McIntyre 1995). This situation regularly occurs in the Earth's polar stratosphere and underlies the formation of the Antarctic ozone hole because of the dynamical isolation of ozone rich air within the stable polar vortex. The extent to which similar effects occur on Venus is currently not known, but could play a significant role in maintaining compositional variations across the planet.

6.7 Atmospheric Interactions with the Surface

The role of surface interactions with the atmosphere on Venus is an aspect that is still relatively sparsely explored, either in models or observations. In general terms, the surface is important in providing a boundary condition for radiative heating and cooling, and in mechanically coupling the atmosphere to the underlying planet.

Winds are believed to be relatively weak close to the surface, as found e.g. by the Venera and Pioneer Venus entry probes, but the high density of the atmosphere may lead to significant stresses exerted at the surface.

In general, winds at the surface will lead to both turbulent frictional stresses and form drag forces due to interactions with topographic features. Both kinds of interaction are important in producing exchanges of linear and angular momentum between the atmosphere and the underlying planet. In a long term equilibrium, frictional and form drag torques on the atmosphere must come into balance to result in zero net torque across the planet. This tends to imply that zonal flow of either sign must occur in different places across the planet, most likely with prograde flow at mid-high latitudes and weak retrograde flow close to the equator, as may be induced by near-surface equator-ward flow in the main Hadley circulations.

Frictional interactions are typically treated by analogy with planetary boundary layer flows on Earth, utilizing Monin-Obukhov similarity theory for the surface layer and some form of bulk closure or turbulence model for the main mixed layer (e.g. see Garratt 1994). The choice of roughness length, z_0, is not well characterized for Venus, but typical values that have been used are around $z_0 \sim 1 - 3\,\mathrm{cm}$ (e.g. Lebonnois et al. 2010), typical of small-medium boulder fields on Earth.

Form drag represents the stress acting on the atmosphere associated with pressure differences across topographic features as large-scale wind patterns interact with topography. In addition to local stresses on the atmosphere close to the ground, such interactions can also lead to non-local stresses through the generation of vertically propagating waves that are stationary in the horizontal. As discussed earlier, such waves may break and dissipate at high altitude within the free atmosphere, leading to eddy-zonal flow interactions that may decelerate the flow at those altitudes and have a significant effect on the overall momentum budget.

Finally, the surface may also play a significant role in mediating thermal interactions with the atmosphere. This can be quantified in a similar way as for the Earth's planetary boundary layer (Garratt 1994), although this again is relatively unexplored in both observations and models. However, the strength of surface solar heating on Venus is comparatively weak compared with the Earth, because of the very high albedo of Venus's clouds and the relatively strong absorption of sunlight by the atmosphere itself. In addition, the lower atmosphere has a relatively large heat capacity because of its high density and is optically thick in the infrared, so the thermal structure of the lower atmosphere and surface is relatively weakly forced by radiative heating and cooling. So surface temperature on Venus is largely controlled by the altitude of the surface along a nearly uniform lapse rate with height.

References

A.C.B. Aguiar, P.L. Read, R.D. Wordsworth, T. Salter, Y.H. Yamazaki, A laboratory model of Saturn's North Polar hexagon. Icarus **206**, 755–763 (2010)

D.G. Andrews, M.E. McIntyre, Generalized eliassen-palm and charney-drazin theorems for waves on axisymmetric mean flows in compressible atmospheres. J. Atmos. Sci. **35**, 175–185 (1978)

D.G. Andrews, J.R. Holton, C.B. Leovy, *Middle Atmosphere Dynamics* (Academy, Orlando, 1987)
N.L. Baker, C.B. Leovy, Zonal winds near Venus cloud top level – a model study of the interaction between the zonal mean circulation and the semidiurnal tide. Icarus **69**, 202–220 (1987)
R.D. Baker, G. Schubert, P.W. Jones, Convectively generated internal gravity waves in the lower atmosphere of venus. part I: No wind shear. J. Atmos. Sci. **57**, 184–199 (2000a)
R.D. Baker, G. Schubert, P.W. Jones, Convectively generated internal gravity waves in the lower atmosphere of venus. part II: Mean wind shear and wave-mean flow interaction. J. Atmos. Sci. **57**, 200–215 (2000b)
S.W. Bougher, M.J. Alexander, H.G. Mayr, Upper atmosphere dynamics: global circulation and gravity waves, in *Venus II: Geology, Geophysics, Atmosphere, and Solar Wind Environment*, ed. by S.W. Bougher, D.M. Hunten, R.J. Philips, University of Arizona Press, AZ, Tucson (1997), pp. 259–291
S. Chapman, S. Lindzen, *Atmospheric Tides* (Reidel, Dordrecht, 1970)
C.C. Counselman III, S.A. Gourevitch, R.W. King and G.B. Loriot, Zonal and meridional circulation of the lower atmosphere of Venus determined by radio interferometry, J. Geophys. Res, **85**, 8026–8030 (1980)
R.A. Craig, A solution of the nonlinear vorticity equation for atmospheric motion. J. Meteor. **2**, 175–178 (1945)
A.D. Del Genio, W.B. Rossow, Planetary-scale waves and the cyclic nature of cloud top dynamics on Venus. J. Atmos. Sci. **47**, 293–318 (1990)
P.G. Drazin and W.H. Reid, Hydrodynamic Stability, Cambridge University Press, Cambridge, UK (1981)
L.S. Elson, Wave instability in the polar-region of Venus. J. Atmos. Sci. **39**, 2356–2362 (1982)
S.B. Fels, R.S. Lindzen, The interaction of thermally excited gravity waves with mean flows. Geophys. Fluid Dyn. **6**, p. 149–191 (1974)
W.G. Fruh, P.L. Read, Experiments on a barotropic rotating shear layer. part 1. instability and steady vortices. J. Fluid. Mech. **383**, 143–173 (1999)
B. Galperin, S. Sukoriansky, P.S. Anderson, On the critical Richardson number in stably stratified turbulence. Atmos. Sci. Lett. **8**, 65–69 (2007)
J.R. Garratt, The atmospheric boundary layer – review. Earth-Science Reviews **37**, 89–134 (1994)
P.J. Gierasch, Meridional circulation and the maintenance of the Venus atmospheric rotation. J Atmos. Sci. **32**, 1038–1044 (1975). doi:10.1175/1520-0469(1975)032
P.J. Gierasch, Waves in the atmosphere of Venus. Nature **328**, 510–512 (1987)
P.J. Gierasch, P.H. Stone, A mechanism for Jupiter's equatorial acceleration. J. Atmos. Sci. **25**, 1169–1170 (1968)
A.E. Gill, Atmosphere-Ocean Dynamics. Academic Press, New York (1982)
D. Grassi, A. Migliorini, L. Montabone, S. Lebonnois, A. Cardesin-Moinelo, G. Piccioni, P. Drossart, L.V. Zasova, Thermal structure of Venusian nighttime mesosphere as observed by VIRTIS-Venus Express. J. Geophys. Res.-Planets **115**, E09007 (2010)
B. Haurwitz, The motion of atmospheric disturbances on the spherical Earth. J. Mar. Res. **3**, 254–267 (1940)
I.M. Held, A.Y. Hou, Non-linear axially-symmetric circulations in a nearly inviscid atmosphere. J. Atmos. Sci. **37**, 515–533 (1980)
R. Hide, Dynamics of the atmospheres of the major planets, with an appendix on the viscous boundary layer at the rigid bounding surface of an electrically-conducting rotating fluid in the presence of a magnetic field. J. Atmos. Sci. **26**, 841–853 (1969)
R. Hide, Equatorial jets in planetary atmospheres. Nature **225**, 254–255 (1970)
D.P. Hinson, J.M. Jenkins, Magellan radio occultation measurements of atmospheric waves on Venus. Icarus **114**, 310–327 (1995)
J.R. Holton, *Introduction to Dynamic Meteorology*, 4th edn. (Academic, New York, 2004)
A.Y. Hou, Axisymmetric circulations forced by heat and momentum sources – a simple-model applicable to the Venus atmosphere. J. Atmos. Sci. **41**, 3437–3455 (1984)
A.Y. Hou, B.F. Farrell, Superrotation induced by critical-level absorption of gravity-waves on Venus – an assessment. J. Atmos. Sci. **44**, 1049–1061 (1987)

A.Y. Hou, R.M. Goody, Diagnostic requirements for the superrotation on Venus. J. Atmos. Sci. **42**, 413–432 (1985)
L.N. Howard, P.G. Drazin, On instability of parellel flow of inviscid fluid in rotating system with variable coriolis parameter. J. Math. Phys. **43**, 83–99 (1964)
S. Iga, Y. Matsuda, Shear instability in a shallow water model with implications for the Venus atmosphere. J. Atmos. Sci. **62**, 2514–2527 (2005)
S. Lebonnois, F. Hourdin, V. Eymet, A. Crespin, R. Fournier, F. Forget, Superrotation of Venus' atmosphere analyzed with a full general circulation model. J. Geophys. Res.-Planets **115**, 6006 (2010). doi:10.1029/2009JE003458
C.B. Leovy, Rotation of the upper atmosphere of Venus.. J. Atmos. Sci. **30**, 1218–1220 (1973). doi:10.1175/1520-0469(1973)030
S.S. Leroy, A.P. Ingersoll, Convective generation of gravity-waves in Venus's atmosphere – gravity-wave spectrum and momentum transport. J. Atmos. Sci. **52**, 3717–3737 (1995)
S.S. Limaye, Venus atmospheric circulation: Known and unknown. J. Geophys. Res. **112**, E04S09 (2007). doi:10.1029/2006JE002814
S.S. Limaye, J.P. Kossin, C. Rozoff, G. Piccioni, D.V. Titov, W.J. Markiewicz, Vortex circulation on Venus: Dynamical similarities with terrestrial hurricanes. Geophys. Res. Lett. **36**, L04204 (2009). doi:10.1029/2008GL036093
R.S. Lindzen, Instability of plane parallel shear-flow (toward a mechanistic picture of how it works). Pure Appl. Geophys. **126**, 103–121 (1988)
M.S. Longuet-Higgins, Eigenfunctions of laplaces tidal equations over a sphere. Phil. Trans. R. Soc. A **262**, 511–607 (1968)
T. Matsuno, Quasi-geostrophic motions in the equatorial area. J. Meteorol. Soc. Japan **44**, 25–43 (1966)
M.E. McIntyre, The stratospheric polar vortex and sub-vortex – fluid-dynamics and midlatitude ozone loss. Phil. Trans. R. Soc. A **352**, 227–240 (1995)
J.M. Mendonca, P.L. Read, C.F. Wilson, S.R. Lewis, Zonal winds at high latitudes on Venus: An improved application of cyclostrophic balance to Venus Express observations. Icarus **217**, 629–639 (2012). doi:10.1016/j.icarus.2011.07.010
D.V. Michelangeli, R.W. Zurek, L.S. Elson, Barotropic instability of midlatitude zonal jets on Mars, Earth And Venus. J. Atmos. Sci. **44**, 2031–2041 (1987)
J.L. Mitchell, G.K. Vallis, The transition to superrotation in terrestrial atmospheres. J. Geophys. Res. **115**, E12008 (2010). doi:10.1029/2010JE003587
S.M. Neamtan, The motion of harmonic waves in the atmosphere. J. Meteor. **3**, 53–56 (1946)
H. Niino, N. Misawa, An experimental and theoretical-study of barotropic instability. J. Atmos. Sci. **41**, 1992–2011 (1984)
J. Peralta, R. Hueso, A. Sanchez-Lavega, G. Piccioni, O. Lanciano, P. Drossart, Characterization of mesoscale gravity waves in the upper and lower clouds of Venus from VEX-VIRTIS images. J. Geophys. Res.-Planets **113**, E00B18 (2008)
R.A. Plumb, Angular-momentum advection by axisymmetric motions. Quart. J. R. Meteor. Soc. **103**, 479–485 (1977)
J.B. Pollack, R. Young, Calculations of radiative and dynamical state of Venus atmosphere. J. Atmos. Sci. **32**, 1025–1037 (1975)
P. Read, Super-rotation and diffusion of axial angular momentum: II. A review of quasi-axisymmetric models of planetary atmospheres. Quater. J. R. Met. Soc. **112**, 253–272 (1986)
C.G. Rossby, Relation between variations in the intensity of the zonal circulation of the atmosphere and the displacements of the semipermanent centers of action. J. Mar. Res. **2**, 38–55 (1939)
W.B. Rossow, G.P. Williams, Large-scale motion in the Venus stratosphere. J. Atmos. Sci. **36**, 377–389 (1979). doi:10.1175/1520-0469(1979)036
E.K. Schneider, Axially-symmetric steady-state models of basic state for instability and climate studies. 2. Nonlinear calculations. J. Atmos. Sci. **34**, 280–296 (1977)
P.J. Schnider, P.J. Gierasch, S.S. Leroy, M.D. Smith, Waves, advection, and cloud patterns on venus. J. Atmos. Sci. **47**, 2037–2052 (1990)

J.T. Schofield, F.W. Taylor, Measurements of the mean, solar-fixed temperature and cloud structure of the middle atmosphere of Venus. Quart. J. R. Meteor. Soc. **109**, 57–80 (1983)

G. Schubert, R.L. Walterscheid, Propagation of small-scale acoustic gravity-waves in the Venus atmosphere. J. Atmos. Sci. **41**, 1202–1213 (1984)

J. Sommeria, S.D. Meyers, H.L. Swinney, Experiments on vortices and Rossby waves in eastward and westward jets, in *Nonlinear Topics in Ocean Physics*, ed. by A.R. Osborne (North-Holland, Amsterdam, 1991)

V.P. Starr, *The Physics of Negative Viscosity Phenomena* (McGraw-Hill, New York, 1968)

P.D. Thompson, The propagation of permanent-type waves in horizontal flow. J. Meteor. **5**, 166–168 (1948)

G.K. Vallis, *Atmospheric and Oceanic Fluid Dynamics: Fundamentals and Large-Scale Circulation* (Cambridge University Press, Cambridge, 2006)

I.C. Walton, Viscous nonlinear symmetric baroclinic instability of a zonal shear-flow. J. Fluid Mech. **68**, 757–768 (1975)

G.P. Williams, Barotropic instability and equatorial superrotation. J. Atmos. Sci. **60**, 2136–2152 (2003)

M. Yamamoto, Gravity waves and convection cells resulting from feedback heating of Venus' lower clouds. J. Meteorol. Soc. Japan **81**, 885–892 (2003)

R.E. Young, H. Houben, L. Pfister, Baroclinic instability in the Venus atmosphere. J. Atmos. Sci. **41**, 2310–2333 (1984)

Chapter 7
Modeling Efforts

Stephen R. Lewis, Jonathan Dawson, Sebastien Lebonnois, and Masaru Yamamoto

In this section we survey the historical development of Venus models and the range of models now available, before discussing some of their remaining limitations. We also consider some approaches which have been taken to model Saturn's moon Titan, also a slowly-rotating body with an optically thick, dense atmosphere which super-rotates compared to Titan's surface.

7.1 Venus Modeling Efforts and Historical Background

In many ways Venus is a natural planet on which to first attempt the application of terrestrial atmospheric modeling techniques to a body other than the Earth, being a rocky body of very similar size to the Earth, a similar distance from the Sun and with a thick neutral, gaseous atmosphere. Historically progress in modeling has, however, been limited by several factors. The slow rotation rate places Venus closer to a cyclostrophic rather than geostrophic balance, and so many of the simplified balance theories, such as quasi-geostrophic balance, developed for the Earth do

S.R. Lewis (✉)
Department of Physical Sciences, The Open University, Milton Keynes, UK
e-mail: S.R.Lewis@open.ac.uk

J. Dawson
Department of Physics & Astronomy, The Open University, Milton Keynes, UK
e-mail: jon.dawson@open.ac.uk

S. Lebonnois
Laboratoire de Meteorologie Dynamique, Paris, France
e-mail: Sebastien.Lebonnois@lmd.jussieu.fr

M. Yamamoto
Research Institute for Applied Mechanics, Kyushu University, Fukuoka, Japan
e-mail: yamakatu@riam.kyushu-u.ac.jp

L. Bengtsson et al. (eds.), *Towards Understanding the Climate of Venus*, ISSI Scientific Report Series 11, DOI 10.1007/978-1-4614-5064-1_7,

not apply. The dense and optically thick atmosphere results in very long radiative relaxation times and so models have to be integrated for many tens of years to approach equilibrium, again in contrast to the Earth or Mars where an atmospheric statistical equilibrium may be reached in a few tens of days. Finally, there has been relatively little wind or thermal data for the Venus lower and middle atmosphere below the ubiquitous cloud-tops and it has been consequently difficult to constrain or validate models. Each of these factors has combined to result in less progress in Venus atmosphere modeling than has been possible for the Earth, or even Mars, although the influx of new spacecraft observations from missions such as Venus Express and advances in computing power have lead to the development of a range of Venus global atmosphere models in recent years.

In this section we briefly survey the historical development of Venus models and the range of models now available, before discussing some of their remaining limitations and lead on to the development of a model intercomparison programme in the following section. We consider lessons which may be learnt from efforts to model the atmosphere of Saturn's moon Titan, also a slowly-rotating body with an optically thick, dense atmosphere which super-rotates compared to Titan's surface.

Early models of the Venus atmosphere, prior to Pioneer Venus in 1979, were hampered by the lack of observational data below the cloud tops with which to constrain models and by the limited computing resources available to researchers. These models were primarily one- and two-dimensional and could not be described as global circulation models in the modern context. From 1975 a few studies began tentatively to apply three-dimensional, global modeling techniques to the atmosphere of Venus.

7.1.1 Early Two- and Three-Dimensional Venus Models

Kalnay de Rivas (1975) presented the results of two-dimensional simulations of the deep circulation of Venus. These showed that the high surface temperature of Venus can only be explained by the greenhouse effect and not by any of the competing theories around at the time (e.g. the Goody and Robinson 1966 dynamical model).

Secondly, Kalnay de Rivas (1975) used results from a quasi-three-dimensional version of her model (obtained by extending the two-dimensional model with a few longitudinal wave terms) to test the, then new, Gierasch mechanism which seeks to explain super-rotation and the 4 day Venus circulation. The three-dimensional model was a quasi-Boussinesq 'pressure type' model where the original momentum equations are used to determine the pressure by the solution of an elliptic equation. The model used a combination of exponential Fourier components in the longitudinal plane (spectral method), and finite differences for the meridional plane (latitude and height).

The three-dimensional model was tested with only zonal wavenumber 0 retained, and 18 grid intervals from equator to pole. In numerical experiments, where the model was integrated for 2.2×10^7 s ($\approx$240 Earth days (Edays), 1 Venus sidereal day (Vsid)), Kalnay de Rivas (1975) obtained a maximum zonal velocity of 17 m/s

at 10° from pole. The model produced a single equator to pole Hadley cell for each hemisphere.

Young and Pollack (1977) used a three-dimensional model with seemingly a great deal of success in modeling the atmosphere of Venus, obtaining results which match observations quite closely. Their model used an equally spaced vertical grid, solving the primitive equations using centered and finite differences, and spectral harmonics to resolve the flow structure horizontally. The model used a maximum of 32 vertical levels, although most integrations used 16, up to 64 km at their model top. Solar and infrared heating rates were computed, the solar energy deposition rates giving a vertical temperature profile that was consistent with Venera 8 measurements. Considerable attention was paid to the discussion of eddy diffusion terms and their parameterization.

Despite short integration times of the order of 15 Venus solar days the results obtained were impressive. Zonal wind speeds in some integrations reached up to ≈100 m/s, in the same sense as the underlying planet's rotation, and the model exhibited stacked Hadley cells and warm poles. A, perhaps more typical, result for the winds was ≈35 at the equator, increasing to a peak of ≈51 at 50°N and then reducing back to zero at the pole.

Young and Pollack (1977) suggest that the main mechanism for maintenance of the equatorial zonal wind, the super-rotation, is transport of angular momentum poleward by the meridional circulation which is offset by equator-ward transport by planetary scale eddies. They state that planetary scale eddies are the principle mechanism for converting potential energy to kinetic energy.

Subsequently, Rossow et al. (1980) argued that the formulation by Young and Pollack (1977) and the conclusions drawn are incorrect. They point out that with the exception of stresses at the surface, all model physics should conserve angular momentum, but the Young and Pollack (1977) vertical momentum diffusion formulation does not. Rossow et al. (1980) also note that there are severe problems arising from the truncation used and the assumed symmetry, which eliminates most of the wave modes.

Rossow and Williams (1979) used a two-dimensional model with a 128 x 128 grid point array and the Arakawa (1966) finite differences scheme, time-stepping with the standard leapfrog method,with the aim of explaining the horizontal distribution of angular momentum in Venus' stratosphere. Despite the relative lack of observational data available at the time, Rossow and Williams (1979) conclude that the circulation is dominated by inertial effects, the turbulent cascade of kinetic energy and enstrophy. They also posit a 'relaxed' state, resembling two-dimensional vorticity conserving flow, which on a slowly rotating planet consists of a solid body rotation plus an advection wave, with zonal wavenumber one, lying symmetrically about the equator.

Rossow and Williams (1979) also concluded that problems would arise in future attempts to model Venus' atmosphere because the inertial cascade process requires a relatively high resolution. They caution that coarse horizontal resolution, or severe spectral truncation, will have two serious effects: that it increases the importance of eddy diffusion, a poorly understood parameter; and that it artificially stabilizes some of the planetary scale waves.

Despite not identifying the processes producing Venus' super-rotation nor investigating directly the role of gravity waves, Rossow and Williams (1979) conclude the stratospheric dynamics of Venus are dominated by two-dimensional interactions.

7.1.2 Three-Dimensional Modeling After Pioneer Venus

At least two global Venus atmosphere models were developed in the years immediately following the Pioneer Venus mission.

Rossow (1983) used a three-dimensional model to investigate whether 1) the mean meridional circulation can provide the dominant vertical and horizontal heat flux in a massive, slowly rotating atmosphere as suggested by Stone (1974), 2) What determines the vertical and horizontal structure of the mean meridional circulation, 3) Can the mean meridional circulation transport momentum over large vertical distances as suggested by Gierasch (1975), and 4) Do some eddy motions behave as if they are barotropic, two-dimensional motions as suggested by Rossow and Williams (1979).

The model used was a version of the GFDL [NOAA/Geophysical Fluid Dynamics Laboratory] 9-levels, 15 wavenumber spectral GCM of the Earth's atmosphere which had been modified to resemble Venus. When run for moderately long integration times >5,000 days, the zonal winds and circulation failed to reach the observed magnitudes. In the lower and middle atmosphere, the zonal flow on Venus is at least 3–5 times stronger than that produced by the model.

Mayr and Harris (1983) also used a spectral model to discuss quasi-axisymmetric circulation in an anisotropic viscous fluid, and super-rotation in planetary atmospheres, with a specific emphasis on Venus. They state that it is understood that the required large eddy diffusivities may arise from longitudinal disturbances and therefore the flow is not completely axisymmetric. Flow in their model was driven by solar radiation absorbed at low latitudes, with air rising near the equator and falling at higher latitudes, a classic Hadley cell.

The assumptions made by Mayr and Harris (1983) included taking a Prandtl number of 1, and a ratio of 10^5 between the horizontal and vertical eddy diffusion coefficients, values which are broadly consistent with mixing length theory. In the Venus atmosphere, which is convectively stable, they found that the 4-day equatorial circulation could be maintained with a single Hadley cell. Above the clouds the latitudinal variation of temperature reverses, leading to warm poles. Depending on the assumptions made, in one case adding a Newtonian cooling term, the wind speeds achieved reach 100 m/s and above. Mayr and Harris (1983) took an essentially heuristic approach and varied many model parameters, noting that atmospheric super rotation is ubiquitous in our solar system.

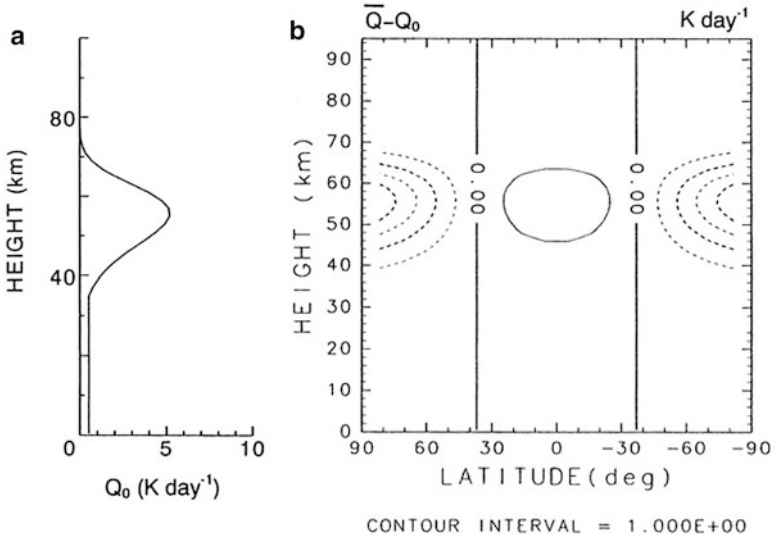

Fig. 7.1 Thermal forcing used in Yamamoto and Takahashi (2003a,b). (**a**) The vertical profile of global mean solar heating rate Q_0 (K day^{-1}), (**b**) the latitude-height cross section of $\overline{Q} - - - Q_0$ ($\overline{Q}$: the zonal mean heating rate). Dashed curve indicates negative value. From Yamamoto and Takahashi (2003a,b)

7.1.3 More Recent Venus Global Atmosphere Modeling

In this section we briefly review existing fully three-dimensional models of the atmosphere of Venus developed in recent years including the group that will be used for the model intercomparison presented in section "Results".

7.1.3.1 CCSR/NIES Model

Yamamoto and Takahashi (2003a,b) used a spectral model developed for terrestrial modeling by the Center for Climate System Research/National Institute for Environmental Study (CCSR/NIES) in Japan. This is a T10 (a triangular spectral truncation at a total wavenumber 10) model with 50 vertical levels (L50) between 0 and 90 km. The grid for the calculation of the physical processes and nonlinear terms is 32×16. The model is adapted to basic Venus planetary parameters, such as radius and rotation rate.

For their simplified Venus GCM, Yamamoto and Takahashi (2003a,b) assumed a simplified radiative process of zonally uniform solar heating and Newtonian cooling. The profile of the solar heating rate is shown in Fig. 7.1.

Yamamoto and Takahashi (2003a) note that the altitude of the maximum heating rate is lower than the cloud top heating maximum by about 10 km.

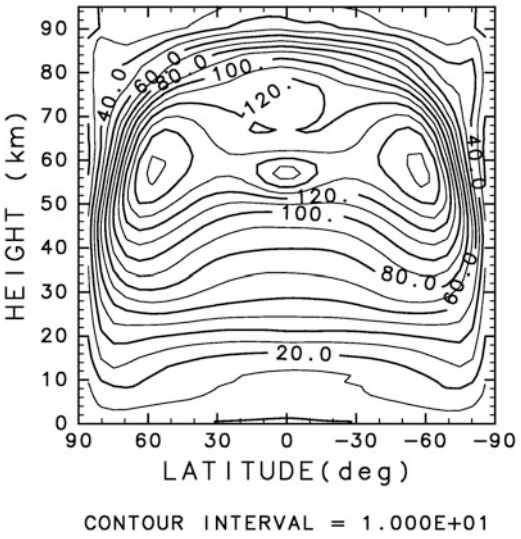

Fig. 7.2 Latitude-height cross section of longitudinally averaged zonal flow (m s^{-1}). From Yamamoto and Takahashi (2003b)

Yamamoto and Takahashi (2003b) further note that this profile produced fully developed super-rotation whereas a heating profile with a maximum at the cloud top did not. Solar heating due to CO_2 above 70 km and surface radiative processes are also neglected.

The parametrization of the atmospheric diffusion was designed not to supply angular momentum from the surface to the atmosphere as is possible in Earth GCMs.

Spun up from rest and reaching equilibrium after ≈50,000 Edays, the zonal wind peaked at approximately 100 m/s near 60 km altitude, at ±60° latitude, with a similar form, though a smaller magnitude, to that shown in Fig. 7.2.

The observed super-rotation is maintained by the Hadley circulation, with a single cell, and various waves, essentially by the Gierasch-Rossow-Williams (GRW) mechanism Gierasch (1975); Rossow and Williams (1979). Vertically propagating gravity waves decelerate the flow above the clouds and enhance the meridional circulation, although the 4-day circulation is fully developed within the cloud layer.

Yamamoto and Takahashi (2003b) present results from a similar model except that the model was now extended to T21 (a spectral truncation at total wavenumber 21, with a 64 × 32 longitude-latitude grid in real space) horizontal resolution and the horizontal diffusion was 8^{th} order. The vertical resolution was 50 levels between the surface and 90 km, as before.

Equilibrium was reached after ≈40,000 Edays. A zonal flow slightly stronger than previously was found, shown in Fig. 7.2, with windspeeds of ≈120 m/s between 50 and 70 km altitude, and mid-latitude jets again peaking at ±60° latitude near the cloud tops. Once again a single pair of Hadley cells was found to be predominant.

With more developments to their model, Yamamoto and Takahashi (2004) refined their earlier simulations further. For these experiments, their model had 52 vertical

levels, and a new three-dimensional solar heating and Newtonian cooling system. Although the description of the heating distribution was improved over the previous model, e.g. the peak solar heating was at higher altitude, a little over 60 km above the surface, they noted that the heating rate below 55 km was much higher than is realistic for Venus.

A 4^{th} order horizontal diffusion with an e-folding time of 4 Edays at the maximum wavenumber is introduced, which is less scale-selective than in Yamamoto and Takahashi (2003a,b). The equator to pole temperature difference at the surface is set to 10 K, again prescribed to be larger than the real atmosphere ($\leq$ 5K). Linear surface drag is imposed with a time constant of 3 days.

These experiments again produced a strongly super-rotating atmosphere, with peak zonal wind-speed of $\approx$100 m/s in the cloud tops at equatorial latitudes. Many waves are found, including an equatorial Kelvin wave and a midlatitude Rossby wave (seen in shear instability) which transport angular momentum towards the equator in the lower atmosphere. There are also thermally-induced, global-scale tides which are now introduced into the model by the more sophisticated thermal forcing. Yamamoto and Takahashi (2004) suggest that thermal tides are a more promising candidate for horizontal eddy momentum transport processes in the middle atmosphere rather than barotropic eddies.

Yamamoto and Takahashi (2006) further investigate the maintenance mechanism of super-rotation and the sensitivities to the surface boundary conditions, using the same model as Yamamoto and Takahashi (2004). Results were similar to Yamamoto and Takahashi (2004) with fully developed super-rotation and several waves with periods similar to those observed in Venus' atmosphere e.g. the 5.5 day, zonal wavenumber 1, Kelvin wave, as well as a range of thermal tides. The experiments to test the sensitivity to the surface conditions revealed that the equator-pole temperature difference and the frictional drag were important parameters in the maintenance of the super-rotation. If any of these parameters were 'tuned' incorrectly then the peak zonal winds were found to be significantly reduced.

Ikeda et al. (2007) modified the radiation code (including aerosol, CO_2 and H_2O absorption and emission) from an Earth GCM to become appropriate for the Venus atmosphere. The simulated vertical structure of temperature below 70 km was found to agree well with observations. A super-rotational flow of about 70 ms^{-1} was maintained primarily by thermal tides and the meridional circulation near the equatorial cloud top. Below 55 km, the zonal wind was found to be much weaker than observations. Ikeda et al. (2007) observe that if a gravity-wave parameterization is introduced, the lower-atmospheric super-rotation below 55 km can become more fully developed by the forced gravity waves.

Takagi and Matsuda (2007) developed a three-dimensional mechanistic model based on a spectral model running at low resolution, T10, also with 50 vertical levels (L50) between 0 and 90 km. Takagi and Matsuda (2007) included a simple representation of the diurnal cycle in which the zonal-mean component of the solar heating was removed. The meridional circulation induced by the zonal mean heating is thus not simulated in their model. In contrast to the results of Yamamoto and Takahashi (2003a,b) for the upper atmosphere, Takagi and Matsuda (2007)

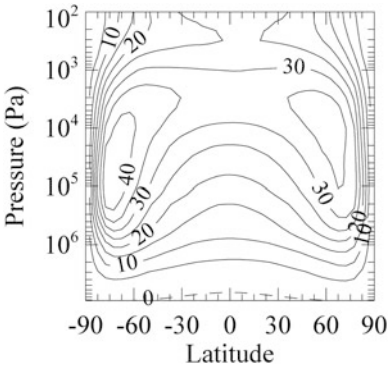

Fig. 7.3 Latitude-height cross section of the zonal mean westward wind speed, averaged over 3 years of data at 100 years. From Lee and Richardson (2010)

suggested that the thermal tides produce lower-atmospheric super-rotation via near-surface deceleration in the absence of the meridional circulation.

A similar mechanism, was suggested by the Ikeda et al. (2007) model which featured a more complete radiation scheme and proposed that the substantial super-rotation produced was driven primarily by vertical transport by the thermal tide modes and not by horizontal transport by waves. The role of the significant horizontal hyper-diffusion in these low horizontal resolution models remains to be fully investigated.

It is worth noting, in relation to some results to be presented in section "Results", that some investigations with these models have noted the sensitivity of the super-rotation produced to the particular form of the model initial conditions. Kido and Wakata (2008, 2009) showed the existence of multiple, super-rotating states Matsuda (1980, 1982) Suarez and Duffy (1992) in the CCSR/NIES GCM using two different initial zonal flows. Yamamoto and Takahashi (2009) found that diabatic heating rates below the cloud layer strongly influence the magnitude of the super-rotation and the formation of such multiple super-rotation states.

7.1.3.2 Oxford and the Open University Models

Lee et al. (2005) began the development of a simplified Venus GCM, with radiative transfer simulated by linear Newtonian cooling specified in a similar, though not identical, distribution to Yamamoto and Takahashi (2003a,b). Using a modification of the UK Meteorological Office Hadley Centre Atmospheric Model, HadAM3, a finite difference, grid-point model run with $5° \times 5°$ horizontal resolution and 32 vertical levels, Lee and Richardson (2010) found a peak equatorial wind speed of $\approx$35 m/s when running with default Venus parameters. A strong meridional circulation was developed in the form of a single Hadley cell in each hemisphere. Zonal jets were produced with a maximum of 45 m/s at 60 km in each hemisphere at mid-latitudes, with a peak equatorial wind of 35 m/s, as shown in Fig. 7.3. This GCM also produced significant warm pole and cold collar features.

The model used by Lee et al. (2005); Lee and Richardson (2010) also maintained super-rotation by a similar GRW mechanism Gierasch (1975) to Yamamoto and Takahashi (2003b), and reproduces many of the observed large-scale wave structures. In the case of Lee and Richardson (2010), the period of the waves is much longer than is observed in the Venus cloud-tops, which is related to the weaker zonal wind speeds found in the GCM with the default parameters. The mixed Rossby-Gravity wave mode has a period of $\simeq$ 30 days, slower than the $\simeq$ 5 days observed Del Genio and Rossow (1990). Similarly the equatorial Kelvin wave is 9 $\pm$1 days rather than the $\simeq$4 days observed. The wave periods were shown to scale with the zonal wind speeds.

Development of this model has continued, with Lee and Richardson (2010) introducing a simple bulk cloud parameterization and transport scheme and Mendonca et al. (2010), Mendonca (2012) introducing a more realistic radiation scheme to include cloud scattering. Parallel development of a simple Venus GCM (Lewis et al. 2006) with a pseudo-spectral dynamical core has been conducted at the Open University in the UK Lewis (2010). The dynamical core is identical to that used in a Mars GCM to identify equatorial super-rotation when the Martian atmosphere is in a dusty state (Lewis and Read 2003). Experiments have been conducted at T21 and T42 horizontal resolution and with from 32 to 200 vertical levels between the surface and roughly 100 km altitude. This model has some more desirable properties when run at relatively low horizontal resolution, in particular, and is used for the model intercomparison described in section "Results". It also offers the ability to make a direct comparison with the Lee and Richardson (2010) model with only the pseudo-spectral rather than finite-difference techniques used in the dynamical core differing. A similar procedure has already been shown to be valuable in identifying subtle differences in dynamical core behavior, when sharing a common physical processes package between grid-point and pseudo-spectral models of Mars and conducting identical experiments (Forget et al. 1999; Lewis et al. 1999). One notable feature is that the pseudo-spectral model has been found to produce significantly stronger super-rotation than was seen in the Lee and Richardson (2010) study, reaching or even exceeding observed values, but only when the thermal forcing is increased beyond realistic magnitudes or when the background thermal lapse rate is modified so that the middle atmosphere becomes much more stably-stratified than is observed.

7.1.3.3 EPIC Model

Herrnstein and Dowling (2007) tested the effects of topography for a Venus atmospheric model. Using this model, which was developed independently and uses a different vertical coordinate, they reproduced the results of Lee and Richardson (2010) for a smooth planet. The super-rotation produced was found by Herrnstein and Dowling (2007) to diminish from 55 m/s to 35 m/s when topography was added, with the mid-latitude jets becoming asymmetric, with a slower jet in the northern hemisphere. The time to reach equilibrium was also reduced with topography included, taking a few years rather than a few decades.

7.1.3.4 ARIES/GEOS and CAM Models

Hollingsworth et al. (2007) adapted another terrestrial GCM, a version of the NASA Goddard Space Flight Center ARIES/GEOS dynamical core, to Venus parameters and then used it to investigate the circulation equilibration and the formation of atmospheric super-rotation on a slowly-rotating planet. This model was run with a $4° \times 5°$ horizontal resolution and used 56 vertical levels. Topography was not included.

Using a thermal structure similar to that of Yamamoto and Takahashi (2003b) the model was run for integrations of up to 20,000 Edays. Super-rotation was achieved but was found to be slightly weaker than observed, at $\approx$88 m/s. A further experiment, performed with more realistic heating, resulted in very weak super-rotation at $\approx$10 m/s, and only weak eddy activity, confirming earlier studies which also used stronger heating Yamamoto and Takahashi (2003a,b); Lee et al. (2005); Lee and Richardson (2010).

The same group has started a new project, adapting the National Center for Atmospheric Research (NCAR) Community Atmosphere Model (CAM) to Venus. This model is based on a finite-volume dynamical core, which is relatively diffusive for high wind speeds, and therefore requires to be run on a very high horizontal resolution (roughly $1° \times 1°$), much higher than previous modeling works. A first set of simulations of the Venus atmospheric circulation has been conducted using a simplified model of radiative forcing that produces Venus-like super-rotation, with no topography nor diurnal cycle included Parish et al. (2011). In these simulations, an unexpected feature is obtained, with a temporal variability on a period of approximately 10 Earth years. The angular momentum transport is found to be following the GRW mechanism, dominated by mean meridional circulation transport with equatorward redistribution of momentum by transient eddies. However, the meridional circulation appears to be more complex below the clouds than the simple Hadley cells obtained in previous works.

7.1.3.5 GFDL Model

Lee and Richardson (2010) compared three different dynamical cores for their response to Venus-like forcing and friction parameters in a pioneering Venus intercomparison study and a fore-runner to the study presented here in section "Results".

The dynamical cores tested were an Arakawa B grid core, a spectral core and a finite volume (FV) core, each from the Geophysical Fluid Dynamics Laboratory (GFDL) terrestrial GCM. Each model was set up to have approximately 5° resolution for longitude and latitude. The thermal forcing, surface Rayleigh friction and 'sponge layer' were all taken from Lee and Richardson (2010).

Lee and Richardson (2010) presented results for integrations of 22 599 Edays. All 3 GCMs were found to produce super-rotating winds of 35 ± 10 m/s at the equator, with faster mid-latitude jets, but there was sensitivity to the dynamical core formulation. The same momentum transport processes as Yamamoto and

Takahashi (2003b) and Lee and Richardson (2010) dominated in all the models tested, unsurprisingly since the GCMs were forced with the same simplified thermal function and had no diurnal tides or topography.

7.1.3.6 LMD Model

Crespin et al. (2006) began the development of a more complete radiative transfer scheme with the aim of producing a more realistic Venus GCM, based on experience with Earth, Mars and Titan models at Laboratoire de Météorologie Dynamique in Paris. The scheme was adapted to work with the LMDZ finite-difference dynamical core, run with 48×32 horizontal grid with 50 vertical levels from the surface up to 95 km altitude.

Crespin et al. (2006) presented initial results for simulations using this model and found zonal winds of $\approx$150 m/s near the cloud tops., after $\approx$50,000 Edays following a start from rest. The temperature structure was not yet fully realistic in these initial experiments.

Lebonnois et al. (2010) present a more comprehensive study of the results obtained with the LMDZ Venus GCM over a large range of parameters. The model now included topography, a diurnal cycle, dependence of the specific heat (c_p) on temperature, and a radiative transfer module which allowed a consistent computation of the temperature field.

Lebonnois et al. (2010) discussed results for the zonal wind and mean meridional circulation under four scenarios. These used both a realistic radiative transfer code and a simplified radiative forcing as used in Lee and Richardson (2010) and similar to that used in Yamamoto and Takahashi (2003a,b, 2004, 2006); Herrnstein and Dowling (2007); Hollingsworth et al. (2007). Both radiation schemes were used with and without surface topography. The results with simplified radiative forcing are broadly consistent with earlier studies. Slightly faster wind-speeds were produced by the realistic radiative transfer experiments, with peak speeds $\approx$ 60 m/s, though this is still somewhat weaker than is observed on Venus. Figure 7.4 shows plots of the zonal wind and meridional circulation for each of these configurations. Note the qualitative differences in the meridional circulation induced by the realistic radiative scheme.

In contrast to Herrnstein and Dowling (2007), Lebonnois et al. (2010) found that the zonal wind peak speed and super-rotation was actually enhanced by the addition of topography.

Lebonnois et al. (2010) conclude that the angular momentum transport is consistent with the Gierasch-Rossow-Williams (GRW) mechanism when no diurnal cycle was used. With the addition of the diurnal cycle, however, the mechanism controlling super-rotation becomes more complex. The mean meridional circulation transports angular momentum upward (despite stacked, multiple Hadley cells in the model) and poleward. The thermal tides weaken this poleward transport and add a significant downward transport at the equator. This transport allows accumulation of angular momentum at low latitudes and prevents the formation of such clear high- and mid-latitude jet peaks as were seen in models without the diurnal cycle.

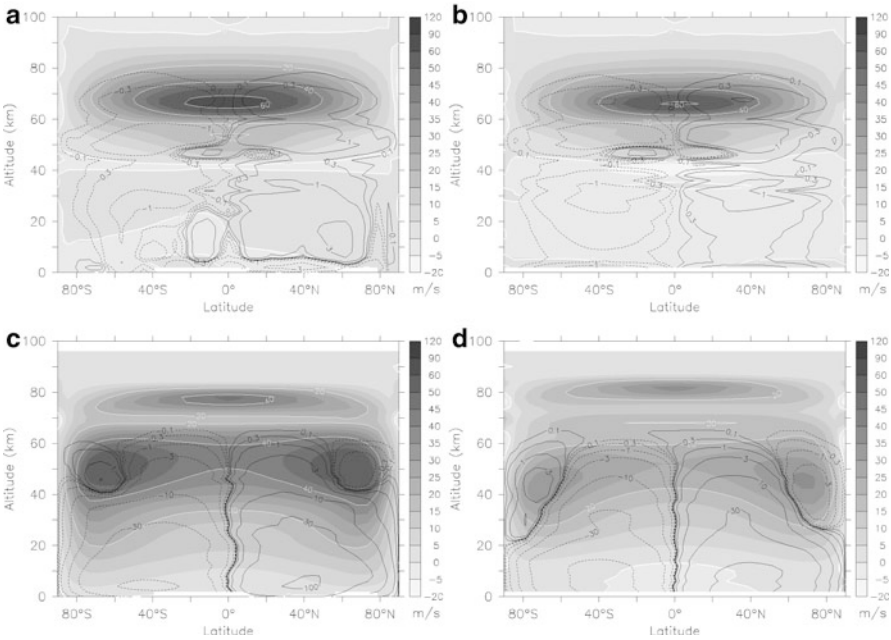

Fig. 7.4 Wind and MMC plots from experiments with (**a**) realistic radiative transfer and topography (**b**) as (**a**) without topography (**c**) Newtonian cooling and forcing with topography (**d**) as (**c**) without topography. From Lebonnois et al. (2010)

7.2 Titan Global Atmosphere Modeling and its Relation to Venus

In this section we briefly discuss some developments in modeling the atmosphere of Titan, which is the other slowly rotating solid body with a substantial gaseous atmosphere in the Solar System. Although Titan and Venus are very different in many aspects, they have three characteristics in common: a slow rotation rate, one to two orders of magnitude less than the Earth and Mars, a high opacity region in a layer many atmospheric scale heights above the surface, and an atmosphere which super-rotates compared to their solid surfaces.

From parametric GCM studies (Del Genio and Zhou 1996; Mitchell and Vallis 2010), it appears that the rotation rate of the planet is a key parameter linked to super-rotation. It controls the latitudinal extent of the Hadley circulation, and therefore the transport of angular momentum by mean meridional circulation. General Circulation Models can provide a detailed analysis of the super-rotation phenomenon in both these atmospheres, and therefore may help us understand whether the mechanism is the same, what the differences may be, and what processes are crucial.

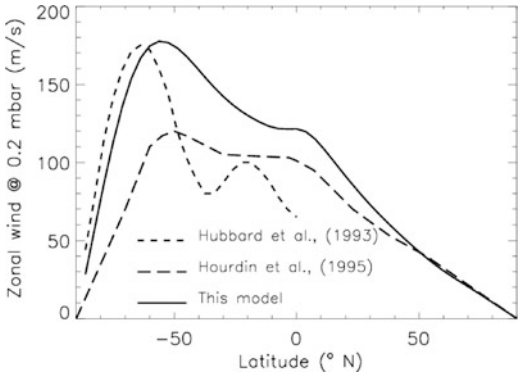

Fig. 7.5 Zonal wind in the IPSL 2-dimensional climate model (at 0.25 mbar), for simulations coupled (*solid line*) and uncoupled (*long-dashed*) with the haze variations. The season is the same as at the time of the 28-Sgr occultation ($L_S \approx 128$). The *short-dashed line* shows the latitudinal zonal wind profile deduced by Hubbard et al. (1993) from the occultation data (southern hemisphere of Titan only). Reprinted from Icarus, 170, Rannou et al. (2004), with permission from Elsevier

Del Genio et al. (1993) and Hourdin et al. (1995) have been the first works to apply General Circulation Models to Titan. This latter GCM was obtaining atmospheric super-rotation comparable to the observed winds. This model was further developed in a 2-dimensional version (IPSL 2-dimensional Climate Model) to include couplings with the haze distribution and the photochemistry (Rannou et al. 2002, 2004; Hourdin et al. 2004). Other models have been developed since, based on different Earth GCMs: the Köln model (Tokano et al. 1999), which has been used for many studies on Titan's troposphere; another 2-dimensional model mainly used to study the tropospheric methane cycle (Mitchell et al. 2006); a non-hydrostatic GCM developed in Russia (Mingalev et al. 2006); a Titan version of the PlanetWRF GCM (Richardson et al. 2007); a Titan version of the CAM model (Friedson et al. 2009). Most of these models have difficulties to reproduce the high zonal winds observed in Titan's stratosphere.

The IPSL 2-D CM has been able to interpret many features in the atmosphere of Titan (Lebonnois et al. 2009). Among the lessons learned from this model, the strong couplings between opacity sources (haze, clouds) located high in the atmosphere, thermal structure and dynamics (wind strength), has been demonstrated (Fig. 7.5). This has significant implications for Venus modeling: the coupling between the cloud structure and the dynamics may be very important to take into account to correctly model the wind structure and amplitude (for both zonal and meridional circulation).

There are certainly many lessons that may be learned by comparing modeling efforts for Titan and Venus, in order to understand these slow-rotators with super-rotating atmospheres, the only examples in the solar system. What is similar? Certainly the role of the global-scale mean meridional circulation in the transport

and redistribution of angular momentum in the atmosphere, and also the coupling with high opacity regions located high in the atmosphere. What is different? Possibly the role of thermal tides, of other planetary-scale and small-scale waves, as well as the impact of seasonal changes, which are much smaller on Venus compared to Titan (see Achterberg et al. 2008; Yamamoto and Takahashi 2007, 2008). A conclusion from the limited amount of Titan modeling conducted so far is certainly that, just as with Venus GCMs, the results obtained differ between each Titan GCM and seem to show a high degree of model sensitivity.

7.3 Key Issues Arising From Previous Studies

Several key issues have emerged from the modeling studies described in the previous section.

Firstly, many Venus GCMs show an insufficiently strong super-rotation, at least when run with supposedly realistic heating rates and best-guess parameters. Most models do now produce a robust and significant amount of super-rotation and most can be 'tuned' to produce plausible cloud-top winds. However, different models show a wide variation in their results under similar conditions.

Secondly, questions remain about the role of various different wave modes in maintaining or eroding the atmospheric super-rotation and whether the wave modes produced by models are realistic, especially at the low resolution at which they are often run in order to spin-up in a practical amount of time. This leads on to questions about what model resolution is required for an adequately realistic experiment and whether the spin-up time to initiate a model unambiguously, or to be sure that the initial transient stage of a model has passed since initiation by an arbitrary wind field, are in fact achievable in practice and whether they will become achievable in the near future.

Thirdly, many models have highly simplified physical parameterizations, again for practical computational reasons, as well as for the more important reason that such schemes are very difficult to validate with the present level of knowledge of the atmosphere of Venus. Several models have begun to introduce more detailed radiation schemes in recent years. How detailed do such schemes have to be to achieve realistic results? And what other schemes, commonly used in comprehensive terrestrial, and now Martian, GCM studies are required? These schemes might include representations of gravity wave drag, convection and turbulence in the planetary boundary layer, interactions between the solid surface and atmosphere, cloud microphysics and atmospheric chemistry. Venus GCMs are still some way off including most of these processes in a fully realistic way, and it is still unclear how important it is to do so in order to model the most important features of the atmospheric dynamics.

Fourthly, while most attention has naturally been focussed on the atmospheric super-rotation at the cloud-tops, and some has been paid to diagnosing global-scale

planetary waves (Kelvin and Rossby modes), relatively little attention has so far been given to how well the GCMs represent other features of the Venus atmosphere, such as the polar vortices and smaller-scale inertia-gravity waves.

The motivation for the present study outlined in Chap. 8 is to see how well these questions might be addressed by the present work and how a program of future work might be designed to progress our understanding, both of the Venus atmosphere itself and, indirectly but perhaps equally usefully, of how well various modeling techniques, in common use in terrestrial weather prediction and climate change studies, operate under conditions of relatively weak forcing and long integration times. The following chapter describes the initial phases of such an international intercomparison study.

References

R.K. Achterberg, B.J. Conrath, P.J. Gierasch, F.M. Flasar, C.A. Nixon, Observation of a tilt of Titan's middle-atmospheric superrotation. Icarus **197**, 549–555 (2008)

A. Arakawa, Computational design for long-term numerical integration of the equations of fluid motion: Two-dimensional incompressible flow. part I. J. Comput. Phys. **1**, 119 (1966). doi: 10.1016/0021-9991(66)90015-5

A. Crespin, S. Lebonnois, F. Hourdin, V. Eymet, R. Fournier, F. Forget, *Simulations of the Dynamics of Venus' Atmosphere with the LMD Venus General Circulation Model*, vol. 38 (Bulletin of the American Astronomical Society, 2006), p. 515

A.D. Del Genio, W.B. Rossow, Planetary-scale waves and the cyclic nature of cloud top dynamics on Venus. J. Atmos. Sci. **47**, 293–318 (1990)

A.D. Del Genio, W. Zhou, Simulations of superrotation on slowly rotating planets: Sensitivity to rotation and initial condition. Icarus **120**, 332–343 (1996). doi:10.1006/icar.1996.0054

A.D. Del Genio, W. Zhou, T.P. Eichler, Equatorial superrotation in a slowly rotating GCM—implications for Titan and Venus. Icarus **101**, 1–17 (1993). doi:10.1006/icar.1993.1001

F. Forget, F. Hourdin, R. Fournier, C. Hourdin, O. Talagrand, M. Collins, S.R. Lewis, P.L. Read, J. Huot, Improved general circulation models of the Martian atmosphere from the surface to above 80 km. J. Geophys. Res. **104**, 24155–24176 (1999). doi:10.1029/1999JE001025

A.J. Friedson, R.A. West, E.H. Wilson, F. Oyafuso, G.S. Orton, A global climate model of Titan's atmosphere and surface. Planet Space Sci. **57**, 1931–1949 (2009). doi:10.1016/j.pss.2009.05.006

P.J. Gierasch, Meridional circulation and the maintenance of the Venus atmospheric rotation. J. Atmos. Sci. **32**, 1038–1044 (1975). doi:10.1175/1520-0469(1975)032

R.M. Goody, A.R. Robinson, A discussion of the deep circulation of the atmosphere of Venus. Astrophys. J. **146**, 339 (1966). doi:10.1086/148898

A. Herrnstein, T.E. Dowling, Effects of topography on the spin-up of a Venus atmospheric model. J. Geophys. Res.-Planets **112**, 4 (2007). doi:10.1029/2006JE002804

J.L. Hollingsworth, R.E. Young, G. Schubert, C. Covey, A.S. Grossman, A simple-physics global circulation model for Venus: Sensitivity assessments of atmospheric superrotation. Geophys. Res. Lett. **34**, 5202 (2007). doi:10.1029/2006GL028567

F. Hourdin, O. Talagrand, R. Sadourny, R. Courtin, D. Gautier, C.P. McKay, Numerical simulation of the general circulation of the atmosphere of Titan.. Icarus **117**, 358–374 (1995). doi:10.1006/icar.1995.1162

F. Hourdin, S. Lebonnois, D. Luz, P. Rannou, Titan's stratospheric composition driven by condensation and dynamics. J. Geophys. Res. **109**, E12005 (2004). doi:10.1029/2004JE002282

W.B. Hubbard, B. Sicardy, R. Miles, A.J. Hollis, R.W. Forrest, I.K.M. Nicolson, G. Appleby, W. Beisker, C. Bittner, H. Bode, M. Bruns, H. Denzau, M. Nezel, E. Riedel, H. Struckmann, J.E. Arlot, F. Roques, F. Sevre, W. Thuillot, M. Hoffmann, E.H. Geyer, C. Buil, F. Colas, J. Lecacheux, A. Klotz, E. Thouvenot, J.L. Vidal, E. Carreira, F. Rossi, C. Blanco, S. Cristaldi, Y. Nevo, H.J. Reitsema, N. Brosch, K. Cernis, K. Zdanavicius, L.H. Wasserman, D.M. Hunten, D. Gautier, E. Lellouch, R.V. Yelle, B. Rizk, F.M. Flasar, C.C. Porco, D. Toublanc, G. Corugedo, The occultation of 28 SGR by Titan. Astron. Astrophys. **269**, 541–563 (1993)

K. Ikeda, M. Yamamoto, M. Takahashi, Superrotation of the Venus atmosphere simulated by an atmospheric general circulation model, in *IUGG/IAMAS Meeting*, Perugia, 2007

E. Kalnay de Rivas, Further numerical calculations of the circulation of the atmosphere of Venus. J. Atmos. Sci. **32**, 1017–1024 (1975). doi:10.1175/1520-0469(1975)032

A. Kido, Y. Wakata, Multiple equilibrium states appearing in a Venus-like atmospheric general circulation model. J. Meteorol. Soc. Japan **86**, 969–979 (2008)

A. Kido, Y. Wakata, Multiple equilibrium states appearing in a Venus-like atmospheric general circulation model with three-dimensional solar heating. Scientific Lett. Atmosphere **5**, 85–88 (2009)

S. Lebonnois, F. Hourdin, P. Rannou, The coupling of winds, aerosols and photochemistry in Titan's atmosphere. Phil. Trans. R. Soc. A **367**, 665–682 (2009). doi:10.1098/rsta.2008.0243

S. Lebonnois, F. Hourdin, V. Eymet, A. Crespin, R. Fournier, F. Forget, Superrotation of Venus' atmosphere analyzed with a full general circulation model. J. Geophys. Res.-Planets **115**, 6006 (2010). doi:10.1029/2009JE003458

C. Lee, M.I. Richardson, A general circulation model ensemble study of the atmospheric circulation of venus. J. Geophys. Res. Planets **115**, E04002 (2010). doi:10.1029/2009JE003490

C. Lee, S.R. Lewis, P.L. Read, A numerical model of the atmosphere of Venus. Adv. Space Res. **36**, 2142–2145 (2005). doi:10.1016/j.asr.2005.03.120

S.R. Lewis, Global models of the lower and middle atmosphere of Venus, in *5 Years of Venus Express and a Look to the Future* (Royal Astronomical Society, London, 2010)

S.R. Lewis, P.L. Read, Equatorial jets in the dusty Martian atmosphere. J. Geophys. Res.-Planets **108**, 5034 (2003). doi:10.1029/2002JE001933

S.R. Lewis, M. Collins, P.L. Read, F. Forget, F. Hourdin, R. Fournier, C. Hourdin, O. Talagrand, J. Huot, A climate database for Mars. J. Geophys. Res. **104**, 24177–24194 (1999). doi:10.1029/1999JE001024

S.R. Lewis, C. Lee, P.L. Read, A Venus atmospheric general circulation model for Venus Express, in European Planetary Science Congress, 2006, p. 457

Y. Matsuda, Dynamics of the four-day circulation in the Venus atmosphere. J. Meteorol. Soc. Japan **58**, 443–470 (1980)

Y. Matsuda, A further study of dynamics of the four-day circulation in the Venus atmosphere. J. Meteorol. Soc. Japan **60**, 245–254 (1982)

H.G. Mayr, I. Harris, Quasi-axisymmetric circulation and superrotation in planetary atmospheres. Astron. Astrophys. **121**, 124–136 (1983)

J.M. Mendonca, P.L. Read, S.R. Lewis, New radiative transfer code in the Oxford Venus GCM, in *3rd International Conference on Venus*, Aussois, 2010

J.M. Mendonca, P.L. Read and S.R. Lewis, Zonal winds on high latitudes on Venus: An improved application of cyclostrophic balance to Venus Experss observations, Icarus, **217**(2), 629–639 (2012) doi:10.1016/j.icarus.2011.07.010

I.V. Mingalev, V.S. Mingalev, O.V. Mingalev, B. Kazeminejad, H. Lammer, H.K. Biernat, H. Lichtenegger, K. Schwingenschuh, H.O. Rucker, First simulation results of Titan's atmospheric dynamics with a global 3-D non-hydrostatic circulation model. Ann. Geophys. **24**, 1–15 (2006)

J.L. Mitchell, G.K. Vallis, The transition to superrotation in terrestrial atmospheres. J. Geophys. Res. **115**, E12008 (2010). doi:10.1029/2010JE003587

J.L. Mitchell, R.T. Pierrehumbert, D. Frierson, R. Caballero, The dynamics behind Titan's methane cloud. Proc. Natl. Acad. Sci. USA **103**, 18 421–18 426 (2006). doi:10.1073/pnas.0605074103

H.F. Parish, G. Schubert, C. Covey, R.L. Walterscheid, A. Grossman, S. Lebonnois, Decadal variations in a Venus General Circulation Model. Icarus, **212**(1), 42–65 (2011) doi:10.1016/j.icarus.2010.11.015

P. Rannou, F. Hourdin, C.P. McKay, A wind origin for Titan's haze structure. Nature **418**, 853–856 (2002)

P. Rannou, F. Hourdin, C.P. McKay, D. Luz, A coupled dynamics-microphysics model of Titan's atmosphere. Icarus **170**, 443–462 (2004). doi:10.1016/j.icarus.2004.03.007

M.I. Richardson, A.D. Toigo, C.E. Newman, PlanetWRF: A general purpose, local to global numerical model for planetary atmospheric and climate dynamics. J. Geophys. Res. **112**, E09001 (2007). doi:10.1029/2006JE002825

W.B. Rossow, A general circulation model of a Venus-like atmosphere. J. Atmos. Sci. **40**, 273–302 (1983). doi:10.1175/1520-0469(1983)040

W.B. Rossow, G.P. Williams, Large-scale motion in the Venus stratosphere. J. Atmos. Sci. **36**, 377–389 (1979). doi:10.1175/1520-0469(1979)036

W.B. Rossow, S.B. Fels, P.H. Stone, Comments on A three-dimensional model of dynamical processes in the Venus atmosphere. J. Atmos. Sci. **37**, 250–252 (1980). doi:10.1175/1520-0469(1980)037

P.H. Stone, The structure and circulation of the deep Venus atmosphere. J. Atmos. Sci. **31**, 1681–1690 (1974). doi:10.1175/1520-0469(1974)031

M.J. Suarez, D.G. Duffy, Terrestrial superrotation: A bifurcation of the general circulation. J. Atmos. Sci. **49**, 1541–1554 (1992)

M. Takagi, Y. Matsuda, Effects of thermal tides on the Venus atmospheric superrotation. J. Geophys. Res.-Atmos **112**, 9112 (2007). doi:10.1029/2006JD007901

T. Tokano, F.M. Neubauer, M. Laube, C.P. McKay, Seasonal variation of Titan's atmospheric structure simulated by a general circulation model. Planet Space Sci. **47**, 493–520 (1999)

M. Yamamoto, M. Takahashi, The fully developed superrotation simulated by a General Circulation Model of a Venus-like atmosphere. J. Atmos. Sci. **60**, 561–574 (2003a). doi:10.1175/1520-0469(2003)060

M. Yamamoto, M. Takahashi, Superrotation and equatorial waves in a T21 Venus-like AGCM. Geophys. Res. Lett. **30**, 090 000–1 (2003b). doi:10.1029/2003GL016924

M. Yamamoto, M. Takahashi, Dynamics of Venus' superrotation: The eddy momentum transport processes newly found in a GCM. Geophys. Res. Lett. **31**, 9701 (2004). doi:10.1029/2004GL019518

M. Yamamoto, M. Takahashi, Superrotation maintained by meridional circulation and waves in a Venus-like AGCM. J. Atmos. Sci. **63**, 3296–3314 (2006). doi:10.1175/JAS3859.1

M. Yamamoto, M. Takahashi, Simulations of superrotation using a GCM for Venus' middle atmosphere. Earth, Planets, and Space, **59**, 971–979 (2007)

M. Yamamoto, M. Takahashi, Prograde and retrograde atmospheric rotation of cloud-covered terrestrial planets. significance of astronomical parameters in the middle atmosphere. Astron. Astrophys. **490**, L11–L14 (2008)

M. Yamamoto, M. Takahashi, Dynamical effects of solar heating below the cloud layer in a Venus-like atmosphere. J. Geophys. Res. **114**, E12004 (2009). doi:10.1029/2009JE003381

R.E. Young, J.B. Pollack, A three-dimensional model of dynamical processes in the Venus atmosphere. J. Atmos. Sci. **34**, 1315–1351 (1977). doi:10.1175/1520-0469(1977)034

Chapter 8
Models of Venus Atmosphere

Sebastien Lebonnois, Christopher Lee, Masaru Yamamoto, Jonathan Dawson, Stephen R. Lewis, Joao Mendonca, Peter Read, Helen F. Parish, Gerald Schubert, Lennart Bengtsson, David Grinspoon, Sanjay S. Limaye, Hauke Schmidt, Håkan Svedhem, and Dimitri V. Titov

In the context of an International Space Science Institute (ISSI) working group, we have conducted a project to compare the most recent General Circulation Models (GCMs) of the Venus atmospheric circulation. A common configuration has been decided, with simple physical parametrization for the solar forcing and the

S. Lebonnois (✉)
Laboratoire de Meteorologie Dynamique, CNRS, Jussieu, Box 99, 75252 Paris, France
e-mail: Sebastien.Lebonnois@lmd.jussieu.fr

C. Lee
Ashima Research, 600 S. Lake Ave, Pasadena, CA 91106, USA
e-mail: lee@ashimaresearch.com

M. Yamamoto
Institute for Applied Mechanics, Kyushu University, 6-1 Kasuga-kouen, 816-8580, Kasuga, Japan
e-mail: yamakatu@riam.kyushu-u.ac.jp

J. Dawson • S.R. Lewis
Department of Physics and Astronomy, The Open University, Walton Hall,
Milton Keynes, MK7 6AA, UK
e-mail: jon.dawson@open.ac.uk

Planetary and Space Science Institute, Open University, Walton Hall,
Milton Keynes, MK7 6AA, UK
S.R.Lewis@open.ac.uk

J. Mendonca • P. Read
Department of Physics, Oxford University, Clarendon Laboratory, Parks Road,
Oxford, OX1 3PU, UK
e-mail: mendonca@atm.ox.ac.uk

Atmospheric, Oceanic and Planetary Physics, University of Oxford, Clarendon Laboratory,
Parks Road, Oxford, 0X1 3PU, UK
e-mail: p.read1@physics.ox.ac.uk

H.F. Parish • G. Schubert
Department of Earth and Space Sciences, University of California Los Angeles, 595 Charles
Young Drive East, Los Angeles, CA 90095-1567, USA
e-mail: hparish@ess.ucla.edu; schubert@ucla.edu

L. Bengtsson et al. (eds.), *Towards Understanding the Climate of Venus*, ISSI Scientific Report Series 11, DOI 10.1007/978-1-4614-5064-1_8,

boundary layer scheme. Six models have been used in this intercomparison project. The nominal simulation was run for more than 200 Venus days, and additional sensitivity runs have been done by several models to test the trends visible in these models when parameters are varied: topography, upper and lower boundary conditions, horizontal and vertical resolution, initial conditions. The results show that even in very similar modeling conditions, the wind speeds obtained with the different GCMs are widely different. Super-rotation is obtained, but the shape (with or without marked high-latitude jets) and amplitude of the maximum zonal wind jet is different from one model to the other, from 15 to 50 m/s. Minor sensitivity is seen in several models to the upper boundary conditions, the topography or the vertical grid. Horizontal resolution and lower boundary conditions induce variations that are significant, affecting the amplitude and shape of the region of maximum zonal wind. Two models were started from an atmosphere already in super-rotation. The simulations did not converge back to the nominal simulations, maintaining maximum zonal winds over 70 m/s (and even 100 m/s) without marked high-latitude jets. This study shows how sensitive GCMs are to the weak forcing of Venus atmosphere, and how difficult it is to draw precise conclusions on the circulation obtained with a single model, as well as on its sensitivity to some parameters.

L. Bengtsson
International Space Science Institute (ISSI), Hallerstrasse 6, 3012 Bern, Switzerland
email:Bengtsson@issibern.ch

D. Grinspoon
Department of Space Science, Denver Museum of Nature and Science,
2001 Colorado Blvd., Denver, CO 80205, USA
email:dgrinspoon@dmns.org

S.S. Limaye
Space Science Engineering Center, University of Wisconsin, 1225 West Dayton Street,
Madison, WI 53706, USA
email:SanjayL@ssec.wisc.edu

H. Schmidt
Atmosphaere im Erdsystem, Max-Planck-Institut fr Meteorologie, Bundestrasse 53,
D-20146, Hamburg, Germany
email:hauke.schmidt@zmaw.de

H. Svedhem • D.V. Titov
ESA/ESTEC, Keplerlaan 1, PO Box 299, 2200 AG, Noordwijk, The Netherlands
email:hsvedhem@rssd.esa.int

ESTEC/ESA, Postbus 299, NL-2200, AG Noordwijk, The Netherlands
email:dmitri.titov@esa.int

8.1 Introduction

With the success of the European Venus Express mission, Venus' atmosphere has been put once more under the lights of international research. Many groups around the world are analyzing observational datasets, from space and ground-based campaigns. To support and complement these analyses modeling of the atmosphere of Venus is needed. The state of worldwide research in this field, as well as the links with the modeling of the Earth's atmosphere, have been the purpose of the ISSI working group producing the present book. In this context, several specialists in the modeling of Venus' and Earth's atmospheres came together, and decided to assess current models of the Venusian atmosphere through an intercomparison project, based on available models, though limited to models that use a simplified thermal forcing.

Starting with the pioneering work of Young and Pollack (1977) more than thirty years ago, the modeling of the circulation of Venus' atmosphere has always been a challenge. Most of the General Circulation Models (GCMs) developed for Venus have been adapted from Earth GCMs. Recently published models include Yamamoto and Takahashi (2003a, 2004, 2006, 2009); Takagi and Matsuda (2007); Dowling et al. (2006); Hollingsworth et al. (2007); Lee (2006); Lee et al. (2005); Lee et al. (2007); Herrnstein and Dowling (2007); Kido and Wakata (2008); Lee and Richardson (2010); Lebonnois et al. (2010); Parish et al. (2011). These models have used simplified physical and radiative parameterizations. Only Lebonnois et al. (2010) used a complete radiative transfer model to compute the temperature field self-consistently. The results presented in these different models vary widely, and may even be contradictory in some aspects.

The idea of comparing the results of different models forced with the same physical parameters is not new. In the case of Venus, it was recently done using numerical experiments with three different dynamical cores Lee and Richardson (2010). We decided to build upon this first work by extending the comparison to five additional models. The models included in this study are:

- **CCSR**—Kyushu/Tokyo CCSR/NIES GCM (simplified forcing version): Masaru Yamamoto (Yamamoto and Takahashi 2003b, 2004, 2006).
- **LMD**—Paris LMD GCM: Sebastien Lebonnois (Lebonnois et al. 2010), in a simplified radiative forcing configuration.
- **OU**—Open University spectral GCM: Jonathan Dawson, Stephen Lewis.
- **UCLA**—UCLA/LLNL Aerospace CAM GCM: Gerald Schubert, Curt Covey, Helen Parish, Richard Walterscheid (Parish et al. 2011). This model had to be run in a very high resolution configuration (approximately $1° \times 1°$) due to numerical dissipation issues.
- **OX**—Oxford GCM: Joao Mendonca, Peter Read. Simulations done by Christopher Lee during his PhD thesis have also been used (Lee et al. 2005; Lee 2006; Lee et al. 2007).

- **LR10**—GFDL FMS GCM: Christopher Lee (Lee and Richardson 2010). The simulations were run before this work, using three different dynamical cores.

The indicated acronyms will be used throughout this text to identify the simulations.

8.2 Intercomparison Protocol

The goal of this study is to build upon the intercomparison of Lee and Richardson (2010) where different GCMs, or different numerical cores, are forced with similar physical parameterizations to test the sensitivity of the simulated atmospheric circulation to the choice of numerical model.

To reach this goal, we have built a common protocol that the different teams involved in the project would have to follow to run a set of simulations, that would be compared together. The first simulation is designed to compare the behavior of the different dynamical cores. Then sensitivity simulations are run to see the sensitivity to several parameters in each model, and check the consistency of these sensitivities among the models.

8.2.1 Dynamical Cores

The set of models includes three different types of dynamical core implementations: three spectral models, three models based on finite differences schemes and two models based on finite volume discretization. The horizontal resolution was chosen close to $5° \times 5°$: 64×32 for grid models (72×36 for OX), T21 for spectral models. The UCLA model had to run at much higher resolution (approximately $1° \times 1°$) due to numerical dissipation issues. This makes direct comparison to other base simulations quite difficult, especially considering the impact of horizontal dissipation, as it will be shown below. However, we will include this simulation in the baseline run discussion. The vertical resolution has been equalized for the protocol, though several models also made some simulations with their usual vertical grid. The common vertical grid used is the one from Lebonnois et al. (2010), based on 50 levels. The OX and LR10 simulations were done only with a 32-level grid given in Lee et al. (2007).

All planetary parameters (e.g., gravity, planetary radius, rotation rate) are fixed to identical values (see e.g., Lee et al. 2007; Lebonnois et al. 2010). The specific heat is taken as constant, $C_p = 900$ J/kg/K. The reference simulations do not include topography. The atmosphere was taken at rest as initial condition, and simulations were run for a couple of hundred Venus days (from 187 Vdays for LR10 up to 600 Vdays for UCLA). One Vday is 117 Earth days, or approximately one third of an Earth year.

The horizontal dissipation scheme is usually deeply embedded in the dynamical cores, and is not a parameter that is easily modified. We left all the different implementations as they were in each dynamical core, though this dissipation was kept as low as possible in each model. The type of horizontal dissipation and typical parameter values used in the different models are listed in Table 8.1.

8.2.2 Common Physical Parameterization

8.2.2.1 Thermal Forcing

All models have been run using the same simplified scheme taken from Lee (2006). The radiative tendency (temporal variation between two model timesteps) on temperature at longitude λ, latitude ϕ and pressure level p is given by

$$\frac{\delta T_{\text{rad}}(\lambda, \phi, p, t)}{\delta t} = -\frac{T(\lambda, \phi, p, t) - T_0(\phi, p)}{\tau}, \tag{8.1}$$

where $T_0(\phi, p)$ is the forcing thermal structure, and τ is the time constant of this forcing. $T_0(\phi, p)$ and τ are taken from Lee (2006)

$$T_0(\phi, p) = T_{\text{ref}}(p) + T_1(p)(\cos(\phi) - C), \tag{8.2}$$

where $T_{\text{ref}}(p)$ is a reference temperature profile Seiff et al. (VIRA model, 1985), and $T_1(p)$ is a perturbation term giving the peak equator-to-pole difference. The constant C is the integral of $\cos\phi$ over the domain ($C = \pi/4$). The profile of $T_1(p)$ was chosen to reflect the peak in absorption of solar insolation within the cloud deck Lee (2006). The value of τ is 25 Earth days, decreasing slightly in the uppermost levels. In this formulation the diurnal cycle is not taken into account.

8.2.2.2 Upper Boundary Conditions

A sponge layer is included in the top four layers of the GCM. In the baseline simulations, this sponge layer includes Rayleigh friction damping horizontal winds to zero. Time constants are ηx$10^6 \approx$ Earth days for the LR10 models. For the other models, these time constants were fixed to 9.6x10^4 s (1.12 Earth days) for the top layer, then 1.20x10^5, 1.23x10^5, and 1.60x10^5 s for the next three layers, following values used in Newman and Leovy (1992). These values are roughly half the values used in the LR10 models and therefore apply a stronger damping at the model top.

For the OX simulation, this damping is applied only to the eddy components of the horizontal wind speed. The other models have adopted this configuration as a sensitivity test (see below). However, we have included the OX simulation in the basic comparison, since the influence of this parameter is small and limited to upper levels (this is discussed below).

Table 8.1 Summary of common and distinct parameters in the GCMs used for this work

Models	CCSR	LMD	OU	UCLA	OX	LR10
Dynamical core[a]	S	FD	S	FV	FD	S, FD, FV
Horizontal resolution	T21	64×32	T21	360x180	72x37	T21, 64x32
Duration of the simulations (Vdays)	250	250-350	500	600	222	187-300
Vertical grid	50 levels	50 levels	50 levels	50 levels	32 levels	32 levels
Horizontal dissipation	6th order	squared Lapl.	Del-8	Del-squared	6th order	8th order (S) 4th order (FD) div. damping (FV)
Time constant	3 Edays	2×10^4 s	4.3×10^4 s	2.2×10^4 s	30 Edays	3 Edays (S,FD) 1 Eday (FV)
Vertical eddy coefficient, K	0.15 m^2 s^{-1}	0.15 m^2 s^{-1}	0.15 m^2 s^{-1}	0.15 m^2 s^{-1}	None	None
Thermal forcing	All models: From Lee (2006)					
Sponge layer	All models: 3 layers					
Surface friction	All models: Rayleigh friction, 1 layer					

[a] S = "spectral" model, FD = "finite differences" and FV = "finite volumes".

Table 8.2 Summary of the simulations done by the different groups

Simulations		CCSR	LMD	OU	UCLA	OX	LR10
base	Baseline	X	X	X			XXX
topo	Topography	X	(X)[a]	X			
spgl	Sponge layer (only eddies)	X	X	X		X	XXX
pbl[n]	Different PBL	X	XX				
lres	Low horizontal resolution	X	X	X			
hres	High horizontal resolution	X	X	X	X		
vgrd	Different vertical grid	X		XX			
uini	Different initial state	X	X				

[a]Parenthesis indicate: for LMD, simulation run before this work (Lebonnois et al. 2010); for OX, simulations run during C. Lee's PhD (Lee 2006)

8.2.2.3 Surface Friction and Vertical Eddy Diffusion

The most simple surface boundary layer is used in the baseline simulation: a Rayleigh friction in the first layer of the model with a time constant fixed to 3 days, together with a constant vertical dissipation coefficient, $k_v = 0.15$ m^2 s^{-1}. For the LR10 simulations, done before this protocol was agreed upon, the Rayleigh friction time constant is fixed to 25 days, and no explicit vertical dissipation is taken into account in the models. Similarly, for the OX simulation, a Rayleigh friction time constant of 32 days is used as well as no explicit vertical dissipation.

Every model kept its own implementation for the temperatures in the soil. For example, in the LMD GCM, a soil model with 11 layers is used.

8.2.3 Sensitivity Simulations

Some sensitivity studies of different parameters could only be done by some of the models. These different simulations are summarized in Table 8.2 and will be discussed in Sect. 8.3.4 of Chap. 7.

8.2.3.1 Topography (topo)

The CCSR and OU models have been run with topography. For the LMD model, the baseline simulation could not be run with topography, due to unsolved instability problems. However, one simulation in Lebonnois et al. (2010) included topography, though the lower boundary conditions are different from the baseline run (see below).

8.2.3.2 Upper Boundary Conditions (spgl)

As was done in the LR10 and OX simulations, we also tried to damp only the eddy terms in the horizontal winds within the sponge layer.

8.2.3.3 Lower Boundary Layer Scheme and Vertical Eddy Diffusion Coefficient (pbl)

For the LMD GCM, two other parameterizations have been used to test the impact of the lower boundary layer scheme and vertical eddy diffusion coefficient. The first one (*pbl2*) was used in Lebonnois et al. (2010), and is described in this paper. This parameterization computes the vertical diffusion flux, the surface drag, and the diffusion coefficient.

The second one (*pbl3*) is a "Mellor and Yamada" parameterization Mellor and Yamada (1982), taken from the Earth version of the LMD GCM. This parameterization is fully described in the Appendix B of Hourdin et al. (2002). The surface drag coefficient is computed as follow: $C_d = (0.4/\ln(1 + z_1/z_0))^2$, where z_1 is the altitude of the center of the first layer, and z_0 is the roughness coefficient, taken equal to 1 cm.

For the CCSR GCM, a "bulk" parameterization has also been used (*pbl1*). We set the drag coefficient C_D to 4x10−3 for temperature and horizontal flow (Del Genio et al. 1993).

8.2.3.4 Horizontal Resolution (lres and hres)

For the CCSR, LMD and OU models, three different resolutions were used, to evaluate the impact of this parameter on the modeled circulations. The horizontal resolutions used are T10, T21 and T42 for the CCSR and OU spectral models, and 32×16, 64×32 and 128×64 for the LMD finite difference model. The UCLA simulation, run at very high horizontal resolution, may also be discussed compared to the *hres* case.

8.2.3.5 Vertical Grid (vgrd)

The CCSR model was run both with its original vertical grid of 52 levels, and with the baseline 50-level grid from Lebonnois et al. (2010). The OX model has only been run with its original 32-level vertical grid. The OU model was also run with this 32-level vertical grid, and also with an increased vertical resolution (100 levels). For this model, the *vgrd* notation will apply to the 32-level run, while the 100-level run is noted *vgrd2*.

8.2.3.6 Different Initial State (uini)

The CCSR and LMD models have also been run starting from a zonal wind field already in super-rotation. This initial field was imposed analytically. The equatorial vertical profile is linear in altitude, from zero at the surface to 110 m s^{-1} at 70 km, then down to zero at 100 km. This profile is then multiplied by a linear latitudinal factor in both polar regions: from zero at the pole to 1 at 50 ° latitude.

The impact of the initial state has been studied with an Earth-like GCM with slow rotation rate (Del Genio and Zhou 1996). In this case, no differences were noted between both initial states (rest vs super-rotation). However, Kido and Wakata (2008) have recently published simulations of the Venus' atmosphere, and they also tested both initial states. In their results, both simulations do not reach the same state, with much stronger winds in the second experiment. As we will show below, this is also the case in the simulations done for this work.

8.2.4 Other Published Works

There are many other published works that may be included in the discussions, though the simulations are not done in the framework detailed here. These works have been described in detailed in the previous chapter.

8.3 Results

8.3.1 Spin-Up Phase and Total Angular Momentum

For most simulations, we decided to run for 250 Vdays, but some simulations were run for longer times to test the stability of the results. In all simulations (except UCLA), the circulation was stabilized after the initial run, though the total angular momentum in the atmosphere was sometimes still increasing slightly.

In Fig. 8.1, the evolution of the total atmospheric angular momentum is plotted for several simulations, normalized to the total angular momentum of the atmosphere rotating with the same speed as the solid surface below, i.e. with the zonal wind equal to zero everywhere, which is the initial state of all the simulations but *uini*. This variable is equal to the super-rotation index used by Del Genio and Zhou (1996), or to 1 plus the super-rotation factor defined by Read (1986). It is mostly sensitive to the deepest regions of the atmosphere, so differences in its evolution and final value are often an illustration of differences in the zonal wind field of the deep atmosphere. The base simulations have a non-dimensional total angular momentum of 2 to 6, with atmospheres in super-rotation. These differences of the total angular momentum are mostly caused by differences among the dynamical cores in atmospheric circulation of the deep atmosphere.

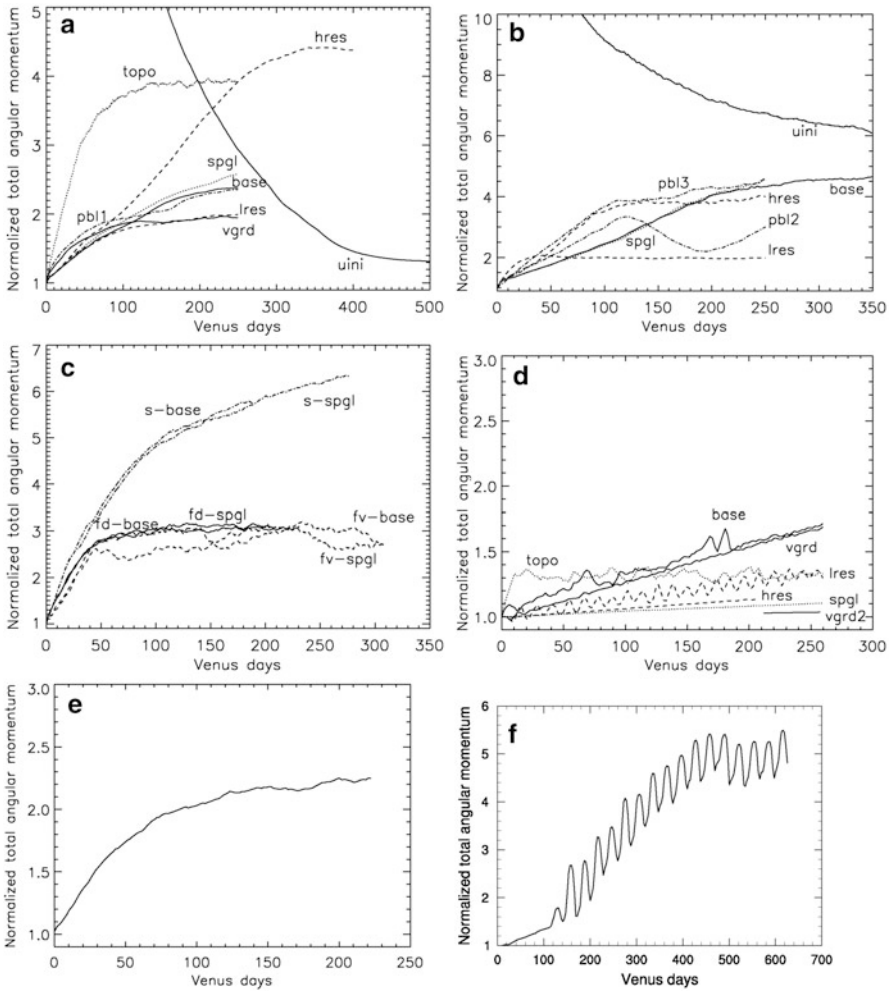

Fig. 8.1 Evolution of the total atmospheric angular momentum, normalized to its initial value (with atmosphere at rest), for all the simulations. (**a**) CCSR, (**b**) LMD, (**c**) LR10, (**d**) OU, (**e**) OX, (**f**) UCLA

The base simulations are almost the same as the *spgl* ones for all cases, which indicates that the total angular momentum is insensitive to the upper boundary parameterization. On the other hand, the sensitivities to the topography (*topo*), horizontal resolution (*lres, hres*), and initial condition (*uini*) are different among the models. These parameters strongly influence the angular momentum processes in the deep atmosphere. It is difficult to find any consistent trends in these temporal evolutions. However, the timescale for stabilization of the simulations are usually

between 100 and 200 Vdays, or even more. This illustrates that simulations of the Venus atmosphere need to be run for very long periods of time before they stabilize.

Two models show peculiar behaviors, the OU and UCLA models. In the OU models (Fig. 8.1d), the amplitude of the super-rotation stays very low compared to other models. The simulations appear to be far from equilibrium even after more than 200 Venus days, except for the *topo* simulation that is stabilized at a very low value (around 1.3). The oscillations seen in UCLA simulation (Fig. 8.1f) are due to large scale oscillations in the zonal wind distribution, particularly in the deep atmosphere, with a period of roughly ten Earth years as discussed in Parish et al. (2011). These oscillations are not seen in other models, though in the LMD-pbl2 simulation, some long-term variations are seen in the total angular momentum (Fig. 8.1b), that are due to oscillations at the cloud level between two different structures of the peak zonal winds. There are also small oscillations visible in the OU-lres simulation (Fig. 8.1d), though these don't affect the circulation much at the cloud level. Due to these oscillations, the UCLA results displayed in the next figures correspond to the average of the fields over a 10-year period.

8.3.2 Zonal Wind Field: Baseline Runs

The zonally averaged zonal wind fields obtained at the end of the simulations are displayed in Fig. 8.2. Temporal averaging is done over the last few Vdays of the simulations.

Super-rotation is obtained in the atmosphere in all the models, with maximum values in the cloud region and above, i.e., in the 10^5–10^3 Pa pressure range (roughly 50–75 km). Jets are predominantly visible at high latitudes, above 50° and are located somewhat deeper than the altitude of the peak equatorial super-rotation. Though this is the general pattern, wind fields are quite different from one model to the other. The jets are not visible in the CCSR and UCLA simulations (Fig. 8.2a and h). However, the UCLA wind field is a temporal average over the period of the oscillations Parish et al. (see 2011). In the LMD and OX simulations (Fig. 8.2b, d), the jets reach deeper into the atmosphere than in other simulations (the maximum peak is at $3x10^5$ Pa for the LMD model). The amplitudes of the wind maxima are also significantly different from model to model. The strongest winds are obtained for the LR10-s simulation (Fig. 8.2e) with jets above 60 m/s while the average peak values are around 30–40 m/s. The vertical gradient and wind distribution in the deepest atmosphere (surface to 10^6 Pa) also vary from model to model. In many cases, the winds are still very small in this region and only develop above about 10^6 Pa level, while in other cases the vertical gradient in the zonal wind is already significant at the surface, with the high-latitude jet shape already visible there.

The nature of the dynamical core does not appear to play a crucial role. Though the two strongest zonal wind peaks are obtained with the CCSR and LR10-s spectral cores, it is not the case with the OU spectral core, in which zonal winds are the

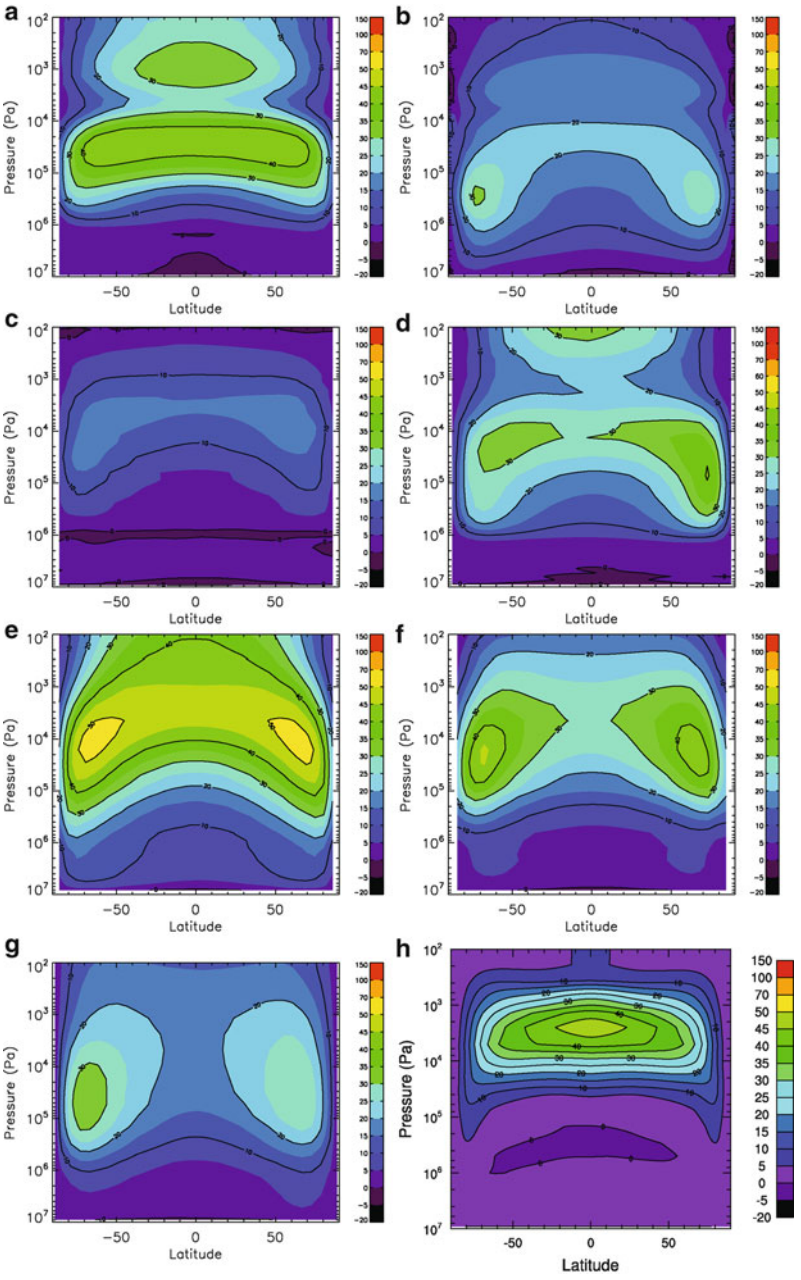

Fig. 8.2 Zonally and temporally averaged zonal wind fields obtained in all the baseline simulations. Unit is m/s. The first column is spectral models: (**a**) CCSR, (**c**) OU, (**e**) LR10-s. The second column is finite difference models: (**b**) LMD, (**d**) OX, (**f**) LR10-fd. The last line is finite volume models: (**g**) LR10-fv, (**h**) UCLA. For the UCLA simulation (**h**), the resolution is much higher than the other baseline runs and the results are averaged over a 10-year period. For the OX simulation, the sponge layer is applied to eddy terms only

weakest. The overall wind field shows many differences between the CCSR and LR10-s models, both in the cloud region and in the deepest part of the atmosphere.

Though the nature of two different dynamical cores may be the same (finite volume, A/B/C grid, spectral), the numerical implementation varies considerably between these models. Ranging from integration method (e.g., Euler vs. Runge-Kutta), to accuracy of the spatial differentiation (grid models), to Fourier filter properties (CFL based, resolution dependence, latitude dependence), these factors aren't equalized in the experiments. These variations probably contribute to the differences in a similar way as the nature of the core.

8.3.3 Related Fields: Temperature Contrasts, Stream Functions

The zonally and temporally averaged temperature contrasts shown in Fig. 8.3 are computed by subtracting the latitudinally averaged temperature field from the temperature field, for each pressure level. These contrasts are dominated by the same feature: cooler polar regions below a transition level corresponding to the zonal wind jet maxima, and warmer polar regions above. An additional inversion is located in the 10^3–10^4 Pa altitude region in the CCSR and LMD simulations. This may be related to the vertical discretization as seen in the *vgrd* simulation (see Sect. 8.3.4 of Chap. 7, Fig. 8.6). A similar inversion is seen close to the top of the OX model. However, it is a consequence of the different sponge layer used in the upper layers of the model. The amplitude of these contrasts are quite similar from model to model, though correlated with the peak zonal winds.

Figure 8.4 shows the zonally and temporally averaged stream function for the baseline simulations. The meridional circulation is dominated by large Hadley-type cells, from the surface up to the top of the models, with ascending air in the equatorial region and descending air over the polar regions. However, polar reverse cells are visible, clearly correlated to the poleward flank of the jets. These reverse cells are more or less visible depending on the model, and may reach the equatorial region in the upper atmosphere for some models (LMD, OX, LR10-s). The amplitude of the circulation in the deep atmosphere is quite similar among models.

8.3.4 Sensitivities

The sensitivity simulations show that many parameters have an impact on the zonal wind field. These effects may be small in some cases, much stronger in other cases. In this section, these effects will be discussed starting from the smallest impacts.

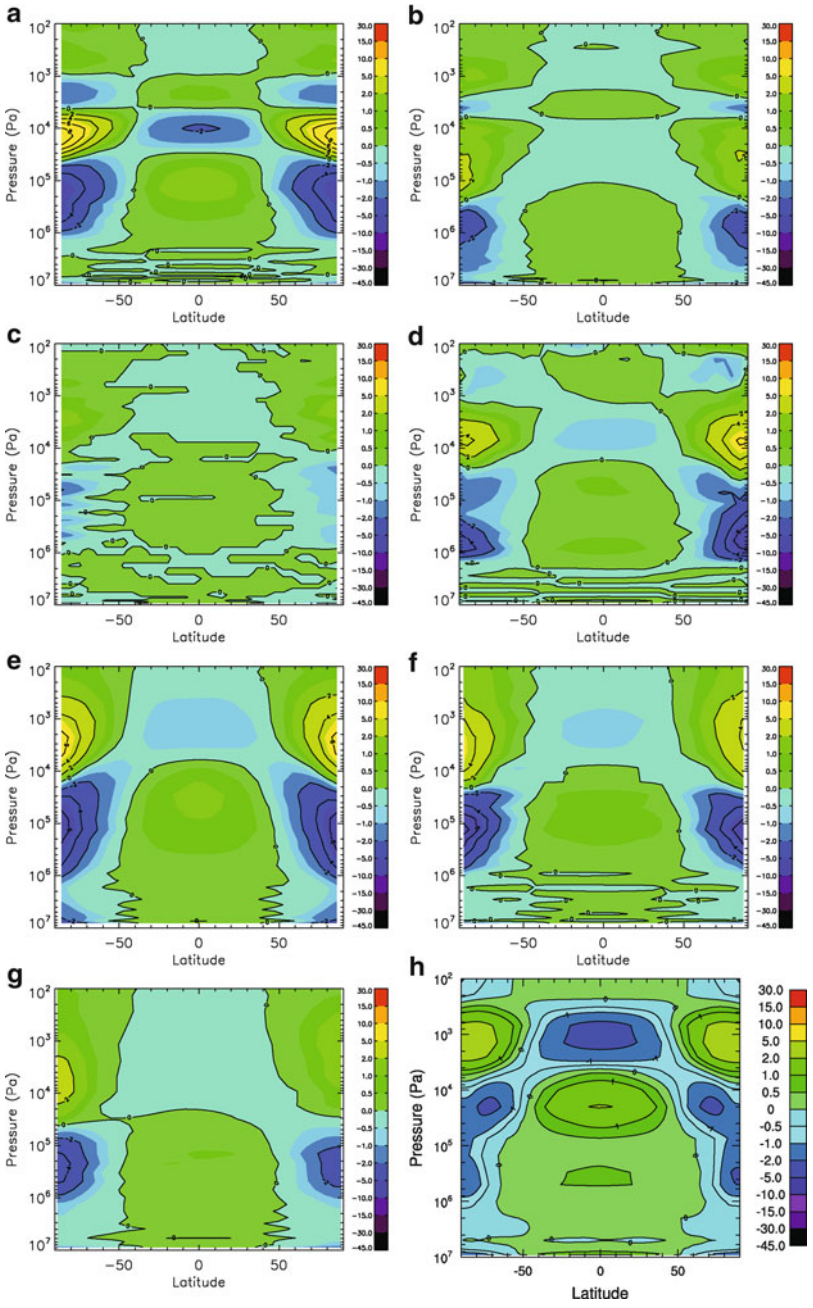

Fig. 8.3 Zonally and temporally averaged temperature contrasts obtained in all the baseline simulations. Unit is K. Models are the same as in Fig. 8.2

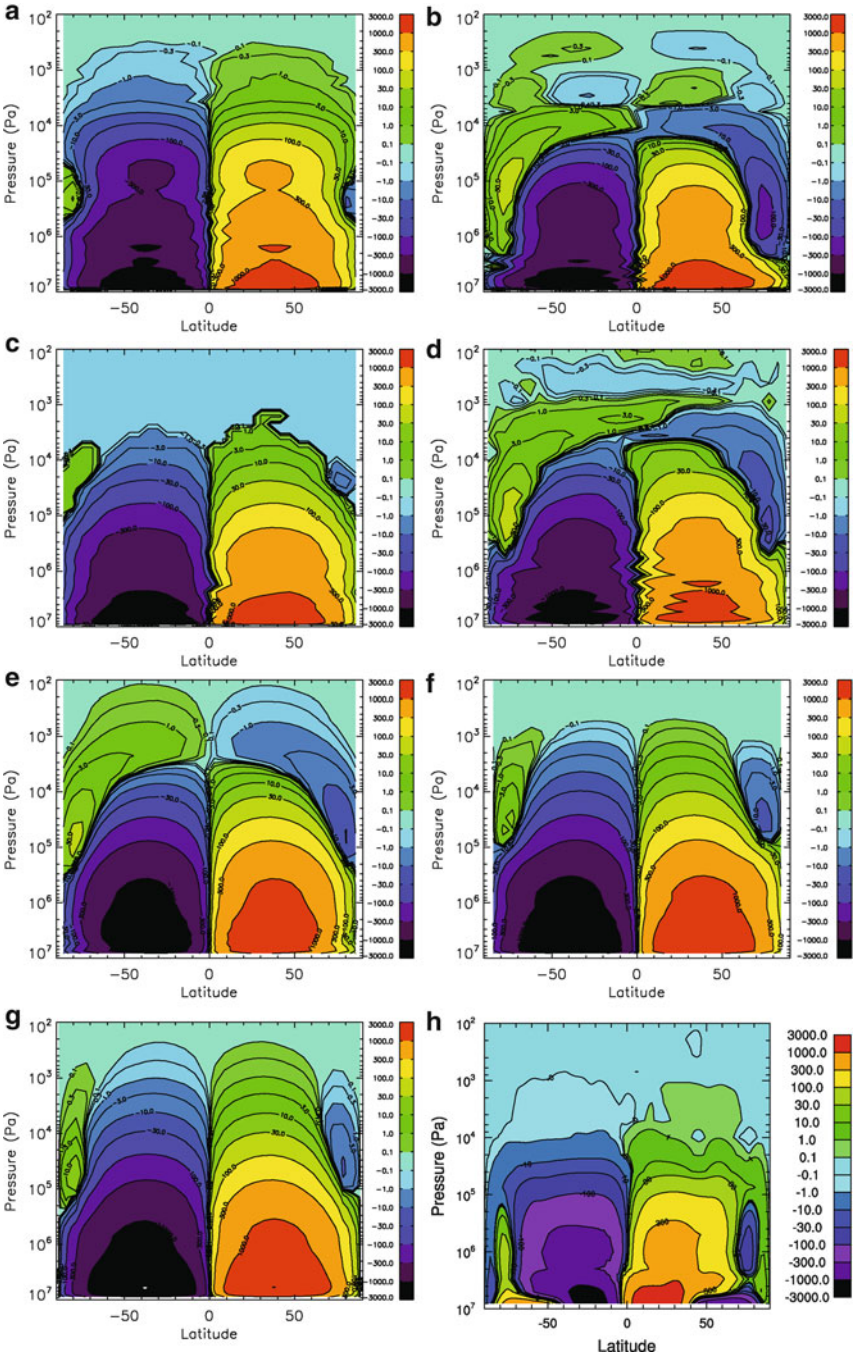

Fig. 8.4 Zonally and temporally averaged stream functions obtained in all the baseline simulations. Unit is 10^9 kg/s. Models are the same as in Fig. 8.2

8.3.4.1 Upper Boundary Conditions

When the upper boundary friction is modified (*spgl*), so that only the eddy part of the horizontal wind is damped in the sponge layer, the results are very similar to the *base* simulations. The corresponding zonal winds are shown in Fig. 8.5, to be compared to Fig. 8.2. For all the models, this change mainly affects the top layers, but not much below. There is not much effect in global budgets from damping the upper atmosphere to the mean, or to zero (Fig. 8.1). The amplitude of the jets is slightly affected (together with the pole-equator temperature contrast, not shown) but not in a consistent way among the different models, and without any correlation to model type. There is some effect on the lower layers because the thermal gradients are slightly modified and the characteristic vertical length scales of the features are larger than the damping region.

8.3.4.2 Vertical Grid

Different vertical grids have been used for the CCSR and OU models (*vgrd* simulations). The resulting fields are shown in Fig. 8.6. In the CCSR case, the feature previously located in the 10^3–10^4 Pa pressure range is not present anymore, suggesting that this feature is related to the distribution of the vertical levels. The shape of the zonal wind maximum has also been affected. In the OU model, the change from 50 to 32 vertical levels has also modified the zonal wind field, slightly reinforcing the jets, though their shape is not affected in the same way in both models. The stream function has also been influenced.

8.3.4.3 Topography

The effect of including Venusian topography in the CCSR and OU models is illustrated in Fig. 8.7. The effect may also be seen in the spin-up of the total angular momentum (Fig. 8.1), though this parameter mainly reflects how the use of topography affects the deepest layers of the atmosphere.

Herrnstein and Dowling (2007) reported a much faster spin up in the EPIC model with topography than without, with a resulting asymmetry between hemispheres because of Ishtar Terra. In the Oxford model used by Lee (2006) and Lee et al. (2007), an asymmetry was also found between hemispheres when including topography, but in the opposite sense to the EPIC model. Though the angular momentum had increased compared to the flat-planet case, no significant change was seen in the zonal wind at altitude or in the spinup speed of the model. In Lebonnois et al. (2010), experiments done with simplified radiative forcing are reported, with and without topography. In these experiments, including topography increases the amplitude of the jets, the total angular momentum, and the spinup speed.

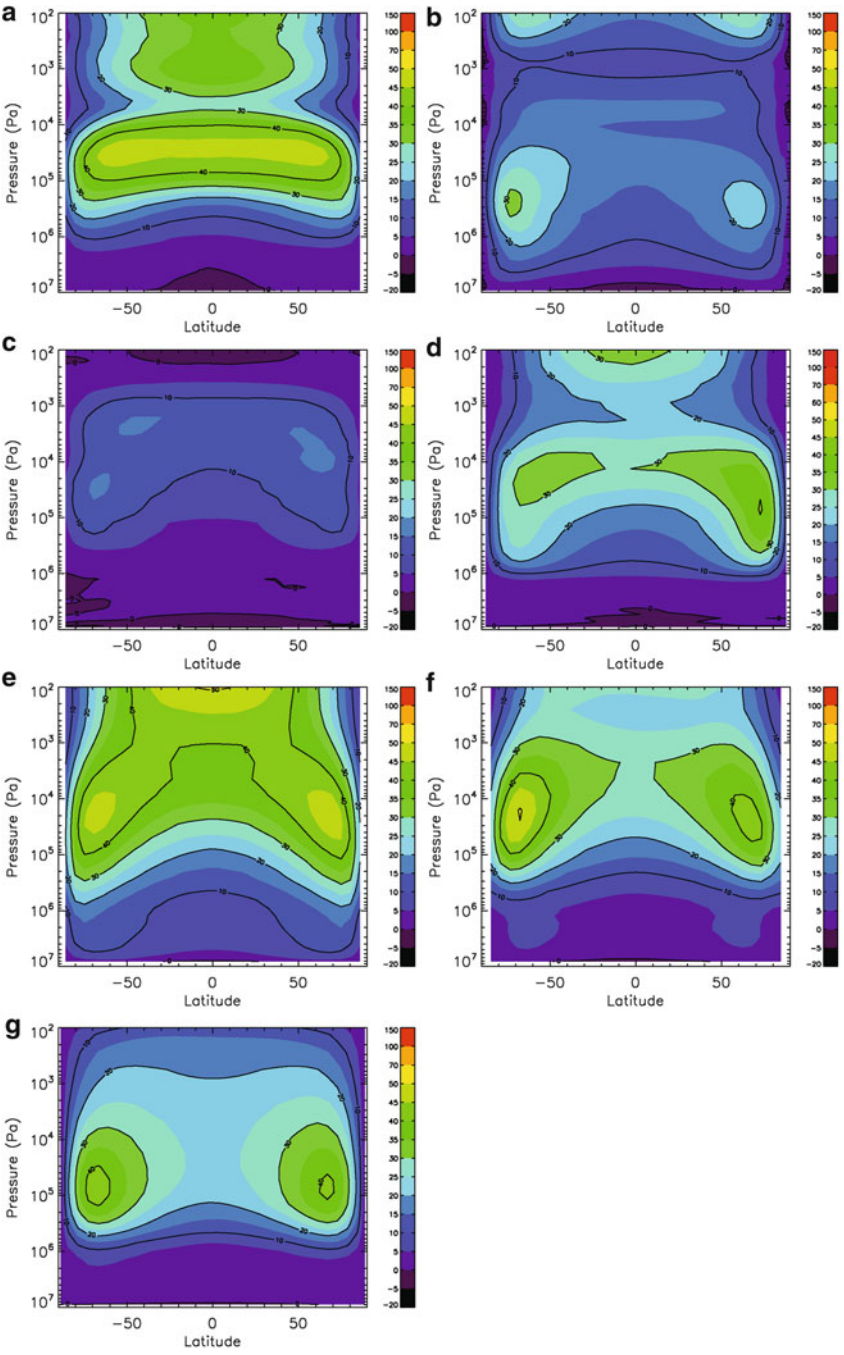

Fig. 8.5 Zonally and temporally averaged zonal wind fields obtained in the simulations with the eddies-only sponge layer *spgl*. For the OX simulation (**d**), Fig. 8.2d is repeated. Models are placed the same way as in Fig. 8.2

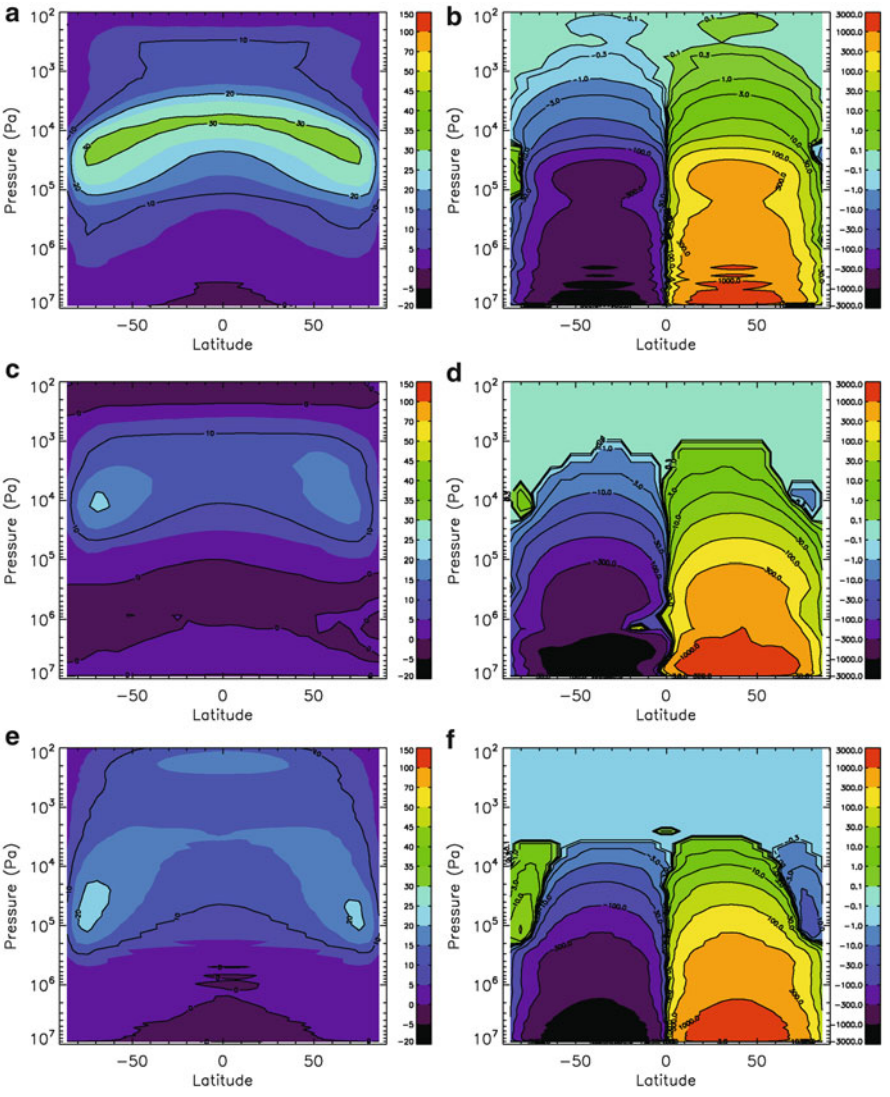

Fig. 8.6 Zonally and temporally averaged zonal wind and stream function obtained with the modified vertical grid (*vgrd*): (**a, b**) CCSR model; OU model (**c, d**) 32-level run and (**e, f**) 100-level run

In the two experiments done with topography for this intercomparison work, the effects on the amplitude of the jets are quite different: in the case of the CCSR model, increased angular momentum is obtained in the deep atmosphere but no effect is visible on the jets, while for the OU model, reduced jets are obtained and the angular momentum in the deep atmosphere decreases.

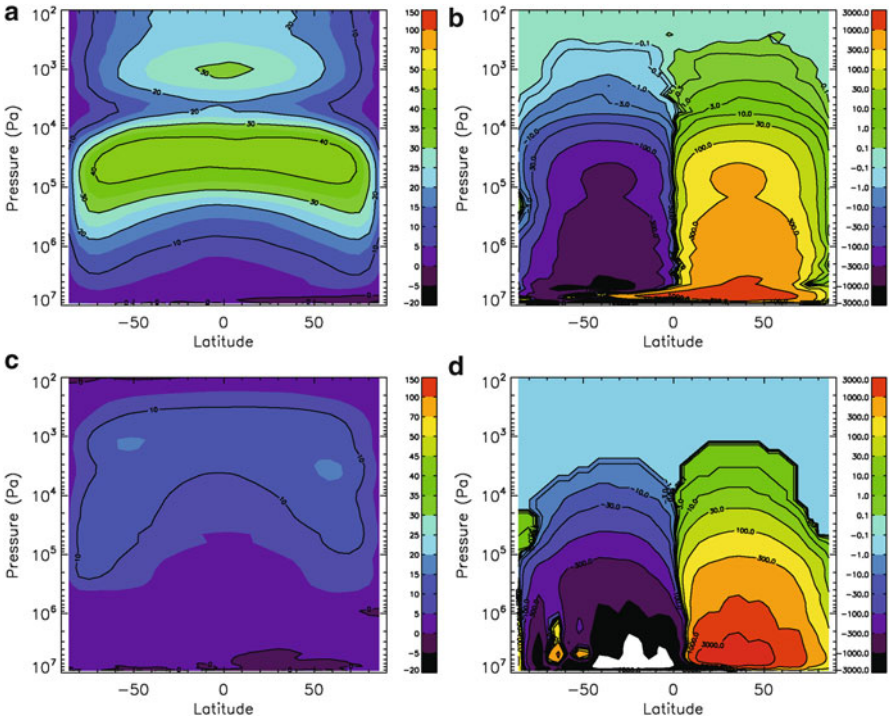

Fig. 8.7 Zonally and temporally averaged zonal wind and stream function obtained with topography (*topo*): (**a, b**) CCSR model, (**c, d**) OU model

Based on all these experiments, and their widely varied results, it is therefore very difficult to extract robust conclusions concerning the impact of the topography on numerical simulations of the Venus' atmosphere.

8.3.4.4 Lower Boundary Conditions

The sensitivity to lower boundary layer parameters and the vertical diffusion coefficient has been evaluated with two models, using alternative parameters: the effect may be quite strong in the deep atmosphere, influencing the angular momentum budget (and spin-up phase), and therefore the whole wind field.

In the CCSR-pbl1 simulation, not much effect is seen compared to the baseline case. This conclusion has also been obtained in the Ph.D. work of Lee (2006), using a (Monin and Obukhov 1954) scheme with a similar roughness length of 3 cm. However, the LMD-pbl2 simulation, with a quite different boundary layer parametrization shows some fluctuations in the wind field over timescales of more than a hundred Venus days, fluctuations especially present in the equatorial wind field within the cloud layer. The results of the LMD-pbl3 simulation, with again a different boundary layer scheme, are very different from the others, with a large

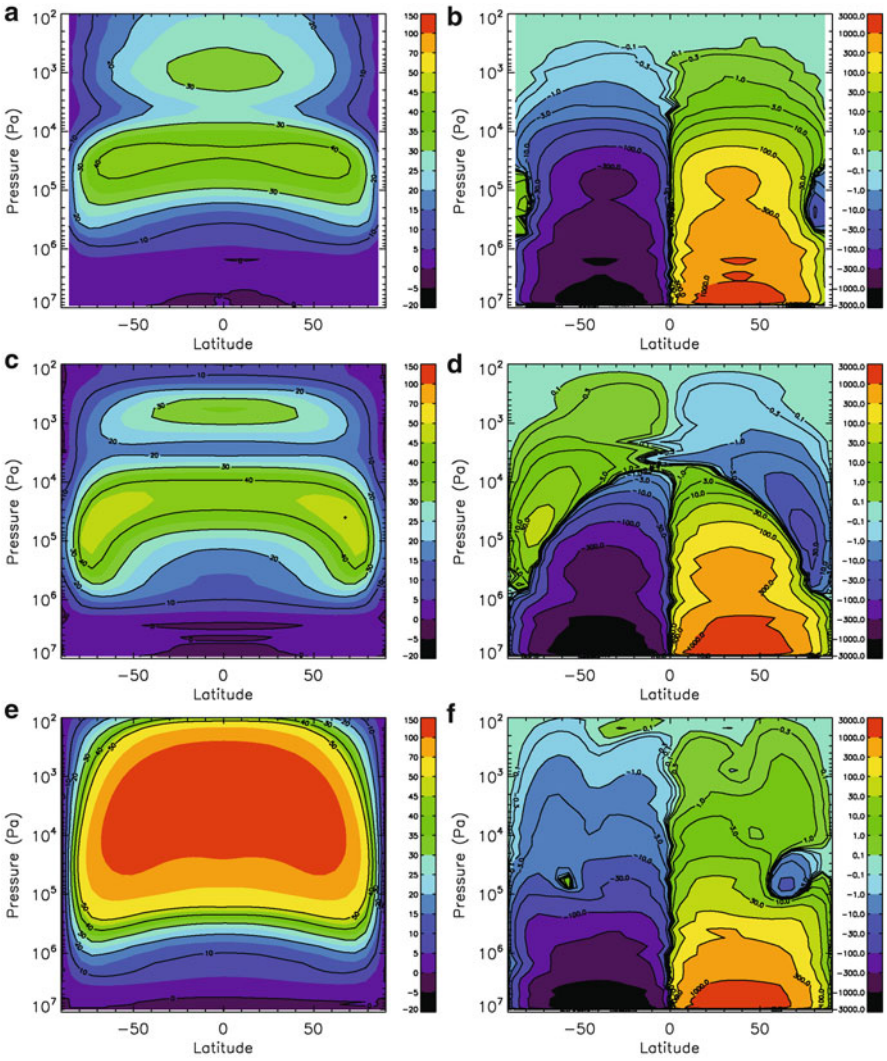

Fig. 8.8 Zonally and temporally averaged zonal winds and stream functions obtained in the simulations using different boundary layers: (**a, b**) CCSR-pbl1, (**c, d**) LMD-pbl2, (**e, f**) LMD-pbl3

impact on the zonal wind field. A large super-rotation is produced, with very high zonal winds in the cloud region, almost uniform from equator to high latitudes. This is one of the most realistic simulations of Venus' circulation obtained with a simplified radiative forcing. It should be noticed from Fig. 8.1b that this simulation has a very similar total angular momentum to the baseline simulation, illustrating the fact that this variable is mostly reflecting the deep atmosphere. It would be interesting to test this more complex boundary layer scheme on other models, to see whether this strong impact is robust or not (Fig. 8.8).

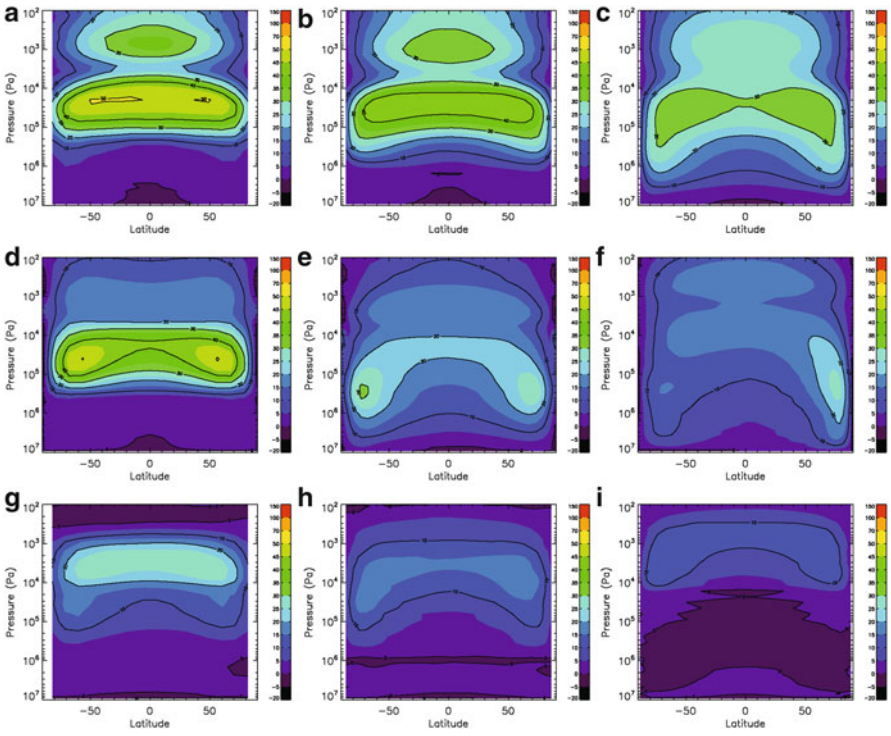

Fig. 8.9 Zonally and temporally averaged zonal winds obtained when varying the horizontal resolution. First row corresponds to the CCSR model, second row to the LMD model and third row to the OU model. First column is the low resolution simulations, middle column is the base runs and third column is the high resolution simulations

8.3.4.5 Horizontal Resolution

The effect of horizontal resolution is quite significant for all the models presented in Figs. 8.9 and 8.10. For both the CCSR and the LMD models, increasing the resolution tends to diminish the peak zonal wind in the 10^5–10^4 Pa pressure range and to increase the deep atmosphere winds over the poles. Though the amplitude and shape of the zonal wind field are not exactly similar between both models, these trends appear to be consistent.

In the case of the OU model, the evolution of the peak zonal wind with the resolution follows the same trend—amplitude decreases when resolution increases. However, the shift of higher winds towards the deep polar regions is not seen in this case.

Due to the high resolution used for the UCLA model, it should also be discussed by comparison to the *hres* simulations. However, comparison between Figs. 8.9 and 8.2h indicates more correspondence between the UCLA simulation and the *lres* simulations rather than with the *hres* simulations. Again, keep in mind that the

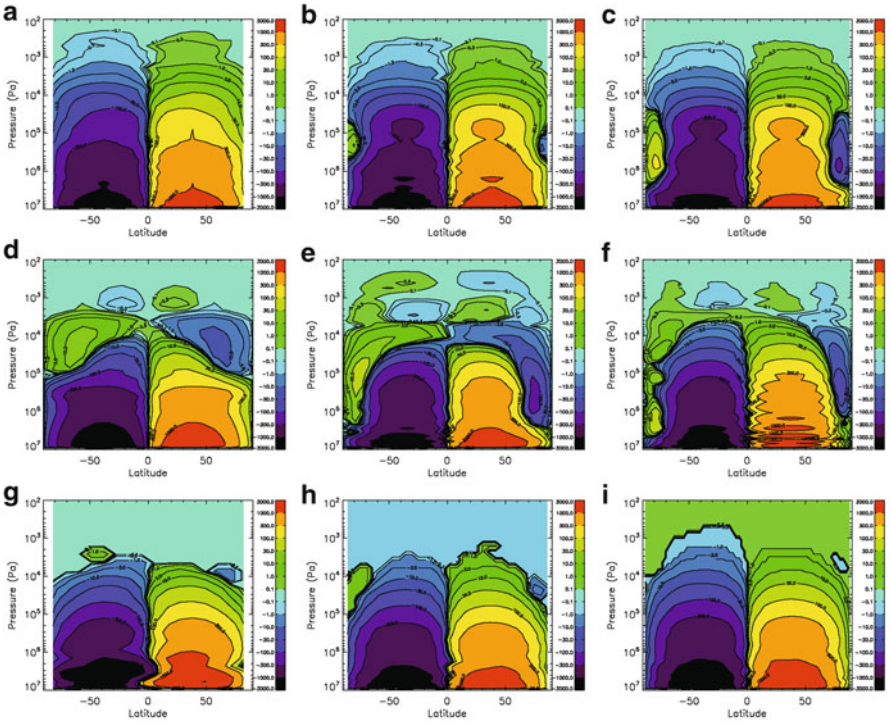

Fig. 8.10 Zonally and temporally averaged stream functions obtained when varying the horizontal resolution. First row corresponds to the CCSR model, second row to the LMD model and third row to the OU model. First column is the low resolution simulations, middle column is the base runs and third column is the high resolution simulations

results of the UCLA run are averaged over a 10-year period. Unfortunately, the impact of the resolution could not be tested with this model.

Changing the resolution clearly affects the zonal wind distributions, even if a consistent trend may not be found for all the models. It also affects the meridional cells, with the development of a much deeper reverse cell over the poles, as seen in Fig. 8.10. The polar regions appear to be very sensitive to the resolution, as well as the amplitude of the zonal winds in the cloud region. The connection between both effects is certainly done through the angular momentum transport budget.

8.3.4.6 Different Initial States

When the zonal wind is initialized with a pre-defined super-rotating field, the initial total angular momentum is high (around 15 times the angular momentum at rest, for the chosen wind distribution). It decreases with time, but the level at which it stabilizes depends on the model, as for the baseline case. The final zonal wind and

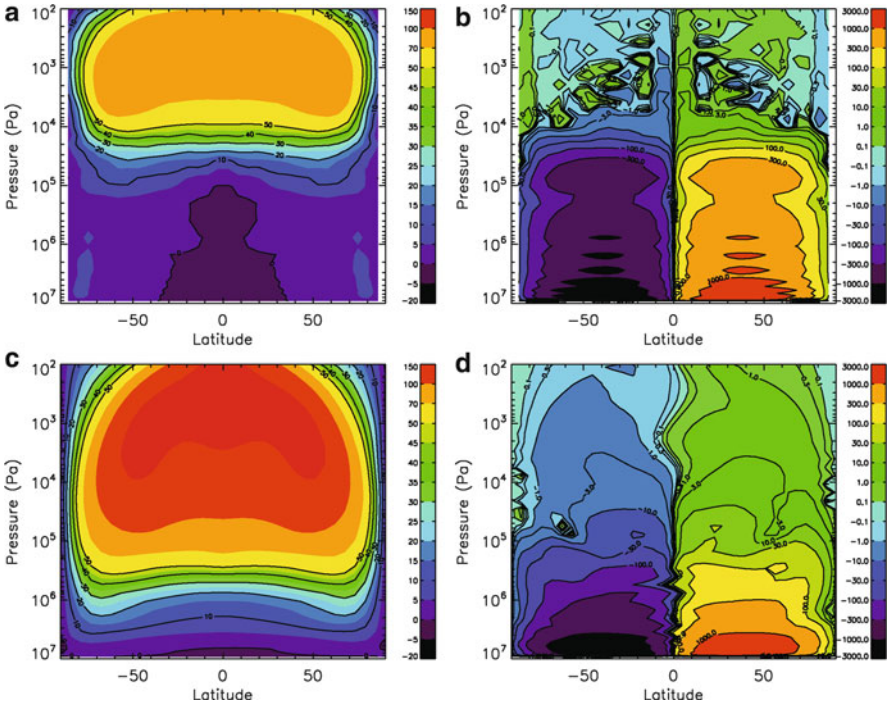

Fig. 8.11 Zonally and temporally averaged zonal wind and stream function obtained in the simulations with modified initial conditions (zonal wind already in super-rotation, *uini*): (**a, b**) CCSR model and (**c, d**) LMD model

stream function fields for the two models that tested this case (CCSR and LMD) are displayed in Fig. 8.11.

In both simulations, the zonal wind maximum is much higher than in the baseline case. However, the shape of the wind distribution is different in each model. In the CCSR-uini simulation, the wind below 10^5 Pa becomes very small, with a region of retrograde winds around the equator, reaching as high as 10^5 Pa. This explains why the total angular momentum goes down to 1.3, even lower than in the baseline simulation (Fig. 8.1). In the case of the LMD model, this region of negative values for u is also present, but confined to the near surface, and the deep atmospheric zonal wind is still comparable to observations. The total angular momentum is then high (factor around 6), though it has not yet reached an equilibrium after the 350 Venus days of the simulation. This simulation looks very similar to the LMD-pbl3 run.

The sensitivity to initial conditions in simulations of super-rotating atmospheres has been previously studied by Del Genio and Zhou (1996) and Kido and Wakata (2008). In the experiments reported in Del Genio and Zhou (1996), the rotation rate of the simulated planet varied, to test the sensitivity to this parameter, but the influence of initial conditions was also tested in the case of Titan-like and Venus-like rotation rate. In both cases, the same equilibrium was reached when starting

from rest or from strong zonal winds. Comparing to previous experiments (Del Genio et al. 1993), where different initial states lead to a different equilibrium in a Venus-like simulation, the authors conclude that the change from single- to double-precision computation may explain the results, due to a better angular momentum conservation.

Using a model based on the CCSR-NIES GCM, Kido and Wakata (2008) explored the impact of initial conditions on the resulting simulations of Venus zonal winds. When starting from rest, the zonal winds obtained show two high-latitude jets with peak values around 60 m/s, a distribution quite similar to the LR10-s baseline simulation (Fig. 8.2e). When starting from an atmosphere already in super-rotation, the wind field appears qualitatively similar, but the jets reach peak zonal winds up to 120 m/s. These two different final states indicate a similar behavior for this model, compared to the behavior obtained in our intercomparison work.

The angular momentum conservation has been checked in baseline configurations for the different models presented here. However, the question of detailed angular momentum budget in the simulations started from an artificially super-rotating state may be investigated further, in order to evaluate the impact of this conservation on the obtained multiple stable states.

8.4 Discussion

We have discussed here several series of simulations obtained by different models but with an effort to equalize the physical forcing and parametrization. The dispersion of the results is quite surprising, but may help to understand the directions where progress is needed in atmospheric modeling, at least in the case of the atmosphere of Venus. Other works have been published previously on GCM simulations of the atmosphere of Venus. They have been described in the previous chapter of this book. Though these simulations were not obtained under similar conditions as those in this present work, some results have been discussed in the previous section. It is also to be noted that many of these simulations show wind fields that fit within the dispersion obtained here. As an example, the wind field displayed in Fig. 8.4 of Del Genio and Zhou (1996), obtained for an Earth-like planet rotating as slowly as Venus, presents similarities (wind amplitude, shape of high-latitude jets) with those of Fig. 8.2.

In most cases, the amplitude and shape of the zonal wind field obtained with these models, though the atmosphere is in super-rotation, may not be exactly comparable to the observations of the latitudinal profile of zonal wind at the cloud-top level (Sanchez-Lavega et al. 2008), or of the vertical profiles of the zonal winds obtained with probes. One point noticed many times before is that to obtain zonal wind peaks around 100 m/s, it is often needed, when using simple radiative forcing, to induce an unrealistically high latitudinal contrast in the deep atmosphere.

How may modelers improve this comparison? Based on the work by Lebonnois et al. (2010), it appears that the radiative forcing chosen does have a strong effect

on the meridional circulation, and therefore on the angular momentum transport in the atmosphere. However, the intercomparison done in the present work clearly indicates that the modeled circulation is highly sensitive to many aspects of the models. In particular, the polar regions and the way they are treated in each model may be responsible for the different behaviors described here.

8.4.1 Simplified Radiative Forcing: Implications

The use of a simplified parametrization for the radiative forcing has a strong impact on the meridional circulation. The circulation obtained in all the previous works using such a parametrization consists of two large Hadley cells, with ascending motion in the equatorial region, poleward motions almost everywhere in the atmosphere, descending motions over each poles, and the returning equator-ward branch very close to the surface. In addition, a reverse cell is sometimes seen over the polar region, in and above the cloud region though it may go deeper in some cases.

In the case of a realistic radiative forcing, as discussed in Lebonnois et al. (2010), the circulation shows a pattern with more layers. The dominant Hadley-type cells are present in the cloud region, with a returning branch below the clouds, and a second set of cells in the deep atmosphere. This circulation is quite different from the circulation obtained with simplified forcing, and therefore it induces a global angular momentum transport pattern that must also be quite different. In the simulation presented in Lebonnois et al. (2010), high zonal winds peaking at roughly 60 m/s are present only in and above the clouds, with a significant role for the thermal tides in the concentration of angular momentum over equatorial regions. The effect of the diurnal cycle, with three-dimensional solar heating, should also be considered in the models with simplified forcing, to investigate the thermal tides.

Therefore, it is clear that the simplified radiative forcing affects the overall circulation significantly. As the radiative modeling suggests, the simplified forcing misses the significant cooling within the cloud deck, and probably overestimates (or incorrectly attributes) the heating in the lower atmosphere. To what extent can the sensitivity results of this intercomparison study be extrapolated to other radiative forcing simulations? The answer to this question is far from obvious. However, with more models using new radiative transfer forcings, the sensitivity of the results to modeling choices will certainly need to be evaluated.

8.4.2 Role of Polar Regions

The polar regions may represent a significant source of differences between the different dynamical cores, e.g., due to the filters used in finite different schemes. The sensitivity tests done with varying resolutions have shown that the zonal wind

field variations were correlated with variations of the stream function over the polar regions. Formations of jets and indirect circulations in the polar regions are clearly sensitive to the horizontal resolutions. The transport of angular momentum in these regions may be a key element to investigate in order to better understand these differences. These investigations have not been possible during this intercomparison campaign, but it should be a goal for future work.

8.4.3 Key Questions, Recommendations

The work we have conducted with these different GCMs illustrate how difficult it is to reproduce the same angular momentum budget and balance with different models, even when most parameterizations are chosen to be identical. This angular momentum balance is extremely sensitive to many model parameters, whether in the dynamical core or in the physical parameterizations. It is also quite complex to build tools accurate enough to investigate details of this budget, to explore how variations on one or the other parameter does affect the overall balance. It would certainly be an interesting direction to explore for future coordinated investigations: build an intercomparison protocol oriented towards angular momentum budget, transport terms and balance. Such detailed studies would also help to quantify and verify angular momentum conservation, which should affect the overall balance of momentum and therefore the meridional and zonal circulations.

Among the most sensitive parameters, this work points out the topography, the planetary boundary layer scheme, and the vertical and horizontal resolutions. Though its role is not obvious from the present work, the topography is certainly affecting the meridional circulation, as well as the budget of angular momentum. Concerning the boundary layer, the LMD-pbl3 simulation may indicate a more efficient upward transport, allowing the atmosphere to transfer quickly angular momentum into the cloud region, and therefore reaching a similar state as when started with an excess of angular momentum (*uini* simulation). For the boundary layer, but also for other aspects such as atmospheric turbulence and convection, or the role of gravity waves, parametrization of subgrid-scale physical processes (meso/micro-scale dynamics of waves and turbulence) is a significant direction for further research in Venus general circulation modeling.

The choice of vertical and horizontal resolutions does affect the results. This is a difficult aspect of the problem, since we are limited by computer power. Therefore, the zonal and meridional wind strength should always be considered with caution until this dependence may be waived. In the case of the vertical resolution, there may be regions where the resolution should be improved, while in other regions this dependence is less significant. This analysis is certainly a study that needs to be done in the near future.

The sensitivity of the circulation to the initial state raises questions. Is this due to very long timescales to reach a completely steady state? Is it related to angular

momentum conservation? Are there other processes to be taken into account that would help solve this problem (such as gravity waves)? These questions need to be addressed by further modeling efforts.

This intercomparison work should be persuade in the future. It should include a quantitative assessment of the angular momentum budget, transport terms and balance, as well as the analysis of waves and their role in the transport of angular momentum. It would also be very interesting work to do when several improved models with realistic radiative transfer modules will be mature.

Acknowledgements SL would like to thank the Centre National d'Etudes Spatiales (CNES), the project Exoclimats financed by the Agence Nationale de la Recherche (ANR), and the computation facilities of both the Institut du Dévelopement et des Ressources en Informatique Scientifique (IDRIS) and the University Pierre and Marie Curie (UPMC). The LR10 simulations were performed on Caltech's Division of Geological & Planetary Sciences Dell cluster, CITerra, funded by a grant from NASA under the Planetary Atmospheres program. MY conducted the numerical experiments at the Information Technology Center of the University of Tokyo and the Information Initiative Center of Hokkaido University, which were supported by Grant-in-Aid for Scientific Research (KAKENHI No. 20740273 and 22244060). HFP and GS acknowledge support from NASA's Planetary Atmospheres Program through Grant NASA NNX07AF27G.

References

A.D. Del Genio, W. Zhou, Simulations of superrotation on slowly rotating planets: Sensitivity to rotation and initial condition. Icarus **120**, 332–343 (1996), doi:10.1006/icar.1996.0054

A.D. Del Genio, W. Zhou, T.P. Eichler, Equatorial superrotation in a slowly rotating GCM - implications for Titan and Venus. Icarus **101**, 1–17 (1993), doi:10.1006/icar.1993.1001

T.E. Dowling, M.E. Bradley, E. Colon, J. Kramer, R.P. LeBeau, G.C.H. Lee, T.I. Mattox, R. Morales-Juberias, C.J. Palotai, V.K. Parimi, A.P. Showman, The EPIC atmospheric model with an isentropic/terrain-following hybrid vertical coordinate. Icarus **182**, 259–273 (2006)

A. Herrnstein, T.E. Dowling, Effects of topography on the spin-up of a Venus atmospheric model. J. Geophys. Res.-Planets **112**, 4 (2007), doi:10.1029/2006JE002804

J.L. Hollingsworth, R.E. Young, G. Schubert, C. Covey, A.S. Grossman, A simple-physics global circulation model for Venus: Sensitivity assessments of atmospheric superrotation. Geophys. Res. Lett. **34**, 5202 (2007), doi:10.1029/2006GL028567

F. Hourdin, F. Couvreux, L. Menut, Parameterization of the dry convective boundary layer based on a mass flux representation of thermals. J. Atmos. Sci. **59**, 1105–1123 (2002)

A. Kido, Y. Wakata, Multiple equilibrium states appearing in a Venus-like atmospheric general circulation model. J. Meteorol. Soc. Japan **86**, 969–979 (2008)

S. Lebonnois, F. Hourdin, V. Eymet, A. Crespin, R. Fournier, F. Forget, Superrotation of Venus' atmosphere analyzed with a full general circulation model. J. Geophys. Res.-Planets **115**, 6006 (2010), doi:10.1029/2009JE003458

C. Lee, Modelling of the atmosphere of Venus, Ph.D. thesis, University of Oxford (2006)

C. Lee, M.I. Richardson, A general circulation model ensemble study of the atmospheric circulation of venus. J. Geophys. Res. Planets **115**, E04002 (2010), doi:10.1029/2009JE003490

C. Lee, S.R. Lewis, P.L. Read, A numerical model of the atmosphere of Venus. Adv. Space Res. **36**, 2142–2145 (2005), doi:10.1016/j.asr.2005.03.120

C. Lee, S.R. Lewis, P.L. Read, Super-rotation in a venus general circulation model. J. Geophys. Res. Planets **112**, L04204 (2007), doi:10.1029/2006JE002874

G.L. Mellor, T. Yamada, Development of a turbulent closure model for geophysical fluid problems. Rev. Geophys. Space Phys. **20**, 851–875 (1982)

A.S. Monin, A.M. Obukhov, Basic laws of turbulent mixing in the ground layer of the atmosphere. Trans. Geophys. Inst. Akad. Nuak. **151**, 1963–1987 (1954)

M. Newman, C.B. Leovy, Maintenance of strong rotational winds in Venus' middle atmosphere by thermal tides. Science **257**, 647–650 (1992)

H.F. Parish, G. Schubert, C. Covey, R.L. Walterscheid, A. Grossman, S. Lebonnois, Decadal variations in a Venus General Circulation Model. Icarus, **212**, 1, 42–65, doi:10.1016/j.icarus.2011.11.015, 2011 accepted (2011)

P. Read, Super-rotation and diffusion of axial angular momentum : II. a review of quasi-axisymmetric models of planetary atmospheres. Quater. J. R. Met. Soc. **112**, 253–272 (1986)

A. Sanchez-Lavega, R. Hueso, G. Piccioni, P. Drossart, J. Peralta, S. Perez-Hoyos, C.F. Wilson, F.W. Taylor, K.H. Baines, D. Luz, S. Erard, S. Lebonnois, Variable winds on Venus mapped in three dimensions. Geophys. Res. Lett. **35**, L13204 (2008)

A. Seiff, J.T. Schofield, A.J. Kliore, F.W. Taylor, S.S. Limaye, H.E. Revercomb, L.A. Sromovsky, V.V. Kerzahanovich, V.I. Moroz, M.Y. Marov, Models of the structure of the atmosphere of Venus from the surface to 100 kilometers altitude. Adv. Space Res. **5**(11), 3–58 (1985)

M. Takagi, Y. Matsuda, Effects of thermal tides on the Venus atmospheric superrotation. J. Geophys. Res.-Atmos. **112**, 9112 (2007), doi:10.1029/2006JD007901

M. Yamamoto, M. Takahashi, The fully developed superrotation simulated by a General Circulation Model of a Venus-like atmosphere. J. Atmos. Sci. **60**, 561–574 (2003a), doi:10.1175/1520-0469(2003)060

M. Yamamoto, M. Takahashi, Superrotation and equatorial waves in a T21 Venus-like AGCM. Geophys. Res. Lett. **30**, 090 000–1 (2003b), doi:10.1029/2003GL016924

M. Yamamoto, M. Takahashi, Dynamics of Venus' superrotation: The eddy momentum transport processes newly found in a GCM. Geophys. Res. Lett. **31**, 9701 (2004), doi:10.1029/2004GL019518

M. Yamamoto, M. Takahashi, Superrotation maintained by meridional circulation and waves in a Venus-like AGCM. J. Atmos. Sci. **63**, 3296–3314 (2006), doi:10.1175/JAS3859.1

M. Yamamoto, M. Takahashi, Dynamical effects of solar heating below the cloud layer in a Venus-like atmosphere. J. Geophys. Res. **114**, E12004 (2009), doi:10.1029/2009JE003381

R.E. Young, J.B. Pollack, A three-dimensional model of dynamical processes in the Venus atmosphere. J. Atmos. Sci. **34**, 1315–1351 (1977), doi:10.1175/1520-0469(1977)034

Chapter 9
Comparing Earth and Venus

Hauke Schmidt

9.1 Introduction

For obvious reasons the atmosphere of Venus has received much less attention in the natural sciences than the atmosphere of Earth. The same is true for numerical modeling efforts concerning the two atmospheres. The circulation of Venus' atmosphere can be described by the same set of basic equations valid for the other planetary atmospheres: the Navier-Stokes equations describing the temporal evolution of momentum plus equations of continuity and the conservation of thermodynamic energy (see Chap. 5). These equations are discretized in the so-called dynamical cores of numerical models, and it is not surprising that Venus models, in general, use dynamical cores originally built for Earth modeling (see Chap. 6). Parameterizations needed in complex planetary models to describe subgrid-scale processes are more difficult to exchange because parameters may differ considerably among planets. Nevertheless, many parameterizations used in Venus models are based on developments made for other planets.

The Venus model presented by Lebonnois et al. (2010), for instance, see also Chaps. 6 and 8, uses several parameterizations applied originally to Earth, but also used for modeling of Mars and Titan. But there may be more to learn for Venus modeling from more or less recent successes in Earth modeling. Consequently, the purpose of this chapter is to describe features of the Earth atmosphere and their numerical simulation that may help in the understanding phenomena of the Venus' atmosphere. The focus will be on the zonally averaged circulation both in the tropics and extra-tropics. Atmospheric dynamics on Earth and Venus exhibit some significant differences. Due to the fast rotation of the Earth, e.g., wind patterns over

H. Schmidt (✉)
Max Planck Institute for Meteorology, Hamburg, Germany
e-mail: hauke.schmidt@zmaw.de

L. Bengtsson et al. (eds.), *Towards Understanding the Climate of Venus*, ISSI Scientific Report Series 11, DOI 10.1007/978-1-4614-5064-1_9,

a large range of scales can be understood assuming geostrophic equilibrium, while cyclostrophic equilibrium is a useful concept for the atmosphere of the slow rotating Venus (see Chap. 5).

However, there are also important similarities that will be the subject of the following sections. For a start, it may be useful to remind the reader of the mean circulation in Earth's atmosphere. Figure 9.1a shows the annual and zonal mean zonal wind as simulated by the Hamburg Model of the Neutral and Ionized Atmosphere (HAMMONIA Schmidt et al. 2006). HAMMONIA is a general circulation and chemistry model covering the atmosphere from the surface to the lower thermosphere. While the observational coverage of the troposphere and lower stratosphere, that are accessible to balloon soundings and remote sensing from satellites, is excellent, the knowledge on the circulation of mesosphere and lower thermosphere is much less complete and except for sparse rocket soundings based on remote sensing from satellite or the surface. Similar to the situation on Venus, modeling is therefore necessary not only to understand the observations but also to fill their gaps. Figure 9.1a shows the westerly jets in the subtropical upper troposphere. Stratosphere and lower mesosphere are dominated by easterlies in the tropics and westerlies in the extra tropics, a picture that reverses in the upper mesosphere. While in the case of Venus the obliquity is close to zero, the relatively high obliquity of the Earth axis leads to a strong seasonality of the circulation. This is indicated by Fig. 9.1b that shows zonal mean winds for July. It is clear from this figure that the annual mean extra-tropical westerlies in the stratosphere are resulting from the strong polar night jets in the respective winter hemispheres. However, even seasonal wind fields provide only limited insight in the actual circulation as strong variability exists on many other (shorter and longer) timescales.

Although this chapter mainly deals with phenomena of the zonally averaged circulation, the importance of eddies or waves (i.e. deviations from a zonally averaged state) for the general circulation on both Venus and Earth can hardly be overestimated. Waves may influence the mean flow by depositing their momentum and depend on the atmospheric background state that defines propagation conditions. Such wave-mean flow interactions play an important role for the phenomena described below. An overview and a theoretical description of important wave modes on Venus (and Earth) are given in Sect. 6.6. Further comprehensive information on waves in the terrestrial atmosphere is provided e.g. in the textbooks from Holton (2004) and Andrews et al. (1987).

9.2 Super-Rotation and the Qbo: The Role of Eddy Momentum Transfer

The strong super-rotation of the Venus atmosphere is arguably one of the most challenging scientific issues in planetary atmospheric studies. Theoretical considerations have shown that momentum transport by eddies and the transfer of their momentum

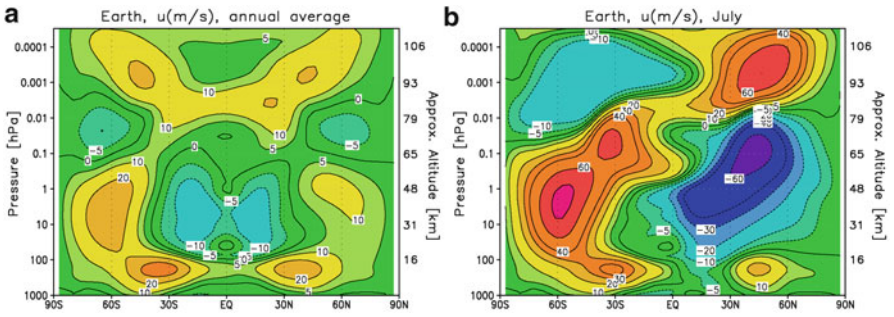

Fig. 9.1 (**a**): Annual and zonal mean zonal wind (m/s) of the Earth atmosphere averaged from a multi-year simulation with the HAMMONIA model. (**b**): same as (**a**) but as an average over all simulated months of July

to the zonal mean flow are necessary to sustain a super-rotation (Chap. 5). Although today's Venus models are able to produce super-rotating atmospheres it is still not completely clear, which role different types of waves may play. Planetary scale waves, but also small scale gravity waves and thermal tides may all have an influence (Chaps. 6 and 8). Zonal winds with westerly speeds up to about 100 m/s in large parts of the Venus atmosphere extend by far the rotational speed of Venus that is of about 2 m/s at the equator. Absolute zonally averaged wind speeds observed in the Earth atmosphere are in general below 100 m/s everywhere (see Fig. 9.1) and thus largely exceeded by the equatorial rotational speed of about 460 m/s. Such high wind speeds have only occasionally and locally been observed on Earth in the high latitude lower thermosphere (Tsuda et al. 2009).

But as on Venus, the momentum transfer through eddies plays an important role in determining the zonally averaged circulation on Earth, as well. In this section, we focus on equatorial zonal winds, and specifically on the phenomenon known as QBO: the quasi-biennial oscillation of stratospheric zonal winds. As shown in Fig. 9.2, the winds change their direction with an observed average period of about 28 months from easterly (of up to about –35 m/s in the middle stratosphere) to westerly (of up to about 15 m/s) and back. Like the super-rotation on Venus the occurrence of the QBO had remained unexplained for a long time and is still subject of scientific research. Periods of one year or harmonics of it are observable in many atmospheric quantities but a period of about 28 months had presented a puzzle over decades. More detailed historical surveys on the discovery of the QBO and a review of the current scientific understanding are given e.g. by Hamilton (1998); Labitzke and van Loon (1999), and Baldwin et al. (2001). Here we want to give only a relatively brief overview.

After the eruption of the tropical volcano Krakatoa in August 1883 a westward transport of the volcanic cloud around the globe at about 25 km of altitude was observed. Based on these global sightings of the cloud, Russell (1888) estimated an easterly wind velocity of slightly more than 30 m/s for the cloud altitude. This fitted nicely to the expectation of having easterly winds in the equatorial region.

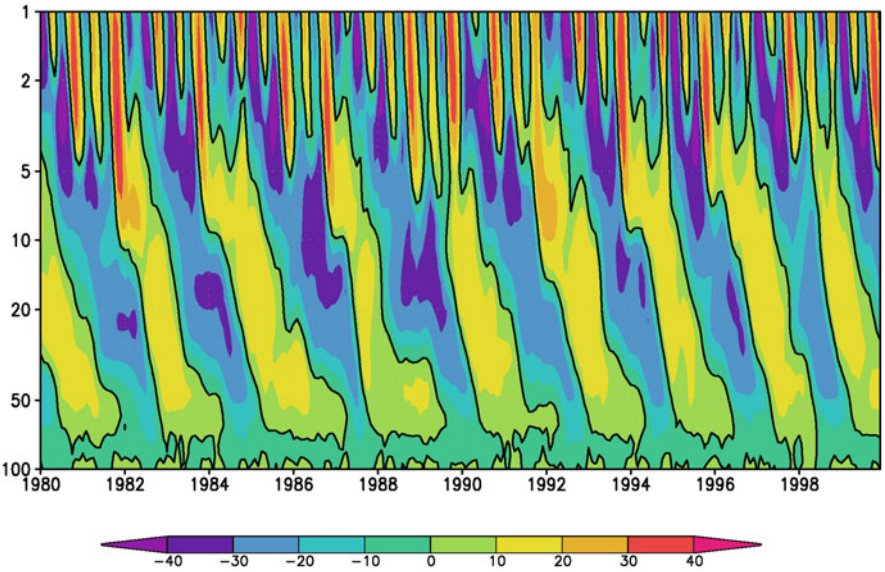

Fig. 9.2 Zonal mean zonal winds (m/s) at the equator for the stratosphere. Pressure levels of 100 and 1 hPa correspond to altitudes of approximately 16 and 48 km, respectively. Winds are simulated by the HAMMONIA model but nudged to radio soundings from Singapore (2°N) in the lower to middle stratosphere

Today we know that if Krakatoa had erupted a year earlier or later, the cloud would likely have moved in the opposite direction. In 1908, the German Meteorologist A. Berson launched balloons in equatorial Africa, and discovered westerly winds in altitudes between about 18 and 20 km. In the first half of the twentieth century it was then assumed that narrow bands of westerly winds (called "Berson westerlies") were embedded in the prevailing easterlies. Only after more regular balloon soundings in the tropics had started in the 1950s the alternation of prevailing easterly and westerly winds, the QBO, was discovered (e.g. Reed et al. 1961). So in the early 1960s, the phenomenon was observed but waited to be understood. Early assumptions that the QBO might be a harmonic of the 11-year solar cycle proved inconclusive. Two main QBO features were difficult to explain: First, why did the structure propagate downward without any change of amplitude over a fairly large part of the stratosphere, and second, why would winds turn westerly at all. They do not represent a super-rotation in the Venusian sense of a zonal wind faster than the rotation, but in the opposite direction. It was shown that the necessary momentum transfer could neither be explained by meridional advection nor by meridional eddy momentum transport (Wallace and Holton 1968). Rather transport of zonal momentum by vertically propagating equatorial waves had to be involved, but by which type of waves? Lindzen and Holton (1968) and Holton and Lindzen (1972) developed conceptual models that explained the QBO with wave-mean flow interactions resulting from a combination of eastward and westward travelling

waves. While in the first paper internal gravity waves were assumed to provide the momentum transport, in the second paper Holton and Lindzen (1972) presented a revised theory based on equatorial planetary waves (Kelvin and mixed Rossby-gravity waves). It took until the turn of the century before the main features of the QBO were successfully simulated in Earth GCMs (e.g. Takahashi 1999; Scaife et al. 2000).

Today it is assumed that momentum deposition from a broad spectrum of small scale gravity waves (that need to be parameterized in standard GCMs) and from planetary waves drives the QBO. Simulations by Giorgetta et al. (2006) indicate that gravity waves provide the dominant forcing for the QBO east phase while planetary waves have a larger contribution to the west phase. Still today, many GCMs do not succeed in reproducing a QBO, although it has become clear that two major requirements have to be met: First, an appropriate parameterization of convective processes that provide energy for planetary waves and second, a high vertical resolution of the model capable of resolving the waves that carry the momentum. Observational confirmation of the mechanism assumed to drive the QBO seems difficult. This is in particular related to the difficulty in quantifying gravity wave parameters on a global scale due to their small spatial scale and inappropriate resolution of satellite observations. Similarly, one can expect for Venus that a conclusive theory of the super-rotation will have to rely heavily on numerical simulations.

The QBO is not the only interesting feature in the equatorial Earth atmosphere. As can be seen from Fig. 9.2, the equatorial stratopause region is dominated by a semi-annuals oscillation (SAO), and also in the upper mesosphere a strong SAO is present. The semi-annual period appears much less mysterious than the 28-month period of the QBO. Many GCMs have successfully simulated the stratopause SAO and it is generally assumed that the east phase of the SAO is forced by a combination of the effect of quasi-stationary planetary waves and by momentum advection by the meridional winds directed from the winter to the summer hemisphere at the stratopause (thus causing the locking to the seasonal cycle). The westerly acceleration is less clearly understood, but several studies point to the importance of gravity waves. This is also supported by the fact that different phases of the SAOs in the different altitudes are modulated by the QBO, which is probably due to the filtering effects of the QBO on gravity waves (see e.g. Pena-Ortiz et al. 2010). To complete the picture it should be noted that also momentum deposition by tidal waves is supposed to play a role in equatorial dynamics, specifically in the mesopause region as discussed e.g. by Lieberman et al. (2011).

9.3 Polar Vortices on Venus and Earth

Polar vortices exist on both Earth and Venus and it is tempting to compare them, and to learn from the better observed Earth vortices about the Venus vortices where the major source of information is the tracking of cloud features at the upper cloud surface close to 70 km of altitude. However, it is suggested by Limaye et al. (2009)

that differences between the planetary vortices are large, and dynamically the Venus vortices may have more similarities with another feature of the Earth atmosphere, namely tropical cyclones.

So what are the obvious similarities and differences? Earth vortices are seasonal features observed to occur in both winter hemispheres. As mentioned earlier, due to an almost vertical obliquity, Venus shows no distinct seasons. Its vortices are observed on both hemispheres and assumed to be of permanent nature. Wind fields of both planets, including their polar vortices, can largely be deduced from the temperature fields via thermal wind equations but while a geostrophic thermal wind is observed on Earth, the Venus equilibrium is of cyclostrophic nature (Chap. 5). The Earth vortices extend in the winter hemisphere over a large vertical range from the upper troposphere to the lower mesosphere (see Fig. 9.1b). Maximum wind speeds are in general obtained close to or slightly above the stratopause near the polar night terminator (hence the name "polar night jet"). They can easily be explained by the meridional gradient in solar heating by ozone absorption. Solar heating in the Venus atmosphere that may be relevant for the vortices occurs mainly at the top of the cloud layer. So the existence of the Venus vortices is likely less related to heating gradients but to the momentum transfer processes mentioned in connection with the super-rotation. Figure 6.4 shows a plausible zonal wind field consistent with angular momentum and momentum transfers that would explain super-rotation. The wind field shows jets in both hemispheres with zonal wind maxima close to 50 degrees of latitude. Many present-day Venus models simulate polar vortices. This can be inferred e.g. from the zonal wind fields from a variety of models presented in Fig. 8.2. Strength and location of high-latitude jet maxima differ however strongly among the models. Further work is required to understand these differences and the role of the high latitudes for the global circulation on Venus in general (see Chaps. 6 and 8). An observed feature in the center of the Venus vortices is a deviation from zonal symmetry occurring as an S-shape (sometimes also referred to as a dipole). Elson (1982) found that the Venus vortex is barotropically unstable. Limaye et al. (2009) confirmed this in a two-dimensional model simulation initialized with a latitudinal vorticity field from Venus observations (see Fig. 6.17). In their model, wave-2 patterns occur that resemble very much the S-shape structure observed on Venus. Figure 9.3 shows the vortex as observed during October 2006 by the VIRTIS instrument on Venus Express. Occasionally, Earth vortices produce similar wave-2 patterns as can be seen in Fig. 9.4. Such events in general belong to the category of "sudden stratospheric warmings" (SSW) that still are an important topic of middle atmosphere research. These events were discovered by R. Scherhag in 1952. His balloon soundings revealed a temperature increase in the middle stratosphere of about 40 K within two days. Today, it is known that the high latitude temperature increase is always accompanied by a reversal (or strong weakening) of the wintertime westerly zonal winds, i.e. it is a signal of an intermediate breakdown of the polar vortex. "Major" stratospheric warmings are defined using as criterion the reversal of the zonal mean zonal wind at 60 degrees latitude and 10 hPa plus a reversal of the usually negative poleward temperature gradient. Such events are relatively frequent in the Northern hemisphere, occurring in about two out of three

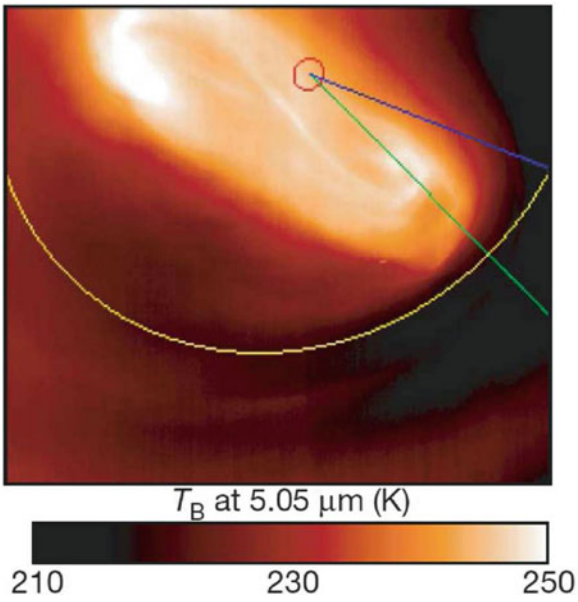

Fig. 9.3 False color image at a wavelength of 5.05 mm of the Venus south polar vortex acquired on 28 May 2006 by the VIRTIS instrument on Venus Express. Color shading indicates the brightness temperature in K. The *blue* and the *green lines* mark the meridians at 330° and 350° of longitude, respectively. The red circle indicates the south pole. The *yellow curve* is the parallel at –70° of latitude. Figure reprinted by permission from Macmillan Publishers Ltd, Piccioni et al. (2007), ©(2007)

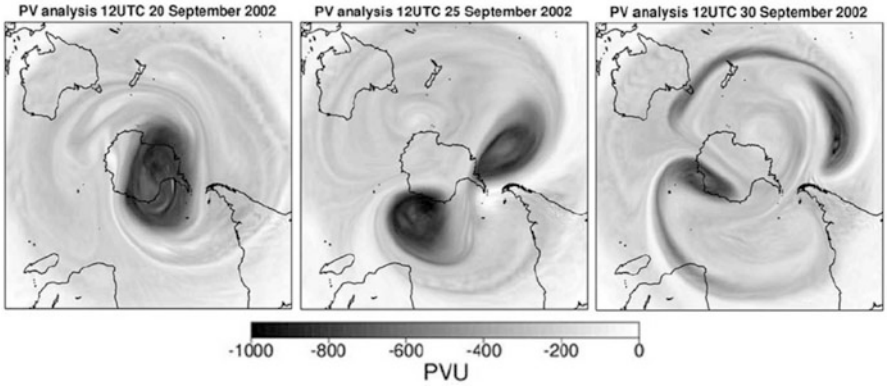

Fig. 9.4 ECMWF analyses of potential vorticity in units of 10^{-6} m^2 s^{-1} $K\,kg^{-1}$ on the 850 K isentropic surface (≈30 km altitude) for 1200 UTC on 20, 25, and 30 September 2002. While the vortex on 20 September has a fairly typical shape, the split vortex at 25 September is indicative of the, so far, unique observed event of a major sudden stratospheric warming in the southern hemisphere. Major warmings characterized by a vortex split occur on average about each three years in the northern hemisphere winter. Figure adapted from Simmons et al. (2005). ©American Meteorological Society. Reprinted with permission

years (Charlton and Polvani 2007), but have been observed only once (in 2002) in the Southern hemispheric winter. In the Northern hemisphere, SSWs can be characterized either as wave 1-events, called "vortex displacements", where the vortex center is significantly displaced from the pole, or as "vortex splits" with a

wave 2-structure as in the middle panel of Fig. 9.4. The occurrence of these events can, however, not be explained with barotropic instability as it seems to be the case on Venus. According to Andrews et al. (1987), early attempts to explain sudden warmings investigated the possibility of barotropic instability of the large scale polar vortex as well as of baroclinic instability of the polar night jet, but the developing instabilities were too small to explain the observed characteristics of warmings. Today, it is generally assumed that SSWs are the result of upward propagating Rossby waves that originate in the troposphere and interact with the stratospheric mean flow. This conceptual idea was first brought up by Matsuni (1971). Many Earth GCMs are able to simulate more or less satisfactorily the polar vortices and their occasional breakdown in the form of an SSW. It is however still a challenge to simulate the correct occurrence frequency of SSWs and its seasonal cycle (Charlton et al. 2007).

As stated in the beginning the dynamical origin of polar vortex instabilities on Venus and Earth is likely to be very different. Limaye et al. (2009) suggested that dynamical similarities rather exist with tropical cyclones on Earth although these have a much smaller scale. They show that S-shaped structures occur also in the eye of cyclones, and mention the occurrence of small scale transverse waves extending radially from the centres of both terrestrial cyclones and the Venus polar vortices. Accordingly, earlier theoretical studies have shown that barotropic instability is of importance in the inner core of tropical cyclones (Schubert et al. 1999). However, it can not be excluded that studies of Venus polar vortices may benefit from comparisons with their terrestrial counterparts. Relatively recently, vertical coupling processes during SSWs have been discussed that reach far beyond the stratosphere. It is observed that stratospheric warmings are in general accompanied by mesospheric coolings and possibly also by thermospheric warmings (e.g. Funke et al. 2010). This is explained by changes in the filtering of upward propagating waves (in particular small scale gravity waves) during SSWs and subsequent changes in wave-mean flow interactions in the upper atmosphere. Hence, SSWs can be seen as a manifestation of dynamical coupling between atmospheric layers from the surface to the thermosphere. It would be interesting to investigate if similar coupling processes occur also on Venus.

9.4 Conclusions and Outlook

What can be learned from the comparison of Earth and Venus phenomena as done above and where could future Venus modeling benefit from current developments in Earth modeling? All phenomena described above, super-rotation and S-shaped vortex instabilities on Venus, the quasi-biennial oscillation and sudden stratospheric warmings on Earth have been observed, first, and then scientists have tried to understand them with the help of numerical models. This is not an unusual sequence in atmospheric science. Labitzke and van Loon (1999) in their book on

the stratosphere cite the German-Russian climatologist and meteorologist Wladimir Köppen (1846–1940). In general, theory has to follow the experience ("die Theorie muss der Erfahrung folgen"). In the above cases, one reason for this is probably that the phenomena can not be simulated from first principles alone. In all cases parameterizations are needed, for instance of the radiative effect of clouds in the case of the Venus circulation and of subgrid-scale gravity waves in the cases of the QBO and of coupling effects during SSWs. The transfer of parameterizations from Earth to Venus models is not generally feasible, because parameter ranges may be very different. A candidate for transfer are parameterizations of subgrid-scale gravity wave effects. A parameterization for non-orographic gravity waves has already been used for Venus and shown to affect super-rotation (Ikeda et al. 2007), but the standard approach in Venus modeling is to parameterize the damping effect of gravity waves on horizontal winds via a Rayleigh friction approach (see Chap. 8).

In Earth models this technique has been largely replaced by more physically based gravity wave parameterizations. But also these parameterizations have severe limitations, as they in general assume a strict vertical and instantaneous propagation of the waves and are poorly coupled to actual sources. Current development efforts try to overcome these deficiencies (e.g. Song and Chun 2008; Richter et al. 2010). Another approach is to eliminate parameterizations completely by strongly increasing the model resolution and actually resolving large parts of the gravity wave spectrum. This was done in a simulation by Kawatani et al. (2009) that successfully reproduced a QBO-like structure albeit with a too short period. These developments might be perspectives for Venus modeling, too. Future transfer of parameterizations and knowledge from Earth to Venus may also be useful in case of the cloud layer. Because of the large uncertainty clouds introduce with respect to climate change on Earth, they are a topic of intensive research. Numerical efforts concentrate on both, improved parameterizations of cloud effects in global climate models and process studies with limited area high resolution models. In most Venus models of today, the cloud layer has been represented only by a simple parameterization of their effect on radiation (see Chap. 8). Obviously, the sulfuric acid clouds on Venus differ strongly from the water clouds on Earth. A link to sulfate aerosol modeling, another important topic in current Earth atmosphere research, may be more promising. A comparison of clouds and cloud modeling for Venus and other terrestrial planets is presented e.g. by Montmessin (2010).

As stated in the beginning, it seems obvious that Venus modeling should exploit efforts made for Earth. But the transfer of code, knowledge, and understanding is not likely to be straightforward. A growing number of terrestrial atmosphere or climate models are applied to extreme cases, such as very different climates in the geological history of Earth. This is done not only to understand these historical climates but also to possibly eliminate parameterizations developed with too narrow a scope. Thereby confidence is gained for the applicability of the models to a broad spectrum of climate states, and in particular confidence in the ability to project future climate change. Venus is an excellent example for such an extreme climate.

References

D.G. Andrews, J.R. Holton, C.B. Leovy, *Middle Atmosphere Dynamics* (Academy, Orlando, Florida, 1987)

M.P. Baldwin, L.J. Gray, T.J. Dunkerton, K. Hamilton, P.H. Haynes, W.J. Randel, J.R. Holton, M.J. Alexander, I. Hirota, T. Horinouchi, D.B.A. Jones, J.S. Kinnersley, C. Marquardt, K. Sato, M. Takahashi, The quasi-biennial oscillation. Rev. Geophys. **39**, 179–229 (2001)

A.J. Charlton, L.M. Polvani, A new look at stratospheric sudden warmings. part I: Climatology and modeling benchmarks. J. Climate **20**, 449–469 (2007)

A.J. Charlton, L.M. Polvani, J. Perlwitz, F. Sassi, E. Manzini, K. Shibata, S. Pawson, J.E. Nielsen, D. Rind, A new look at stratospheric sudden warmings. part II: Evaluation of numerical model simulations. J. Climate **20**, 470–488 (2007)

L.S. Elson, Wave instability in the polar-region of Venus. J. Atmos. Sci. **39**, 2356–2362 (1982)

B. Funke, M. Lopez-Puertas, D. Bermejo-Pantaleon, M. Garcia-Comas, G.P. Stiller, T. von Clarmann, M. Kiefer, A. Linden, Evidence for dynamical coupling from the lower atmosphere to the thermosphere during a major stratospheric warming. Geophys. Res. Lett. **37**, L13803 (2010)

M.A. Giorgetta, E. Manzini, E. Roeckner, M. Esch, L. Bengtsson, Climatology and forcing of the quasi-biennial oscillation in the MAECHAM5 model. J. Climate **19**, 3882–3901 (2006)

K. Hamilton, Dynamics of the tropical middle atmosphere: A tutorial review. Atmos.-Ocean **36**, 319–354 (1998)

J.R. Holton, *Introduction to Dynamic Meteorology*, 4th edn. (Academic, New York, 2004)

J.R. Holton, R.S. Lindzen, Updated theory for quasi-biennial cycle of tropical stratosphere. J. Atmos. Sci. **29**, 1076–1080 (1972)

K. Ikeda, M. Yamamoto, M. Takahashi, Superrotation of the Venus atmosphere simulated by an atmospheric general circulation model. IUGG/IAMAS Meeting, Perugia, Italy (2007)

Y. Kawatani, M. Takahashi, K. Sato, S.P. Alexander, T. Tsuda, Global distribution of atmospheric waves in the equatorial upper troposphere and lower stratosphere: AGCM simulation of sources and propagation. J. Geophys. Res.-Atmos. **114**, D01102 (2009)

G.K. Labitzke, H. van Loon, *The Stratosphere: Phenomena, History, and Relevance* (Springer, Berlin, 1999)

S. Lebonnois, F. Hourdin, V. Eymet, A. Crespin, R. Fournier, F. Forget, Superrotation of Venus' atmosphere analyzed with a full general circulation model. J. Geophys. Res.-Planets **115**, 6006 (2010), doi:10.1029/2009JE003458

R.S. Lieberman, D.A. Ortland, D.M. Riggin, Q. Wu, C. Jacobi, Momentum budget of the migrating diurnal tide in the mesosphere and lower thermosphere. J. Geophys. Res.-Atmos. **116**, D07110 (2011)

S.S. Limaye, J.P. Kossin, C. Rozoff, G. Piccioni, D.V. Titov, W.J. Markiewicz, Vortex circulation on Venus: Dynamical similarities with terrestrial hurricanes. Geophys. Res. Lett. **36**, L04204 (2009), doi:10.1029/2008GL036093

R.S. Lindzen, J.R. Holton, A theory of Quasi-Biennial Oscillation. J. Atmos. Sci. **25**, p. 1095–1107 (1968)

T. Matsuno, Dynamical model of stratospheric sudden warming. J. Atmos. Sci. **28**, 1479–1494 (1971)

F. Montmessin, Clouds of Venus: comparison with other terrestrial planets. In VEXAG2010 workshop abstract, Madison, WI, USA (2010)

C. Pena-Ortiz, H. Schmidt, M.A. Giorgetta, M. Keller, QBO modulation of the semiannual oscillation in MAECHAM5 and HAMMONIA. J. Geophys. Res.-Atmos. **115**, D21106 (2010)

G. Piccioni, P. Drossart, A. Sanchez-Lavega, R. Hueso, F.W. Taylor, C.F. Wilson, D. Grassi, L. Zasova, M. Moriconi, A. Adriani, S. Lebonnois, A. Coradini, B. Bezard, F. Angrilli, G. Arnold, K.H. Baines, G. Bellucci, J. Benkhoff, J.P. Bibring, A. Blanco, M.I. Blecka, R.W. Carlson, A. Di Lellis, T. Encrenaz, S. Erard, S. Fonti, V. Formisano, T. Fouchet, R. Garcia, R. Haus, J. Helbert, N.I. Ignatiev, P.G.J. Irwin, Y. Langevin, M.A. Lopez-Valverde, D. Luz, L.

Marinangeli, V. Orofino, A.V. Rodin, M.C. Roos-Serote, B. Saggin, D.M. Stam, D. Titov, G. Visconti, M. Zambelli, South-polar features on venus similar to those near the North Pole. Nature **450**, 637–640 (2007)

R.J. Reed, L.A. Rasmussen, W.J. Campbell, D.G. Rogers, Evidence of a downward-propagating,annual wind reversal in equatorial stratosphere. J. Geophys. Res. **66**, 813–818 (1961)

J.H. Richter, F. Sassi, R.R. Garcia, Toward a physically based gravity wave source parameterization in a General Circulation Model. J. Atmos. Sci. **67**, 136–156 (2010)

F.A.R Russell, Spread of the phenomena round the world. *The Eruption of Krakatoa and Subsequent Phenomena* (Trübner & co, London, 1888)

A.A. Scaife, N. Butchart, C.D. Warner, D. Stainforth, W. Norton, J. Austin, Realistic quasi-biennial oscillations in a simulation of the global climate. Geophys. Res. Lett. **27**, 3481–3484 (2000)

H. Schmidt, G.P. Brasseur, M. Charron, E. Manzini, M.A. Giorgetta, T. Diehl, V.I. Fomichev, D. Kinnison, D. Marsh, S. Walters, The HAMMONIA chemistry climate model: Sensitivity of the mesopause region to the 11-year solar cycle and CO2 doubling. J. Climate **19**, 3903–3931 (2006)

W.H. Schubert, M.T. Montgomery, R.K. Taft, T.A. Guinn, S.R. Fulton, J.P. Kossin, J.P. Edwards, Polygonal eyewalls, asymmetric eye contraction, and potential vorticity mixing in hurricanes. J. Atmos. Sci. **56**, 1197–1223 (1999)

A. Simmons, M. Hortal, G. Kelly, A. McNally, A. Untch, S. Uppala, ECMWF analyses and forecasts of stratospheric winter polar vortex breakup: September 2002 in the Southern Hemisphere and related events. J. Atmos. Sci. **62**, 668–689 (2005)

I.-S. Song, H.-Y. Chun, A Lagrangian spectral parameterization of gravity wave drag induced by cumulus convection. J. Atmos. Sci. **65**, 1204–1224 (2008)

M. Takahashi, Simulation of the quasi-biennial oscillation in a general circulation model. Geophys. Res. Lett. **26**, 1307–1310 (1999)

T.T Tsuda, S. Nozawa, S. Oyama, T. Motoba, Y. Ogawa, H. Shinagawa, N. Nishitani, K. Hosokawa, N. Sato, M. Lester, R. Fujii, Acceleration mechanism of high-speed neutral wind observed in the polar lower thermosphere. J. Geophys. Res.-Space Phys. **114**, A04322 (2009)

J.M. Wallace, J.R. Holton, A diagnostic numerical model of the Quasi-Biennial Oscillation. J. Atmos. Sci. **25**, 280–292 (1968)

Part III
Outlook

Chapter 10
Future Prospects

Håkan Svedhem and David Grinspoon

In spite of all spacecraft that have visited our nearest planetary neighbor a large number of questions remain to be answered. Exploration of Venus is far from completed. In this chapter we summarize the most important questions to be answered, both in the short term, feasible with the technology of today, and those that only can be addressed in the medium to long term, after additional technology development. A large number of missions have been proposed in recent years but since Venus Express (Svedhem et al. 2007) and the ill fated Akatsuki (Nakamura et al. 2007) none of these have been selected for flight. Short descriptions of these mission proposals, as much as the information is openly available, are given in the following section. The next section deals with future ground based observations and joint space-ground observations. Finally the priorities for future missions, both for the benefit of improving on the theoretical models for atmospheric circulation, as dealt with in this book, and for an improved understanding of the evolution of Venus as a planet and of terrestrial planets in general, are discussed.

10.1 Major Questions

A large number of major questions have been debated in several multidisciplinary groups during recent years and there is at the moment a reasonable level of consensus in the Venus science community about which questions are the most burning. A "top ten" collection of questions has been agreed upon by the Venus

H. Svedhem (✉)
ESA/ESTEC, The Netherlands
e-mail: hsvedhem@rssd.esa.int

D. Grinspoon
Denver Museum of Nature & Science, Denver, USA

L. Bengtsson et al. (eds.), *Towards Understanding the Climate of Venus*, ISSI Scientific Report Series 11, DOI 10.1007/978-1-4614-5064-1_10,

Exploration Analysis Group, VEXAG, a NASA chartered community-based group of US and international scientists (Smrekar and Limaye 2011). The questions all fall within the three major themes of the 2010 Planetary Decadal Survey (to which VEXAG also contributed input); (1) Building New Worlds-understanding solar system beginnings; (2) Planetary Habitats-searching for the requirements for life; and (3) Workings of Solar Systems-revealing planetary processes through time. The questions also fit well within two out of the four Grand Themes of the Cosmic Vision Programme of ESA, namely; (4) What are the conditions for life and planetary formation?; and (5) How does the solar system work?

From these general themes the top ten questions can be arranged into three main groups: Questions related to understanding the origin and diversity of terrestrial planets (1 and 4 above) are,

- What was Venus' initial rock and volatile composition and what processes determined this inventory?
- What processes controlled Venus' thermal and chemical evolution throughout history?
- What are the mechanisms and timescales of resurfacing on Venus and is it still active today?

Questions related to understanding how the evolution of terrestrial planets enables and limits the origin and evolution of life (2 and 4 above) are,

- What is the origin and evolution of Venus' volatile inventory in its interior and atmosphere?
- Was Venus ever habitable?
- What are the past and present tectonic systems on Venus?
- How and when did Venus lose its volatiles?

Questions related to the understanding the processes that control climate on Earth-like planets and questions related to direct comparisons between Venus and the Earth (3 and 5 above) are,

- What processes control Venus' present climate?
- How did the climate of Venus evolve into its current state?
- What processes were responsible for the original atmosphere of Venus?

In order to answer these high level questions a large number of measurement objectives have had to be defined. This has to a large extent been done by the different teams that have been conducting mission studies or proposing missions in response to recent mission calls under various programmes. It becomes obvious that several questions are addressed by different measurements as well as that those individual measurements provide parts of answers to more than one question. For detailed measurement objectives and the corresponding scientific objectives of the different proposed missions the reader is referred to the individual mission descriptions in the reference list.

10.2 Prospects for the Next 20 Years

Exploration of planets beyond our own Earth in order to answer major questions as outlined above is a major undertaking and often comes with a need for a significant technology development. However, many of the listed questions can be addressed with measurements from orbit, or in situ in the atmosphere or on the surface, by scientific instruments similar to those existing today. For complete answers to all questions a number of complex missions will be required, and most likely missions focussed on dedicated topics will need to be flown together with larger more general and complex missions.

Many of the major questions are related to the evolution and the early history of the planet. To answer these it is essential to get better information on the noble gases and isotopes in the atmosphere. This can be done with existing instrumentation. Remote studies of the atmospheric dynamics, chemistry and clouds from orbit can be done well with existing cameras, and (imaging) spectrometers from the UV to mid IR, and by sub-mm wave sounders. As shown already in the 1980s by the Vega balloons, in situ investigations of the mesosphere are feasible and the troposphere and the lower cloud layer can be studied in situ with properly equipped descent probes. Surface studies from orbit are basically limited to radar investigations and to imaging in the infrared spectral windows between 1 and 3 micrometer wavelength. Spatial resolution on the surface at IR wavelengths is however limited to about 50 km due to scattering in the atmosphere and in cloud layers. In addition the spectral windows are fairly narrow making it difficult to acquire reliable information on surface elemental composition and mineralogy from orbit.

Spatial resolution of topography and surface structure can be significantly improved over the Magellan data with modern radar instruments, in particular by using an Interferometric Synthetic Aperture Radar, I-SAR, though such an instrument may need further development in order to be compatible with mission mass and data transfer restrictions.

In situ surface studies are possible for durations up to two to 3 h with well insulated landers, possibly in combination with the use of phase change materials. This is sufficient for a number of critical surface measurements like mineralogical and compositional investigations and local surface and panoramic imaging.

Long lived stations and mobile stations/rovers will require significant technology development, as they will need both advanced power systems and cooling systems that do not exist today. Such systems are therefore not likely to be ready for flight within the next 20 years. This limits the possibilities for extended lower atmosphere studies, like meteorology monitoring stations, and the deployment of seismic networks. This will have implications for the understanding of the status of the deep interior structure of today, and even more so for the investigation of interior history. The lack of mobility on the surface will, in the absence of a very large number of landers, leave questions on how representative a landing site and the related measurements will be. However, good progress is being made in development of high temperature electronics and it might be possible to have

a working high temperature seismometer a decade from now, although power generation and data transmission will remain a challenge. A possible alleviation for the mobility problem may be a "hopper", a lander using an inflatable bellows to achieve sufficient buoyancy to lift off and drift with the wind to several different landing sites, but again power and data transfer will remain difficult problems to solve.

If new missions are approved within the next 5–10 years, significant scientific progress can still be expected before 2030, using contemporary technology. Progress in modeling and theory usually go together with new empirical data and therefore there are good prospects for getting answers to many of the driving questions related to present status of the planet, to the atmosphere of the planets and to climate studies. It may perhaps be more difficult in the short term to answer questions about the deep interior and the early evolution of the planet.

10.3 New Mission Studies and Proposals

10.3.1 The NASA Venus Flagship Mission Study

In 2008 NASA appointed a Science and Technology Definition Team to study a Design Reference Mission, The Venus Flagship Mission (Hall et al. 2009). The team came up with a truly impressive and very capable concept designed to be compatible with a launch in 2021. The science was focussed under three Themes, with each Theme covering three scientific objectives:

1. What does the Venus greenhouse tell us about climate change? (i. Understand radiation balance in the atmosphere and the cloud and chemical cycles that affect it. ii. Understand how super-rotation and the general circulation work. iii. Look for evidence of climate change at the surface.)
2. How active is Venus? (i. Identify evidence of current geologic activity and understand the geologic history. ii. Understand how surface/atmosphere interactions affect rock chemistry and climate. iii. Place constraints on the structure and dynamics of the interior.)
3. When and where did the water go? (i. Determine how the early atmosphere evolved. ii. Identify chemical and isotopic signs of a past ocean. iii. Understand crustal composition differences and look for evidence of continent-like crust)

The mission concept is based on an orbiter, two balloons and two landers. The landers and balloons will be launched mounted on a carrier spacecraft and will be launched first and the orbiter will be launched separately six months later. The orbiter has a design lifetime of 4 years and a launch mass of 5,300 kg and carries an Interferometric SAR, a Vis-NIR imaging spectrometer, a Neutral and Ion mass spectrometer, a sub-mm wave sounder, a magnetometer, a Langmuir probe, and an Ultra Stable Oscillator (for radio science). The two balloons will float at 55.5 km

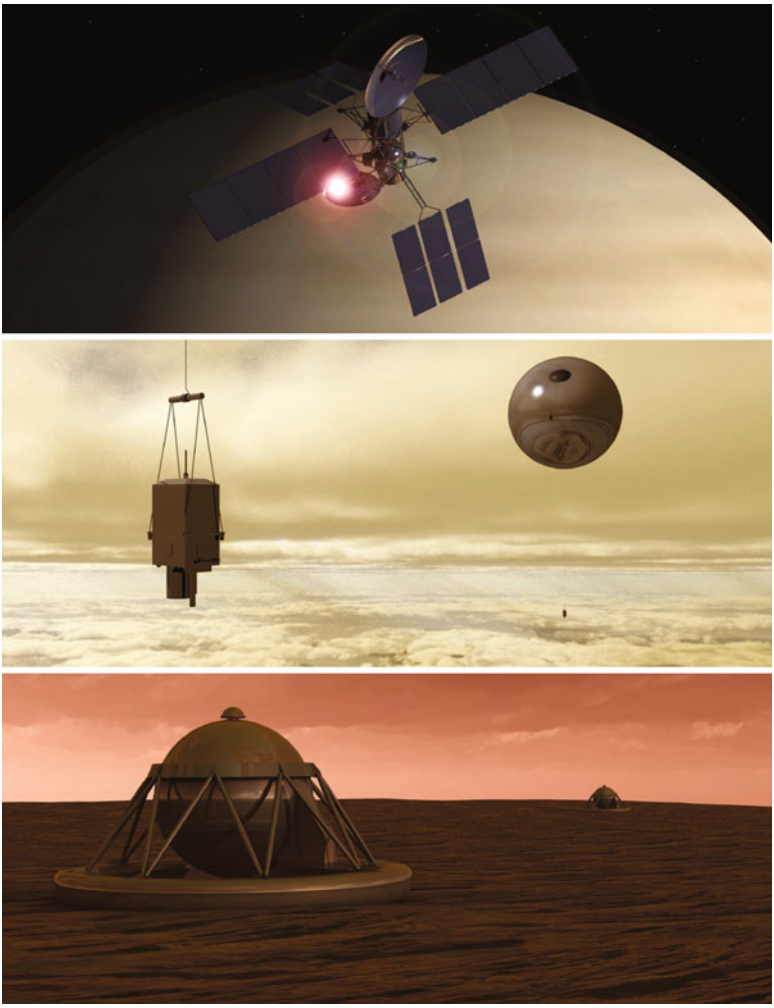

Fig. 10.1 An artist's impression of the major elements of NASA's Venus Flagship Mission showing the orbiter with the solar panels, I-SAR antennas and communication antennas clearly identifiable (*top*). The two balloons (only one visible) with gondolas drifting with the high velocity winds inside the cloud layer (*middle*). The two landers with their spherical well insulated outer structure on the surface of Venus (*bottom*). In the real flight configuration the separation of the two balloons and the two landers will be much larger. Credit: T. Balint, JPL/SWRI

altitude and will each carry an Atmospheric Structure Instrument, a GC/MS, a Nephelometer, a Vis-IR camera, a Magnetometer, and Radio Tracking. Because of the high temperatures on the surface of Venus the two landers have limited lifetimes (Fig. 10.1).

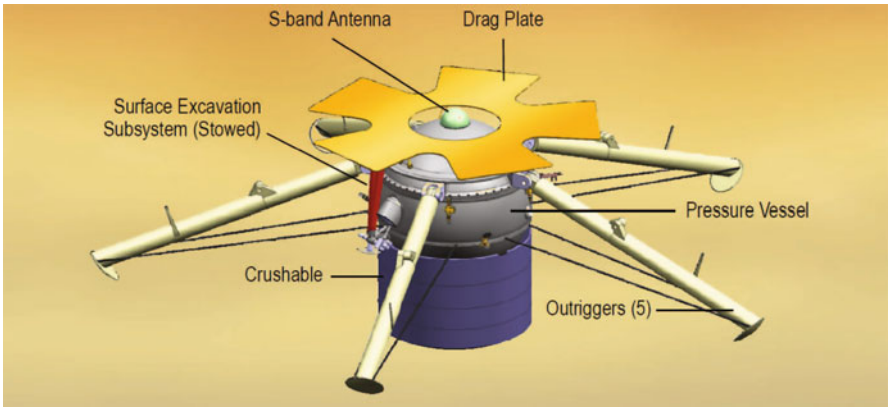

Fig. 10.2 A conceptual view of the SAGE lander. A soft landing is ensured by the crushable structure on the lower part of the body (in *blue* above) while the lateral stability is maintained by the long legs. The small drag plate at the top is sufficient to maintain attitude and ensure a low velocity during the final descent and the landing thanks to the high atmospheric density at low altitudes. Credit: LASP/JPL

10.3.2 The NASA New Frontiers Programme

In 2009 The Surface and Atmosphere Geochemical Explorer (SAGE) was selected for a study in competition with two other missions as a part of the New Frontiers 3 selection (Esposito 2011).

The leading scientific questions and the related measurement objectives were:

1. Why is Venus so different from Earth? (i. Measure noble gases, isotopes and sulphur compounds)
2. Was Venus ever like Earth? (i. Measure surface and subsurface composition at volcanic hotspot. ii. Determine surface rock type, mineralogy, and texture. iii. Provide ground truth for Magellan images and VIRTIS emissivity)
3. Does Venus represent Earth's fate? (i. Model the history of Venus and predict its future. ii. Predict observable characteristics of Venus-like extra solar planets.)

This mission is based on a single lander attached to a carrier spacecraft with a nominal launch date in December 2016. After separation the lander will descend onto the flank of Mielikki Mons, a volcano identified by Venus Express as having excessive surface emissivity and therefore believed to have a fresh surface structure, possibly due to recent activity. The carrier spacecraft will change course and slow down so that communication between the lander and the carrier spacecraft can be maintained after landing during the 3 h mission on the surface (Fig. 10.2).

The scientific payload includes the following elements: A Flyby Camera (on the carrier s/c), an Atmospheric Structure Investigation (ASI), including sensors for Temperature, Pressure, Wind and an accelerometer, a Doppler Wind Experiment (DWE), a Neutral Mass Spectrometer (NMS), a Tunable Laser Spectrometer

(TLS), a Descent Panoramic Camera and Microscopic Camera (DPC/MC), a Neutron-Activated Gamma-Ray Spectrometer (NAGRS), a Raman/Laser Induced Breakdown Spectroscopy (Raman/LIBS), and a robotic arm to access the surface.

Unfortunately, SAGE did not succeed in the final NF-3 selection in spring 2011. The Planetary Decadal Survey however does recommend maintaining SAGE as a candidate for NF-4 and NF-5.

10.3.3 The NASA Discovery Programme

In the most recent round of proposals, submitted in 2010 and selected in June 2011, seven out of the 28 proposals were missions to Venus. Out of these four were orbiters carrying radars as their main instrument and three were atmospheric/surface probes or balloons. Unfortunately none of these seven proposals were selected for a further study. As there is fierce competition and many of the proposers intend to resubmit similar proposals in response to a following Discovery announcement only limited information on these proposed missions is available. Therefore no further details are given here.

10.3.4 The NASA Planetary Decadal Survey 2010

As a part of and in support of the 2010 Decadal survey three brief studies for Venus missions were performed (Squyres 2011):

10.3.4.1 Venus Climate Mission

The Science objectives of this mission are: to characterize the strong CO_2 greenhouse atmosphere of Venus, including its variability; to characterize the dynamics and the variability of Venus' super rotating atmosphere; to characterize the surface/atmosphere chemical exchange in the lower atmosphere; to search for atmospheric evidence of climate change on Venus; to determine the origin of Venus' atmosphere and the sources and sinks driving the evolution of the atmosphere; and to understand the implications of Venus' climate evolution for the long term fate of the Earth (Fig. 10.3).

The mission concept is based on a gondola and balloon system, a mini probe, and two drop sondes, all accommodated inside an entry capsule/heat shield, which in turn is attached to a carrier spacecraft for the Earth-Venus trajectory. The carrier spacecraft will enter orbit around Venus and carries a Visible-Infrared monitoring camera and handles the communication between all elements and the Earth. The gondola/balloon system will float at 55 km altitude for 21 days and carries a Neutral Mass spectrometer (NMS), a Tunable Laser Spectrometer (TLS), an Atmospheric

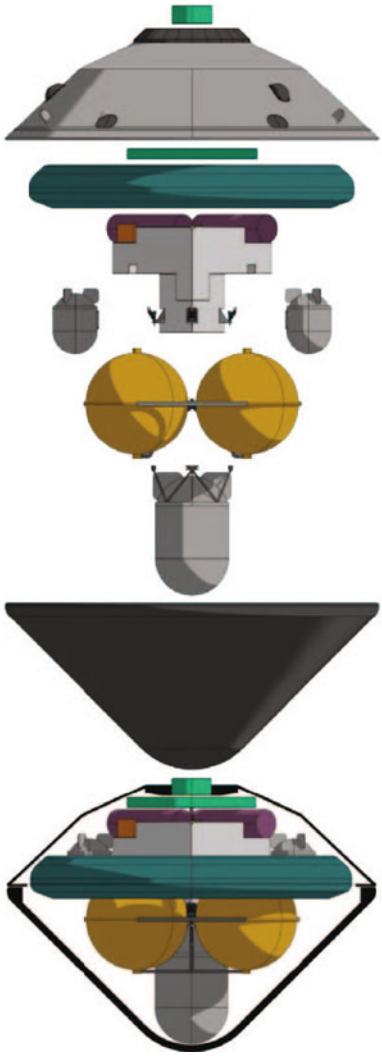

Fig. 10.3 An exploded view of the entry system of the Venus Climate Mission concept. From *top to bottom*: Drogue parachute; Backshell; Main parachute; Balloon; Gondola; Drop sondes (2); Helium tanks (4); Mini probe; Front aeroshell (Pioneer Venus heritage). At the *bottom* the stowed configuration of the complete entry system is shown. Credit: GSFC/JPL/ARC

Structure Instrument (ASI), a Nephelometer, and a Net-Flux Radiometer (NFR). The mini probe carries a Neutral Mass Spectrometer, a Net Flux radiometer and an Atmospheric Structure Instrument. Both drop sondes carry an Atmospheric Structure Instrument and a Net Flux Radiometer. Both the mini probe and the drop sondes will, once released from the gondola, descend from 55 km to the surface in 45 min.

The Venus Climate Mission can be seen as a downsized version of the Flagship mission described above excluding the landers, but with significantly less technology development required. The launch date for the purpose of the study is 2021. The Venus Climate mission was recommended as the 4th or 5th priority Flagship

Mission by the Decadal Survey for the decade 2013–2022. It could conceivably be chosen by NASA if the higher priority missions are deemed too expensive or cannot be flown for other reasons.

10.3.4.2 Venus Intrepid Tessera Lander

The Venus Intrepid Tessera lander is the second of the Decadal survey mission studies. The science objectives of this mission are: to characterize the chemistry and the mineralogy of the surface; to place constraints on the size and temporal extent of a possible ocean in Venus' past; and to characterize the morphology and relative stratigraphy of the various surface units.

The mission concept is based on a lander and a fly-by carrier. The lander shall sample the upper and the lower atmosphere during the descent and make 25 surface measurements on tessera terrain plus relevant context images. The scientific payload is composed of a Raman/LIBS, a NIR descent imager, a Neutral Mass Spectrometer, a Tunable Laser Spectrometer and a surface panoramic camera. The lifetime on the surface shall be 2 h and communication with the Earth is through the fly-by carrier.

10.3.4.3 Venus Mobile Explorer

The Venus Mobile Explorer is the third of the Decadal Survey mission studies. The science objectives of this mission are: to determine the origin and the evolution of Venus' atmosphere; to determine the rates of exchange of key chemical species between the surface and the atmosphere; to characterize the fundamental geologic units in terms of major rock forming elements, minerals in which those elements are sited, and isotopes; and to characterize the geomorphology and the relative stratigraphy of the major surface units.

The mission concept is based on a fly-by carrier spacecraft and a lander capable of moving to a second site using buoyancy generated by extending a gas filled bellows. It will perform compositional analysis in two locations and low altitude imaging during the drift from the first to the second landing site. The scientific payload is composed of a Raman/LIBS spectrometer, a NIR descent imager, a Neutral Mass Spectrometer, and a Tunable Laser Spectrometer. The lifetime on the surface and in the lower atmosphere shall be 4 h or more. This includes the horizontal traverse time, following the wind, at an altitude of about 5 km.

10.3.5 The ESA Cosmic Vision Programme

10.3.5.1 European Venus Explorer, EVE

The European Venus Explorer, EVE, was proposed in response to the 2010 call for M-class missions (Wilson and Chassefiere 2012). It was a modified version of a

more extended proposal that was submitted in response to the 2007 call for missions where it also included an orbiter and a lander (Chassefiere et al. 2009).

The scientific objectives of the EVE mission are: to understand the formation of the terrestrial planets and the origin of their atmospheres; to characterize and understand the strong greenhouse effect; to characterize and understand all aspects of the cloud layer; and to characterize and understand the atmospheric dynamics (Fig. 10.4).

The EVE 2010 concept is based on a single spacecraft carrying an entry probe containing a balloon and a gondola to Venus. The balloon is a superpressure Helium filled balloon floating at 55 km altitude. The communication will be via a direct gondola to Earth link at x-band. The gondola scientific payload is composed of, an Aerosol Collector and Pyrolyzer Gas Chromatograph Mass Spectrometer (ACP-GCMS), a Cloud X-ray fluorescence (XRF) spectrometer, an Isotopic Noble Gas Mass Spectrometer (INGMS), a Tunable Diode Laser (TDL) spectrometer, a Nephelometer, a radiometer, a meteorological package, an electric/magnetic package, and a camera. Optional instruments are, an Attenuated Total Reflection Spectrometer (ATRS), a 3d Fluxgate magnetometer and a microbalance for cloud microphysics investigations.

10.3.6 The Russian Venera-D Mission

The Venera-D mission is a future concept following in the footsteps of the long series of past Soviet Venus missions (Zasova 2011). The concept is in design phase-A and the present scientific objectives include: to investigate the structure and chemical composition of the atmosphere, including noble gases abundance and isotopic ratios and the structure and chemistry of the clouds; to study the atmospheric dynamics and the nature of the super-rotation; to characterize the radiative balance and the nature of the greenhouse effect; to study the structure, mineralogy and geochemistry of the surface; to search for seismic and volcanic activity and lightning; to investigate the interaction of the atmosphere and the surface; to investigate the upper atmosphere, the ionosphere and the magnetosphere and to determine the escape rates of the atmosphere.

The mission concept is based on an orbiter, a sub-satellite and a lander. The orbiter is derived from the Phobos-Grunt spacecraft and will be inserted into a 24 h polar orbit (Fig. 10.5).

The orbiter payload includes several spectrometers in the spectral range from UV to MM-wave, mapping spectrometers, a monitoring camera and a plasma package. The sub-satellite is aimed for plasma investigations by simultaneous measurement with plasma instruments on the orbiter. The lander payload includes, a GC-MS, a pressure-temperature-wind (PTW) package, a Nephelometer, an optical package, an active gamma spectrometer, a Mössbauer spectrometer, a Multichannel Tunable Diode Laser Spectrometer (MTDL), a Laser-Induced Plasma Spectrometer (LIPS),

Fig. 10.4 An artist's impression of the European Venus Explorer, EVE. The helium filled super pressure balloon/gondola combination will float at 55 km altitude and will make at least one full revolution around the planet during its minimum lifetime of ten days. Courtesy of T. Balint, JPL/Univ. Paris-Sud/Univ. Oxford

and a TV-complex containing panoramic high resolution cameras and descent cameras. The landing site is preliminary chosen as one of Tessera terrains, the oldest areas, where non-basaltic material is likely to be found.

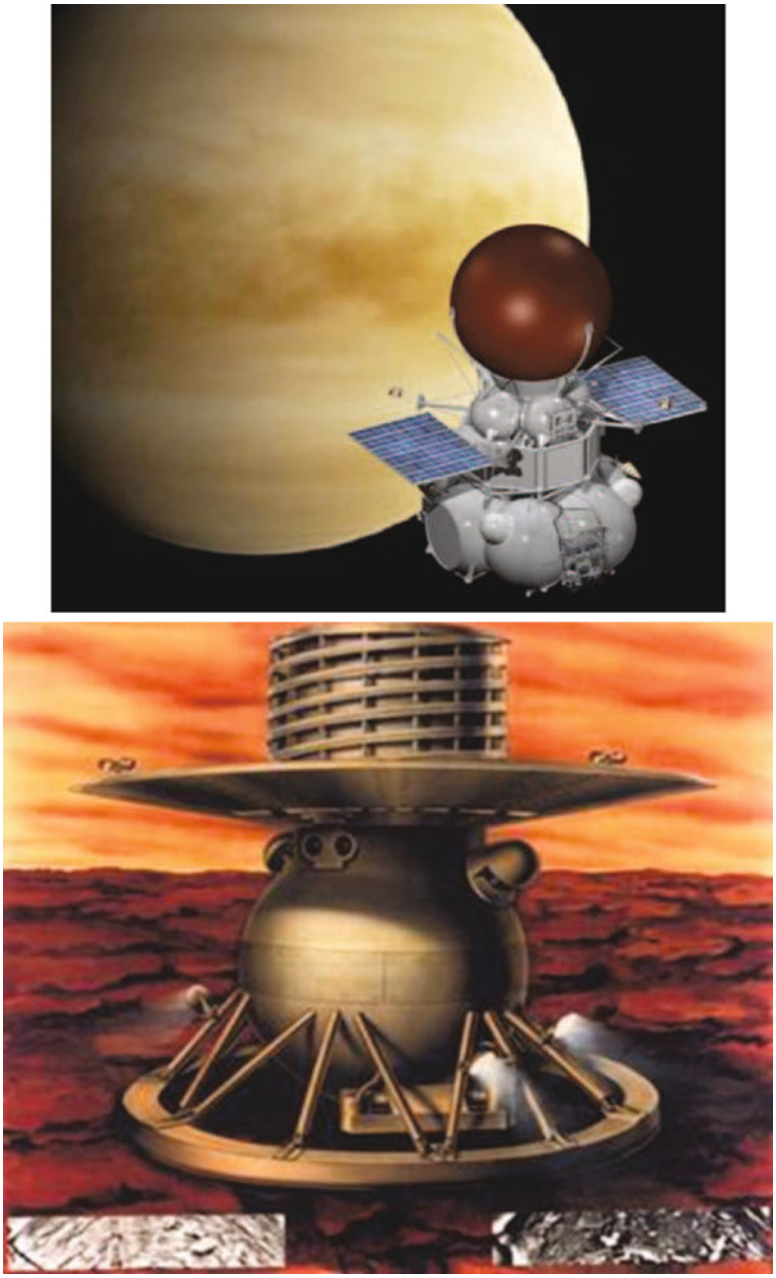

Fig. 10.5 An artist's impression of the Russian Venera-D mission. The orbiter is based on the Phobos-Grunt platform, launched on 8 November 2011. The brown sphere at the *top* of the spacecraft is the entry module, containing the lander and descent system (*left panel*). The lander has a strong heritage from the Vega1 and Vega 2 landers—the last landers that reached the surface of Venus. The *black and white* inserts at the *bottom* of the picture are images of the surface from the Venera-9 and -10 landers (*right panel*). Credit: NPO Lavochkin/IKI

10.3.7 Missions to Venus by Other Nations

Interest has been reported from additional countries, including for example China and India, which are planning or considering missions to Venus. At the moment the authors are not aware of any firm plans and no articles have yet been published in the open literature on such new projects. It may, however, not take too long before also new players will get seriously interested in studying Venus from orbit or even within the atmosphere or from the surface.

10.4 Advances in Earth Based Observations

Recent Earth based observations, in particular observations that have been done jointly by Venus Express and ground based observers, have shown that such observations have a great value. Especially the high spectral resolution observations available in mm wave and, thanks to new heterodyne receivers, also in the infrared range, have shown great value in determining atmospheric circulation at a global scale. These observations complement the space based observations very well. It is expected that such observations will play a role in the future, both as independent observations and as joint observations with new missions to Venus. The advantage of such observations is that they can be performed over a large portion of the year since they are not necessarily limited to the short periods of Venus maximum elongations from the Sun as are the conventional observations in the visible wavelength range. Also other observations, such as mapping of different kinds of airglow, are important and complementary to the space based observations. Improved spatial resolution, thanks to adaptive optics, indeed already is making such observations increasingly valuable. With future technical progress this is likely to improve further.

10.5 Priorities

For significant progress in wide fields addressing major topics like planetary evolution and general topics like understanding of planetary systems discussed in Sects. 10.1 and 10.2 it is necessary to design and fly missions at a level comparable to one or more flagship missions, which include landing elements as major components. Questions related to geology, petrology, seismic activity, local meteorology and local surface history can only be answered fully by landing on the surface of the planet. Even if the priority of such complex missions are high they may need to stand back in order to allow for additional technology development to take place. On the other hand, the main questions in this book are related to atmospheric circulation and GCMs. Here significant progress can be made without landing on the surface. Data required for this include measurements

of 3-d wind fields, 3-d temperatures, cloud structure and microphysics, radiation balance, atmospheric waves and tides, and energy and momentum transport. This will requires at least one orbiter, two or more balloons, preferably at different altitudes and a number of drop probes. The orbiter and the balloon will be of major importance for the understanding of the dynamics above the clouds, where an orbit that allows tracking the winds and the clouds for an extended time, like the concept of the semi stationary Akatsuki orbit, would be very beneficial, while the balloons would circle the planet inside the cloud layer at different latitudes, driven by the winds. Present knowledge on the temperature profiles and winds below the clouds is extremely sparse. Drop probes, launched from the balloons at different latitudes and local times are therefore needed. It is not expected that temperatures and winds at low altitudes will vary to a large extent (even if this is not proven yet). The number of probes can therefore be limited as long as a reasonable coverage in local time and latitude is provided. Flying such a set of platforms would have the highest priority for improving the present GCMs, and perhaps aid in understanding why the present Earth-Optimized GCMs have severe limitations when applied to Venus, as shown in Chap. 8. A mission of this kind could be based on one or two major complex projects, or could be made up of several coordinated missions of the size of NASA Discovery Class or the ESA Medium Class missions. A trade off study may be required to evaluate which strategy would be the most cost effective way to address these important questions. A serious attempt to solve the questions outlined in this chapter is a major undertaking and international collaboration would be very beneficial, if not essential.

References

E. Chassefiere, O. Korablev, T. Imamura, K.H. Baines, C.F. Wilson, D.V. Titov, K.L. Aplin, T. Balint, J.E. Blamont, C.G. Cochrane, C. Ferencz, F. Ferri, M. Gerasimov, J.J. Leitner, J. Lopez-Moreno, B. Marty, M. Martynov, S.V. Pogrebenko, A. Rodin, J.A. Whiteway, L.V. Zasova, European Venus Explorer: An in-situ mission to Venus using a balloon platform. Adv. Space Res. **44**, 106–115 (2009)

L. Esposito et al., Sage fact sheet, Tech. Rep., SAGE, URL http://lasp.colorado.edu/sage/ (2011)

J. Hall, M.A. Bullock, D.A. Senske, T.S. Balint, A. Benz, B.A. Campbell, E. Chassefiere, A. Colaprete, J.A. Cutts, L. Glaze, S. Gorevan, D.H. Grinspoon, G.L. Hashimoto, J.W. Head, G. Hunter, N. Johnson, V.V. Kerzhanovich, W.S. Kiefer, E.A. Kolawa, T. Kremic, J. Kwok, S.S. Limaye, S.J. Mackwell, M.Y. Marov, A. Ocampo, G. Schubert, E.R. Stofan, H. Svedhem, D.V. Titov, A.H. Treiman, Venus flagship mission study: Report of the Venus science and technology definition team, Tech. Rep., Jet Propulsion Laboratory, Pasadena, CA (2009)

M. Nakamura, T. Imamura, M. Ueno, N. Iwagami, T. Satoh, S. Watanabe, M. Taguchi, Y. Takahashi, M. Suzuki, T. Abe, G.L. Hashimoto, T. Sakanoi, S. Okano, Y. Kasaba, J. Yoshida, M. Yamada, N. Ishii, T. Yamada, K. Uemizu, T. Fukuhara, K.-I. Oyarna, Planet-C: Venus climate orbiter mission of Japan. Planet Space Sci. **55**, 1831–1842 (2007)

S. Smrekar, S.E.A. Limaye, Venus exploration goals & objectives. Tech. Rep., VEXAG report (2011)

E.A.S. Squyres, *Vision and Voyages for Planetary Science in the Decade 2013–2022* (The National Academies Press, Washington D.C, 2011)

H. Svedhem, D.V. Titov, D. McCoy, J.P. Lebreton, S. Barabash, J.L. Bertaux,P. Drossart, V. Formisano, B. Haeusler, O. Korablev, W.J. Markiewicz, D. Nevejans, M. Paetzold, G. Piccioni, T.L. Zhang, F.W. Taylor, E. Lellouch, D. Koschny, O. Witasse, H. Eggel, M. Warhaut, A. Accomazzo, J. Rodriguez-Canabal, J. Fabrega, T. Schirmann, A. Clochet, M. Coradini, Venus Express – the first european mission to Venus. Planet Space Sci. **55**, 1636–1652 (2007)

C. Wilson, E.A.E. Chassefiere, The 2010 european Venus Explorer (EVE) mission proposal. Experimental Astronomy, **33**(2–3), 305–335, doi:10.1007/s10686-011-9259-9 (2012)

L.E.A. Zasova, Russian mission Venera-D, new conception. EPSC Abstracts **6**, 2011–1334 (2011)